The corrosion of magnesium: the influence of inorganic ions and selected organic compounds

Dissertation

Zur Erlangung des akademischen Grades

Doktor der Ingenieurwissenschaften

(Dr.-Ing.)

Der Technischen Fakultät

Der Christian-Albrechts-Universität zu Kiel

Vorgelegt von

Di Mei

Aus

Henan, VR China

Kiel 2020

Gutachtern der Dissertation:

1. Gutachter: Prof. Dr. Mikhail Zheludkevich

2. Gutachter: Prof. dr. ir. J.M.C. (Arjan) Mol

3. Gutachter: Prof. Dr. rer. nat. Franz Faupel

4. Gutachter: Prof. Dr. Regine Willumeit-Römer

Vorsitzender des Promotionsausschusses:

Prof. Dr. rer. nat. Franz Faupel

Tag der mündlichen Prüfung:

17th November 2020

Eidesstattliche Erklärung

Hiermit erkläre ich, dass die beigefügte Dissertation, abgesehen von der Beratung durch die Betreuerin, nach Inhalt und Form meine eigene Arbeit ist.

Die Arbeit, ganz oder zum Teil, wurde nie schon einer anderen Stelle im Rahmen eines Prüfungsverfahrens vorgelegt und ist abgesehen, von den im Anhang angegebenen Veröffentlichungen, nicht anderweitig zur Veröffentlichung vorgelegt worden.

Außerdem ist die Arbeit unter Einhaltung der Regeln guter wissenschaftlicher Praxis der Deutschen Forschungsgemeinschaft entstanden.

Signiature

Geesthacht, den 10. 07. 2020

Table of contents

Abstract

Magnesium (Mg) and its alloys have been extensively investigated for engineering, energy storage, and biomedical applications owing to their suitable properties. However, the intrinsic high corrosion rate of Mg alloys restricts their general applicability. In the recent years, a number of new-type alloys, surface modification methods, processing routes, and corrosion inhibitors have been developed in order to obtain Mg materials with suitable anticorrosion properties that meet all requirements for the targeted application. For this sake, corrosion tests are frequently employed to evaluate the corrosion resistance and degradation behavior of the investigated materials prior to real application. However, this is complicated by the fact that there are no generally accepted protocols for Mg corrosion tests, especially for testing Mg as implant biomaterials. Until now, a variety of media has been used in these tests and the applicability of these media has not been fully described until now impeding the comparability of results from different research groups. In this thesis, the influence of media components, (e.g. inorganic ions, synthetic pH buffer and selected organic compounds) on the degradation of Mg is systematically studied to provide more insight into the influence of the media composition on Mg corrosion tests.

The results show that the synthetic pH buffer (Tris/HCl) accelerates Mg corrosion in simulated body fluid (SBF). Its acceleration effect can be attributed to three factors: the consumption of OH^- (caused by the buffering effect), which is needed for the formation of corrosion products, the complexation ability of Tris for Ca^{2+} and Mg^{2+}, and the increased concentration of Cl^-. Moreover, in SBF without synthetic pH buffer, the synergy between Ca^{2+}, carbonates and phosphates plays a significant role in the corrosion protection of Mg. In Tris-free electrolytes, the corrosion rate of Mg in SBF (with Ca^{2+}, HCO_3^- and HPO_4^{2-}) is significantly lower than that in the electrolytes missing one of the three ions. The trio of ions leads to the continuous growth of the protective co-precipitation layer above the normal $MgO/Mg(OH)_2$ corrosion products on corroded Mg surface and then slows down the Mg corrosion. In terms of bio-relevant organic compounds, amino acids, vitamins, and saccharides at low concentration have no critical influence on Mg corrosion in NaCl solution and SBF electrolyte. The antibiotics, penicillin and streptomycin, at operating concentration (around 10^{-4} M), also have no significant influence on Mg corrosion in minimum essential medium (MEM) and SBF. While streptomycin, as a Ca^{2+} chelating agent, at higher concentration (10^{-2} M and 10^{-3} M) increases the corrosion rate of Mg in MEM and SBF, the importance of free Ca^{2+} concentration on the protection of Mg corrosion in HCO_3^- and HPO_4^{2-}-containing media is emphasized. In addition, the influence of albumin on Mg corrosion is investigated. The results demonstrated that the influence of albumin on Mg corrosion is susceptible to the albumin sources, test methods, and test conditions. Its influencing mechanism can be summarized in three aspects, adsorption, Ca^{2+}/Mg^{2+} chelation and pH buffering effects.

The results of this work highlight the significant influence of the composition of the used media on Mg corrosion tests. Based on these finding, a general discussion about the advantages, shortcomings, and applicability of the commonly used media is provided and potential medium selection criteria for Mg corrosion tests for various research purposes are suggested. The systematic investigation of the corrosion behavior of Mg in pseudophysiological media presented in this work provides a deeper understanding of the underlying mechanism and lays the foundation for the standardization of the corresponding testing protocols.

Zusammenfassung

Magnesium (Mg) und magnesiumbasierte Legierungen wurden wegen ihrer vielversprechenden mechanischen Eigenschaften, intensiv auf ihre Eignung als Basismaterial im Konstruktionswesen, in biomedizinischen Anwendungen sowie für die Energiespeicherung untersucht. Jedoch schränkt die intrinsische Korrosionsanfälligkeit von Mg-Legierungen ihre Verwendung im unbehandelten Zustand ein. In den letzten Jahren wurden daher bereits eine Reihe neuer Legierungen, Oberflächenmodifizierungsverfahren, Verarbeitungstechniken und Korrosionsinhibitoren entwickelt, um Mg-Materialien mit geeigneten Korrosionsschutz-eigenschaften zu entwickeln, die allen nötigen Anforderungen eines spezifischen Anwendungsfeldes genügen. Um die Korrosionsbeständigkeit und das Abbauverhalten der verwendeten Materialien abzuschätzen, werden in der Regel Korrosionstests im Labor durchgeführt, bevor der Werkstoff in einer Anwendung genutzt wird. Bisher wurden dabei keine allgemeingültigen Protokolle für Mg Degradationstests festgelegt, was insbesondere für biorelevante Anwendungsfelder ein Problem darstellt. Die notwendigen Studien werden zurzeit in einer Vielzahl von Medien durchgeführt, wodurch die Forschungsergebnisse verschiedener Arbeitsgruppen nicht vergleichbar sind. Eines der Ziele dieser Arbeit ist daher die systematische Untersuchung der Auswirkung verschiedener Zusammensetzungen des Testmediums (z.B. anorganische Ionen, synthetische pH-Puffer und ausgewählte organische Verbindungen) auf die Degradation von Mg, um ein tieferes Verständnis des Einflusses des verwendeten Mediums auf Mg-Korrosionstests zu erhalten.

Die Ergebnisse zeigen, dass der synthetische pH-Puffer (Tris/HCl) die Mg-Korrosion in simulierter Körperflüssigkeit (SBF) beschleunigt. Diese Beobachtung kann auf drei Faktoren zurückgeführt werden: den Verbrauch von OH^- Ionen durch die Pufferlösung, die für die Bildung von Korrosionsprodukten benötigt werden, die Affinität von Tris für Ca^{2+} und Mg^{2+} Ionen sowie die erhöhte Konzentration von Cl^- Ionen. Darüber hinaus spielt die Synergie zwischen Ca^{2+}, Carbonaten und Phosphaten in SBF in Abwesenheit eines synthetischen pH-Puffer eine wichtige Rolle beim Korrosionsschutz von Mg. In Tris-freien Elektrolyten ist die Korrosionsrate von Mg in SBF (mit Ca^{2+}, HCO_3^- und HPO_4^{2-}) signifikant niedriger als in den Elektrolytlösungen, in denen eines der drei Ionen fehlt. Das Ionentrio führt zu einem kontinuierlichen Wachstum einer zusätzlichen Präzipitationsschicht über den normalen $MgO/Mg(OH)_2$-Korrosionsprodukten auf der korrodierten Mg-Oberfläche. Diese zusätzliche Schicht resultiert in einer stärkeren Verlangsamung der Materialdegradation. In Bezug auf biorelevante organische Verbindungen haben Aminosäuren, Vitamine und Saccharide in geringer Konzentration keinen ausgeprägten Einfluss auf die Korrosionsrate von Mg in NaCl- sowie SBF-basierter Elektrolytenlösung. Die Antibiotika Penicillin und Streptomycin haben in der üblicherweise verwendeten Konzentration (ca. 10^{-4} M) ebenfalls keinen signifikanten Einfluss auf die Mg-Korrosion in minimal essentiellem Medium (MEM) und SBF. Bei höherer Konzentration (10^{-2} M und 10^{-3} M) beschleunigt Streptomycin (Ca^{2+}-Chelatbildner) die

Degradation von Mg in MEM und SBF. Dieser Sachverhalt unterstreicht den Einfluss der freien Ca^{2+}-Konzentration auf die Korrosionsrate von Mg in HCO_3^- und HPO_4^{2-} haltigen Medien. Zusätzlich wird der Einfluss von Albumin auf die Mg-Korrosion untersucht. Die Ergebnisse zeigen, dass die Korrosionsrate von Mg in Gegenwart des Proteins stark von der Albuminquelle, den Testmethoden und Testbedingungen abhängig ist. Der grundlegende Wirkungsmechanismus kann dabei in drei Aspekten zusammengefasst werden: Adsorption, Ca^{2+}/ Mg^{2+}-Komplexierung und pH-Puffereffekte.

Die Ergebnisse der vorliegenden Arbeit heben den ausgeprägten Einfluss der Zusammensetzung des Testmediums auf Mg Korrosionstests hervor. Auf Grundlage dieser Ergebnisse wurden die Vorteile, Mängel und Anwendbarkeit der üblicherweise in Korrosionstests verwendeten Medien diskutiert. Darüber hinaus werden Auswahlkriterien für Testmedien für Materialdegradationsuntersuchungen in verschiedenen Forschungsfeldern umrissen. Die systematische Untersuchung des Degradationsverhaltens von Mg in pseudophysiologischen Medien, die im Rahmen dieser Arbeit durchgeführt wurde, ermöglicht ein tieferes Verständnis der zu Grunde liegenden Mechanismen und schafft die Grundlage für die Standardisierung der entsprechenden Untersuchungsverfahren.

1. Introduction

1.1 Brief introduction to Mg corrosion and corrosion protection

Magnesium and its alloys have been extensively investigated for various applications, such as engineering, energy storage, and biomedical applications, thanks to their varieties of advantages [1-3]. Specifically, Mg attracts much attention in automotive light weighting due to its low density (which is 2/3 of that of Al and 1/5 to 1/4 of that of Fe) and high specific strength [2, 4, 5]. The appealing electrochemistry qualities of Mg, including a relatively negative electrode potential (−2.37 V vs. SHE) and high volumetric capacity (3832 mA·h·cm^{-3}), are beneficial for energy storage [3, 6-8]. Regarding the biomedical applications, Mg and its alloys have become promising biodegradable implant materials for bone fixation and cardiovascular applications [9-13] because of its good biocompatibility and appropriate mechanical properties [1, 10, 12]. However, a shortcoming of Mg, relatively high corrosion rate, is limiting its widespread application in aforementioned areas.

1.1.1 Why and how Mg corrodes

Basic corrosion processes of Mg in aqueous solution

In aqueous solution, the basic corrosion process of magnesium can be described by the following formulas [14-18]:

Anodic reaction:

$$Mg \rightarrow Mg^{2+} + 2e^{-} \tag{1.1}$$

Cathodic reaction:

(Main, Hydrogen evolution reaction (HER))

$$2H_2O + 2e^{-} \rightarrow 2OH^{-} + H_2 \uparrow \tag{1.2}$$

(Secondary, Oxygen reduction reaction (ORR))

$$2H_2O + O_2 + 4e^{-} \rightarrow 4OH^{-} \tag{1.3}$$

Normally, HER (**Eq. 1.2**) was regarded as the cathodic reaction of Mg corrosion process. Recently, the contribution of O_2 to the cathodic reaction during Mg corrosion process has also been gradually valued (as shown in **Eq. 1.3**) [16-20]. In NaCl solution, the localized measurement was employed to investigate the corrosion procedure of commercially pure Mg (CP Mg), and it was found that the dissolved oxygen in the medium was consumed [16]. Not only in the aqueous solution, the contribution of ORR to the cathodic reaction during atmospheric Mg alloy corrosion was also proven by *in situ* monitoring setup [17, 18]. The contribution of ORR to the corrosion of AZ91 alloy even reached 60% in certain cases depending on relative humidity [18].

Negative difference effect (anomalous hydrogen evolution)

During the anodic polarization, hydrogen is evolved on Mg surface, and the increase in anodic polarization leads to the higher hydrogen evolution rate. This effect is termed as negative difference effect (NDE) [21], which is also defined as anomalous hydrogen evolution (anomalous HE) [22]. Although NDE was firstly reported over 150 years ago [23], the community has not reached a consensus on the origin of this effect.

The theory of unipositive Mg^+ has been discussed as one of the possible explanations of NDE [24]. In this theory, Mg electrochemically dissolves to Mg^+ firstly, and then Mg^+ reacts with water to generate hydrogen (**Eq. 1.4** and **1.5**). When anodic potential is applied, the rate of the first reaction (**Eq. 1.4**) increases, which results in in the increased rate of hydrogen evolution (**Eq. 1.5**). However, the presence of Mg^+ has not been validated by the experimental results. Therefore, this theory is trended to be considered as a hypothesis [22]. Besides, the presence of MgH_2 was also considered as one of the possible origin of NDE. Seyeux [25] et al. identified the formed MgH_2 on Mg after 2 min's immersion in ultra-pure water by Time of Flight-Secondary Ion Mass Spectrometry (ToF-SIMS). MgH_2 may contribute to NDE through the reaction shown by **Eq. 1.6-1.7**.

$$Mg \rightarrow Mg^+ + e^- \quad (1.4)$$

$$Mg^+ + 2H_2O \rightarrow H_2 + Mg(OH)_2 \quad (1.5)$$

$$Mg + 2H^+ + 2e^- \rightarrow MgH_2 \quad (1.6)$$

$$MgH_2 + 2H_2O \rightarrow Mg(OH)_2 + 2H_2 \uparrow \quad (1.7)$$

Another explanation of NDE is based on the theory of breakdown of corrosion products film on Mg surface during the anodic polarization. Anodic polarization leads to the increase in the uncovered area on Mg surface, and then enhances the NDE. As a further development of the film theory, Curioni [26] reported that anodic polarization led to propagation of dark regions (on Mg surface) where show higher cathodic activity than that of silvery regions. These dark regions consist of a compact inner MgO layer and an outer $Mg(OH)_2$ layer [27]. The impurity element, Fe, which may further promote the cathodic reaction [27].

Based on the investigation of the behavior of impurities during the Mg corrosion process, another theory was proposed, Fe re-deposition, to strengthen the aforementioned dark regions theory to explain NDE [28]. **Fig. 1.1** shows the schematic of the effect of Fe re-deposition on Mg surface. In this theory, Fe would detach from the Mg matrix with the dissolution of Mg, and then the detached Fe would be oxidized to Fe(II), Fe(III), or α-Fe_2O_3 compounds. These dissolved Fe pieces can be reduced to metallic Fe and redeposit on the matrix by a galvanic replacement reaction with Mg. As shown in **Fig. 1.1. (b)**, Fe re-deposition is believed to promote the propagation of dark regions and increase the active area with corrosion progress.

The Fe re-deposition theory not only provides a new perspective of NDE, but also points out a new strategy of suppressing Mg corrosion, which is discussed in the part of "*Corrosion inhibitors*" in Section 1.1.2.

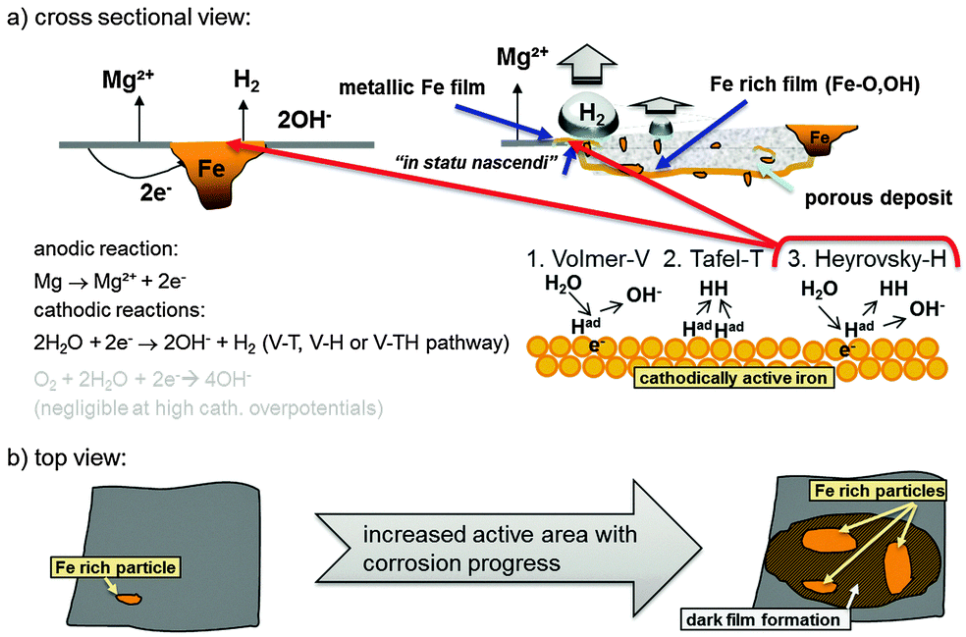

Fig. 1.1 Schematic illustration to the effect of Fe re-deposition on Mg surface. Reprinted from [28] under a Creative Commons Attribution 3.0 Unported Licence.

The role of impurities and second phases

Due to its high reactivity, Mg is susceptible to the galvanic corrosion owing to the Volta potential difference between Mg matrix and impurities or second phases. Fe is the common impurity element in raw Mg produced by Pidgeon process that is currently the main production method of Mg. According to Mg-Fe phase diagram, the tolerance limit of Fe in heat-treated Mg is less than 5 ppm. This limit is much lower than the average impurity content of Fe in high pure Mg and commercial Mg alloys (around 20-50 ppm). It means that iron impurity particles are apt to appear in the heat-treated and slow-cooled Mg and its alloys. In addition, the presence of Si in Mg promotes the precipitation of Fe-containing impurity [29]. Fe-containing impurities act as local cathodes during Mg corrosion owing to the high potential of iron, and then significantly reduce the corrosion resistance of Mg alloys [30]. In addition, a number of transition elements, such as Cu, Co, Ni, Mo, and Cr, are considered to significantly deteriorate the corrosion resistance of Mg when they are beyond the tolerance limits [22]. Thus, the international standards, such as ASTM B94-18 [31] and ASTM B91-17 [32], have strictly regulated the tolerance limits of impurities in Mg alloys.

Dissimilar to impurities, second phases in Mg alloys do not always act as cathode during the corrosion process. **Table 1.1** lists the corrosion potential for pure Mg and several intermetallic phases in 0.1 M NaCl solution. It could be found that most of the Mg-containing intermetallic phases have more positive corrosion potential than Mg matrix, while Mg_2Ca shows more

negative potential. Besides, a rare earth-containing intermetallic phase (Mg-Y-Gd-Nd) in EW75 Mg alloy and the $Mg_{41}Sm_5$ in Mg-Sm-Zn-Zr alloy were also reported to be more active than Mg matrix [33, 34].

Table 1.1 The corrosion potentials for intermetallic phases and pure Mg in 0.1 M NaCl solution [35].

Intermetallic phases	Corrosion potential (V_{SCE})
Mg_2Ca	-1.75
Mg	-1.65
$Mg_{24}Y_5$	-1.60
$Mg_{12}La$	-1.60
Mg_3Nd	-1.55
Mg_2Si	-1.54
$Mg_{12}Ce$	-1.50
$Mg_{17}Al_{12}$	-1.35
$MgZn_2$	-1.03

Herein, we select Mg-Al alloy (containing $Mg_{17}Al_{12}$ phase) and Mg-Ca alloy (containing Mg_2Ca phase) as examples to describe the different role of second phases during Mg corrosion process, as schematically shown in **Fig. 1.2**. In the as-cast Mg-Al alloy, $Mg_{17}Al_{12}$, the main second phase, distributes along the grain boundary. The potential difference between Mg matrix and $Mg_{17}Al_{12}$ accelerates the anodic dissolution (Mg matrix) leading to the decrease in corrosion resistance at initial stage. However, if the $Mg_{17}Al_{12}$ distributes along the grain boundary continuously, the second phases with network structure can prevent the propagation of corrosion. For discontinuous second phases, the dissolution of surrounding Mg matrix makes the undercutting of these second phases and results in the pitting corrosion of the alloy. On the contrary, Mg_2Ca is an anodically active second phase, which also distributes along the grain boundary of as-cast Mg-Ca alloys. In the as-cast high Ca-content (>1.0 wt. %) Mg-Ca alloys, the Mg_2Ca of network structure dissolves first during the corrosion process due to its more negative potential as compared to Mg matrix. The dissolution of net-like Mg_2Ca results in the detachment of undissolved grain, which significantly damages the mechanical integrity of the alloy. This phenomenon was called “chunk effect” [36]. In this type of alloys, the discontinuous second phase is beneficial for the corrosion resistance.

In practical applications, the real phase composition of the alloys is usually more complicated than that in the ideal state. It is worth noting that the second phases in Mg alloy are not only influenced by the alloying elements, but are also determined by the impurities in the materials. For example, besides the often-mentioned CaMgZn ternary phase and Mg_2Ca phase, Jin [37] et al. found the MgCaSi phase in micro-alloyed Mg-Zn-Ca alloy, because of the

presence of Si impurity with the content of 150 ppm in this alloy. Unlike Mg_2Ca phase, MgCaSi phase has more positive potential than Mg matrix, which influenced the corrosion behavior of this alloy.

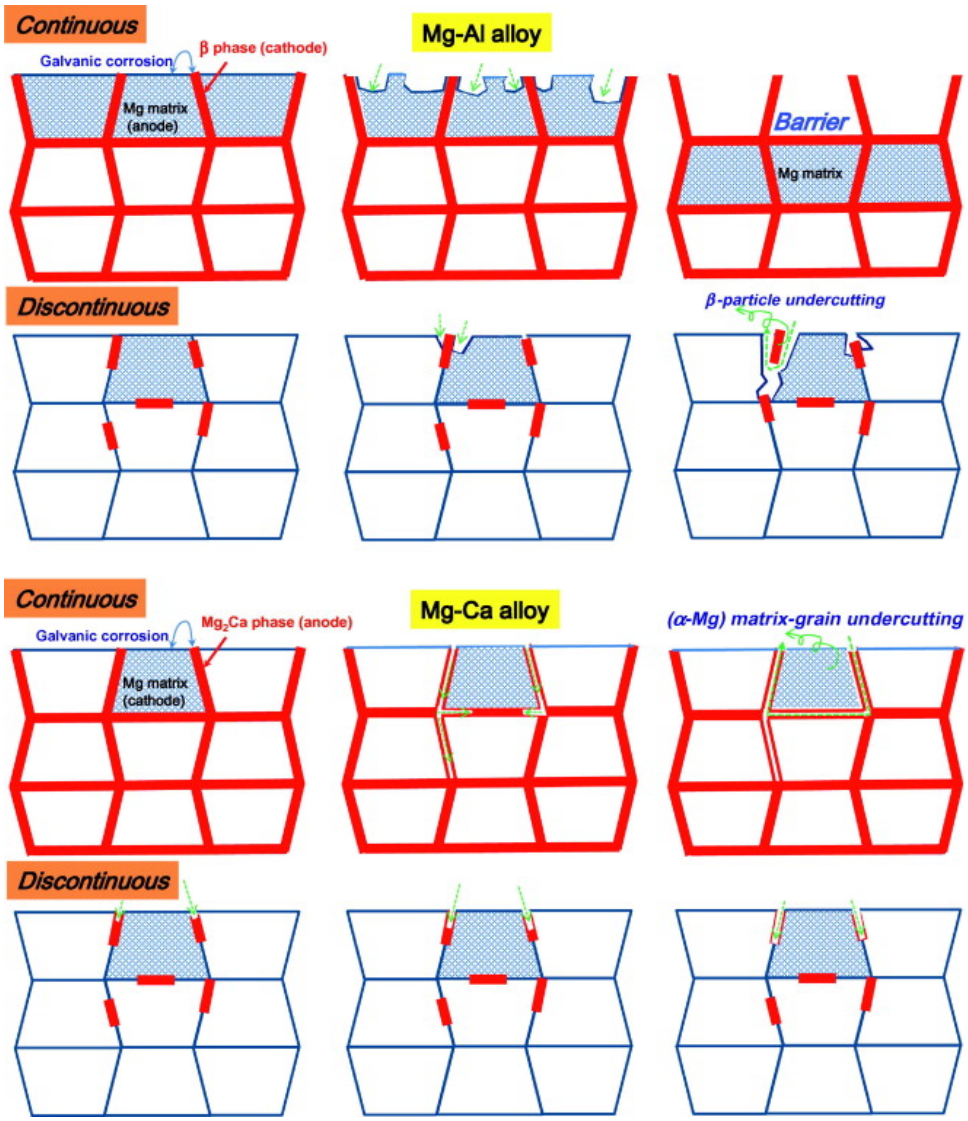

Fig. 1.2 Schematic illustration of the role of $Mg_{17}Al_{12}$ and Mg_2Ca phases in the Mg matrix where their distribution is continuous or discontinuous. Reprinted from [38] with permission.

Corrosion products of Mg in NaCl electrolyte

In the previous section, the role of impurities and the second phases have been discussed based on the Mg corrosion in simple NaCl solution (which is the representative test environment for Mg in engineering application). After decades of research, the understanding of Mg corrosion behavior in NaCl solution is getting deeper. $MgO/Mg(OH)_2$ is the main corrosion product of Mg in NaCl solution, which has insufficient protection efficiency against corrosion. **Fig. 1.3** shows the local pH results near the HP Mg surface exposed in 0.05 M NaCl solution. The high local pH (10.30-10.97) indicates the active corrosion reaction of Mg in NaCl solution.

Even for Al, a metal that can form passive Al_2O_3 film, the presence of chloride causes localized corrosion (e.g. pitting corrosion) [39]. Similarly, chloride is also an aggressive ion for Mg corrosion. In general, $MgO/Mg(OH)_2$ corrosion product consists of outer porous $Mg(OH)_2$ layer and inner relatively dense MgO layer [40]. Danaie [41] et al. investigated the chemical composition of corrosion products on AM50 alloy after immersion in NaCl solution. It was found that Cl^- was uniformly distributed throughout the cross-section of the $MgO/Mg(OH)_2$ corrosion products on α-Mg. One of the possible reasons of the distribution of Cl^- in the corrosion products is that the formation of hydroxychlorides [42, 43]. Giner [44] et al. found that the infiltration of the chloride into the corrosion products led to the destabilization of the hydroxylated interface in NaCl solution and accelerated Mg corrosion.

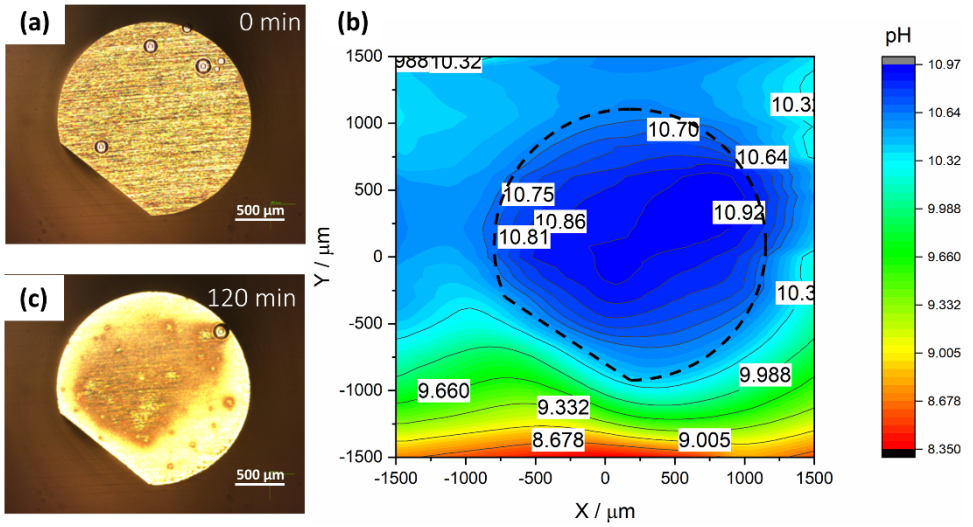

Fig. 1.3 Local pH mapping at 50 µm from the surface of HP Mg immersed in 0.05 M NaCl solution. The contour line of the sample is shown by dashed line. (a, c) Visual appearance of scanned area during the local measurement.

Mg corrosion in complex pseudophysiological media

Considering various potential applications of Mg, not only NaCl solution, other multiple media have also been employed to investigate the corrosion resistance and behavior of Mg. In some cases, the target service environment of Mg materials is much more complicated than NaCl solution.

For some engineering applications, the Mg corrosion tests, which were performed in artificial seawater [45], NaCl dissolved in tap water [15] and deicing salt solution [46, 47] indicated the combination of Ca^{2+} and HCO_3^- (which are the components in above media) and alkaline pH at Mg interface led to formation of $CaCO_3$, which slowed down the corrosion rate of Mg.

In terms of biomedical implant application, in body fluids (typically interstitial fluid and plasma/serum), there are not only Na^+ and Cl^-, but also abundant inorganic ions (such as K^+, Mg^{2+}, Ca^{2+}, SO_4^{2-}, carbonates, phosphates etc.), small-molecule organic compounds (such as

amino acids, vitamins, saccharides etc.), and proteins. During the service period of metallic implants in animal body, ion exchange between the implant and surrounding environment, corrosion products formation induced by inorganic ions/organic compounds and the adsorption/desorption or precipitation of organic compounds significantly influence the surface state of implants and alter their degradation behavior. Mg, C, O, P, Ca and Na were found as the main elements of formed corrosion products on WZ21 Mg alloy after 2 months' implantation in animal body [48]. Obviously, the corrosion products formed in the real service environment of biomedical application are more complicated than those formed in NaCl solution. Therefore, more efforts are still necessary to deepen the understanding of Mg corrosion behavior in such complex environment. Undoubtedly, *in vivo* animal trials are the most direct approaches to investigate the degradation behavior of Mg for biomedical application. However, the broader application of animal trials for the early screening procedure has some limitations, including: 1) lack of high resolution and *in situ* characterization methods; 2) high cost and ethical concerns for animal models at the later stages of implant development prior to clinical trials. Therefore, although the corrosion rate of Mg calculated by corrosion tests does not show a quantitative relationship to that from *in vivo* trials [49], corrosion tests in pseudophysiological environment are still necessary to deepen the understanding of the degradation behavior of Mg during the service period. Until now, more and more complex media have been used for testing corrosion behavior of Mg for biomedical application in order to mimic the real body fluids (e.g. interstitial fluid and plasma/serum). PBS (phosphate buffer solution), Ringer's solution, SBF (simulated body fluid), HBSS (Hank's balanced salt solution), cell culture media and protein-containing solutions are the representatives of the complex media for Mg corrosion test in biomedical applications. The advantages, shortcomings and applicability of these media are discussed in detail in the *General Discussion* (Chapter 5) part of this thesis.

Among these aforementioned complex corrosive media, SBF-like media, cell culture media and protein-containing solutions are most commonly employed due to their similar components as compared to interstitial fluid and plasma/serum. We have performed the local pH measurements of Mg alloys in HBSS solution (as shown in **Fig. 1.4**). The results showed the relatively low local pH (in the range of 7.8 to 8.6), which corresponded to the slight corrosion of Mg alloys in this medium and different nature of corrosion products compared to that in simple NaCl solution (compare to **Fig. 1.3**). They are completely different from the results in NaCl solution. These local pH values (below 9) are significantly lower than that in simple NaCl solution (as shown in **Fig. 1.3**).

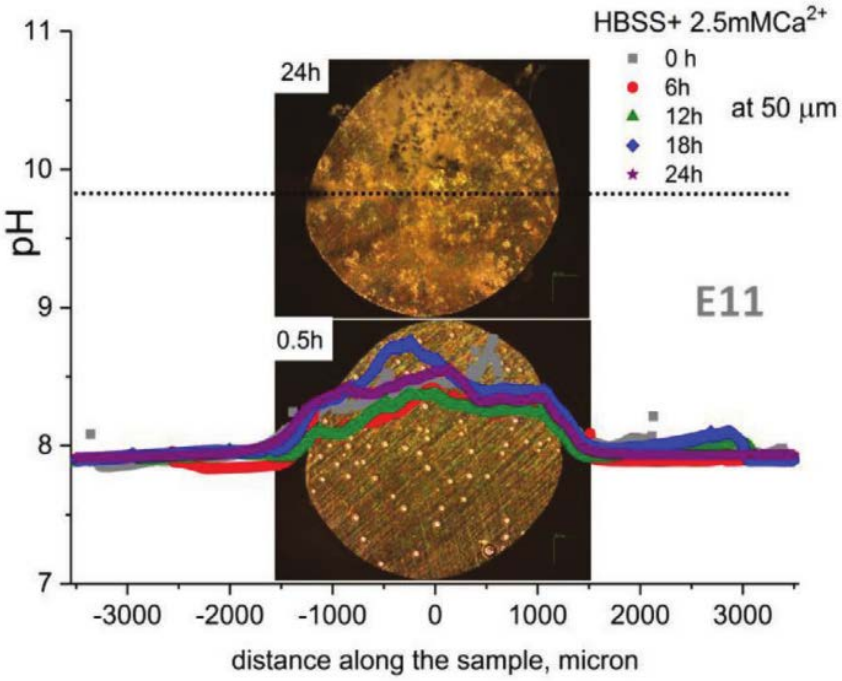

Fig. 1.4 Local pH measurements over E11 (Mg-10Gd-1Nd-0.3Ca) immersed in HBSS+Ca at 50 µm from the surface. Reprinted from [50] with permission.

Unlike Mg corrosion in simple NaCl solution, the corrosion behavior of Mg in pseudophysiological media is not only influenced by the intrinsic corrosion resistance of materials itself, but is also determined by the precipitates of corrosion prodcuts (controlled by media) on the surface of Mg. Hydra-Medusa software [51] can be employed to calculate formation of inorganic ions and precipitates based of thermodynamic stability constants (hence, kinetic limitations may apply). Based on Hydra-Medusa simulation, $MgCO_3$, $Ca_5(PO_4)_3OH$ and $CaCO_3$ were identified as the possible precipitates in HBSS solution within the pH range of 7.5-9.0 (**Fig. 1.5**). However, the simulation in this software relies on the available thermodynamic stability constants. Formation of other compounds, especially co-precipitates, is possible; however, their stability constants are often unavailable and hence cannot be taken into account while drawing the thermodynamic predictions. Nevertheless, predicted products correspond to the descriptions in a number of publications about the corrosion behavior of Mg in SBF-like media. In these works, the precipitation of Mg products was described by the following reactions [52]:

$$Mg^{2+} + 2OH^- \rightarrow Mg(OH)_2 \quad (1.8)$$

$$Mg^{2+} + CO_3^{2-} \rightarrow MgCO_3 \quad (1.9)$$

$$Ca^{2+} + CO_3^{2-} \rightarrow CaCO_3 \quad (1.10)$$

$$3Mg^{2+} + zPO_4^{3-} \rightarrow Mg_3(PO_4)_2 \quad (1.11)$$

$$xMg^{2+} + yCa^{2+} + zPO_4^{3-} \rightarrow Mg_xCa_y(PO_4)_z \quad (1.12)$$

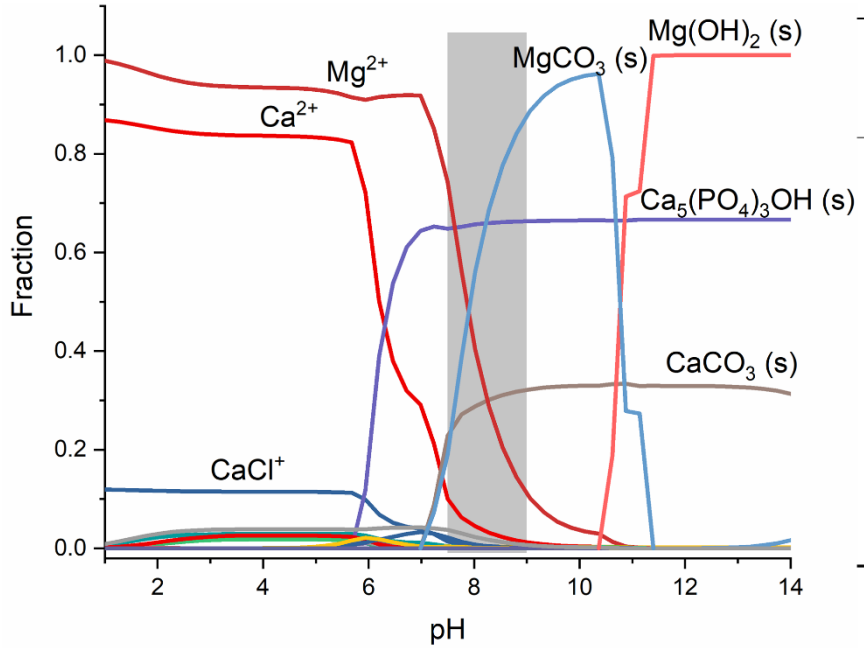

The concentration of participating ions for this calculation (mM)	
Na^+	142.8
K^+	5.8
Mg^{2+}	0.9
Ca^{2+}	1.3
Cl^-	146.8
SO_4^{2-}	0.4
HCO_3^-	4.2
$HPO_4^{2-}/H_2PO_4^-$	0.8

Fig. 1.5 Fraction of either Ca^{2+} or Mg^{2+} species as a function of pH in HBSS based on thermodynamic stability constants, at 25 °C. Simulated by Hydra-Medusa.

Although these complex media, like SBF, HBSS and cell culture media, have been reported to be broadly used for testing the degradation behavior of Mg for biomedical applications, none of them has been initially designed for Mg corrosion test, neither for testing any bioabsorbable metal. Their applicability for corrosion test is still unclear. As a prerequisite, it is necessary to perform systematic studies to investigate the effect of components of these media (including inorganic ions, small-molecule organic compounds, and proteins) on Mg corrosion and clarify the applicability of these media for corrosion testing. It is of paramount significance for the selection or design of suitable corrosive media and understanding of Mg corrosion mechanisms in pseudophysiological environment.

1.1.2 Corrosion protection strategies

Considering the relatively high intrinsic corrosion rate of Mg, continuous efforts are made to develop new alloys [53-57], surface modification technologies [58-62], deformation process routes [63, 64] and corrosion inhibitors [30] in order to improve the corrosion resistance of Mg to fit the actual service requirements. In this section, these commonly employed strategies for corrosion protection of Mg are briefly introduced.

Melt purification, alloying and deformation

As discussed previously, the impurities play a significant role in Mg corrosion. Thus, some effort has been made to improve the corrosion resistance of Mg alloys through melt purification [65]. Dai [66] et al. found that the corrosion rate of AZ61 alloys decreased by

reducing the content of iron impurity in the materials. Similarly, the corrosion rate of AM series alloys was found to be dependent on the content of iron impurity in the alloys [67]. In addition to melt purification, the addition of alloying elements also reduces the impact of impurities on Mg corrosion. For example, Kim [68] et al. found that the small additions of Y in Mg-3Al alloy reduced the content of iron impurities by forming Al_8Fe_4Y phase and then significantly decreased the corrosion rate of Mg.

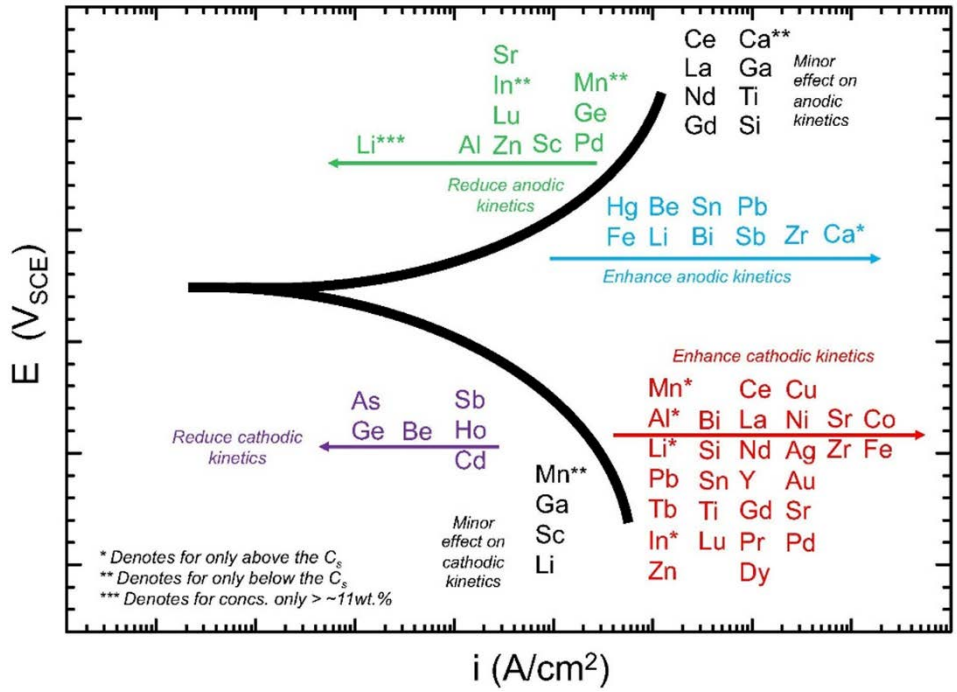

Fig. 1.6 Schematic representation of the electrochemical impact of alloying elements on Mg. The schematic depicts the ability of alloying additions to modify either anodic or cathodic kinetics (or both). C_S represents solid solubility. Reprinted from [22] under the terms of the Creative Commons CC-BY license.

Fig. 1.6 shows electrochemical impact of alloying elements on Mg. It is found that Ge inhibits the cathodic kinetics and has only minor influence on anodic reaction; this corresponds to the reduced corrosion rate of Mg with addition of Ge [57, 69]. As shown in **Fig. 1.6**, a large number of elements can activate cathodic kinetics or/and anodic kinetics. Therefore, from the electrochemical impact prospective, most of these elements might not significantly reduce the corrosion rate of Mg through alloying. However, the influence of alloying elements on the corrosion resistance of Mg alloys cannot be judged only by their electrochemical impact. The addition of alloying elements might influence grain size, second phases and the existence of impurities. Al is the most common alloying element added to Mg alloy. With the increase of Al content in AZ-series alloys, the anomalous HE was reduced [70]. In AZ-series alloys, the addition of Mn decreased the corrosion rate of materials by reducing the precipitation of the iron-rich impurity phase [71]. Sm was also found to had a positive effect on the corrosion protection of AZ91 alloy by influencing the type and existence of second phases [72]. Ca is the

commonly employed alloying element in Mg alloys. Deng [36] et al. found that the addition of Ca in small amount (less than 0.5 wt.%) significantly increased the corrosion resistance of Mg.

Severe plastic deformation (SPD) techniques, such as equal-channel angular pressing (ECAP) [73, 74], high pressure torsion (HPT) [75, 76] and friction stir process (FSP) [77, 78], have been used to fabricate the fine grained Mg materials. The improvement of microstructural homogeneity after processing restricts the localized corrosion of Mg. Other common processing methods, such as extrusion and rolling, are also believed to improve the corrosion resistance of Mg alloys by changing the texture or microstructural homogeneity of the materials [79-81]. However, deformation does not always improve the corrosion resistance of Mg alloys. The residual stress after deformation or defects caused by deformation may accelerate the corrosion of Mg. Besides, for micro-alloyed Mg alloys, the homogenization heat treatments before processing and the heat input during the processing may cause the precipitation of impurities, which likely to reduce the corrosion resistance of Mg alloys.

In general, it is possible to improve the corrosion resistance of Mg alloys by melt purification, alloying or/and plastic deformation. However, the effect of these strategies is affected by complex metallurgical factors and deformation parameters during preparation process of alloys. Impurity content, solidification speed, residual stress and homogeneity of microstructure etc. may significantly affect the corrosion resistance of materials. Therefore, when targeting good corrosion performance, it is still necessary to introduce surface protection techniques to strengthen the corrosion resistance of materials in the real service environment.

Surface modification

Surface modification is an effective approach to improve the properties (such as corrosion resistance, wear resistance and bio-function) of Mg alloys. **Fig. 1.7** lists the commonly investigated coating technologies for Mg alloys.

Plasma electrolyte oxidation (PEO) (also known as micro-arc oxidation (MAO)) is a relatively mature coating technology, and has been used in actual production to improve the corrosion resistance and wear resistance of light metals (Al, Ti, Mg) [82]. PEO coating is an oxide-based ceramic layer formed on the metal surface under the action of high-voltage locally discharge in electrolytes that normally contain silicate, phosphate, fluoride, or aluminate. However, the high porosity of PEO coating restricts its corrosion protection for Mg alloys. Sol-gel [62, 83, 84], electrodeposition [85] and organic coating [86] have been employed as post treatments to seal the pores of PEO coating, which consequently enhance its corrosion resistance. Application of conversion coating is another complementary coating technology for Mg corrosion protection [87]. In the past two decades, phosphate [88-90], permanganate [91], vanadate [92, 93], zirconate [94], titanate [95] and stannate [96, 97] conversion coatings have been extensively investigated. In the recent years, the coatings with self-healing function, like

layered double hydroxide (LDH) [98], PEO coating with corrosion inhibitors [62, 83, 99] and sol-gel coating with corrosion inhibitors [100], have been given more and more attention.

Although a number of surface modification technologies has been developed, the widespread application of these technologies still faces some challenges. For engineering applications, the development of eco-friendly, durable and high-efficient coating technology is an eternal topic. For biomedical applications, the controllable degradability and biocompatibility are the main concerns of the coatings. In particular, the further investigations are still necessary for understanding the corrosion behavior of coatings in the complex service environment.

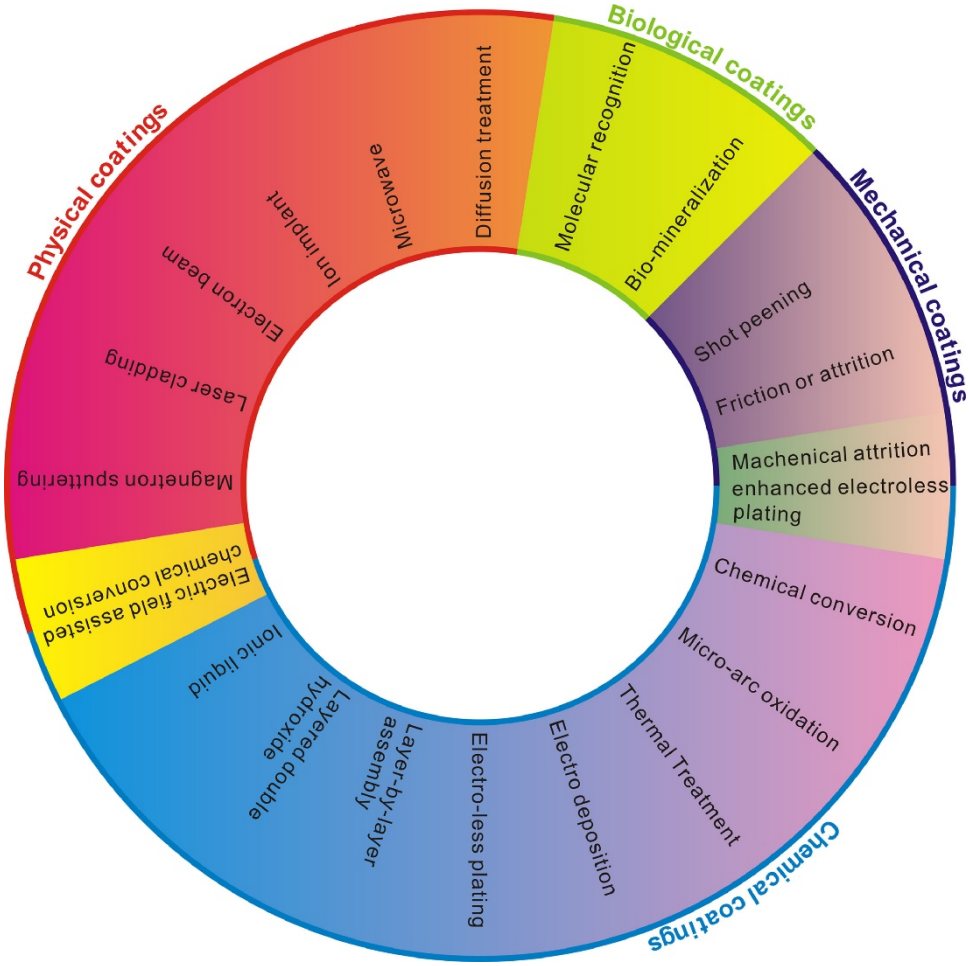

Fig. 1.7 The typical coating technologies explored for Mg alloys. Reprinted from [101] under the terms of the Creative Commons Attribution-NonCommercial-No Derivatives License (CC BY NC ND).

Corrosion inhibitors

One of the promising options for an active corrosion control of Mg is utilization of corrosion inhibitors. A corrosion inhibitor is a compound added in a small amount in corrosion media, which has a strong inhibitory effect on corrosion of metallic materials [102]. The application of the corrosion inhibitors is low cost, easy to operate and requires no special equipment, which is more advantageous than other strategies for corrosion protection. Corrosion

inhibitors are widely used to suppress the corrosion of other structural metallic materials, such as Cu alloys [103], Al alloys [104, 105] and steels [106, 107].

Several inorganic compounds, such as chromate [108], phosphate [109], fluoride [110] and molybdate [111], have been reported to have significant inhibition effect on Mg corrosion by forming insoluble protective film. However, they should be regarded as conversion coating technologies. The focus, in this section, is on the organic compounds as corrosion inhibitors. Until now, the most widely studied organic corrosion inhibitors are surfactants, which adsorb on Mg surface and inhibits corrosion by blocking the contact between the substrate and the electrolyte [112-115].

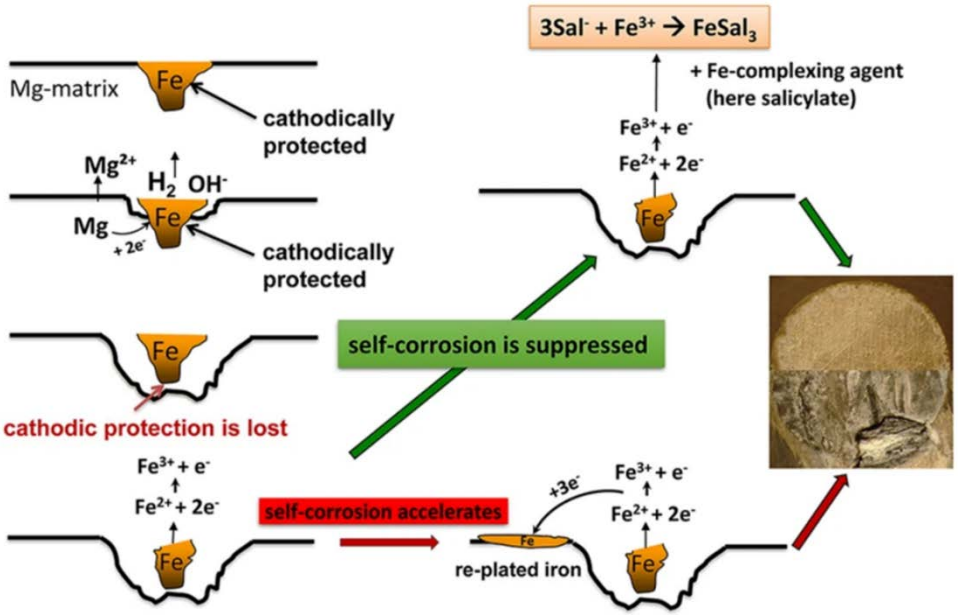

Fig. 1.8 Schematic illustration of the inhibition mechanism of Fe-complexing agent on the corrosion of pure Mg. Reprinted from [116] under a Creative Commons Attribution 4.0 International License.

In the recent years, according to the previously mentioned Fe re-deposition effect, another approach, inhibition of cathodic activity, to suppress Mg corrosion was proposed and validated [28, 116-118]. **Fig. 1.8** schematically shows the inhibition mechanism of Fe-complexing agent on the corrosion of pure Mg. Based on this, the inhibition efficiency (IE) of over 150 chemicals for nine different Mg materials has been experimentally investigated [30]. In addition to experimental methods, machine learning combined with density functional theory calculations have also been used to screen modulators (inhibitors and accelerators) of Mg corrosion [119]. A number of high efficiency corrosion inhibitors were discovered, such as salicylates, pyridinedicarboxylates, and fumarate. Maltseva [120] et al. investigated the influence of salicylate, pyridinedicarboxylate, and fumarate on the formation and evolution of surface film on Mg surface during the corrosion in Cl^--containing electrolyte. The results

pointed out three different inhibition mechanisms for these three types of high efficiency inhibitors: Salicylate adsorbs chemically on $Mg(OH)_2$ and inhibits Fe re-deposition by binding dissolved Fe^{3+} ; Fumarate adsorbs on the surface of metallic Mg or MgO via carboxylate group; Pyridinedicarboxylate precipitates in the form of coordination polymer. These findings enrich the theory of corrosion inhibitors for Mg alloy and are beneficial for further development of highly effective corrosion inhibitors.

Although some highly effective corrosion inhibitors for Mg have been reported, the development and applications of corrosion inhibitors for Mg is still a relatively new field. Especially, more efforts are still necessary to expand the applications of inhibitors, i.e. their incorporation in various types of protective coatings.

1.2 Influence of inorganic ions, small-molecule organic compounds and proteins on Mg corrosion

In the recent years, a number of publications have focused on the influence of media components, including inorganic ions, synthetic pH buffers, small-molecule organic compounds, and proteins, on Mg corrosion. In this section, these relevant results and findings are overviewed.

1.2.1 The influence of inorganic ions

Commonly used corrosive media contain various inorganic ions, including Na^+, K^+, Mg^{2+}, Ca^{2+}, Cl^-, SO_4^{2-}, HCO_3^- and $H_2PO_4^-/HPO_4^{2-}$. Their influence on Mg corrosion has drawn much attention.

Cl^- is normally regarded as the corrosion accelerator for Mg due to its destructiveness towards $MgO/Mg(OH)_2$ layer covering Mg surafce. A number of studies found that the increased concentration of Cl^- promotes the Mg corrosion in simple NaCl solution [121-124]. However, in the complex media (e.g. SBF and HBSS), the increase of Cl^- concentration does not always show higher aggressiveness on Mg corrosion. Taltavull [125] et al. investigated the influence of Cl^- on the corrosion of HP Mg, AZ91 and ZE41 in simple NaCl solution and Hank's solution. After comparing the corrosion rate of these three Mg materials in Hank's solution (0.14mM) and simple NaCl solution (0.1mM Cl^-), the lower corrosion rate was found in Hank's solution. In addition, the increase of Cl^- in Hank's-based solutions did not significantly accelerate the corrosion of HP Mg. Clearly, the presence of various inorganic ions in Hank's solution (like Ca^{2+}, HCO_3^- and $H_2PO_4^-/HPO_4^{2-}$) offsets the corrosion acceleration effect of Cl^- to a certain extent.

HCO_3^- is another widely studied ion in Mg corrosion field, since it is one of the main components in SBF-like corrosive media and is also part of HCO_3^-/CO_2 natural pH buffer in human body environment. Besides, HCO_3^-/CO_2 balance plays important role in atmospheric

corrosion of Mg alloys. There are divergences between published results about the influence of HCO_3^- on Mg corrosion. In simple NaCl solution, Zeng [126] et al. investigated the influence of HCO_3^- concentration (from 4.2 mM to 12 mM) on the corrosion of AZ31 alloy. The results showed that the corrosion rate of AZ31 initially decreased and then increased with the increased concentration of HCO_3^-. In complex environment, HCO_3^- with the increased concentration (from 4 mM to 27 mM) was found to have an increased corrosion inhibition effect on pure Mg in Tris-buffered SBF electrolytes [127]. In the same basic electrolyte, Li [128] et al. found that HCO_3^- with higher concentration (40 mM) activated Mg surface. In Tris-free SBF-like electrolytes, Ma [129] et al. reported that the corrosion rate of Mg increased in the first hours and then decreased with immersion time in HCO_3^--containing electrolyte. However, Agha [130] et al. reported that the change of HCO_3^- concentration had minor influence on Mg corrosion in Ca^{2+}/Mg^{2+}-free HBSS+FBS (fetal bovine serum) (**Fig. 1.9**). In contrast, in Ca^{2+}, Mg^{2+}-containing HBSS+FBS, the increase in HCO_3^- concentration slowed down the Mg corrosion, which vaguely indicated the synergy of HCO_3^-, Ca^{2+} and Mg^{2+} (probably with other ions) on the protection of Mg corrosion.

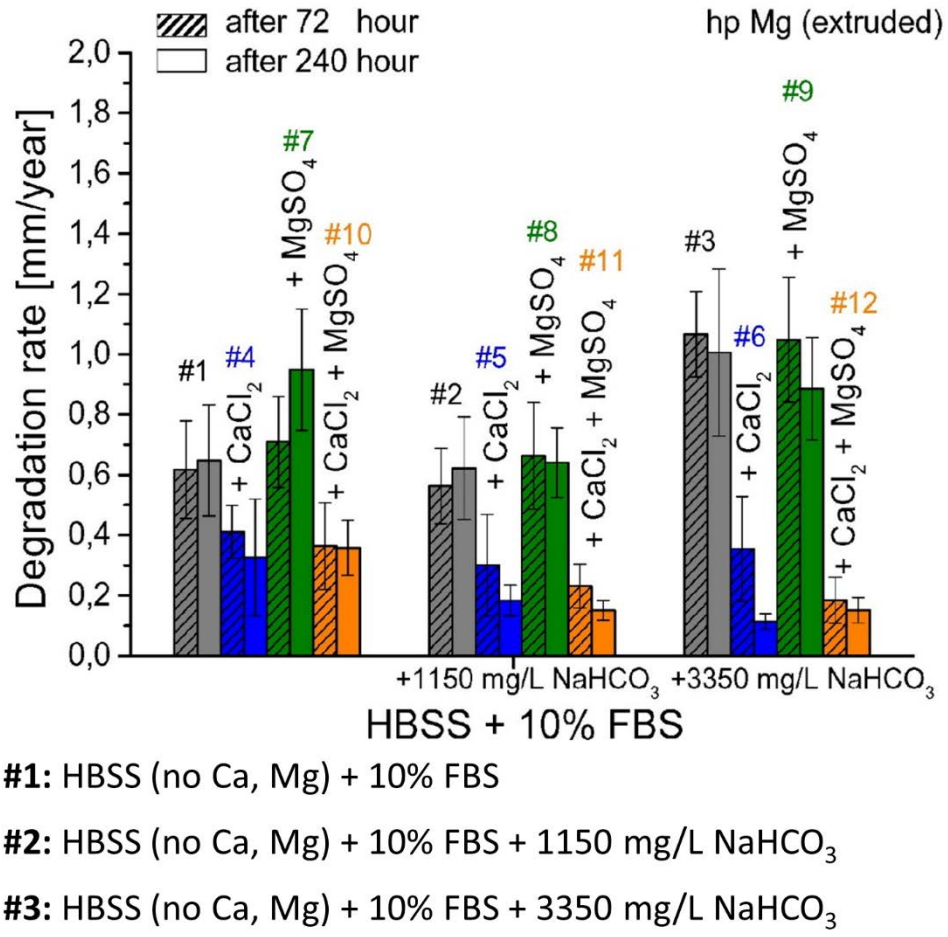

Fig. 1.9 The degradation rate after immersion for 72 and 240 h in the immersion media under cell culture conditions. Numbers over columns present the conditions numbering in text. Reprinted from [130] with permission.

Dissimilar to HCO_3^-, the research results about the influence of phosphates ($H_2PO_4^-/HPO_4^{2-}$) on Mg corrosion are basically consistent. Zeng [126] et al. reported that the presence of phosphates decreased the corrosion rate of AZ31 alloy in NaCl solution. Similar results were reported by Jang [131] et al. In the complex media, including Tris-buffered SBF, Tris-free SBF, and calcium/magnesium-free HBSS+FBS, phosphates were also found to have inhibition effect on the corrosion of pure Mg [127, 129, 130]. In addition, phosphates with higher concentration provide more protection on Mg corrosion. The inhibition effect of phosphates is attributed to the formation of (Ca, Mg)-phosphate corrosion products (as described by **Eq. 1.11** and **1.12**) which provide partial protection against Mg corrosion.

Regarding SO_4^{2-}, at physiological concentration of 0.5 mM, none of relevant works reported its significant influence on Mg corrosion in simple NaCl solution [126] and complex media [127, 129, 130]. On the other hand, at higher concentration of 0.05M Na_2SO_4 in 0.5% (0.085M) NaCl sulfate inhibited corrosion of most of the tested magnesium alloys [30]. In line with this findings, inhibiting effect of sulfate in artificial seawater was ascribed to its possible competitive absorption, hindering absorption of chloride [45].

For the cations in the corrosive media, Na^+ and K^+ were found to have no significant influence on Mg corrosion [132]. However, as compared to the corrosion test in NaCl solution, the slightly higher corrosion rate of AZ31 alloy was found in KCl solution with same concentration of Cl^- [132], which indicated the slight acceleration effect of K^+ on Mg corrosion. The other two cations, Mg^{2+} and Ca^{2+}, play important roles during Mg corrosion process. Ning [132] et al. reported higher corrosion rate of AZ31 in $CaCl_2$ solution (142 mM) as compared to that in $MgCl_2$ solution (142 mM). In NaCl solution, single Ca^{2+} does not have obvious influence on Mg corrosion [133]. However, in carbonate and phosphate containing complex media, the combination between Ca^{2+} and these anions slowed down the corrosion of pure Mg [130]. As shown in **Fig. 1.10**, local pH of four Mg alloys in HBSS and HBSS with 2.5 mM Ca^{2+} showed that the addition of Ca^{2+} affected Mg corrosion by altering the Mg/media interface evolution. This inhibition effect of Ca^{2+} and carbonate/phosphate combination has been employed to develop the anticorrosion coating on Mg alloy [89], albeit at different concentration/ratios of the constituents.

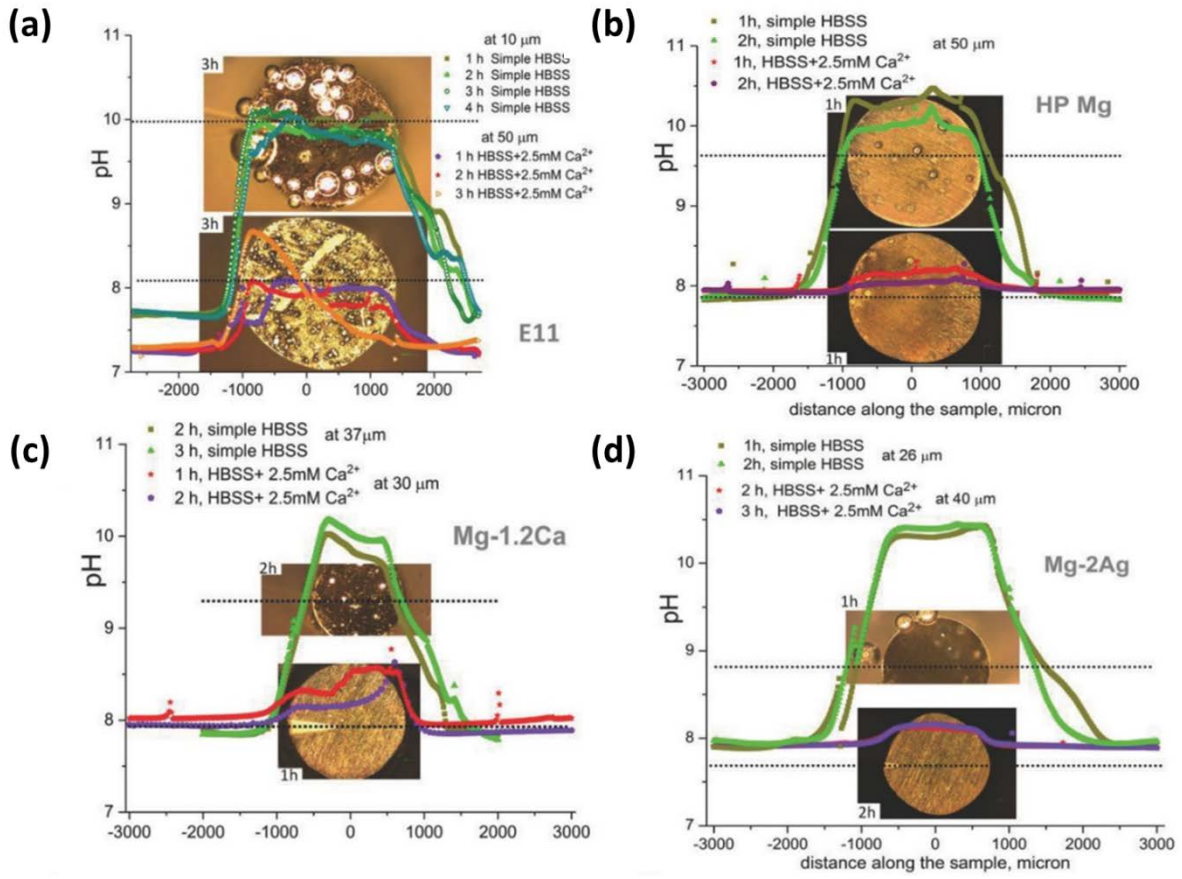

Fig. 1.10 Local pH profiles across (a) E11, (b) HP-Mg, (c) Mg-1.2Ca, and (d) Mg-2Ag sample immersed in constantly flowing simple HBSS and HBSS with 2.5 mM Ca^{2+}. The dotted line across the optical image indicates the exact scanning path. The distance between the surface and the probe is indicated at each part of the figure and varied between 10 to 50 µm. Reprinted from [50] with permission.

As shown in **Fig. 1.9**, in calcium/magnesium-free HBSS+FBS, the addition of $MgSO_4$ showed no significant influence on corrosion of HP Mg [130]. Under the same conditions, the influence of co-addition of $CaCl_2$ and $MgSO_4$ on Mg corrosion was similar to that of single addition of $CaCl_2$ [130]. This indicates the probable minor influence of Mg^{2+} on Mg corrosion in the mild complex media (e.g. HBSS-like).

In addition to these main inorganic ions in body fluids (typically interstitial fluid and plasma/serum), the influence of other inorganic ions/compounds on Mg corrosion has been also noticed [134-136]. NH_4^+ was found to dissolve the MgO layer of Mg corrosion products, and then accelerated Mg corrosion in alkaline solutions [134]. The influence of individual constituents of PM 2.5 in haze on the corrosion behavior of Mg was systematically investigated [136]. $(NH_4)_2SO_4$ showed a more pronounced aggressiveness on corrosion of pure Mg in a $Mg(OH)_2$-saturated solution than that of NH_4Cl and NaCl [136]. This finding provides a new perspective about the test environment for investigating the corrosion behavior of Mg alloys for engineering applications.

1.2.2 The influence of synthetic pH buffers

In order to mimic the constant pH environment of human body, pH buffers have been employed in the corrosion test. $NaHCO_3/CO_2$, the natural pH buffer similar to that in human body, is often used in cell culture tests and corrosion tests under cell culture conditions. Given the required experimental setup, this natural buffer is not easily applicable to corrosion testing at conventional laboratory environments. In this case, some synthetic pH buffers, such as HEPES and Tris/HCl, which are easier to be applied, have been added into the corrosive media to keep the constant pH environment during the corrosion test period.

Kirkland [137] et al. investigated the mass loss of pure Mg in multiple media with different pH buffer. The results indicated that HEPES had stronger acceleration effect on Mg corrosion in all employed media as compared to $NaHCO_3/CO_2$ (shown in **Fig. 1.11**). The electrochemical tests of pure Mg showed that the addition of HEPES inhibited the formation of insoluble phosphates/carbonates products layer on corroded Mg surface and accelerated Mg corrosion in EBSS [138]. This finding was confirmed by the local pH measurement performed in HBSS (with Ca) + HEPES [50]. As compared to the local pH of E11 shown in **Fig. 1.4**, the presence of HEPES prominently affected the Mg/media interface and resulted in the high local pH near E11 alloy in HBSS+Ca (even reached 11, as shown in **Fig. 1.12 (a)**). The local measurement for HP Mg showed similar high local pH in the same medium (**Fig. 1.12 (b)**). This findings are in line with previous local pH measurement which shows high local pH value during the corrosion of AZ31 in HEPES-buffered SBF [139].

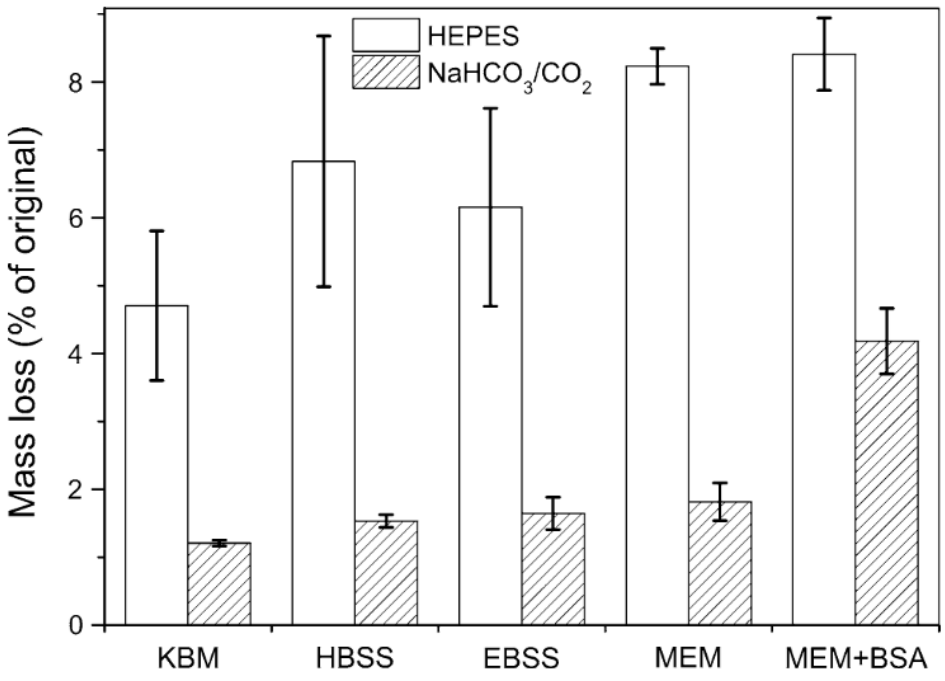

Fig. 1.11 Mass loss of pure Mg after 1 week of immersion in multiple media with HEPES or $NaHCO_3/CO_2$. KBM (Kirkland's biocorrosion medium, which has compositions similar to HBSS and EBSS). Reprinted from [137] with permission.

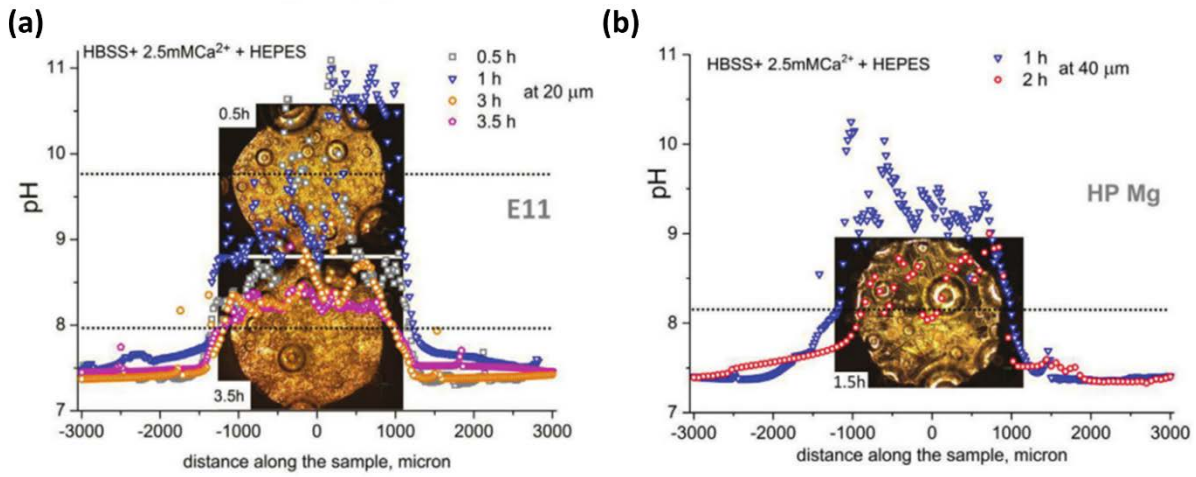

Fig. 1.12 pH profiles across (a) E11, (b) HP-Mg sample immersed in constantly flowing simple HBSS with 2.5 × 10^{-3} M Ca^{2+} and HEPES. Reprinted from [50] with permission.

Similar to HEPES, another synthetic pH buffer, Tris/HCl, was also found to accelerate Mg corrosion. Xin [140] et al. pointed out that Tris/HCl accelerated the corrosion of pure Mg by consuming the generated OH^-, which has participated in the formation of corrosion products. It is also found that Tris/HCl promoted the pitting corrosion of Mg. Cui [141] et al. investigated the influence of Tris/HCl on the corrosion of AZ31 alloy in SBF. The results confirmed the inhibition effect of Tris/HCl on the precipitation of corrosion product on Mg surface.

Above all, since the synthetic pH buffers are not the components of any physiological fluids and show significant influence on Mg corrosion, they should not be allowed in the medium for testing Mg corrosion behavior for biomedical applications.

1.2.3 The influence of small-molecule bio-relevant organic compounds

Besides inorganic ions, there are small-molecule organic compounds, including amino acids, vitamins, saccharides, and organic compounds from Krebs cycle, in physiological fluids (e.g. plasma/serum and interstitial fluid). Additionally, other additional components, such as pH indicator, antibiotics etc., are included in some commonly used corrosive media (like cell culture medium). Thus, a number of published works focused on the influence of these small-molecule bio-relevant organic compounds on Mg corrosion.

Yamamoto [142] et al. compared the corrosion rate of pure Mg in EBSS and E-MEM. They reported a higher corrosion rate of Mg in E-MEM. The difference between EBSS and E-MEM is the presence of amino acids (0.86 $g \cdot L^{-1}$) and vitamins (0.008 $g \cdot L^{-1}$) in E-MEM. Thus, the slight acceleration of Mg corrosion in E-MEM was attributed to the acceleration effect of combination of amino acids and vitamins. Similarly, as shown in **Fig. 1.11**, Kirkland [137] et al. also reported that the corrosion rate of pure Mg in MEM is higher than that in HBSS and EBSS, but the increase is slight. Although these publications have repeatedly confirmed the slight

acceleration effect of the combination of amino acids and vitamins on Mg corrosion, their individual effect is still not fully understood.

Helal [143] et al. investigated the inhibition effect of 9 amino acids on Mg corrosion in stagnant naturally aerated chloride free neutral solution. The results showed that inhibition efficiency (IE) depended on the structure and concentration of amino acids. Phenylalanine with concentration of 2mM had 93% of IE on the corrosion of Mg-Al-Zn alloy by the physical adsorption in naturally aerated aqueous buffer solution of pH 7. Fang [144] et al. studied the adsorption of arginine, glycine and aspartic acid on Mg and its alloys by first principle calculation and found that the functional groups of amino acid influenced their adsorption on Mg. In simple NaCl solution (0.5 wt.%), several individual amino acids and vitamins with concentration of 0.05M were found to have inhibition or acceleration effect on Mg corrosion [30]. For example, L-lysine has over 60% IE on the corrosion of CP Mg and folic acid (Vitamin B9) has general inhibition effect on the corrosion of pure Mg and Mg-RE alloys and Mg-Al alloys. Wang [145] et al. examined the influence of amino acids with different isoelectric points and molecular structures on Mg corrosion in phosphate buffer solution. The results showed that amino acids suppressed Mg corrosion in PBS to some extent. According to different isoelectric points of amino acids, alanine and glutamic acid (negatively charged in aqueous solution) showed higher IE on Mg corrosion as compared to the positively charged amino acid, lysine. This finding corresponds to the results reported by Zhao [146] et al. Based on metadynamics simulations, it was found that the reversed hydration layer on the hydroxylated Mg surface significantly weakened the binding affinities of positively charged amino acid analogues [146]. In addition, the molecular structure of amino acid contains amino and carboxyl groups, which makes the group of amino acids a possible pH buffer. The potential pH buffering effect might alter the test environment and then influence the corrosion behavior of Mg in amino acids-containing media.

Aforementioned publications pointed out the influence of amino acids on Mg corrosion and preliminarily revealed the possible action mechanism. However, the comprehensive understanding of the effects of amino acids on Mg corrosion is still insufficient. It is worth noting that there are hundreds of amino acids in nature, and more than 20 are involved in protein synthesis in the human body. However, only a few of them were considered in the Mg corrosion tests. This is also the case for studies on the influence of saccharides, vitamins and other organic compounds of Krebs cycle.

Glucose, as a representative saccharide, was found to have the acceleration effect on the corrosion of pure Mg and Mg-Ca in NaCl solution [147, 148]. The acceleration effect was attributed to the formation of gluconic acid transferred by glucose in the solution. In Hank's solution, the increased concentration of glucose (1 $g \cdot L^{-1}$ to 3 $g \cdot L^{-1}$) slightly decreased the corrosion rate of pure Mg [148]. However, although some of other saccharides (like

glucosamine, galactose) have similar concentration in plasma/serum to that of glucose, their influence on Mg corrosion have never been considered.

For vitamins and organic compounds from Krebs cycle, Hou [52] et al. found that ascorbic acid (862 mg·L^{-1}) and L-alanyl-L-glutamine (862 mg·L^{-1}) did not significantly affect Mg corrosion in HBSS under cell culture conditions. We have tested the influence of a number of vitamins and organic compounds on Mg corrosion in NaCl solution [30], but that work focused on the potential application of these compounds as corrosion inhibitors and tested concentration (0.05M) is much higher than that in plasma/serum.

Except for these organic compounds from human plasma/serum, other small-molecule organic compounds that are often included in test media, such as pH indicator and antibiotics, are not taken into consideration. The investigation of their influence on Mg corrosion is still lacking.

The effects of single small-molecule organic compound on Mg corrosion are worth investigating. However, considering the rich variety of organic compounds, it is necessary to reach a more comprehensive understanding of their influence on Mg corrosion through extensive testing of organic compounds. These findings can be employed for evaluating the applicability of the organics-containing corrosive media for testing Mg corrosion behavior for biomedical applications.

1.2.4 The influence of macromolecule organic compounds (proteins)

In human blood, there are a number of different proteins, including but not limited to albumins, globulins, fibrinogen, regulatory proteins, and clotting factors.

Table 1.2 The proteins in blood [149].

Blood protein	Content/g·dL^{-1}	Percentage/%	Function
Albumins	3.5-5.0	55	create and maintain osmotic pressure; transport insoluble molecules
Globulins	2.0-2.5	38	participate in immune system
Fibrinogen	0.2-0.45	7	Blood coagulation
Regulatory proteins		<1	Regulation of gene expression
Clotting factors		<1	Conversion of fibrinogen into fibrin

As shown in **Table 1.2**, proteins have relatively high concentration (over 60 g·L^{-1}) in human blood as compared to that of the aforementioned inorganic ions and small-molecule organic compounds. Among these proteins in human blood, albumin has highest content, which is always taken as an example of proteins and employed as the research subject in the Mg corrosion tests.

A number of related publications pointed out the inhibition effect of albumin on Mg corrosion through its adsorption effect, while some other works indicated that albumin also accelerates Mg corrosion. Liu [150] et al. found that, in simple NaCl solution, the presence of bovine serum albumin (BSA) changed the degradation behavior of Mg-1.5Ca alloys at the initial stage of tests, and the higher concentration of BSA resulted in higher inhibition efficiency of Mg corrosion. Similarly, Heakal [151] et al. explored the inhibition effect of BSA with concentration of 40 $g \cdot L^{-1}$ on the corrosion of AZ80 in NaCl solution and the inhibition was attributed to the competition between albumin, OH^- and Cl^-. In the same work, Heakal [151] et al. also investigated the influence of BSA on Mg corrosion in simulated blood plasma (SBP), which has compositions similar to that of HBSS and SBF. The electrochemical tests showed that the addition of BSA with concentration of 10-20 $g \cdot L^{-1}$ increased the corrosion resistance of Mg by forming a protective adsorption layer and BSA with the higher (40 $g \cdot L^{-1}$) or lower (5 $g \cdot L^{-1}$) concentration accelerated the corrosion of AZ80 in SBP. Li [152] et al. studied the corrosion behavior of Mg-Zn-Zr-Sc in albumin-containing HBSS during the 7 days of immersion. The weight loss results showed that albumin inhibited Mg corrosion in the first 6 hours of immersion and then accelerated it. Similar results were reported by Harandi [153] et al., the addition of BSA (40 $g \cdot L^{-1}$) inhibited the corrosion of AZ91 in HBSS solution in the first 48 hours and significantly accelerated it afterwards.

Walker [154] et al. performed the weight loss measurements and reported results of the BSA influence on the corrosion of different Mg alloys in MEM (shown in **Fig. 1.13**). BSA showed significant acceleration effect on the corrosion of HP Mg, Mg-0.8Ca, and Mg-1Mn in MEM, but inhibited degradation of quickly corroding Mg-1.34Ca-3Zn alloy. This is important notion as it shows that the effect of albumin might be alloy dependent and is also influenced by the degradation rate of an alloy. The results indicated that the effect of albumin on Mg corrosion is alloy dependent. Similarly, Gu [155] et al. reported that the addition of 10% FBS increased the corrosion rate of Mg-1.2Ca alloy, but decreased the corrosion rate of AZ91 alloy. Johnson [156] et al. found that the surface states of the Mg materials influenced the protein effect on Mg corrosion in DMEM. The results showed that the addition of 10% FBS just slightly influenced the corrosion of CP Mg with or without the oxide layer, but it slowed down the corrosion of Mg-Y alloy with oxide layer and increased the corrosion rate of Mg-Y alloy with metallic surface. The influence of surface state on the effect of protein could be attributed to the difference in the adsorption capacity of proteins on different surfaces. Hou [157] et al. investigated adsorption of albumin and fibrinogen (Fib), which are two of the main proteins in blood, on Mg surface during the Mg degradation process. The results revealed that pH, surface roughness and wettability influenced the proteins adsorption. The different effects of single protein and protein mixtures on Mg corrosion have been also given due attention. Hou [158] et al. found that BSA, Fib and FBS showed different effect on Mg corrosion in HBSS (no Ca^{2+}), HBSS+Ca^{2+} and DMEM.

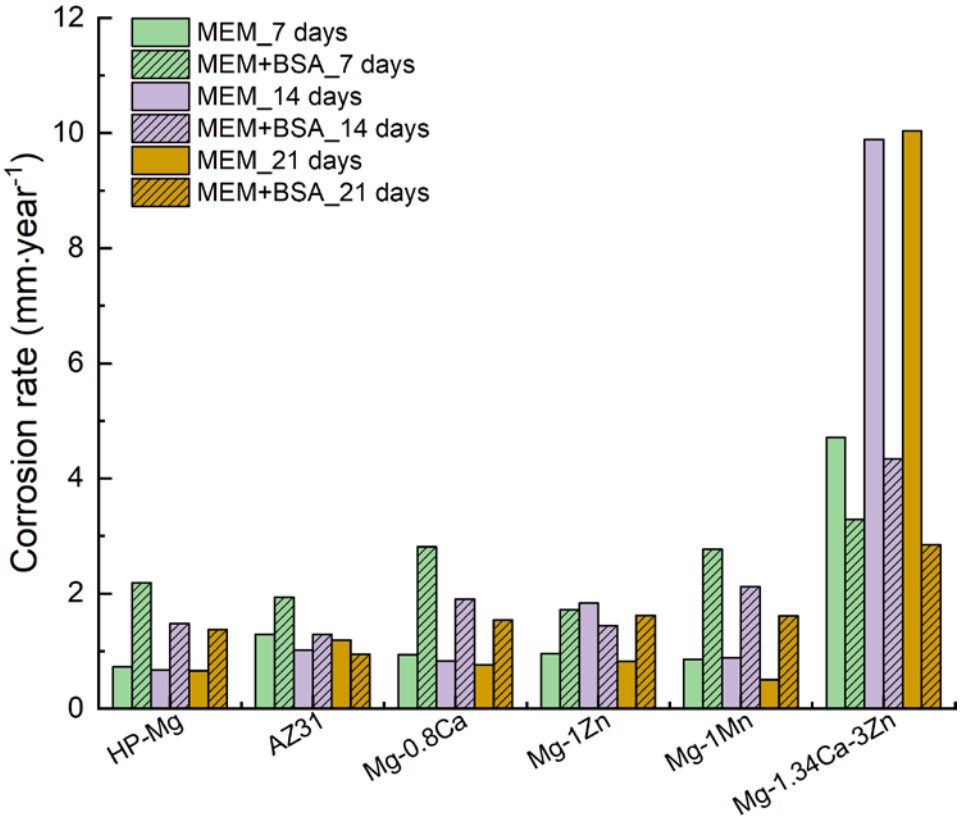

Fig. 1.13 Corrosion rate of various Mg alloys measured by weight loss after 7, 14, and 21 days of immersion in MEM and MEM+BSA. This graph was drawn based on the results reported in Ref. [154].

In a number of publications, besides albumin, FBS was also selected as the protein source in Mg corrosion tests. In most cases, it was regarded as a type of protein mixture. FBS is a very complex physiological medium. It contains not only albumin, but also inorganic ions, globulins, fibrinogen, growth factors, hormones, amino acids, vitamins, fatty acids, lipids etc. Although FBS-containing cell culture media is now also used for testing corrosion behavior of Mg and its alloys, it was originally derived from the media for cell culture in biological research. The usual amount of addition is 10%-20%. In this case, the maximum amount of protein actually added in media is no more than 20 $g \cdot L^{-1}$, which is less than the content of proteins in blood plasma (60-80 $g \cdot L^{-1}$). The works reported by same group of authors showed that 10 % addition of FBS decreased the corrosion rate of Mg-0.8Ca in MEM [159], while 40 $g \cdot L^{-1}$ of BSA accelerated the corrosion of the same alloy in the same basic medium [154].

Thus, although a number of published works focused on the influence of proteins on Mg corrosion, there is no consensus about whether they increase or decrease the corrosion rate of Mg. Although it is not easy to answer this question because the existing studies were conducted in different test conditions, basic media, test materials etc., yet it is possible to clarify the influence mechanisms of proteins through systematic investigations. The adsorption effect of proteins is the most widely mentioned mechanism of its influence on Mg

corrosion. However, it cannot be used to explain the acceleration effect of proteins reported by some works. Some publications reported that proteins thicken the corrosion products on Mg surface and pointed out the affinity of proteins to cations (e.g. Ca^{2+} and Mg^{2+}) [158, 160]. In addition, similar to what was mentioned in Section 1.2.3, the functional groups in the chemical structure of proteins give them a potential pH buffering effect. The effects of the latter two factors in the corrosion process of Mg alloys have not been fully elucidated.

2. Motivation and objectives

The investigation of Mg corrosion behavior has been performed over many decades. However, from the large number of works published about Mg corrosion for biomedical applications, it is clear that the understanding of Mg corrosion behavior is still not complete at present stage, especially in the complex environments. Specifically, the published results showed divergences in some cases due to the different employed test methods and test environment, even if the same materials were tested. Therefore, it is imperative to reveal the inner relationship between different published works through the systematic research. The motivation of this thesis is to reveal the influence of media components on Mg corrosion. Therefore, several representative media components were selected as the research objects, including inorganic ions, small-molecule organic compounds and proteins. Although some works have already covered this area, most of them focused on the individual effect of these components. The synergies between inorganic ions, as well as between organic compounds are not always taken into consideration.

The objectives for this thesis:

- To understand the individual influence and synergy of inorganic ions on Mg corrosion.
- To investigate the effect of small-molecule organic compounds (including amino acids, vitamins, saccharides, antibiotics, several other organic compounds from Krebs cycle and other organic components) at low concentration on Mg corrosion in simple medium (NaCl solution) and complex medium (simulated body fluid).
- To elucidate the mechanisms of protein influence on Mg corrosion.
- To discuss the possible influence of test environments/conditions on Mg corrosion test.

3. Experimental

3.1 Materials and electrolytes

3.1.1 Materials

As-cast commercially pure Mg (CP Mg) and as-cast Mg-0.8Ca alloy were used in this study. Optical discharge emission spectroscopy (SPECTROLAB with Spark Analyser Vision software, Germany) was employed to determine the elemental composition of these two materials. The results are listed in **Table 3.1**.

Table 3.1 The elemental composition of commercial pure Mg (CP Mg) and Mg-0.8Ca alloy.

	Element content/ wt. %				
CP Mg	**Fe**	**Cu**	**Ni**	**Al**	**Mn**
	0.0342	0.00037	<0.0002	0.00402	0.00237
	Si	**Ca**	**Ce**	**Zn**	**Mg**
	0.00071	<0.0001	0.0007	0.00046	Bal.
Mg-0.8Ca	**Fe**	**Cu**	**Ni**	**Al**	**Mn**
	0.0046	0.0021	0.0019	0.024	0.052
	Si	**Ca**	**Ce**	**Zn**	**Mg**
	0.045	0.83	0.001	0.0052	Bal.

These two materials were selected since they are commonly used for biomedical research, and they are also representatives of two types of Mg alloys: with anodic second phase and cathodic intermetallic particles. **Fig. 3.1** shows the SEM images of the used two materials. The second phase in Mg-0.8Ca alloy is Mg_2Ca that is anodically active as compared to Mg matrix [35, 36, 38, 161-163]. In contrast, CP Mg contains iron-rich impurities acting as cathodic second phases. In addition, pure Mg and binary Mg alloy were selected to exclude the potential influence of alloying elements and to get the general influencing mechanisms of inorganic ions and selected organic compounds on Mg corrosion as far as possible.

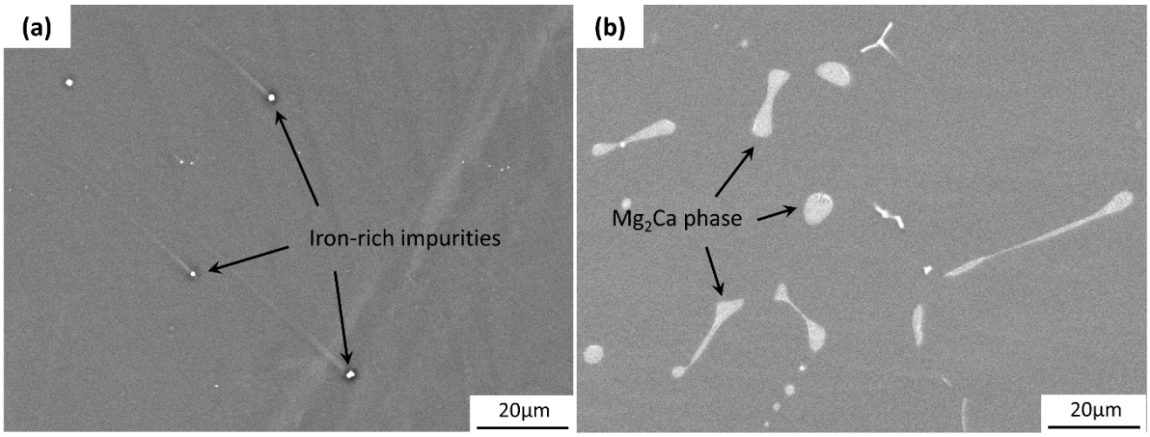

Fig. 3.1 SEM micrographs of the used materials. (a) CP Mg; (b) Mg-0.8Ca.

In order to speed up the hydrogen evolution tests, small metallic chips with a large surface area were produced by a milling machine. Besides, the employment of metallic chips can exclude the influence of orientation (caused by solidification or processing) on Mg corrosion to some extent. **Fig. 3.2** shows the visual appearance of the used Mg chips. For calculation of the surface area of chips, 0.5 g chips were manually unrolled and the size was measured by using an optical microscope (Wild Heerbrugg M3C) equipped with a micrometer (Mitutoyo). **Table 3.2** lists the surface area of these used metallic chips. For the immersion tests and electrochemical impedance measurements, bulk samples with a size of 13x13x4 mm were used.

Fig. 3.2 Visual appearance of used Mg Chips.

Table 3.2 The surface area of the used metallic chips.

Material	Surface area of the chips / $cm^2 \cdot g^{-1}$
CP Mg	47.7 ± 5.0
Mg-0.8Ca	52.3 ± 3.8

3.1.2 Electrolytes in Chapter 4.2

The main focus of Chapter 4.2 is to reveal the individual influence and synergy of the synthetic pH buffer and inorganic ions on Mg corrosion.

Kokubo's simulated body fluid (SBF) [164], which is prepared by various inorganic salts and synthetic pH buffer (Tris/HCl), was selected as the basic electrolyte. Contrary to the most of the relevant works, in this chapter, the influence of synthetic pH buffer and inorganic ions on Mg corrosion was investigated by removing the specific component from the complex media instead of adding it to the simple NaCl solution. The chemical components of the electrolytes used in Chapter 4.2 are listed in **Table 3.3**. Solution No. 2 to 6 were designed to investigate the influence mechanisms of Tris/HCl pH buffer. Solution No. 7 to 10 were designed to investigate the individual influence of Ca^{2+}, SO_4^{2-}, HCO_3^-, and $H_2PO_4^-$, respectively. Solution No. 11 to 12 were designed to investigate the synergy of Ca^{2+}, HCO_3^-, and $H_2PO_4^-$ on Mg corrosion.

Table 3.3 The chemical composition of electrolytes in Chapter 4.2.

No.	Electrolytes	Initial pH value	Ion concentration (mM)								
			Na^+	K^+	Mg^{2+}	Cl^-(inorganic salt and buffer)	Ca^{2+}	HCO_3^-	HPO_4^{2-}	SO_4^{2-}	Tris
1	SBF	7.35-7.45	142.0	5.0	1.5	186.8	2.5	4.2	1.0	0.5	50.5
2	SBF (Ca^{2+}, HCO_3^-, HPO_4^{2-}, SO_4^{2-}/ no Tris/HCl)		142.0	5.0	1.5	147.8	2.5	4.2	1.0	0.5	/
3	SBF (no Tris, adjust pH by NaOH)		>142.0	5.0	1.5	186.8	2.5	4.2	1.0	0.5	/
4	SBF (Cl^- concentration the same as in No. 2)		102.8	5.0	1.5	147.8	2.5	4.2	1.0	0.5	50.5
5	SBF (buffering capacity was depleted by adding NaOH)	9.5	>142.0	5.0	1.5	186.8	2.5	4.2	1.0	0.5	50.5
6	SBF (no Tris/HCl, adjust pH by NaOH)		?142.0	5.0	1.5	186.8	2.5	4.2	1.0	0.5	50.5
7	SBF (HCO_3^-, HPO_4^{2-}, SO_4^{2-}/ no Tris/HCl, no $CaCl_2$)	7.35-7.45	142.0	5.0	1.5	142.8	/	4.2	1.0	0.5	/
8	SBF (Ca^{2+}, HCO_3^-, HPO_4^{2-}/ no Tris/HCl, no $NaSO_4$)		141.0	5.0	1.5	147.7	2.5	4.2	1.0	/	/
9	SBF (Ca^{2+}, HPO_4^{2-}, SO_4^{2-}/ no Tris/HCl, no $NaHCO_3$)		142.0	3.0	1.5	147.8	2.5	/	1.0	0.5	/
10	SBF (Ca^{2+}, HCO_3^-, SO_4^{2-}/ no Tris/HCl, no K_2HPO_4)		137.8	5.0	1.5	147.8	2.5	4.2	/	0.5	/
11	SBF (HPO_4^{2-}, SO_4^{2-}/ no Tris/HCl, no $CaCl_2$, no $NaHCO_3$)		137.8	5.0	1.5	142.8	/	/	1.0	0.5	/
12	SBF (HCO_3^-, SO_4^{2-}/ no Tris/HCl, no $CaCl_2$, no K_2HPO_4)		142.0	3.0	1.5	142.8	/	4.2	/	0.5	/

3.1.3 Electrolytes in Chapter 4.3

In Chapter 4.3, the influence of 53 bio-relevant small-molecule organic compounds (constituting plasma/serum or cell culture media) on Mg corrosion was investigated.

Three different basic electrolytes were employed in this part of work, namely 0.85 wt. % NaCl solution (isotonic solution), simulated body fluid (Kokubo's SBF, refer to [164] but without Tris/HCl buffer), and Minimum Essential Medium (MEM, Thermofisher, 61100-103). The detailed composition of these electrolytes is listed in **Table 3.4**.

To test the individual influence of small-molecule organic compounds, 0.85 wt.% NaCl solution was used. The effect of group of amino acids, vitamins and saccharides on Mg corrosion was investigated in both NaCl solution and SBF. For preparing the test media, organic compounds were regarded as additives and dissolved in NaCl solution, SBF, or MEM and the initial pH was adjusted by NaOH or HCl to 6.8±0.5.

Table 3.4 The chemical compositions of three basic electrolytes.

	Concentration/ mM		
	0.85 wt. % NaCl	SBF	MEM
Na^+	145.4	142.0	144.4
K^+	-	5.0	5.3
Mg^{2+}	-	1.5	0.8
Ca^{2+}	-	2.5	1.8
Cl^-	145.4	147.8	126.1
HCO_3^-	-	4.2	26.2
HPO_4^{2-}/ $H_2PO_4^-$	-	1.0	1.0
SO_4^{2-}	-	0.5	0.8
Synthetic pH buffer (i.e. Tris/HCl, HEPES)	No	No	No
Amino acids (13 kinds)	-	-	848.0 mg/L
Vitamins (8 kinds)	-	-	8.1 mg/L
Glucose	-	-	5.5
Phenol red	-	-	10 mg/L
Initial pH value	5.6-5.9	7.35-7.45	7.0-7.4

Table 3.5 lists the tested small-molecule organic compounds and their tested concentration. There are 24 amino acid, 9 vitamins, 4 saccharides, 2 antibiotics and 14 other small-molecule organic compounds. These small-molecule organic compounds were selected due to their relatively high concentration (>10E-6 M) in human plasma/serum or MEM electrolyte [165-167]. The tested concentration of these compounds was chosen so as to correspond to their concentration in human plasma/serum or MEM electrolyte.

The individual influence and then the group effect of 20 essential amino acids, 4 non-essential amino acids, 9 water-soluble vitamins, 4 saccharides were tested in NaCl. The group effects were also tested in SBF. The individual influence of 14 other organic compounds from Krebs cycle and the additives in MEM were only tested in NaCl solution. The individual influence of antibiotics (penicillin and streptomycin) of three different concentrations and the combined effect of antibiotics with concentration of 10E-4 M were tested in MEM and SBF (where they are typically added to prevent the microbial growth).

Table 3.5 The tested small-molecule organic compounds and their concentration

Amino acid

Compound	Concentration/ M	Compound	Concentration/ M
Alanine	**8.53×10^{-4}**	Serine	**1.90×10^{-4}**
Aspartic	**9.01×10^{-5}**	Proline	**4.95×10^{-4}**
Glutamic	**1.90×10^{-4}**	Cysteine	**4.13×10^{-4}**
Glycine	**7.19×10^{-4}**	Asparagine	**1.00×10^{-4}**
Leucine	**3.96×10^{-4}**	Isoleucine	**3.20×10^{-4}**
Methionine	**1.01×10^{-4}**	Arginine	**2.07×10^{-4}**
Histidine	**2.45×10^{-4}**	Valine	**3.59×10^{-4}**
Tryptophan	**1.47×10^{-4}**	Threonine	**2.69×10^{-4}**
Phenylalanine	**2.42×10^{-4}**	Glutamine	**7.25×10^{-4}**
Lysine	**3.97×10^{-4}**	Tyrosine	**1.38×10^{-4}**
Ornithine	**1.06×10^{-4}**	α-Aminobutyric acid	**1.94×10^{-5}**
Taurine	**1.68×10^{-4}**	Cystine	**9.90×10^{-5}**

Vitamin

Compound	Concentration/ M	Compound	Concentration/ M
Ascorbic acid (VC)	**1.14×10^{-4}**	Folic acid (VB9)	**2.27×10^{-6}**
Inositol (VB8)	**3.89×10^{-5}**	Riboflavin (VB2)	**2.66×10^{-7}**
Pyridoxine-HCl (VB6)	**4.82×10^{-6}**	Thiamine-HCl (VB1)	**2.96×10^{-6}**
Nicotinamide (VB3)	**8.19×10^{-6}**	Choline chloride (VB4)	**7.16×10^{-6}**
Calcium pantothenate (VB5)	**2.10×10^{-6}**		

Saccharide

Compound	Concentration/ M	Compound	Concentration/ M
Glucose	**5.83×10^{-3}**	Galactose	**1.11×10^{-3}**
Glucosamine	**4.97×10^{-3}**	Fructose	**4.44×10^{-4}**

Several other organic compounds

Compound	Concentration/ M	Compound	Concentration/ M
Phenol red	**2.82×10^{-5}**	β-Hydroxybutyric acid	**9.00×10^{-6}**

Lactate	**2.20×10^{-3}**	Glucuronic acid	**5.67×10^{-5}**
Malic acid	**6.70×10^{-5}**	Creatinine	**1.00×10^{-4}**
Glycerol	**1.87×10^{-4}**	Urea	**6.66×10^{-3}**
Uric acid	**4.82×10^{-4}**	Citric acid	**1.66×10^{-4}**
Succinic acid	**4.23×10^{-5}**	Acetone	**3.44×10^{-4}**
Pyruvic acid	**1.40×10^{-4}**	Lecithin	**2.25 g/L**

Antibiotic

Compound	Concentration/ M	Compound	Concentration/ M
Penicillin	**1×10^{-4}**	Streptomycin	**1×10^{-4}**
	1×10^{-3}		**1×10^{-3}**
	1×10^{-2}		**1×10^{-2}**
Penicillin + Streptomycin	**$1 \times 10^{-4} + 1 \times 10^{-4}$**		

3.1.4 Electrolytes in Chapter 4.4

The mechanisms of protein influence on Mg corrosion was investigated in Chapter 4.4. In this part of work, HBSS was selected as the corrosive medium since it is more stable (free of precipitate during long time storage) than other SBF-like media. The detail composition of HBSS is listed in **Table 3.6**.

Table 3.6 The composition of Hank's balanced salt solution (HBSS).

	Concentration/ mM
	HBSS
Na^+	142.8
K^+	5.8
Mg^{2+}	0.9
Ca^{2+}	1.3
Cl^-	146.8
HCO_3^-	4.2
HPO_4^{2-}/ $H_2PO_4^-$	0.8
SO_4^{2-}	0.4
Synthetic pH buffer (i.e. Tris/HCl, HEPES)	No
Initial pH value	7.0-7.4

As previously mentioned, albumin is the most abundant protein in human plasma/serum. Its concentration is 3.5-5.0 $g \cdot dL^{-1}$. Thus, albumin was regarded as the representative of proteins. In this part of work, bovine serum albumin (BSA, Carl Roth, 8076.3) was selected as the source of albumin. Although the structure of BSA is different from that of human serum albumin (HSA), the findings based on the work with BSA can be cautiously deepen the understanding

of the influence of HSA on Mg corrosion since some of their physicochemical properties are similar [168]. Here, 40 $g \cdot L^{-1}$ of BSA was added to HBSS to investigate its influence on Mg corrosion. This added concentration was determined based on the albumin concentration in human plasma. The initial pH value of the media (HBSS/HBSS+BSA) was 7.2 ± 0.2. Besides, chicken egg albumin (CEA, Alfa Aesar, A16951) was also preliminarily tested for comparison.

3.2 *In situ* characterization methods

3.2.1 Hydrogen evolution test

Hydrogen evolution test is a continuous corrosion test for Mg and its alloys. As shown in **Eq. 1.2**, it reflects the corrosion rate of Mg. However, as mentioned earlier in Chapter 1, ORR also occurs as secondary cathodic process during Mg corrosion. It is obviously not taken into account during hydrogen evolution tests. This leads to underestimated values of corrosion rate of Mg presented by HER, as compared to that given by weight loss method. In this study, the hydrogen evolution tests were performed by using the commercial eudiometers (Art. Nr. 2591-10-500 from Neubert-Glas, Germany). It is noteworthy that the eudiometer is a closed setup, thus the oxygen in the air does not continuously contribute to the ORR during Mg corrosion process. Besides, we found that the ratio of ORR to total cathodic process is smaller for fast corroding materials [169]. Using Mg chips, which have large surface area, in hydrogen evolution test can accelerate the corrosion reaction. These strategies help to minimize the underestimation of the total cathodic reaction of Mg corrosion during hydrogen evolution tests. However, there are some other experimental artifacts, such as the dissolution of hydrogen in electrolyte and in Mg, can also lead to a discrepancy between hydrogen evolution and weight loss tests.

Fig. 3.3 shows the schematic of the eudiometer for hydrogen evolution test. The corrosive medium (500 mL) and Mg metallic chips (0.50 g) were put in the matched wide-mouth bottle. Silicone vacuum grease was employed to ensure the air tightness of the device. Before test, the H_2O in the eudiometer was pumped up to "0" mL. During the test, the medium is continuously stirred by a magnetic stirrer at a rate of 200 rpm. The generated H_2 pushed H_2O back to the reservoir. The volume of evolved hydrogen was shown by the drawdown of liquid level in the eudiometer. Additionally, the evolution of hydrogen can be also reflected by the weight change of the reservoir. The weight of the reservoir was measured by the electronic balance (OHAUS, SKX series) in real time, and the weight values were recorded by using a UBS data logger (OHAUS, 30268984) after every fixed time interval (freely adjustable from 1 s to 1 h; 15 min in this work). As compared to the device normally used in hydrogen evolution test (combined burette, funnel and beaker), the remarkable advantage of the device here is that the volume of evolved hydrogen can be recorded automatically, thus the subtle changes in corrosion rate are easier to be shown. It is also beneficial for the long-term tests, where

continuous manual recording is difficult. In this thesis, hydrogen evolution test was employed to compare Mg corrosion in different electrolytes under the same test conditions rather than to accurately calculate the corrosion rate of materials, thus, the listed results are original results without correction by atmospheric pressure change and eventual temperature.

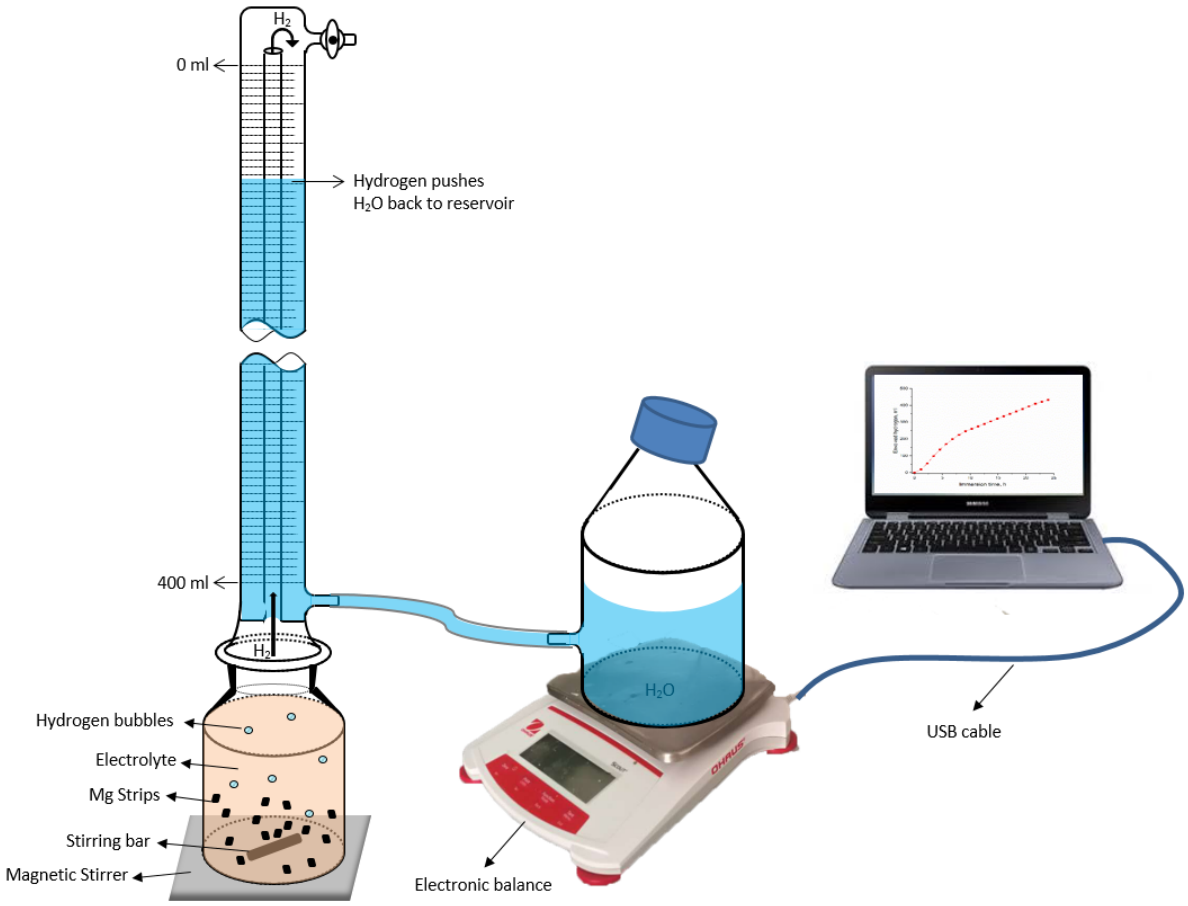

Fig. 3.3 The schematic setup of an eudiometer experiment used for hydrogen evolution test. Reprinted from [170] with permission.

In Chapter 4.2 and 4.4, the hydrogen evolution tests of Mg were performed for 22-24 hours to compare corrosion rate of Mg in various electrolytes.

In Chapter 4.3, the influence of selected small-molecule organic compounds on Mg corrosion was described by inhibition efficiency (IE/ %) that was calculated according to the volume of evolved hydrogen after 20 hours' test by the following equation:

$$\mathrm{IE}/\,\% = \frac{V_{Ref.} - V_{Additive}}{V_{Ref.}} \times 100\,\%$$

Where $V_{Ref.}$ is the cumulative volume of generated hydrogen after 20 h immersion in the three basic media that were listed in Section 3.1.3. The tests in basic media were repeated 3-6 times to confirm the reproducibility, and the average value of the parallel experimental results was

finally employed as $V_{Ref.}$. $V_{Additive}$ refers to the cumulative hydrogen volume of Mg after 20 h immersion in the basic medium with the addition of organic compounds to be measured. The group effects of organic compounds and part of tests of individual compounds (which show relatively significant influence) were repeated to verify the reproducibility. The positive value of IE means the tested organic compound inhibits Mg corrosion in the corresponding basic medium, while negative value indicates the acceleration effect of the organic compound on Mg corrosion.

3.2.2 Electrochemical impedance spectroscopy

Electrochemical impedance spectroscopy (EIS) measurements were performed to continuously evaluate the degradation behavior of Mg in various media and to *in situ* investigate the formation of corrosion products during the immersion period. The compositions of the used electrolytes are listed in Section 3.1.2-3.1.4. Before the measurement, the bulk samples were ground with SiC paper up to 1200 grit, followed by the cleaning with ethanol and drying process in a stream of pressurized cold air. For the EIS measurements, a conventional three-electrode setup was employed, including a working electrode (Mg samples with an exposure area of 0.5 cm^2), a counter electrode (a platinum wire coil), and a reference electrode (saturated Ag/AgCl). EIS measurements were performed at open circuit potential (OCP) applied sinusoidal perturbation with amplitude of 10 mV RMS over a frequency range from 100 kHz to 0.1 Hz in 330-350 mL electrolyte. All the EIS measurements were performed by a potentiostats (Gamry Interface 1000) at room temperature in air-conditioned lab (around 22±2 ℃) under constant stirring conditions (200 rpm).

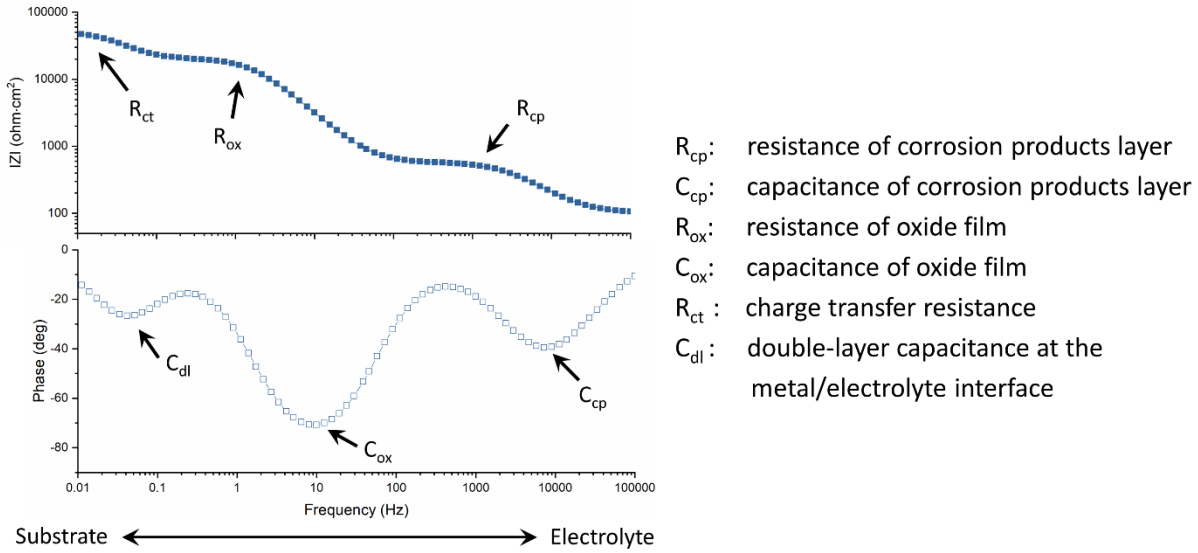

Fig. 3.4 Simulated typical Bode plots of Mg in simulated body fluids (such as HBSS, SBF).

The EIS spectrum can be presented in two formats, Nyquist plot and Bode plot. The former one shows the real and imaginary parts of the impedance. The latter one shows the total

impedance modulus and the phase shift with frequency. Here, we focused on the impedance change in the mid- to high-frequency range, which usually reflects the growth of the corrosion product layer on the sample surface. Thus, all the EIS results are shown in the format of Bode plot in this thesis. **Fig. 3.4** shows the simulated typical Bode plots of Mg in complex saline electrolytes (such as HBSS, SBF). Generally, the response at higher frequency is related to the interface reaction more close to electrolyte, and the response at lower frequency reflects the interface reaction close to the substrate. The frequency-phase angle curve clearly shows the layered structure of corrosion products on Mg surface. The EIS tests can be performed continuously to evaluate the change and formation of coating/corrosion products on Mg surface during the immersion period.

Normally, for the EIS measurement of Mg, 30 min to 1 h pre-immersion is desirable to reach stationarity of the system prior to test. Here, we omitted this procedure and started the measurement immediately after the sample was exposed to the media. Thus, the rapid changes in the corrosion behavior of Mg at the initial stage of immersion can be observed. It helps make the comparison between EIS results and other experimental results (like hydrogen evolution test). However, in order to avoid the possible sample polarization caused by the change of OCP in this case, the measurements were stopped before upon the first signs of sample polarization, typically before reaching to lower frequency range (0.1-0.01 Hz).

3.2.3 Monitoring of local and global pH during Mg corrosion

Bulk pH measurement

A pH meter (Metrohm-691, Switzerland) was employed to measure the bulk pH of all electrolytes before all the tests. Prior to measurement, the pH meter was calibrated by buffer solutions (pH=4, 7 and 10). The bulk pH of the electrolytes after hydrogen evolution tests was also recorded.

In Chapter 4.2, the bulk pH change of selected electrolytes during the hydrogen evolution test was recorded. The bulk pH monitoring was repeated at least three times to confirm the reproducibility.

Local pH measurement

Due to the high mobility of OH^-, a thick Nernstian diffusion layer was quickly established when Mg was exposed to the electrolyte [50]. As shown in **Fig. 3.5**, pH of the medium near the corroded surface is controlled by the diffusion of OH^-; therefore, a pH gradient is formed in the diffusion layer. The local pH in this thesis means the pH value measured in the electrolyte 10-100 µm from the surface of the corroded sample. As opposed to bulk pH of the medium, the local pH measured in the diffusion layer reflects the pH at the Mg-medium interface. **Fig. 3.6 (a)** shows the schematic representation of the cell for the local pH measurement under hydrodynamic conditions. The probes were positioned at 50±5 µm above the sample surface. The volume of the electrolyte in the cell was 5 mL. The measurements were performed under

hydrodynamic conditions (by Medorex TL15E peristaltic pump) at a flow rate of 1.0-1.5 $mL \cdot min^{-1}$. The electrolyte in the flow-through cell was fully refreshed once every 3.3-5 min. A commercial instrument for a scanning ion-selective electrode technique (SIET, from Applicable Electronics) was used and controlled by LV4 software from Science Wares. Two types of pH-sensitive probes were employed: homemade glass-capillary ion-selective microelectrodes (tip orifice diameter was 1.8±0.2 µm) with a liquid membrane (H^+ ionophore I, cocktail B from Fluka 95293) (**Fig. 3.6 (b)**), and microelectrodes with a tip made of pH-sensitive glass from Unisense (pH-10, tip diameter was 10 micron, tip length was 50 micron) (**Fig. 3.6 (c)**). A homemade Ag/AgCl/0.1M KCl, 0.01M KH_2PO_4 reference electrode was used. Mg samples were prepared by embedding a machined rod with diameter of 2±0.2 mm in transparent epoxy resin (Buehler 20-3430064/20-3432-016). The embedded sample was ground with SiC paper up to 4000 grit.

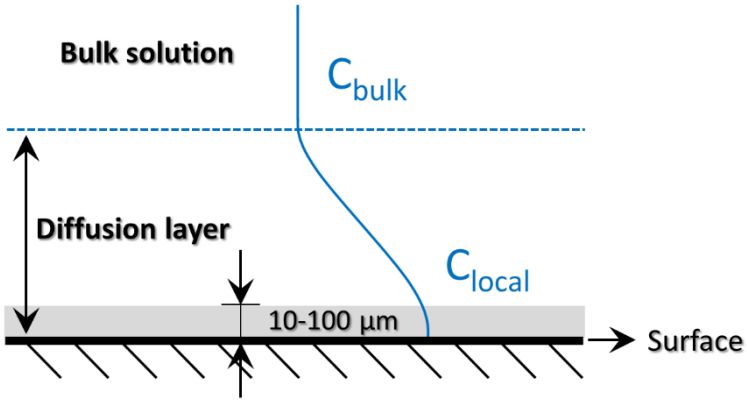

Fig. 3.5 Schematic diagram of the Nernstian diffusion layer and the measuring area of local pH.

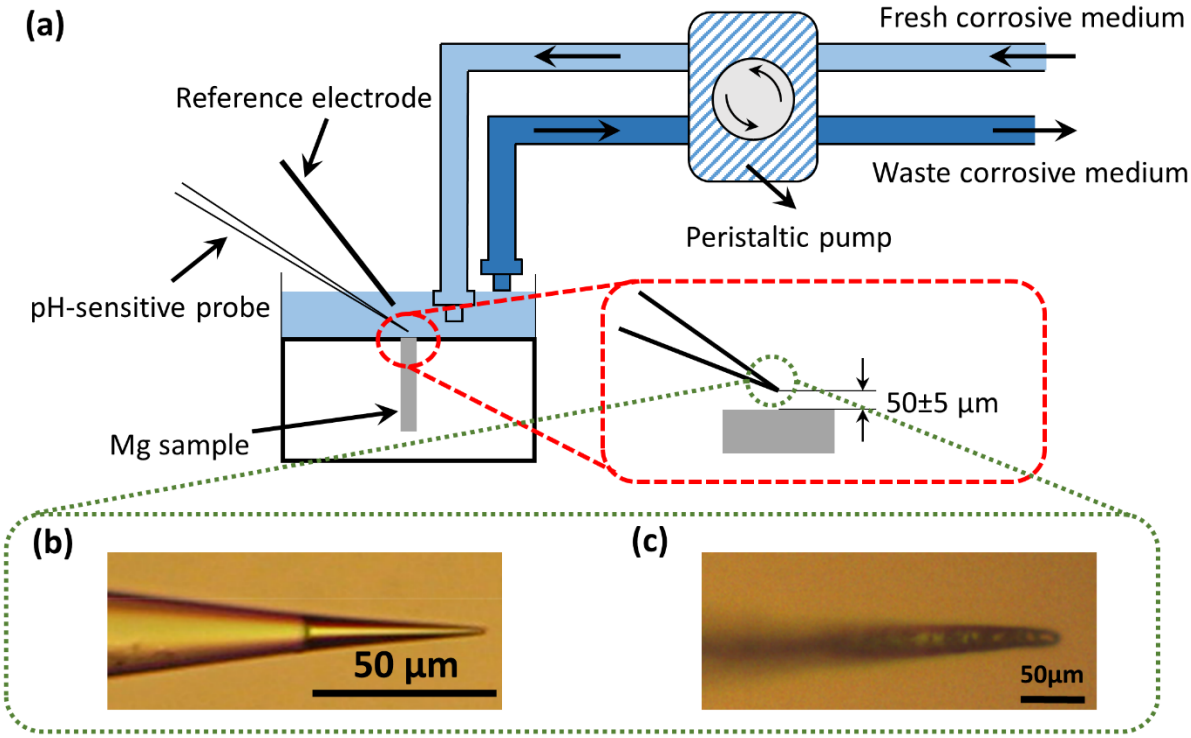

Fig. 3.6 (a) The schematic representation of the cell for the local pH measurement under hydrodynamic conditions; (b) homemade glass-capillary ion-selective microelectrodes; (c) commercial microelectrodes with a tip made of pH-sensitive glass.

In Chapter 4.2, the homemade pH microelectrode was employed. It was calibrated by using SBF, with different pH adjusted (by NaOH/HCl) over a range from 6.4 to 10.2. The local pH measurements were performed in the line scan mode. The 200-points line scans were performed during the immersion of Mg in Kokubo's SBF with or without Tris-HCl.

In Chapter 4.4, bearing in mind the addition of protein in HBSS, and their possible adsorption on the pH sensitive part of the microelectrode, commercial pH microelectrodes with higher stability of potential were employed. Prior to measurement, the microelectrode were calibrated by the buffer solutions (pH=4 and 10). Two measure modes, point measurement and line scan, were employed.

3.2.4 Immersion / weight loss

Immersion for corrosion morphology observation

To investigate corrosion products on Mg surface in different electrolytes, bulk samples were used for the immersion tests. The ratio of the electrolyte volume to the sample surface area (V/A ratio) remained similar to that of hydrogen evolution tests (around 20:1 mL·cm^{-2}). The immersion was performed under constant stirring conditions (200 rpm), which is also similar to the hydrogen evolution tests. After immersion, the corroded samples were cleaned with deionized water/ethanol and in a stream of hot dry air.

Weight loss under semi-static condition

In Chapter 4.4, in order to clarify the influence of V/A ratio on the corrosion rate of Mg, the weight loss measurements were performed.

Schematic setup of the experimental setup of weight loss measurement under semi-static condition is shown in **Fig. 3.7 (a)**. Under this condition, the medium was changed once a day. The ratios of electrolyte volume to sample surface area (V/A) were 3:1 and 10:1 mL·cm^{-2}, respectively. Before immersion, the samples were ground with SiC paper up to 1200 grit. The initial weight and surface area of the samples were recorded. After 3 days' immersion, according to the ASTM G31-12a [171], the samples were cleaned by chromic acid (200 g·L^{-1}) to remove the corrosion product, dried, and weighed. The corrosion rate was calculated by the following formula:

$$Corrosion\ rate\ (mm \cdot year^{-1}) = \frac{(M_0 - M_1)}{\rho \cdot S \cdot t} \qquad (3.1)$$

Where M_0 is the initial weight of samples in mg, M_1 denotes the final weight after immersion in mg, ρ is the density of Mg in mg·cm^{-2}, S represents the surface area of samples before test in cm^2, and t is the immersion time in day.

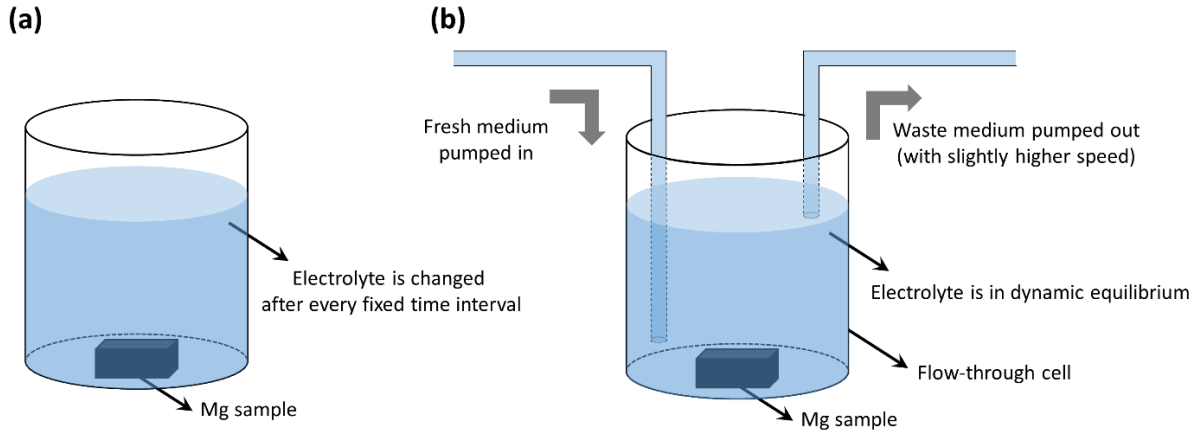

Fig. 3.7 Schematic setup of the experimental setup of immersion/weight loss (a) under semi-static condition and (b) under hydrodynamic condition.

Weight loss under hydrodynamic condition

The weight loss measurements of Mg were also performed in selected electrolytes under hydrodynamic condition for comparison about the influence of test condition on Mg corrosion rate. **Fig. 3.7 (b)** shows the schematic of the experimental setup of immersion/weight loss under hydrodynamic condition. During the immersion period, the medium was constantly renewed by a peristaltic pump at a rate of 0.5 mL·min^{-1}. The pre-/post-treatment of samples is same with that of weight loss under semi-static condition. The Mg corrosion rate was also calculated by **Eq. 3.1**.

3.3 *Ex situ* characterization methods

3.3.1 Scanning electron microscopy (SEM) and Energy dispersive X-ray (EDS)

When the high-energy electron beam bombards the sample, the sample surface emits some characteristic signals, including secondary electrons (SE), back-scattered electrons (BSE), characteristic X-rays etc. SEM is employed to observe the surface morphology of the sample by detecting SE and BSE. EDS performs the semi-quantitative analysis of the elemental composition on sample surface by identifying characteristic X-rays. **Fig. 3.8** shows an example of the SEM images for the same position in both BSE and SE mode, as well as the EDS spectrum conducted on the selected point. Secondary electrons provide information about geographical morphology of the sample surface. The intensity of the back-scattered electrons is closely related to the atomic number of elements on the sample surface. EDS spectrum shows the detected elements on the selected point.

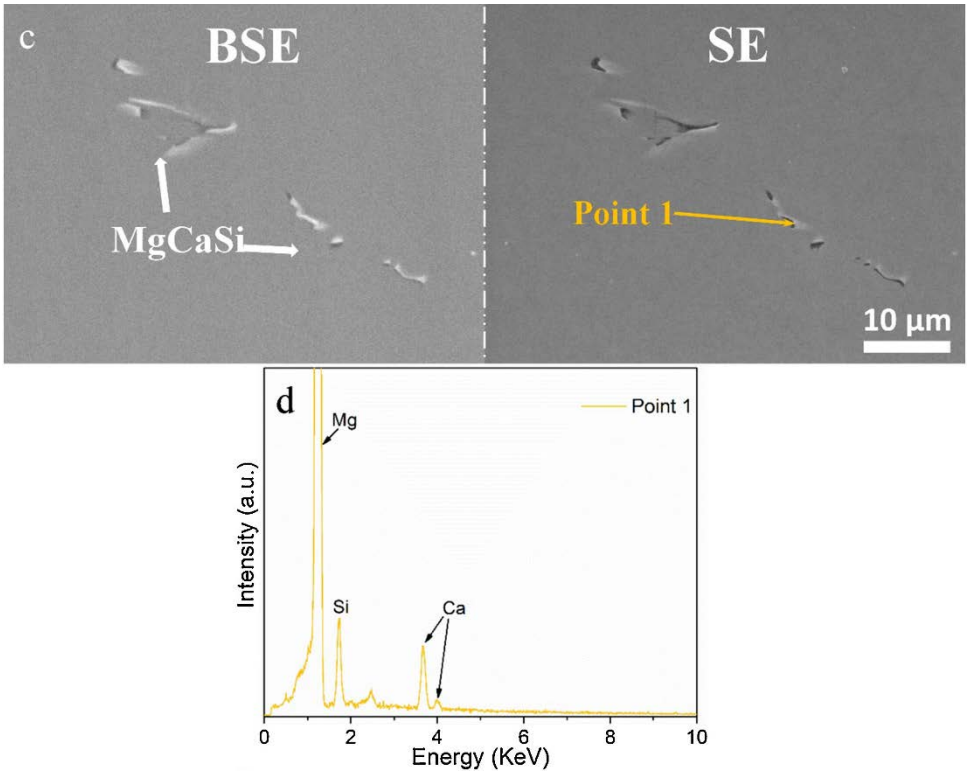

Fig. 3.8 SEM images in BSE and SE mode: Mg, Ca, Si-containing phase in Mg alloy and the EDS spectrum conducted on point 1. Reprinted from [37] with permission.

In this thesis, the corrosion morphologies of the corroded Mg in various media were observed by a scanning electron microscope (TESCAN, Vega3 SB) at accelerating voltage of 15kV. The chemical composition of corrosion products was investigated using an energy dispersive X-ray spectrometer (EDS). In order to have better resolution for SEM/EDS characterization, gold sputtering machine was employed to improve the conductivity of sample surface.

3.3.2 X-ray diffraction (XRD)

XRD is a non-destructive testing method that can be used to identify the crystallized phases by the diffraction of X-ray in crystals. **Fig. 3.9** shows an example of XRD pattern of Mg alloy after immersion in NaCl solution for 7 days. It shows that the common corrosion product of Mg in NaCl solution ($Mg(OH)_2$) was identified in the patterns. In Chapter 4.2, the corroded CP Mg samples after immersion in various electrolytes were characterized *ex situ* by X-ray diffraction to analysis the crystallographic phase in the corrosion products. A Bruker D8 Advance diffractometer was employed. The measurements were performed in the range of 2-theta angles from 10 to 80° with Cu Kα radiation (incidence angle 3°, exposure time 1 s, step 0.02°).

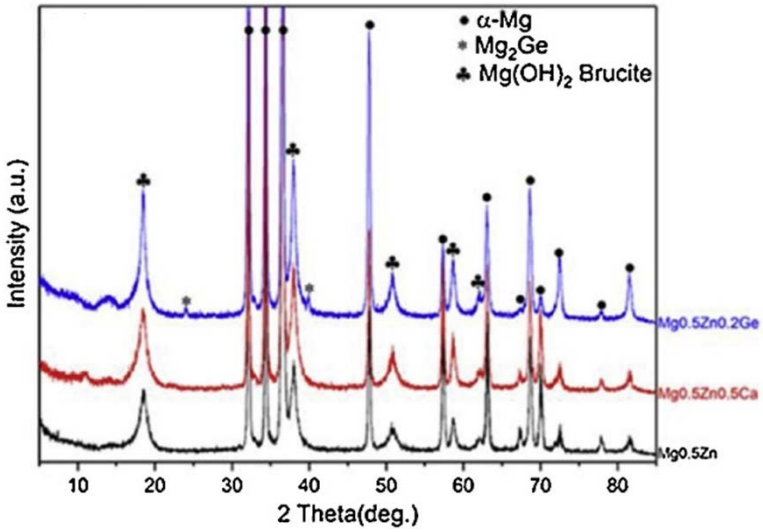

Fig. 3.9 XRD patterns for Mg0.5Zn, Mg0.5Zn0.5Ca and Mg0.5Zn0.2Ge alloys after immersion in 0.9 wt.% NaCl solutions for 7 days. Reprinted from [15] with permission.

4 Results and discussion

4.1 Overview and structure of the results

The obtained results in the frame of thesis have been separately published in scientific journal or accepted for publication. This chapter, as the results and discussion part of this thesis, consists of 3 complementary published/accepted papers. The effect of synthetic pH buffer, inorganic ions, small-molecule organic compounds and protein has been investigated. The brief introduction of these papers are provided as below and the schematic illustration of the thesis structure is shown in **Fig. 4.1**.

Paper 1: The role of individual components of simulated body fluid on the corrosion behavior of commercially pure Mg

In this paper, the influence mechanisms of inorganic ions and synthetic pH buffer on Mg corrosion in simulated body fluid are investigated by hydrogen evolution test, bulk and local pH monitoring, immersion tests, and EIS measurements. The acceleration effect of synthetic pH buffer on Mg corrosion is clarified. The synergy of Ca^{2+}, carbonate and phosphate on the protection of Mg corrosion is emphasized.

Paper 2: The effect of small-molecule bio-relevant organic components at low concentration on the corrosion of commercially pure Mg and Mg-0.8Ca alloy: An overall perspective

In this paper, the individual influence and group effect of 53 small-molecule bio-relevant organic compounds, constituting plasma/serum or cell culture medium, on Mg corrosion in NaCl solution, SBF and cell culture medium are investigated by hydrogen evolution tests. The slight influence of these tested organic compounds at low concentration on Mg corrosion is pointed out. In addition, the similarity between cell culture medium and simulated body fluid as the corrosive medium for Mg corrosion test are clarified. The precipitation of corrosion products from the medium, which is mainly controlled by the inorganic components in the medium, significantly influences the degradation behavior of Mg in pseudophysiological medium.

Paper 3: Clarifying the influence of albumin on the initial stages of magnesium corrosion in Hank's Balanced Salt Solution

In this paper, hydrogen evolution test, EIS measurement, local pH measurements and immersion/weight loss test were employed to investigate the mechanisms of protein influence on the degradation behavior of Mg in Hank's balanced salt solution by taking bovine

serum albumin (BSA) as an example. It is found that the influence of protein on Mg corrosion stems from the synergy of the three factors, namely, adsorption, Ca^{2+}/Mg^{2+} chelation, and pH buffering effects. However, the Influence of albumin on Mg corrosion is susceptible to experimental conditions.

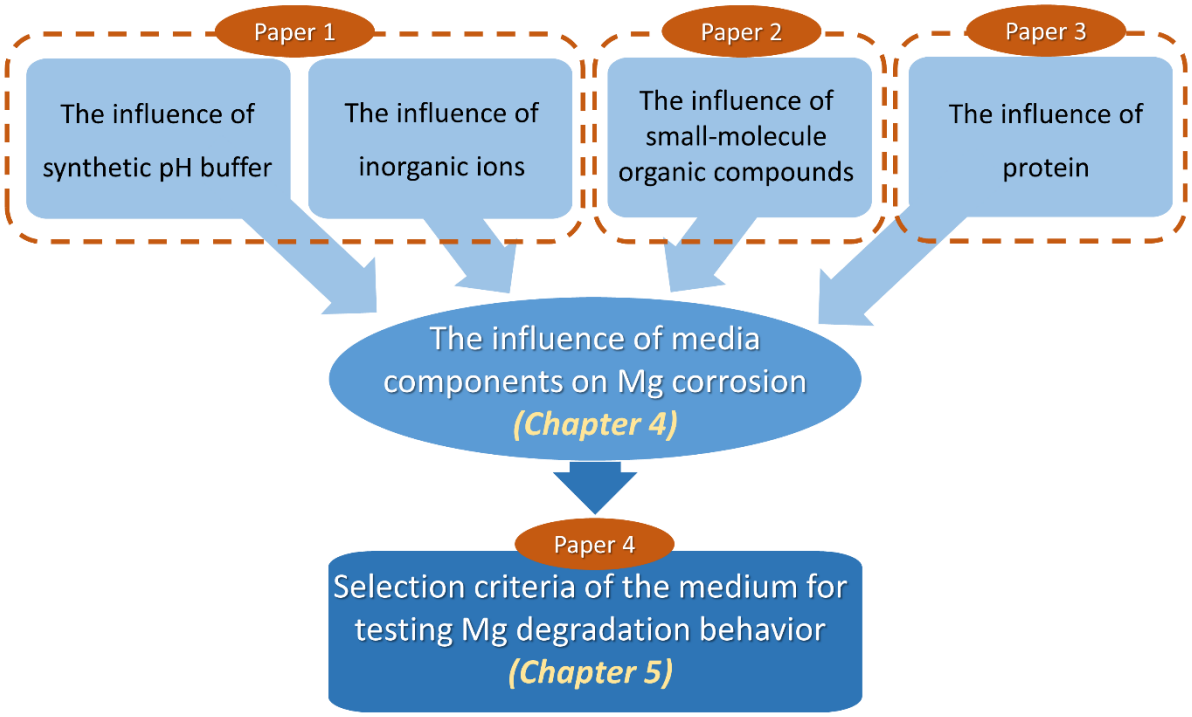

Fig. 4.1 Schematic illustration of the thesis structure

4.2 The individual influence and synergy of inorganic ions and synthetic pH buffer on Mg corrosion

The following published paper was incorporated as Chapter 4.2 (with permission from Elsevier):

D. Mei, S.V. Lamaka, J. Gonzalez, F. Feyerabend, R. Willumeit-Römer, M.L. Zheludkevich, The role of individual components of simulated body fluid on the corrosion behavior of commercially pure Mg, Corrosion Science 147 (2019) 81-93. https://doi.org/10.1016/j.corsci.2018.11.011

D. Mei conceived and designed the study based on the discussion with S.V. Lamaka. D. Mei and S.V. Lamaka carried out the experimental work. J. Gonzalez, F. Feyerabend and R. Willumeit-Römer provided suggestions on the experimental design. S.V. Lamaka and M.L. Zheludkevich gave constructive comments on data analysis. All the authors contributed to the interpretation of the results and to writing of the paper.

Corrosion Science 147 (2019) 81–93

Contents lists available at ScienceDirect

Corrosion Science

journal homepage: www.elsevier.com/locate/corsci

The role of individual components of simulated body fluid on the corrosion behavior of commercially pure Mg

Di Mei[a,*], Sviatlana V. Lamaka[a], Jorge Gonzalez[b], Frank Feyerabend[b], Regine Willumeit-Römer[b,c], Mikhail L. Zheludkevich[a,c]

[a] Magnesium Innovation Centre – MagIC, Institute of Materials Research, Helmholtz-Zentrum Geesthacht, Geesthacht, 21502, Germany
[b] Division Metallic Biomaterials, Institute of Materials Research, Helmholtz-Zentrum Geesthacht, Geesthacht, 21502, Germany
[c] Institute for Materials Science, Faculty of Engineering, Kiel University, Kiel, 24103, Germany

ARTICLE INFO

Keywords:
Magnesium
Corrosion
Degradation
Biodegradable
Simulated body fluid
Tris (tris (hydroxymethy) aminomethane)

ABSTRACT

Simulated body fluid (SBF) is a common medium for *in vitro* corrosion analysis. The individual influence and synergy of the SBF components on the corrosion of commercially pure Mg are investigated in this study. The results demonstrate that corrosion acceleration in presence of the synthetic pH buffer, Tris/HCl, is attributed to the combined effect of three factors: increased Cl^- concentration, complexation of Mg^{2+} and Ca^{2+} and consumption of OH^- needed for products formation. In Tris/HCl-free SBF, the synergy between Ca^{2+}, Mg^{2+}, HPO_4^{2-} and HCO_3^- assures slowest Mg degradation due to growth of partially protective layer that becomes thicker with time.

1. Introduction

Magnesium and its alloys have become one of the most promising biodegradable implant materials in recent years because of its good biocompatibility, low density and good mechanical properties [1–3]. One of the most important properties for a potentially biodegradable implant material is a tailored corrosion that matches the healing rate of damaged bone. However, the corrosion resistance of magnesium is often not sufficient, limiting its application [4,5]. In recent years, efforts have been made to develop new alloys [6–10], surface modifications [11–15] or deformation processes [16,17] to improve the corrosion resistance of magnesium. Meanwhile, to predict the corrosion performance of magnesium during its service period, a variety of techniques have been used [5,18,19], such as electrochemical impedance spectroscopy (EIS), potentiodynamic polarization, immersion tests and hydrogen evolution tests. Obviously, the corrosion performance of magnesium *in vivo* cannot be fully reflected by these *in vitro* corrosion tests. However, compared with *in vitro* corrosion tests, *in vivo* animal trials have certain limitations: 1) lacking resolution of analysis methods (e.g. μCT, MRT); 2) missing implantable sensors to be placed at the implantation site; and 3) ethical concerns for animal models to be used for screening purposes. Thus, at preliminary screening/selection stages, the applicability of *in vitro* corrosion tests is justified.

Currently, a number of different electrolytes are used as test media for *in vitro* corrosion tests for biomedical applications [20,21], such as Ringer and Hank's solutions [22–24], simulated body fluid (SBF) [25–27], cell culture medium (modified Eagle media like MEM, DMEM, α-MEM) [23,28,29] and others. Yamamoto [30] et al. compared the corrosion property of pure Mg in different media and found that the corrosion rate of pure magnesium largely depended on the composition of electrolytes. Some scientists aim to find or develop a more reasonable corrosive medium for *in vitro* testing, such as MEM/DMEM with the addition of fetal bovine serum (FBS) or fetal calf serum (FCS) [23,31], which contains not only inorganic ions but also a number of organic compounds and proteins. There is no doubt that these complex solutions are closer to the composition of actual body fluid. Yet, there are still some limitations in using these media for *in vitro* corrosion tests, particularly when they are used in longer-term tests or in an open environment (such as the influence of bacterial multiplication and insufficient CO_2 level). Therefore, some saline solutions, such as SBFs and especially Tris (tris (hydroxymethyl) aminomethane)/HCl buffered SBF, are still frequently used for *in vitro* corrosion tests [26,32–36], as they contain all the inorganic components found in body fluids and do not need elaborate physiological setups.

Kokubo [37] et al. presented Tris/HCl-buffered SBF. Initially, this type of SBF was developed for the *in vitro* assessment of the bone bioactivity of materials rather than for corrosion tests [37–40], however, also in this area the use of this solution is highly disputed [41].

* Corresponding author.
E-mail address: Di.Mei@hzg.de (D. Mei).

https://doi.org/10.1016/j.corsci.2018.11.011
Received 28 June 2018; Received in revised form 2 November 2018; Accepted 12 November 2018
Available online 20 November 2018
0010-938X/

Tris/HCl-buffered SBF contains Na^+, K^+, Mg^{2+}, Ca^{2+}, Cl^-, SO_4^{2-}, HCO_3^-, HPO_4^{2-} and Tris/HCl buffer. The latter is a common synthetic pH buffer (buffer range: 7.0–9.0) that covers the physiological pH range. However, it might not be suitable for use in magnesium corrosion tests [42,43]. Ott [44] et al. suggested that Tris/HCl buffer prevents the formation of a protective product layer on the surface of magnesium. In our previous work, we also found that Tris/HCl buffer significantly accelerated the corrosion rates of several magnesium alloys in a 0.5 wt. % NaCl solution [45]. Additionally, another buffer, HEPES, which is often used in corrosion tests, was also found to have an acceleration effect on the corrosion of magnesium [46–50]. Therefore, it is necessary to clarify the other roles that a pH buffer may have aside from buffering in corrosion test media.

As for the inorganic ions in SBF, the influence of Cl^-, SO_4^{2-}, HCO_3^- and HPO_4^{2-} on the corrosion behavior of magnesium has been investigated for a long time [51–55]. However, these results could not thoroughly explain the role of these ions in the corrosion process. The main weakness is that in most previous studies, the influence of the ions on the corrosion was tested individually in a simple saline solution (such as NaCl). Thus, the synergy of the different ions was not fully described. Moreover, the role of cations, especially Ca^{2+}, are still not understood. Ning [56] et al. and Grabowski [57,58] et al. observed the influence of cations but the synergy between cations and anions were not fully described. Agha [59] et al. considered the synergy of Ca^{2+}, $PO_4^{3-}$and HCO_3^- on the corrosion of pure magnesium in a complex saline solution as Ca^{2+}, PO_4^{3-} and HCO_3^- influence the formation of precipitate on the surface of magnesium. However, this study was performed under cell culture conditions and was operated in a limited volume of solution. It is possible that the consumption of these ions in the solution and rapid pH increase influenced the experimental results. In recent work from our group, local pH over the degrading Mg alloys was found to remain at around 8.0 if Ca^{2+} was present in HBSS. In contrast, if HBSS did not contain any Ca^{2+}, the local pH rapidly increased to 10.0–10.5. It has also been found that presence of Ca^{2+} in testing electrolyte decreases the corrosion rate of four different Mg alloys [50]. However, that study mainly focused on the local pH of the electrolyte near the degrading Mg.

In this work, several different electrolytes were designed in a way to elucidate the individual influence of each of the components on the degradation rate of pure Mg. Hydrogen evolution and immersion tests, monitoring of the local and bulk pH values and electrochemical impedance spectroscopy were used to investigate the influence of each of inorganic ions, Tris/HCl buffer and their combinations on the corrosion of pure magnesium.

2. Experimental

Commercially pure Mg (CP Mg) was used in this study. The elemental composition of this material was tested by spark discharge optical emission spectroscopy (SPECTROLAB with Spark Analyser Vision software) and the results are shown in Table 1. Small metallic chips with a large surface area (47.7 ± 5.0 cm^2/g) were produced by a milling machine and used for the hydrogen evolution experiments. Bulk samples with a size of 13 × 13 x 4 mm were used in the immersion tests and impedance measurements. Before the tests, the bulk samples were ground with SiC paper up to 1200 grit, cleaned with ethanol and dried in a stream of pressurized cold air.

Hydrogen evolution tests were performed by using eudiometers (Art. Nr. 2591-10-500 from Neubert-Glas, Germany; as described in ref [45]), for 22–24 h. Metallic chips (0.5 g) were placed in a bottle containing 500 ml of electrolyte. The electrolyte was constantly agitated by a magnetic stirrer but not refreshed during the test period. Given the eudiometer configuration, neither additional air nor CO_2 could enter the testing media after the measurements have started. The components of the different electrolytes are listed in Table 2. The bulk pH evolution of the electrolytes was monitored via a pH meter (Metrohm-691, Switzerland) during the selected tests. All experiments were repeated at least three times. The average and standard deviation of the parallel tests are shown in the figures (Figs. 1, 2, 5, 7, 8 and 9).

Local pH measurements were performed under hydrodynamic conditions with a commercial Scanning Vibrating Electrode Technique (SVET)/ Scanning Ion-selective Electrode Technique (SIET)/ Difference Viewer Imaging Technique (DVIT) system from Applicable Electronics, which was controlled by LV4 software from Science Wares. CP Mg, shaped as an approximately 2 mm diameter rod, was embedded in epoxy mount and fixed in a sample holder, embedded CP Mg constituted a part of a home-made flow-through cell (5 ml) with an electrolyte-pumping speed of 1.5 mL·min^{-1}. The local pH over Mg samples was measured using a glass-capillary microelectrode with a tip orifice diameter of 1.8 ± 0.2 μm. Glass-capillaries were back-filled with an inner reference solution (0.01 M KH_2PO_4 + 0.1 M KCl) and tip-filled with a H^+-selective membrane cocktail based on tridodecylamine (Fluka, Ref. 95293). A homemade Ag/AgCl/0.1 M KCl, 0.01 M KH_2PO_4 electrode was used as the external reference electrode. The microelectrodes were calibrated using three different SBF electrolytes, with the pH adjusted over a range from 6.4 to 10.2. A point by point, move - wait (0.6 s) - measure (0.8 s) scheme took approximately 20 min to complete a 200-points line scan. More details of the experimental setup can be found elsewhere [50,60].

To investigate corrosion products on magnesium in different electrolytes, plate-like samples with a surface area of 4.7 ± 0.1 cm^2/g were used in the immersion tests. The ratio of the sample surface area to the electrolyte volume remained unchanged during the immersion tests. The morphologies of the degraded surface of the samples were observed by scanning electron microscopy (TESCAN, Vega3 SB) and the chemical composition was investigated using an energy dispersive X-ray spectrometer (EDS).

Crystallographic analysis of the corrosion products on the surface was performed *ex situ* using a Bruker D8 Advance diffractometer. The measurements were carried out with Cu Kα radiation in the range of 2-theta angles from 10 to 80° (incidence angle 3°, exposure time 1 s, step 0.02°).

For the EIS measurements, a conventional three-electrode setup was used consisting of a working electrode (with an exposure area of 0.5 cm^2, in electrolyte volume of 330 ml), counter electrode (a platinum wire coil) and reference electrode (saturated Ag/AgCl). EIS measurements were performed at OCP with respect to amplitude of 10 mV RMS sinusoidal perturbation over a frequency range from 100 kHz to 0.1 Hz. EIS was not measured at lower frequencies to avoid sample polarization and make sure that the fast scans can be taken to assess evolution of the system during the initial minutes of exposure to the electrolytes. Room temperature measurements at constant steering were performed using a Gamry Reference 600 potentiostat/galvanostat.

Table 1
The elemental composition of commercial pure Mg (CP Mg).

Element	Fe	Cu	Ni	Al	Mn	Ce	Zn	Si	Zr	Mg
Content/ wt. %	0.0342	0.00037	< 0.00020	0.00402	0.00237	0.00070	0.00046	< 0.00010	< 0.00050	Bal.

Table 2
The chemical composition of electrolytes in this study.

No.	Electrolytes	Initial pH value	Ion concentration (mM)								
			Na^+	K^+	Mg^{2+}	Cl^-(inorganic salt and buffer)	Ca^{2+}	HCO_3^-	HPO_4^{2-}	SO_4^{2-}	Tris
1	SBF	7.35	142.0	5.0	1.5	186.8	2.5	4.2	1.0	0.5	50.5
2	SBF (Ca^{2+}, HCO_3^-, HPO_4^{2-}, SO_4^{2-}/ no Tris/HCl)	~ 7.45(No. 1-4)	142.0	5.0	1.5	147.8	2.5	4.2	1.0	0.5	–
3	SBF (no Tris, adjust pH by NaOH)		> 142.0	5.0	1.5	186.8	2.5	4.2	1.0	0.5	–
4	SBF (Cl^- concentration the same as in No. 2)		102.8	5.0	1.5	147.8	2.5	4.2	1.0	0.5	50.5
5	SBF (buffering capacity was depleted by adding NaOH)	9.5 (No. 5, 6)	> 142.0	5.0	1.5	186.8	2.5	4.2	1.0	0.5	50.5
6	SBF (no Tris/HCl, adjust pH by NaOH)		> 142.0	5.0	1.5	186.8	2.5	4.2	1.0	0.5	50.5
7	SBF (HCO_3^-, HPO_4^{2-}, SO_4^{2-}/ no Tris/HCl, no $CaCl_2$)	7.35 ~	142.0	5.0	1.5	142.8	–	4.2	1.0	0.5	–
8	SBF (Ca^{2+}, HCO_3^-, HPO_4^{2-}/ no Tris/HCl, no $NaSO_4$)	7.45 (No. 7-12)	141.0	5.0	1.5	147.8	2.5	4.2	1.0	–	–
9	SBF (Ca^{2+}, HPO_4^{2-}, SO_4^{2-}/ no Tris/HCl, no $NaHCO_3$)		142.0	3.0	1.5	147.8	2.5	–	1.0	0.5	–
10	SBF (Ca^{2+}, HCO_3^-, SO_4^{2-}/ no Tris/HCl, no K_2HPO_4)		137.8	5.0	1.5	147.8	2.5	4.2	–	0.5	–
11	SBF (HPO_4^{2-}, SO_4^{2-}/ no Tris/HCl, no $CaCl_2$, no $NaHCO_3$)		137.8	5.0	1.5	142.8	–	–	1.0	0.5	–
12	SBF (HCO_3^-, SO_4^{2-}/ no Tris/HCl, no $CaCl_2$, no K_2HPO_4)		142.0	3.0	1.5	142.8	–	4.2	–	0.5	–

3. Results and discussion

3.1. Influence of Tris/HCl buffer on the corrosion of CP Mg

The curves of the hydrogen evolution tests in electrolytes No.1–7 are shown in Fig. 1. These seven electrolytes were divided into two groups, with (No. 1, 4 and 5) or without Tris/HCl buffer (No. 2, 3, 6 and 7). When the Tris/HCl buffer was removed from SBF, the corrosion rate decreased significantly (curves of No.1 and 2 in Fig. 1). Thus, the presence of the Tris/HCl buffer accelerated the corrosion of magnesium in this complex saline electrolyte. The detrimental effect of Tris on magnesium corrosion in simple saline electrolyte has been shown before [42–44]. However, the reason of acceleration of the degradation rate was still not thoroughly investigated.

The addition of Tris/HCl led to an increase of Cl^- concentration by 39 mM beyond that of Cl^- introduced as chloride of inorganic salts. This factor might also influence the corrosion behavior [51]. From the curves of No. 1 and 3 in Fig. 1, it was apparent that when the Tris was removed, the corrosion behaviors were completely different even though the concentration of Cl^- was the same. From curves No. 1 and 4 in Fig. 1, the decrease in the Cl^- concentration (by partial removal of NaCl) retarded the corrosion rate in the Tris/HCl buffered electrolyte, but the effect was not significant. From curves No. 2 and 3 in Fig. 1, it is observed that without Tris/HCl buffer, the hydrogen evolution rates were similar even though the concentration of Cl^- differed by 39 mM. All of the results above suggest that the concentration variation of Cl^- from 147.8 mM to 186.8 mM affects the corrosion rate of Mg, but the effect is rather limited.

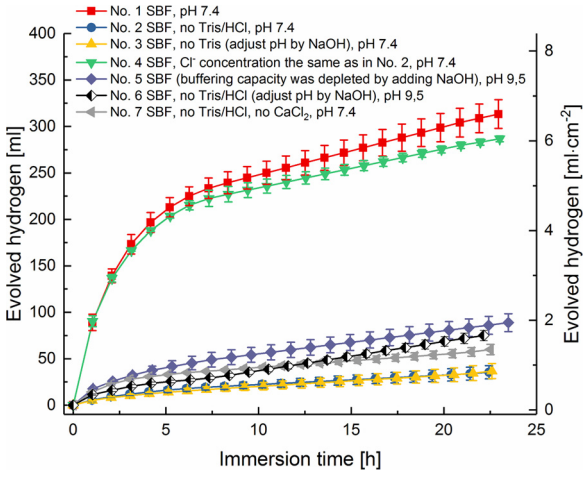

Fig. 1. Hydrogen evolution tests of CP Mg in electrolytes No. 1-7. (The legend shows the difference between different electrolytes.)

Tris is a strong chelating agent [61]. The complexing reaction between Tris and cations should also be taken into account. Ott [44] et al. presented the idea that the strong interaction between Tris and dissolved cations or corrosion products leads to activation of the alloy surface. It has been reported that Tris forms weak complexes with Mg^{2+} ($lg\beta_1 = 0.30$) and Ca^{2+} ($lg\beta_1 = 0.25$) and relatively strong complexes with Fe^{3+} ($lg\beta_1 = 8.59$) [61]. In our previous work, the complexing agents that formed strong Lig-$Fe^{II/III}$ complexes were found to have an inhibiting effect on the corrosion rate of magnesium [45,62,63]. On the other hand, the complexing agents that formed strong Lig-Mg^{II} complexes accelerate the dissolution of magnesium. As shown in and Fig. 1, Tris does not possess any inhibiting effect on the corrosion of magnesium likely due to its pH buffering capacity that plays an adverse role here. The pH values of the electrolytes were maintained over the range of 7.0–9.0 for a long time, and this pH condition influenced the formation of a partially protective corrosion product layer. Furthermore, the light complexation between Ca^{2+} and Tris influenced the concentration of Ca^{2+} in the electrolyte and, consecutively, the formation of a corrosion products layer. To confirm this assumption, another electrolyte, No. 5, was designed in which the buffering capacity of Tris/HCl was depleted by an excessive amount of NaOH. The titration was stopped after the abrupt increase of the pH to 9.5. In this electrolyte, the pH buffering effect was "switched off" so that pure Me^{n+} complexation effect could be observed. In order to exclude the influence of high initial pH on the corrosion behavior, No. 6 electrolyte with an initial pH value of 9.5 but without Tris/HCl was designed for comparison. Comparing the curves of No.1, 2, 5 and 6, it is clear that Tris still accelerates the corrosion of magnesium even in the absence of the OH^- collecting ability. Considered the light complexation of Tris with Mg^{2+} and Ca^{2+}, the influence of the lack of Ca^{2+} in Tris-containing SBFs and the accelerated dissolution of Mg via complexation, becomes apparent. The corrosion rate of CP Mg in electrolyte No. 5 was slightly higher than in electrolyte No. 6 and 7, which supports the conclusion regarding the influence of the complexation between Tris and Ca^{2+} or

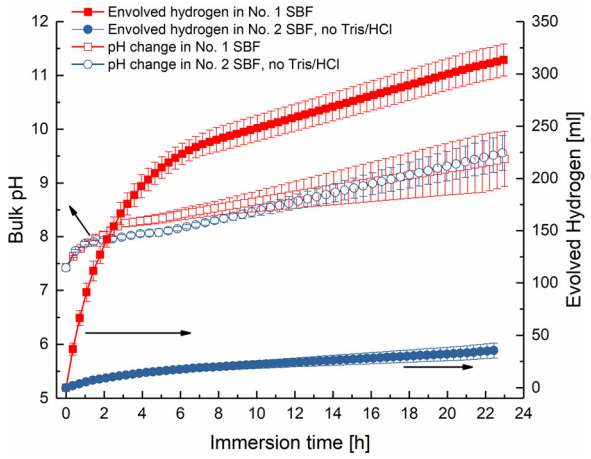

Fig. 2. Bulk pH change and hydrogen evolution curves of CP Mg in SBF (No. 1) and SBF without Tris/HCl (No. 2).

Mg^{2+} on the faster corrosion rates.

Therefore, the influence of Tris/HCl buffer on the corrosion behavior of magnesium is constituted by three aspects: 1) an increase of Cl^- due to the addition of HCl as a component of Tris/HCl; 2) a pH buffering capacity that allows Tris to consume generated OH^- (that otherwise could be used for formation of the partially protective layer); and 3) complexation between Tris and Ca^{2+} or Mg^{2+}. All three lead to accelerated degradation of Mg in presence of Tris/HCl.

Fig. 2 shows the bulk pH change and hydrogen evolution curves of CP Mg in electrolytes No. 1 and 2. During the immersion period, the differences in the evolved hydrogen in two electrolytes are obvious. Mg degraded 10 times faster in the Tris containing SBF electrolyte. However, the change in the bulk pH in electrolytes No. 1 and 2 was similar and the changes were gradual which means that the pH of electrolyte No. 2 was maintained at a relatively stable state even though there was no Tris/HCl in the electrolyte. Moreover, as shown in Fig. 3, the synthetic pH buffer was not able to maintain a stable pH near the surface of degrading Mg, in the Nernstian diffusion layer. The local pH, measured at 50 µm from the surface of degrading Mg, was above 9.0 in Tris containing SBF. The local pH values, fluctuating at approximately 9.0 ± 0.3, were not stable due to the active formation of H_2 bubbles. The local pH value even exceeded 10.5 in several active spots. In SBF electrolyte without Tris (No. 2), the pH (9.0 ± 0.3) recorded during the first few minutes stabilized at approximately 8.3 ± 0.3 after 30 min of exposure and remained at this pH for the next 3 h. We believe that in electrolyte No. 2, the pH was maintained at approximately 8.3 due to the formation of partially protective corrosion products. The partially protective layer that formed on the surface in a low pH environment inhibited the subsequent corrosion. This layer is also visible in the optical micrographs presented in Fig. 3. The bright appearance of the surface in Fig. 3(**a**) is indicative of the absence of the main corrosion products, while the pale white appearance of the surface in Fig. 3(**b**), that is visible even at 10 min of exposure demonstrates the formation of corrosion products. With the immersion time, corrosion products were also formed on Mg exposed to electrolyte No. 1. Fig. 4 shows the typical corrosion morphology after 24 h of immersion in electrolytes No. 1 and 2. The presence of Tris/HCl led to a thicker and looser corrosion product layer.

In summary, the detrimental, corrosion acceleration effect of Tris was demonstrated. In the following experiments, Tris/HCl buffer was removed from the electrolytes. The concentration changes of Cl^- influenced the corrosion rate of magnesium in Tris/HCl buffered SBF, but the change was not significant. Compared with normal SBF, the corrosion rate of CP Mg was 10 times lower in the Tris-free electrolyte, which is attributed to the formation of a partially protective layer. Therefore, the formation of the protective product layer and the individual effects or the synergy of the ions on the formation of the layer is the focus in the subsequent parts of this study.

3.2. Individual influence and synergy of ions in SBF without Tris/HCl buffer on the corrosion of CP Mg

There are eight ions in SBF, namely Na^+, K^+, Mg^{2+}, Ca^{2+}, Cl^-, SO_4^{2-}, HCO_3^- and HPO_4^{2-}. According to our previous work, SO_4^{2-}, HCO_3^- and HPO_4^{2-} have an inhibitory effect on the corrosion of pure Mg in NaCl solution [45], and Ca^{2+} significantly slowed down the corrosion rate in more complex saline solution [50]. Therefore, they were selected as our study objects to investigate the individual effects of these ions on the corrosion behavior of CP Mg in SBF without Tris/HCl buffer. Electrolyte No. 2, which contained all of the ions, was selected as the reference. Fig. 5 shows the curves of the hydrogen evolution tests in electrolytes No. 2 and No. 7-10. The legends of the Fig. 5 indicates which ions are included in the electrolyte (except for Na^+, K^+, Mg^{2+} and Cl^-, which had no influence on the corrosion rate within the studied concentration variations). From the hydrogen evolution tests, HCO_3^- and HPO_4^{2-} were found to have an obvious effect on the corrosion behavior of CP Mg, as well as Ca^{2+}. On the other hand, SO_4^{2-} had no significant influence on corrosion in this complex electrolyte. In the electrolyte without Ca^{2+} (No. 7), the corrosion rate after approximately

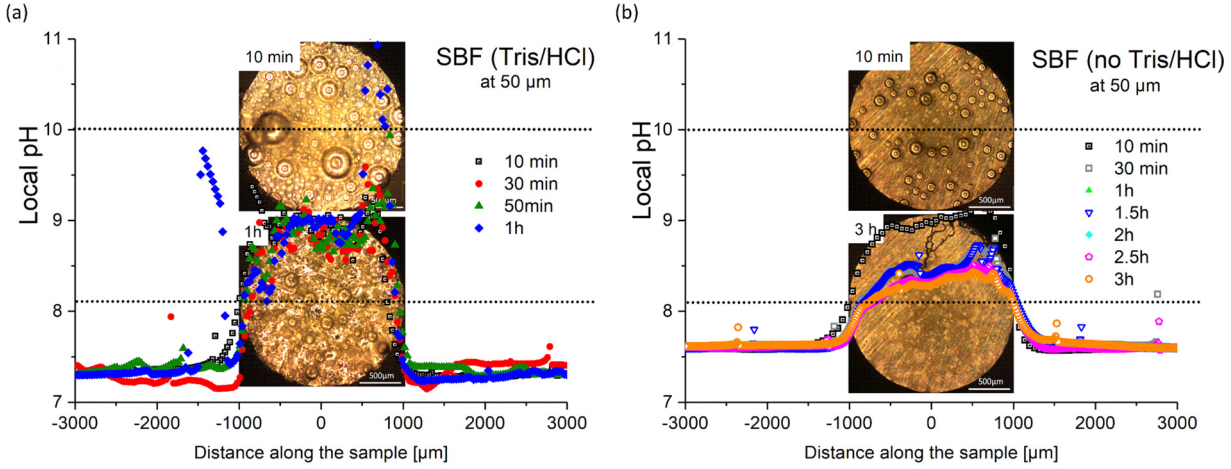

Fig. 3. Local pH measurements 50 µm from the surface of CP Mg immersed in either (a) SBF (No. 1) or (b) SBF without Tris/HCl (No. 2). Performed under hydrodynamic conditions, flow rate 1.5 ml/min. Optical micrographs show the visual appearance of the sample before and after the test. Round features are the bubbles of evolved H_2. Dotted line shows the exact location of the line scan pH measurement.

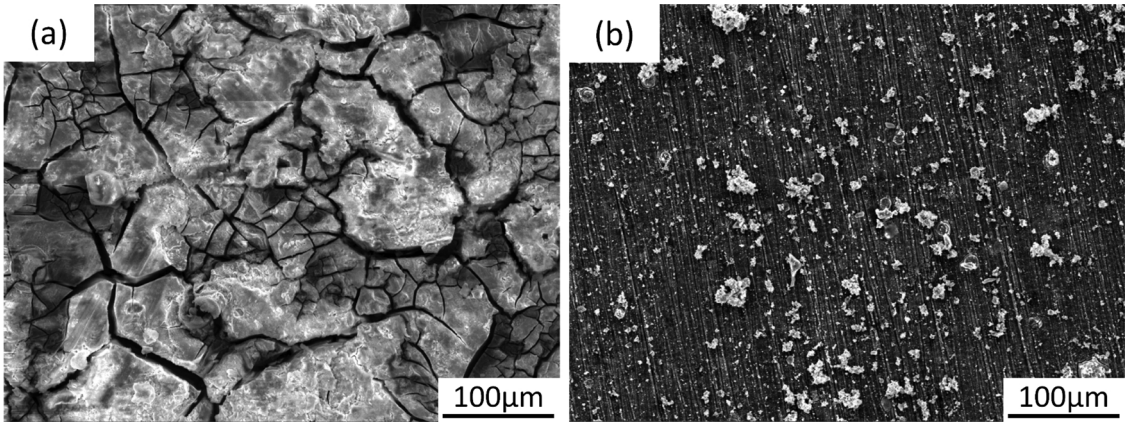

Fig. 4. Typical corrosion morphology after 24 h immersion in (a) SBF (No. 1) or (b) SBF without Tris/HCl (No. 2).

4 h of immersion was similar to the corrosion rate of No. 2, even though the initial corrosion rates were obviously different. These results indicates that a partially protective layer was formed on the surface of magnesium during or after the initial 4 h of immersion in electrolyte No. 7. As shown in the inset in Fig. 5, the differences in the corrosion behavior in different electrolytes appeared at the beginning of the tests. In the electrolyte containing Ca^{2+} and HPO_4^{2-} (No. 8 and 9), the corrosion rate was slow at the beginning (0–1 h). However, in the electrolyte without HCO_3^- (No. 9), the corrosion rate became faster after 1 h of immersion.

The formation of a partially protective layer is the key to magnesium protection in these complex electrolytes. To predict the type and formation order of the corrosion products on the surface of magnesium during the immersion period, Hydra-Medusa software [64], which uses thermodynamic stability constants, was used to simulate the precipitate formation in the different electrolytes. The ion concentrations of the different electrolytes provided in Table 2 were set as equilibrium concentration. The initial concentration of Mg^{2+} in the electrolytes was 1.5 mM, however the concentration of Mg^{2+} obviously increased as magnesium corroded. Thus, the concentration of Mg^{2+} was calculated based on the final hydrogen volume and used in the simulation. These concentrations might be considered overestimated at first glance due to Mg^{2+} consumption for the formation of corrosion products. On the other hand, the momentary local concentration of Mg^{2+}, actually participating in local equilibria (including precipitation of corrosion products) can be several times higher than the bulk one [65,66]. A fraction of the Ca^{2+} and Mg^{2+} species as a function of pH simulated by Hydra-Medusa in electrolytes No. 2, 7, 9 and 10 are shown in Fig. 6. It is found that phosphate ions reacted with Ca^{2+} preferentially and that $Ca_5(PO_4)_3OH$ (hydroxyapatite) could be formed under neutral pH conditions in electrolytes containing Ca^{2+} and HPO_4^{2-}. However, the amount of hydroxyapatite was limited due to the limited amount of HPO_4^{2-} in SBF electrolytes. The hydroxyapatite coating, mimicking this, has been reported for corrosion protection of magnesium [67–69]. In the electrolyte without HCO_3^- (No. 9), carbonate could not be formed and the presence of Ca^{2+} limited the reaction between HPO_4^{2-} and Mg^{2+}. Obviously, without either Ca^{2+} or HPO_4^{2-} (No. 7 and No. 10), hydroxyapatite was not predicted.

The predictions of possible precipitate in different electrolytes at pH from 8.0 to 11.0 are listed in Table 3. The absence of SO_4^{2-} made no difference on the possible precipitate, which was why SO_4^{2-} has no apparent influence on the corrosion of CP Mg. It is important to note

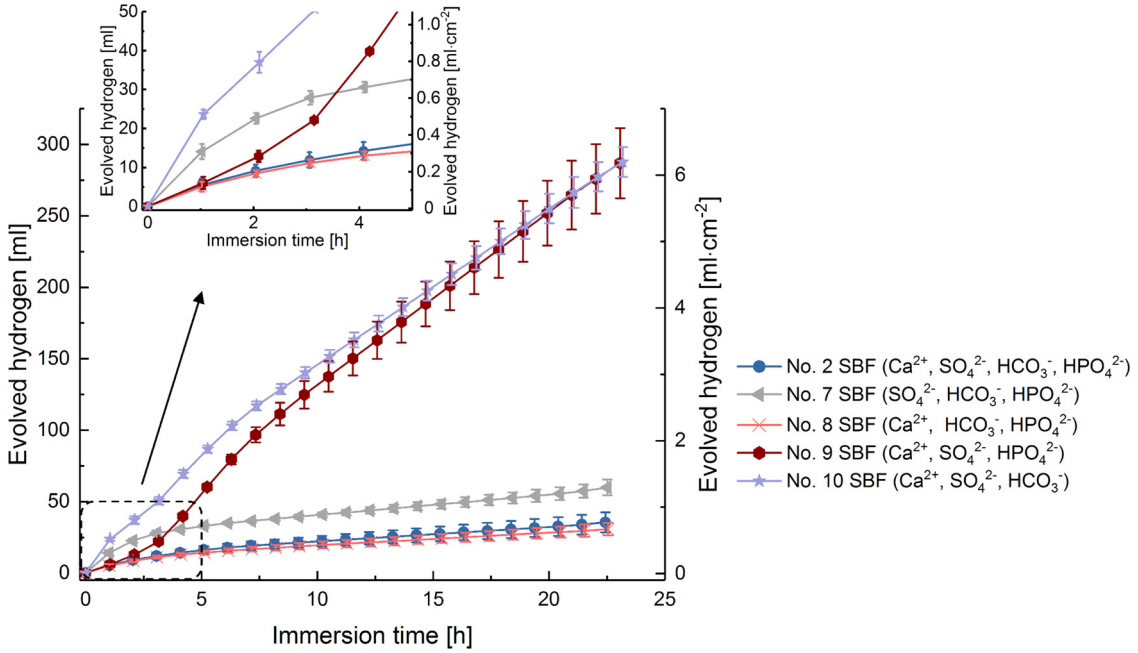

Fig. 5. Hydrogen evolution tests of CP Mg in electrolytes No. 2 and No. 7-10. (The legend shows relevant ions present in each electrolyte.)

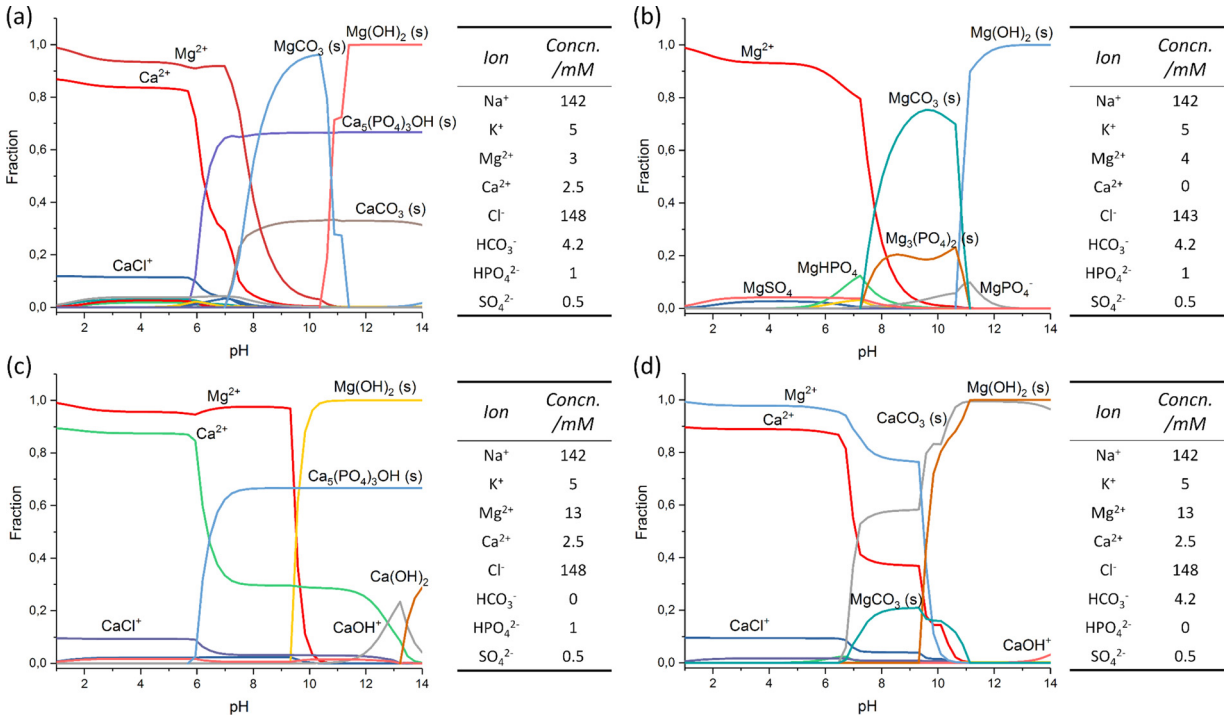

Fig. 6. Fraction of either Ca^{2+} or Mg^{2+} species as a function of pH based on thermodynamic stability constants, at 25 °C and simulated by Hydra-Medusa in (a) No. 2 SBF (Ca^{2+}, HCO_3^-, HPO_4^{2-}, SO_4^{2-}), (b) No. 7 SBF (HCO_3^-, HPO_4^{2-}, SO_4^{2-}), (c) No. 9 SBF (Ca^{2+}, HPO_4^{2-}, SO_4^{2-}), (d) No. 10 SBF (Ca^{2+}, HCO_3^-, SO_4^{2-}). ($CaMg(CO_3)_2$ (cr) in prediction results is already separated into $CaCO_3$ and $MgCO_3$. The concentration of ions that were used in simulation are listed in tables.).

Table 3
The predictions of possible precipitate in electrolyte No. 7-12 at pH 8.0–11.0 by Hydra-Medusa. ($CaMg(CO_3)_2$ (cr) in prediction results is already separated into $CaCO_3$ and $MgCO_3$.).

No.	Prediction of corrosion products				
	$Ca_5(PO_4)_3OH$	$CaCO_3$	$MgCO_3$	$Mg_3(PO_4)_2$	$Mg(OH)_2$
2	×	×	×		×
7			×	×	×
8	×	×	×		×
9	×				×
10		×	×		×
11				×	×
12			×		×

that Hydra-Medusa's predictions are somewhat limited. The formation of even more complex species, such as $Mg_3Ca_3(PO_4)_4$, $Ca_2Mg_7(PO_4)_6$, $Na_2CaMg_7(PO_4)_6$ and $Ca_{9.74}(PO_4)_6(OH)_{2.08}$, has been reported in literature, but stability constants or solubility products for these species are not known, and hence, these values cannot be added to Medusa to generate a more precise simulation. Moreover, the thermodynamic stability constants used by the Medusa software predict the existence of certain species, but do not have the power to predict the kinetics (when precipitation occurs) and how much of each component precipitates at a specific point in time. Therefore, the predictions generated in Hydra-Medusa only provide general ideas to explain the observed experimental phenomena.

Additional pH monitoring is beneficial for the investigation. Fig. 7 shows the bulk pH change and hydrogen evolution curves of CP Mg in electrolytes No. 2 and 7. Similar to electrolyte No. 2, the corrosion rate of CP Mg in electrolyte No. 7 was significantly lower than that in SBF (as shown in Fig. 1), although the pH changes in No. 2 and 7 were completely different. Combined with the prediction and pH monitoring, the absence of Ca^{2+} in electrolyte No. 2 enabled formation of only Mg-containing corrosion products. The absence of hydroxyapatite led to a

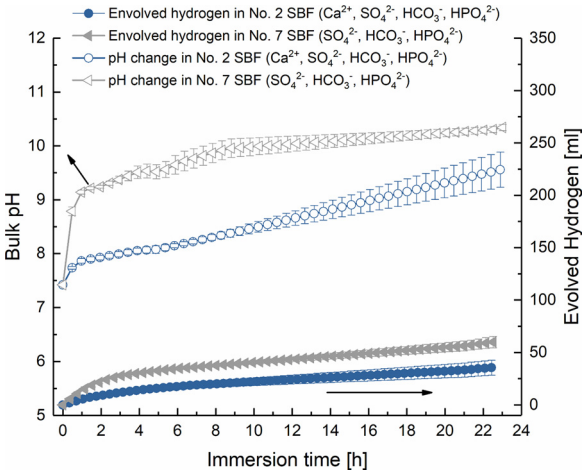

Fig. 7. Bulk pH change and hydrogen evolution curves of CP Mg in No. 2 and 7 electrolytes.
(The legend shows relevant ions present in each electrolyte.)

fast rise of pH at the beginning of the experiment. However, the corrosion rate became slower after several hours of immersion due to the relatively high pH value promoting the formation of $Mg_3(PO_4)_2$, $MgCO_3$ and $Mg(OH)_2$ layer. Observed pH trend correlates well with our previous results [50] where it was measured in dynamic conditions that near surface pH in Ca^{2+} containing electrolyte does not rise above 8.5, while in Ca^{2+}-deficient electrolytes, pH raises to above 10. The difference though needs to be clarified. A local pH below 8.5 was observed in our previous work [50] for the entire duration of 24 h experiment, while bulk pH of electrolyte No. 2 gradually increased to above 9 in present work. This is explained by the gradual depletion of Ca^{2+} and other ions in electrolyte No. 2, while in our previous work the local pH measurements have been performed in hydrodynamic conditions with constantly flowing fresh electrolyte.

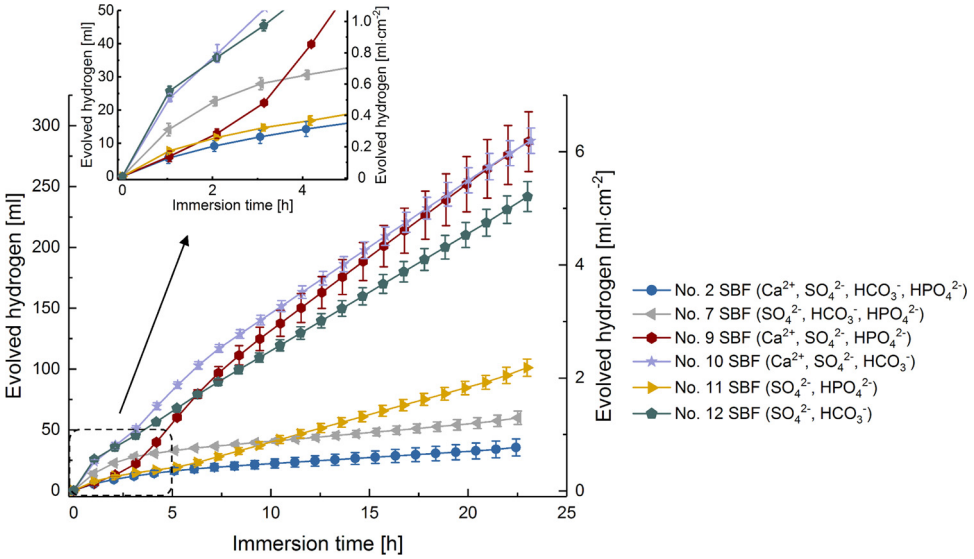

Fig. 8. Hydrogen evolution tests of CP Mg in electrolytes No. 2, No. 7 and No. 9-12.
(The legend shows relevant ions present in each electrolyte.)

From the results discussed above, it is found that the presence of Ca^{2+} delayed the reaction between Mg^{2+} and HPO_4^{2-} or HCO_3^-. The reaction between Ca^{2+} and HPO_4^{2-} provides an initial protection, but either in HCO_3^- or HPO_4^{2-} deficient electrolytes, the presence of Ca^{2+} seems to accelerate corrosion (No. 9 and No. 10). Therefore, electrolytes No. 11 and 12 were designed. These electrolytes lack either Ca^{2+}/HCO_3^- or Ca^{2+}/HPO_4^{2-} compared to the typical SBF electrolytes. The hydrogen evolution curves of No. 11 and 12 are shown in Fig. 8; the curves recorded in electrolytes No. 2, 7, 9 and 10 also included in this figure for comparison.

Comparing the hydrogen evolution curves in electrolytes No. 9 and 11, it is clear that the absence of Ca^{2+} significantly decreased (by factor 2.8) the corrosion rate of CP Mg in a carbonate-free electrolyte. As shown in the insert in Fig. 8, the corrosion rates in the carbonate-free electrolyte with or without Ca^{2+} are similar at the beginning of the immersion. However, after a 3 h immersion, an inflection point appeared on the hydrogen evolution curve in the Ca^{2+} containing electrolyte (No. 9), which means that the corrosion rate of CP Mg in this electrolyte increased at that time. Meanwhile, the corrosion rate in No. 11 had no significant change during the whole immersion time. Fig. 9(**a**) shows the bulk pH changes and hydrogen evolution curves of CP Mg in electrolytes No. 9 and 11. During the first several hours, the trend of the pH change, as well as of evolved hydrogen, were different in these electrolytes. As discussed above, likely formation of hydroxyapatite in the No. 9 electrolyte, provided an initial protection for magnesium. The hydroxyapatite layer inhibited the pH increase at the beginning of the immersion. However, the limited amount of hydroxyapatite did not provide long-term protection for magnesium. According to the predicted results (also listed in Table 3), without Ca^{2+}, HPO_4^{2-} reacted with Mg^{2+} to form a magnesium phosphate layer on the surface of Mg in electrolyte No. 11. The absence of hydroxyapatite led to the quick rise of the pH up to approximately 10. However, the relatively high pH value was helpful for the formation of magnesium phosphate, which delayed the further corrosion of magnesium.

Similarly, the absence of Ca^{2+} also decreased the corrosion rate of CP Mg in the phosphate-free electrolyte, but the change was less pronounced (as shown in Fig. 8). Fig. 9(**b**) shows the bulk spH changes and hydrogen evolution curves of CP Mg in electrolytes No. 10 and 12. The corrosion rate remained at a high level during the whole immersion period in electrolyte No. 10 and was slightly higher than that in electrolyte No. 12. Furthermore, the pH changes were almost the same. However, in the Ca^{2+}-containing electrolyte (No. 10), the pH of first 2 h was slightly lower than that in electrolyte No. 12. In the phosphate-free electrolyte, the lack of HPO_4^{2-}-containing products led to a fast pH increase at the first stage. Ca^{2+}- and HCO_3^--containing products formed in the electrolyte and covered the surface of the magnesium in

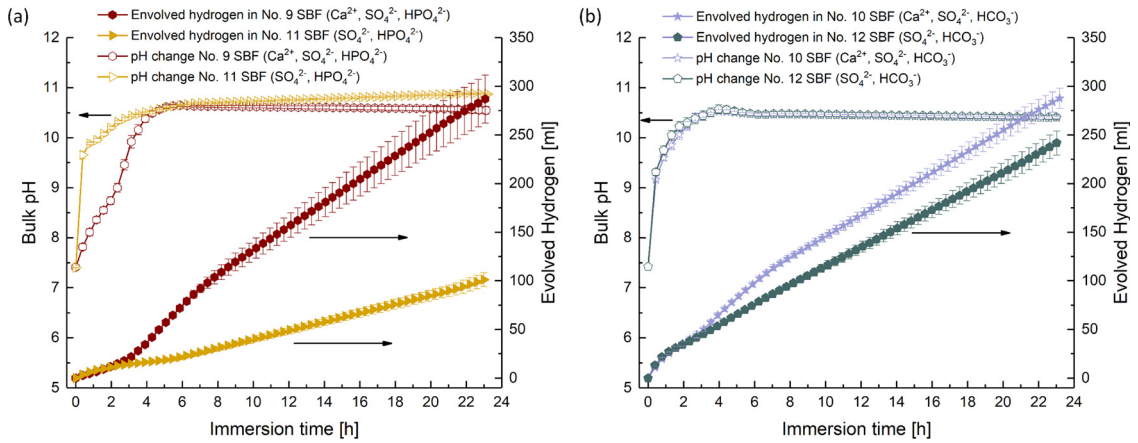

Fig. 9. Bulk pH change and hydrogen evolution curves of CP Mg in different electrolytes: (a) No. 9 and 11, (b) No. 10 and 12.
(The legend shows relevant ions present in each electrolyte.)

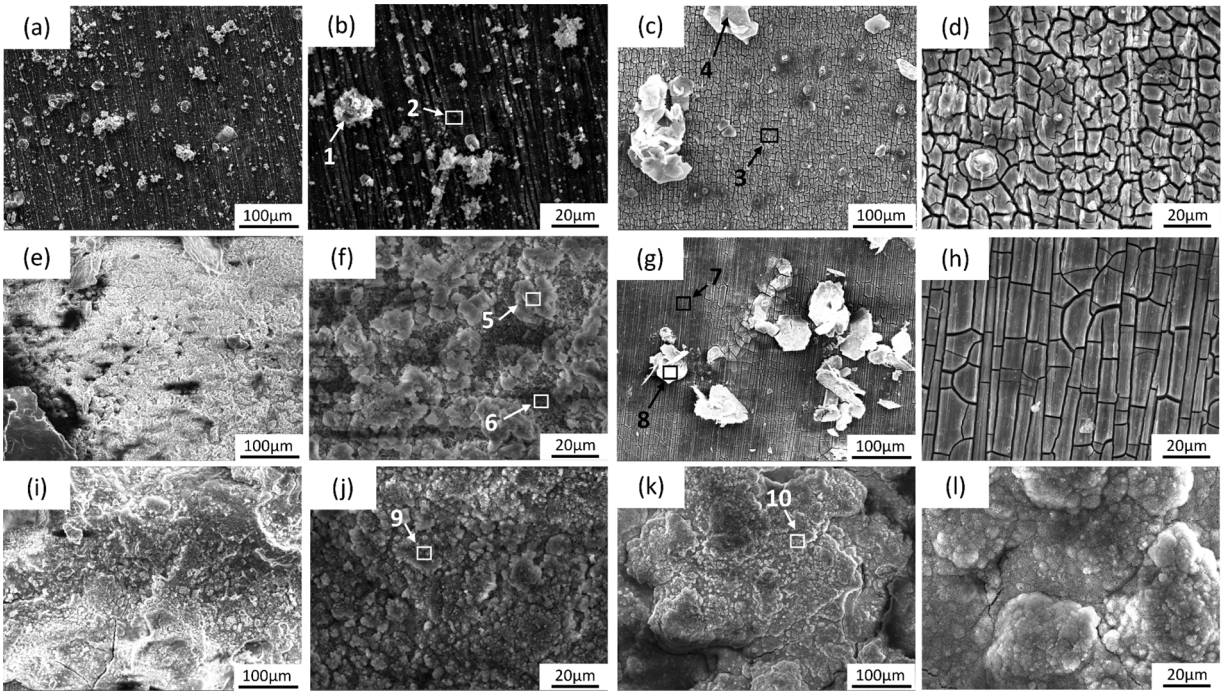

Fig. 10. Corrosion morphologies of samples after 24 h immersion in different electrolytes: (a–b) No. 2 SBF (Ca^{2+}, HCO_3^-, HPO_4^{2-}, SO_4^{2-}), (c–d) No. 7 SBF (HCO_3^-, HPO_4^{2-}, SO_4^{2-}), (e–f) No. 9 SBF (Ca^{2+}, HPO_4^{2-}, SO_4^{2-}), (g–h) No. 11 SBF (HPO_4^{2-}, SO_4^{2-}), (i–j) No. 10 SBF (Ca^{2+}, HCO_3^-, SO_4^{2-}), (k–l) No. 12 SBF (HCO_3^-, SO_4^{2-}).

the Ca^{2+}-containing electrolyte, which inhibits the corrosion and rise of pH. The protective effect of Ca^{2+}- and HCO_3^--containing products was not efficient because of its formation mode. Meanwhile, the reaction between Ca^{2+} and HCO_3^- also influenced the reaction between Mg^{2+} and HCO_3^-. When Ca^{2+} was removed from electrolyte, all of HCO_3- reacted with Mg^{2+} and the (Mg^{2+}, HCO_3^-)-containing products layer provided some protection. However, compared with the (Mg^{2+}, HPO_4^{2-})-containing products layer, this carbonate layer could not significantly slow down the corrosion rate.

3.3. Morphology and composition of the corrosion products of CP Mg after corrosion in different electrolytes

The above discussions were on the individual influence and synergy of some ions on the corrosion rates of CP Mg in SBF. Additionally, precipitation of Ca and Mg containing corrosion products were suggested by the thermodynamic Medusa calculations. To assess these predictions, SEM/EDS and XRD were used to investigate the corrosion morphology (Fig. 10) and compositions of corrosion products (Table 4 and Fig. 11) of CP Mg after 24 h immersion.

The corrosion morphologies in SBF without Tris/HCl are shown in Fig. 10(**a–b**). It was observed that the scratches caused by the grinding process on the surface of the samples were still there and that the corrosion product layer on the surface was thin and compact. These observations indicate that the corrosion in this electrolyte was not profound. The main elements of the corrosion products cluster (point 1) are Ca, P, O and C. It was previously observed that calcium phosphate-containing products form a stable and compact layer [69], especially on the cathodic sites [44]. In CP Mg, the iron-rich impurity particles were the local cathodes in the micro-galvanic couples. We propose that these product clusters were hydroxyapatite forming on the iron particles. The formation of hydroxyapatite on the cathodic sites inhibited galvanic corrosion and thus reduced the corrosion rate. The elements of the thin corrosion product layer are Mg, O, C, Ca and P (point 2). However, no other phase appeared in the XRD pattern except for metallic Mg, also indicating that the corrosion products layer is very thin. The products layer that contained Mg, O, C, Ca and P provided strong corrosion protection. When Ca^{2+} was removed from the electrolyte, the corrosion products layer was significantly thicker (Fig. 10(**c–d**)) and cracks were clearly observed as a result of dehydration. $Mg_3(PO_4)_2{\cdot}22H_2O$ and $Mg_2CO_3(OH)_2{\cdot}3H_2O$ were determined by XRD in the corrosion products formed in electrolyte No. 7, as shown in Fig. 11(**b**). The results confirm Medusa thermodynamic predictions. It should be noted that a similar surface morphology also can be seen in Fig. 10(**g–h**), corresponding to the second Ca^{2+} deficient electrolyte. From EDS analysis, it was found that the composition of the two products layers (in electrolytes No. 7 and 11) were similar, even though electrolyte No. 11 did not contain HCO_3^-. This result is understandable because the dissolution of CO_2 from air provides a low amount of carbonate in electrolyte, and some carbonate is also formed during the air-drying process after the immersion test. In our study, the hydrogen evolution tests and immersion tests were run in a closed environment. Therefore, the dissolution of CO_2 was non-continuous and the amount of dissolved CO_2 was limited. The dissolution of CO_2 cannot fully offset the influence of the absence of HCO_3^- in electrolyte. Thus, the absence of HCO_3^- in electrolyte still had a large influence on hydrogen evolution and the corrosion morphology (Fig. 10(**e–f**)). After a 24 h immersion in electrolyte No. 9, the surface of the sample was covered by a non-uniform thick product layer

Table 4
Composition of corrosion products by EDS after 24 h immersion in different electrolytes.

Electrolytes	Position	Elements/ at. %						
		C	O	Mg	P	Ca	Na	Cl
No. 2	1	9.7	44.5	4.1	16.4	22.1	1.8	1.4
	2	10.1	19.5	63.9	3.4	3.1	–	–
No. 7	3	13.3	50.2	26.3	7.8	–	2.4	–
	4	11.6	54.1	20.3	14.0	–	–	–
No. 9	5	7.2	59.6	30.2	2.7	0.3	–	–
	6	6.2	60.5	33.3	–	–	–	–
No. 11	7	12.4	50.3	25.2	6.8	–	5.4	–
	8	12.1	50.4	18.5	11.8	–	7.2	–
No. 10	9	8.4	58.5	33.1	–	–	–	–
No. 12	10	8.7	55.9	35.4	–	–	–	–

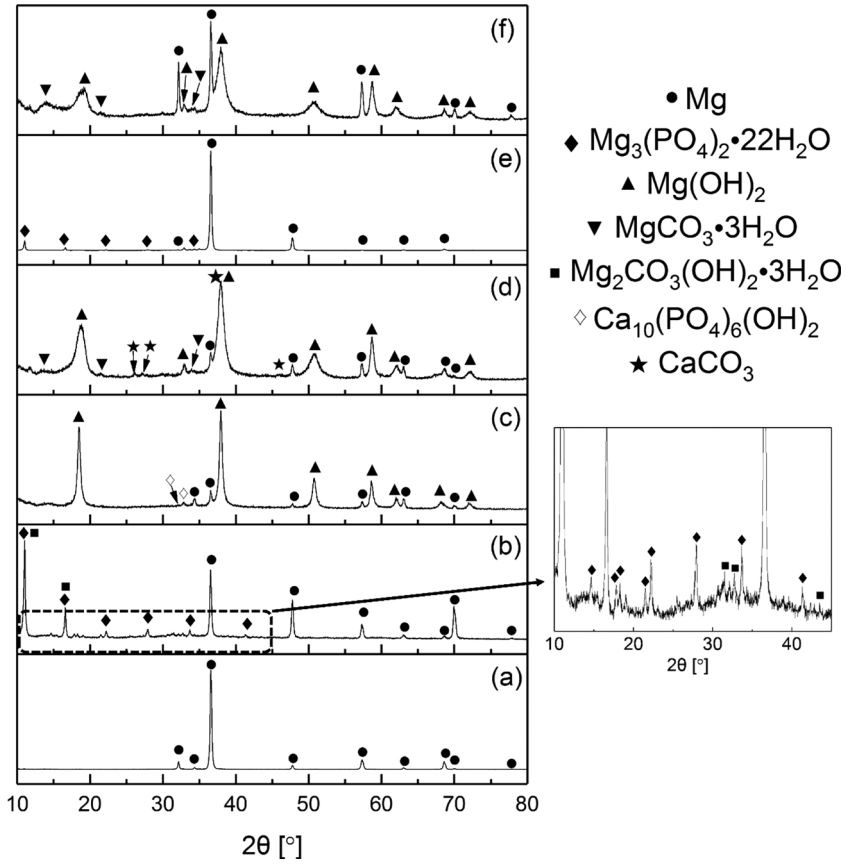

Fig. 11. XRD patterns of the samples after 24 h immersion in different electrolytes, (a) No. 2 SBF (Ca^{2+}, HCO_3^-, HPO_4^{2-}, SO_4^{2-}), (b) No. 7 SBF (HCO_3^-, HPO_4^{2-}, SO_4^{2-}), (c) No. 9 SBF (Ca^{2+}, HPO_4^{2-}, SO_4^{2-}), (d) No. 10 SBF (Ca^{2+}, HCO_3^-, SO_4^{2-}), (e) No. 11 SBF (HPO_4^{2-}, SO_4^{2-}), (f) No. 12 SBF (HCO_3^-, SO_4^{2-}).

with deep cracks. The conductivity of the sample was not sufficient, even after continuous gold sputtering for SEM observations. The corrosion products were divided into two layers; the composition of upper layer was Ca and P (point 5 in Fig. 10(**f**)) and the inner layer contained hydroxide and carbonate. Similar results were also found by XRD, Fig. 11(**c**); the main corrosion products were $Mg(OH)_2$ and $Ca_{10}(PO_4)_6(OH)_2$. As shown in Fig. 10(**i–l**), the corrosion products layer in phosphate-free electrolyte (No. 10 and 12) are thick and loose. From the SEM and EDS results, the corrosion products in these two electrolytes were found to be similar, not only in their morphology but also in their elemental composition. From the EDS results, no obvious Ca containing deposits were found on the surface of the samples immersed in both electrolytes. The similar corrosion products agree well the trends of the hydrogen evolution tests and pH monitoring in these electrolytes. The XRD results showed that there was a small amount of $CaCO_3$ involved in the corrosion products formed in electrolyte No. 10.

3.4. Discussion of the corrosion mechanisms of CP Mg in SBF electrolytes

Based on the SEM/EDS results, product clusters formed on some sites and a thin layer formed on the surface after 24 h immersion in electrolyte No. 2. The main elements of the corrosion products were Mg, Ca, P, C and O. Although forming very thin layer, these products provided best corrosion protection among all tested electrolyte compositions. In Section 3.3, it is mentioned that high Ca-P content products formed around the iron particles (cathodic sites) during the immersion period. To confirm this statement, a semi *in-situ* method was used. Fig. 12 shows the surface morphology of CP Mg prior to and following 30 min of immersion in electrolyte No. 2. The same site is shown. In Fig. 12(**a**), the light spots indicated by arrows are Fe-rich impurity particles (proven by EDS). Impurity particles in CP Mg are abundant and very rich in Fe (5.6–67.2 at. %, results listed in Fig. 12). After a 30 min immersion in electrolyte No. 2, the corrosion products covered the surface, with preferential coverage of iron-rich particles. From the EDS mapping results, the composition of products around most of the initial Fe-rich sites had higher Ca and P, which provides evidences to proof the formation of calcium phosphate-rich precipitates on the iron particles. Given that these iron particles are the starting points of galvanic corrosion, the high pH value around the iron particles due to the cathodic reaction promoted the precipitation of Ca-P products. Unfortunately, there were no other obvious peaks except Mg in the XRD pattern (Fig. 11(**a**)), and the phase composition of products layer was not very clear. In a recent publication, Agha and Liu et al. [70] investigated the corrosion products on the pure Mg after the immersion in DMEM by using synchrotron IR, the results demonstrated that amorphous and/or crystalline $MgCO_3$ on account of $CaCO_3$ can be formed on the surface of the samples, as well as Mg-poor amorphous calcium phosphate. However, more proofs could not be provided in our study, but according to the results and discussions above, it is reasonable to assume that the partially protective layer formed from a co-deposition of Ca^{2+}, Mg^{2+}, carbonate and phosphate.

To verify the partially protective layer forming during the immersion, EIS was employed to characterize the barrier protective ability of the formed layers. The evolution of Bode plots is shown in Fig. 13. It compares the changes of the impedance spectra of samples during immersion in five different SBF electrolytes. Initially, all the samples in different electrolytes displayed a similar pattern of an increasing low frequency impedance, indicating growth of the intrinsic $MgO/Mg(OH)_2$ layer. However, the growth was not always sustainable, and the impedance values at low frequencies were even lower than the original value after 24 h of immersion in electrolytes No. 1, 9 and 10. The most limited growth of the protective layer was observed for electrolyte No.

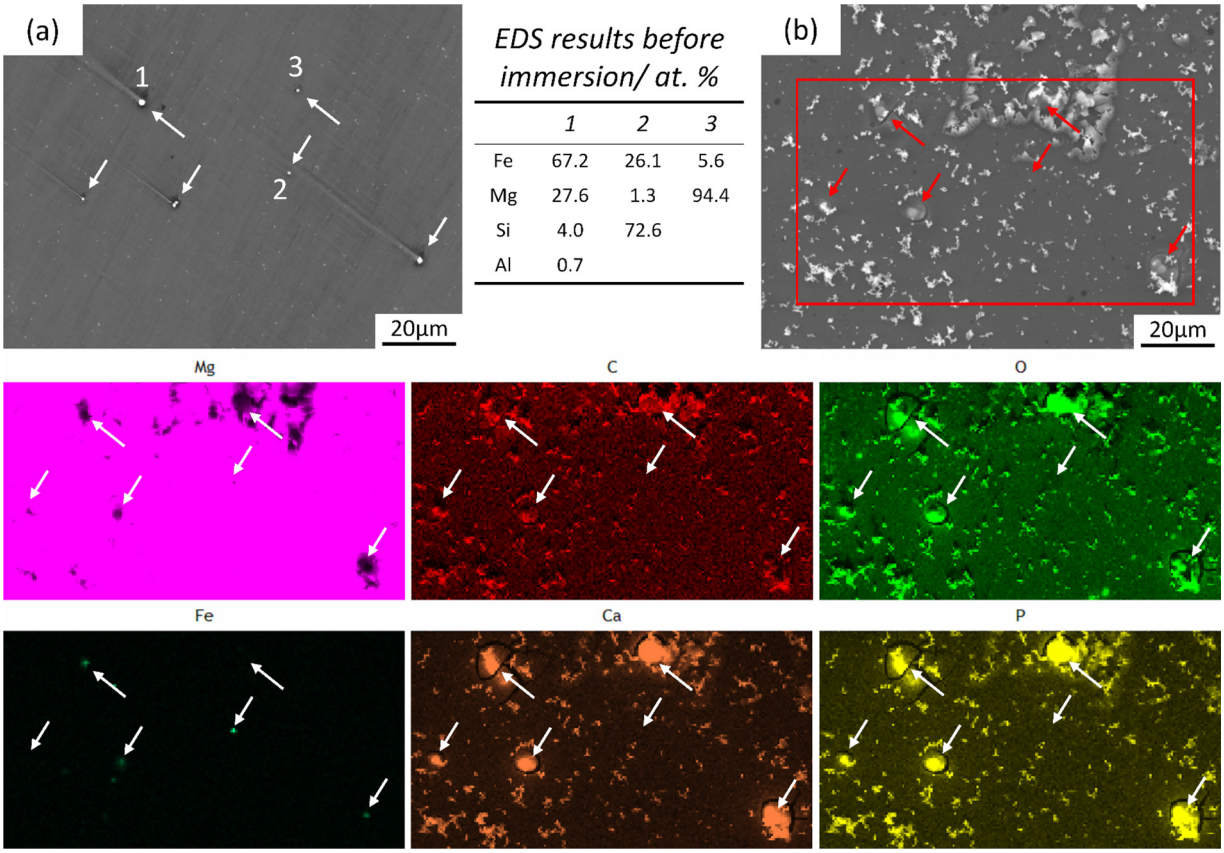

	1	2	3
Fe	67.2	26.1	5.6
Mg	27.6	1.3	94.4
Si	4.0	72.6	
Al	0.7		

Fig. 12. Surface morphology of the same site on polished sample before immersion (a), after 30 min immersion (b) in No. 2 (SBF (Ca^{2+}, HCO_3^-, HPO_4^{2-}, SO_4^{2-})) and the EDS elemental mapping of the selected area in (b).

1, which contained a synthetic pH buffer Tris. This result confirmed previous observations that Tris prevents stabilization of the interface due to the limited growth of corrosion products. The evolution of the middle frequency response in various electrolytes has some differences. The most important change observed in the high frequency domain was for the sample exposed to electrolyte No. 2. Here, an additional time constant steadily grows in the high frequency range throughout the entire 24 h immersion. This indicates steady growth of an additional insoluble partially protective layer on top of existing $MgO/Mg(OH)_2$. The latter also grew up to 7 h of immersion and then slightly decreased.This distinct growing layer only appeared in electrolyte No. 2. In addition, there is an inconspicuous time constant appeared at high

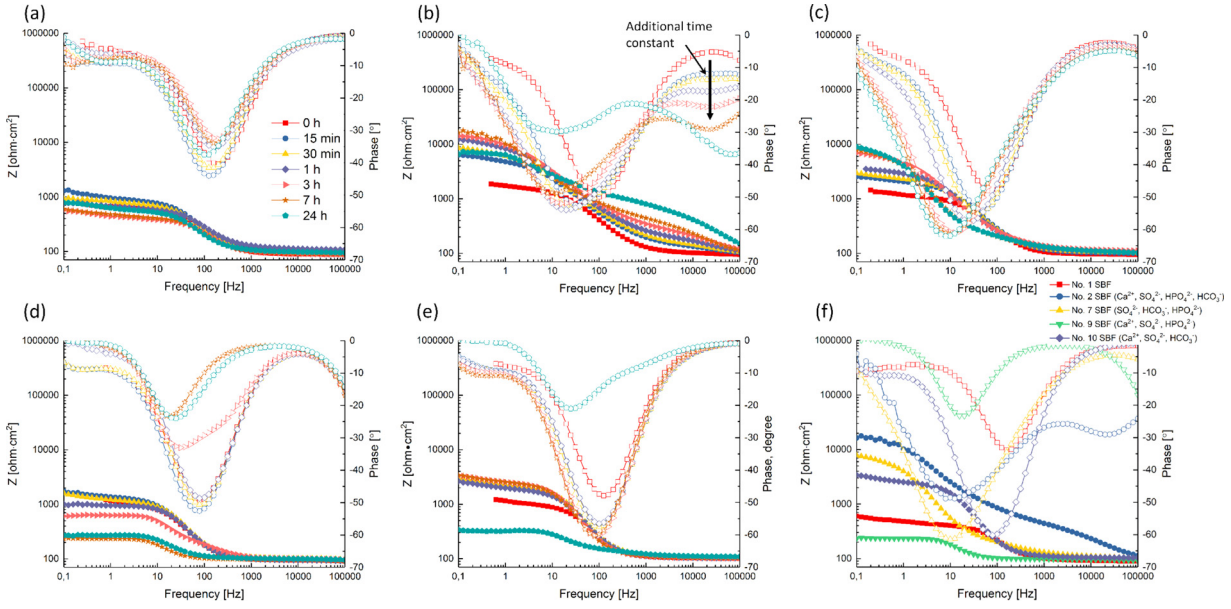

Fig. 13. Bode plots for CP Mg after different immersion duration in (a) No. 1 SBF, (b) No. 2 SBF (Ca^{2+}, HCO_3^-, HPO_4^{2-}, SO_4^{2-}), (c) No. 7 SBF (HCO_3^-, HPO_4^{2-}, SO_4^{2-}), (d) No. 9 SBF (Ca^{2+}, HPO_4^{2-}, SO_4^{2-}), (e) No. 10 SBF (Ca^{2+}, HCO_3^-, SO_4^{2-}) and the comparison of Bode plots that were obtained in different electrolytes after 7 h of immersion (f).

frequency after 30 min immersion in electrolyte No. 7, it indicates the formation of magnesium phosphate on the surface of sample. However, compared with the partially protective layer in electrolyte No. 2, the formation of layer in No. 7 is slow and not sustained throughout the entire 24 h immersion. The comparison of Bode plots that were obtained in different electrolytes after 7 h of immersion was shown in Fig. 13(**f**). The values of low frequency impedance differ significantly for the samples exposed to electrolytes No. 1, 2, 7, 9 and 10 reflecting different composition and protective properties of corrosion products formed in these electrolytes. Additional high frequency time constant observed for the sample exposed to electrolyte No. 2 also stands out in Fig. 13(**f**). The impedance measurements point to the synergistic effect of Ca^{2+}, HPO_4^{2-} and HCO_3^- (and dissolving Mg^{2+}) that promotes formation of an additional partially protective layer growing beside the thickening $MgO/Mg(OH)_2$ also observed in other electrolytes.

Combined with the results discussed above, the strongest surface protection effect came as the result of the synergistic combination of Ca^{2+}, HPO_4^{2-} and HCO_3^- (and dissolving Mg^{2+}) of promoting fast formation of additional partially protective layer of corrosion products. Precipitation of Ca^{2+}, HPO_4^{2-} and HCO_3^- containing corrosion layer occurs at near surface pH of around 8.5. This layer provided constant protection during immersion. Its effect can be separated into two aspects: the corrosion products formed on the cathodic sites (iron impurities), which inhibit cathodic activity, and the layer formed on the anodic matrix partly isolates it from the corrosive medium. In the Ca^{2+}-free electrolyte, the formation of calcium phosphate was not happening and the corrosion rate at the beginning was fast. However, the lack of Ca^{2+} was beneficial to the formation of magnesium phosphate and magnesium carbonate that also provided protection. In the carbonate-free or phosphate-free electrolyte, Ca^{2+} reacted with HPO_4^{2-} or HCO_3^- preferentially. The limited amount of anions inhibit the formation of Mg corrosion products, $Mg_3(PO_4)_2$ and $MgCO_3$, but formed Ca-containing layers did not provide protection comparable to that obtained in absence of Ca^{2+} (electrolyte No. 7). When Ca^{2+} was removed from the carbonate-free or phosphate-free electrolyte, the decreased corrosion rate suggested that magnesium phosphate or magnesium carbonate provide considerable protection effect which is well known from previously reported results [71].

Ca^{2+}, Mg^{2+}, carbonate and phosphate widely exist in bodily fluids where their concentrations are maintained nearly constant. Lack of any of these ions and addition of synthetic pH buffers like Tris or HEPES [50] to the testing electrolytes, might be causing differences between corrosion test results *in vitro* and *in vivo* [21]. It is essential that the *in vitro* tests are conducted in presence of Ca^{2+}, Mg^{2+}, HPO_4^{2-} and HCO_3^- and that concentration of these ions is maintained constant during the course of experiment. Flow-through cells [72–74], although they are more complicated to assemble and requiring significant amount of electrolytes, might be the optimal setup for *in vitro* tests.

4. Conclusion

SBF electrolyte stabilized with a synthetic pH buffer Tris/HCl is a common test medium used for the *in vitro* corrosion tests. In this study, the influence of Tris/HCl buffer and some inorganic ions on the corrosion of CP Mg was investigated. The conclusions are summarized as follows:

(1) Tris/HCl buffer in SBF is found to have a highly negative influence on the corrosion of CP Mg. The corrosion rate of Mg is accelerated in Tris/HCl containing SBF due to three factors: the pH buffering capacity of Tris inhibits the formation of stable corrosion products; the complexation between Tris and Ca^{2+} prevents formation of Ca-containing corrosion products possessing high protective ability and complexation between Tris and Mg^{2+}, promotes the dissolution of Mg; and, eventually, increased concentration of Cl^- (from Tris/HCl) accelerates the corrosion rate.

(2) Usage of Tris is pointless from the point of view of pH stabilization. The buffering effect of Tris is limited in SBF electrolyte. The bulk pH values of SBF with and without Tris are the same and increase from 7.4 to 9.5 within 24 h of immersion. Meanwhile, the local pH in Tris-free electrolyte remains lower (pH = 8.3 ± 0.3) than that in Tris-buffered electrolyte (pH = 9.0 ± 0.3 and exceeding 10 in specific points), at least during the initial hours of immersion.

(3) In SBF without Tris/HCl, a combination of Ca^{2+}, HPO_4^{2-} and HCO_3^- significantly slows down corrosion of CP Mg. The corrosion rate is 8 times lower compared to that with electrolytes lacking either HPO_4^{2-} or HCO_3^-. However, in the carbonate-free or phosphate-free electrolytes, the presence of Ca^{2+} accelerates the corrosion rate. Particularly in the carbonate-free electrolyte, the acceleration effect of Ca^{2+} is more significant.

(4) The synergy of Ca^{2+}, Mg^{2+}, HPO_4^{2-} and HCO_3^- causes growth of partially protective film on top of $MgO/Mg(OH)_2$ layer which becomes thicker in time. Hydrogen evolution and especially EIS results provide clear evidence of the unique protective properties of corrosion products formed in presence of Ca^{2+}, Mg^{2+}, HPO_4^{2-} and HCO_3^- in SBF electrolyte.

Data availability

The raw/processed data required to reproduce these findings cannot be shared at this time as the data also forms part of an ongoing study.

Acknowledgements

Mr. Di Mei thanks China Scholarship Council for the award of fellowship and funding (No. 201607040051). Dr. S. V. Lamaka acknowledges the financial support of Alexander von Humboldt Foundation via Experienced Researcher Grant. “MMDi” IDEA project funded by HZG is gratefully acknowledged. Mr. Jorge Gonzalez, Dr. Frank Feyerabend and Prof. Dr. Regine Willumeit-Römer acknowlegde the financial support of the Helmholtz Virtual Institute via VH-VI-523-In vitro studies of biodegradable magnesium-based implant materials. The technical support of Mr. Volker Heitmann and Mr. Ulrich Burmester during this work is gratefully acknowledged.

References

[1] F. Witte, N. Hort, C. Vogt, S. Cohen, K.U. Kainer, R. Willumeit, F. Feyerabend, Degradable biomaterials based on magnesium corrosion, Curr. Opin. Solid State Mater. Sci. 12 (2008) 63–72.
[2] Y.F. Zheng, X.N. Gu, F. Witte, Biodegradable metals, Mater. Sci. Eng. R Rep. 77 (2014) 1–34.
[3] D. Zhao, F. Witte, F. Lu, J. Wang, J. Li, L. Qin, Current status on clinical applications of magnesium-based orthopaedic implants: a review from clinical translational perspective, Biomaterials 112 (2017) 287–302.
[4] R. Zeng, W. Dietzel, F. Witte, N. Hort, C. Blawert, Progress and challenge for magnesium alloys as biomaterials, Adv. Eng. Mater. 10 (2008) B3–B14.
[5] M. Esmaily, J.E. Svensson, S. Fajardo, N. Birbilis, G.S. Frankel, S. Virtanen, R. Arrabal, S. Thomas, L.G. Johansson, Fundamentals and advances in magnesium alloy corrosion, Prog. Mater. Sci. 89 (2017) 92–193.
[6] G. Song, Control of biodegradation of biocompatable magnesium alloys, Corros. Sci. 49 (2007) 1696–1701.
[7] J. Wang, L. Wang, S. Guan, S. Zhu, C. Ren, S. Hou, Microstructure and corrosion properties of as sub-rapid solidification Mg–Zn–Y–Nd alloy in dynamic simulated body fluid for vascular stent application, J. Mater. Sci. Mater. Med. 21 (2010) 2001–2008.
[8] N. Li, Y. Zheng, Novel magnesium alloys developed for biomedical application: a review, J. Mater. Sci. Technol. 29 (2013) 489–502.
[9] H. Qin, Y. Zhao, Z. An, M. Cheng, Q. Wang, T. Cheng, Q. Wang, J. Wang, Y. Jiang, X. Zhang, G. Yuan, Enhanced antibacterial properties, biocompatibility, and corrosion resistance of degradable Mg-Nd-Zn-Zr alloy, Biomaterials 53 (2015) 211–220.
[10] R.L. Liu, J.R. Scully, G. Williams, N. Birbilis, Reducing the corrosion rate of magnesium via microalloying additions of group 14 and 15 elements, Electrochim. Acta 260 (2018) 184–195.
[11] J. Wang, J. Tang, P. Zhang, Y. Li, J. Wang, Y. Lai, L. Qin, Surface modification of magnesium alloys developed for bioabsorbable orthopedic implants: A general review, J. Biomed. Mater. Res. Part B: Appl. Biomater. 100B (2012) 1691–1701.
[12] H. Hornberger, S. Virtanen, A.R. Boccaccini, Biomedical coatings on magnesium

alloys – a review, Acta Biomater. 8 (2012) 2442–2455.
[13] G. Wu, J.M. Ibrahim, P.K. Chu, Surface design of biodegradable magnesium alloys — a review, Surf. Coat. Technol. 233 (2013) 2–12.
[14] X. Lu, C. Blawert, D. Tolnai, T. Subroto, K.U. Kainer, T. Zhang, F. Wang, M.L. Zheludkevich, 3D reconstruction of plasma electrolytic oxidation coatings on Mg alloy via synchrotron radiation tomography, Corros. Sci. 139 (2018) 395–402.
[15] J. Yang, C. Blawert, S.V. Lamaka, D. Snihirova, X. Lu, S. Di, M.L. Zheludkevich, Corrosion protection properties of inhibitor containing hybrid PEO-epoxy coating on magnesium, Corros. Sci. 140 (2018) 99–110.
[16] G.-L. Song, Z. Xu, Effect of microstructure evolution on corrosion of different crystal surfaces of AZ31 Mg alloy in a chloride containing solution, Corros. Sci. 54 (2012) 97–105.
[17] C.Z. Zhang, S.J. Zhu, L.G. Wang, R.M. Guo, G.C. Yue, S.K. Guan, Microstructures and degradation mechanism in simulated body fluid of biomedical Mg–Zn–Ca alloy processed by high pressure torsion, Mater. Des. 96 (2016) 54–62.
[18] N.T. Kirkland, N. Birbilis, M. Staiger, Assessing the corrosion of biodegradable magnesium implants: a critical review of current methodologies and their limitations, Acta Biomater. 8 (2012) 925–936.
[19] Z. Zhen, T.-f. Xi, Y.-f. Zheng, A review on in vitro corrosion performance test of biodegradable metallic materials, Trans. Nonferrous Met. Soc. China 23 (2013) 2283–2293.
[20] E. Willbold, A. Weizbauer, A. Loos, J.-M. Seitz, N. Angrisani, H. Windhagen, J. Reifenrath, Magnesium alloys: A stony pathway from intensive research to clinical reality. Different test methods and approval-related considerations, J. Biomed. Mater. Res. A 105 (2017) 329–347.
[21] J. Gonzalez, R.Q. Hou, E.P.S. Nidadavolu, R. Willumeit-Römer, F. Feyerabend, Magnesium degradation under physiological conditions – best practice, Bioact. Mater. 3 (2018) 174–185.
[22] A.D. Forero López, I.L. Lehr, S.B. Saidman, Anodisation of AZ91D magnesium alloy in molybdate solution for corrosion protection, J. Alloys. Compd. 702 (2017) 338–345.
[23] R.-Q. Hou, N. Scharnagl, F. Feyerabend, R. Willumeit-Römer, Exploring the effects of organic molecules on the degradation of magnesium under cell culture conditions, Corros. Sci. 132 (2018) 35–45.
[24] C. Cai, R. Song, L. Wang, J. Li, Surface corrosion behavior and reaction product film deposition mechanism of Mg-Zn-Zr-Nd alloys during degradation process in Hank's solution, Surf. Coat. Technol. 342 (2018) 57–68.
[25] E. Willbold, X. Gu, D. Albert, K. Kalla, K. Bobe, M. Brauneis, C. Janning, J. Nellesen, W. Czayka, W. Tillmann, Y. Zheng, F. Witte, Effect of the addition of low rare earth elements (lanthanum, neodymium, cerium) on the biodegradation and biocompatibility of magnesium, Acta Biomater. 11 (2015) 554–562.
[26] Y. Feng, X. Ma, L. Chang, S. Zhu, S. Guan, Characterization and cytocompatibility of polydopamine on MAO-HA coating supported on Mg-Zn-Ca alloy, Surf. Interface Anal. 49 (2017) 1115–1123.
[27] M. Ascencio, M. Pekguleryuz, S. Omanovic, Corrosion behaviour of polypyrrole-coated WE43 Mg alloy in a modified simulated body fluid solution, Corros. Sci. 133 (2018) 261–275.
[28] L. Yang, L. Ma, Y. Huang, F. Feyerabend, C. Blawert, D. Höche, R. Willumeit-Römer, E. Zhang, K.U. Kainer, N. Hort, Influence of Dy in solid solution on the degradation behavior of binary Mg-Dy alloys in cell culture medium, Mater. Sci. Eng.: C 75 (2017) 1351–1358.
[29] R. Willumeit, J. Fischer, F. Feyerabend, N. Hort, U. Bismayer, S. Heidrich, B. Mihailova, Chemical surface alteration of biodegradable magnesium exposed to corrosion media, Acta Biomater. 7 (2011) 2704–2715.
[30] A. Yamamoto, S. Hiromoto, Effect of inorganic salts, amino acids and proteins on the degradation of pure magnesium in vitro, Mater. Sci. Eng. C 29 (2009) 1559–1568.
[31] V. Wagener, S. Virtanen, Protective layer formation on magnesium in cell culture medium, Mater. Sci. Eng. C 63 (2016) 341–351.
[32] H. Ma, Y. Gu, S. Liu, J. Che, D. Yang, Local corrosion behavior and model of micro-arc oxidation HA coating on AZ31 magnesium alloy, Surf. Coat. Technol. 331 (2017) 179–188.
[33] J. Yang, X. Lu, C. Blawert, S. Di, M.L. Zheludkevich, Microstructure and corrosion behavior of Ca/P coatings prepared on magnesium by plasma electrolytic oxidation, Surf. Coat. Technol. 319 (2017) 359–369.
[34] X. Song, L. Chang, J. Wang, S. Zhu, L. Wang, K. Feng, Y. Luo, S. Guan, Investigation on the in vitro cytocompatibility of Mg-Zn-Y-Nd-Zr alloys as degradable orthopaedic implant materials, J. Mater. Sci. Mater. Med. 29 (2018) 44.
[35] J. Wang, Y. Zhou, Z. Yang, S. Zhu, L. Wang, S. Guan, Processing and properties of magnesium alloy micro-tubes for biodegradable vascular stents, Mater. Sci. Eng. C 90 (2018) 504–513.
[36] V. Wagener, S. Virtanen, Influence of electrolyte composition (simulated body fluid vs. Dulbecco's Modified Eagle's Medium), temperature, and solution flow on the biocorrosion behavior of commercially pure Mg, Corrosion 73 (2017) 1413–1422.
[37] T. Kokubo, H. Takadama, How useful is SBF in predicting in vivo bone bioactivity? Biomaterials 27 (2006) 2907–2915.
[38] A. Oyane, H.-M. Kim, T. Furuya, T. Kokubo, T. Miyazaki, T. Nakamura, Preparation and assessment of revised simulated body fluids, J. Biomed. Mater. Res. A. 65A (2003) 188–195.
[39] L. Müller, F.A. Müller, Preparation of SBF with different HCO3- content and its influence on the composition of biomimetic apatites, Acta Biomater. 2 (2006) 181–189.
[40] D. Rohanová, A.R. Boccaccini, D.M. Yunos, D. Horkavcová, I. Březovská, A. Helebrant, TRIS buffer in simulated body fluid distorts the assessment of glass–ceramic scaffold bioactivity, Acta Biomater. 7 (2011) 2623–2630.
[41] M. Bohner, J. Lemaitre, Can bioactivity be tested in vitro with SBF solution? Biomaterials 30 (2009) 2175–2179.
[42] Y. Xin, P.K. Chu, Influence of Tris in simulated body fluid on degradation behavior of pure magnesium, Mater. Chem. Phys. 124 (2010) 33–35.
[43] L.-Y. Cui, Y. Hu, R.-C. Zeng, Y.-X. Yang, D.-D. Sun, S.-Q. Li, F. Zhang, E.-H. Han, New insights into the effect of Tris-HCl and Tris on corrosion of magnesium alloy in presence of bicarbonate, sulfate, hydrogen phosphate and dihydrogen phosphate ions, J. Mater. Sci. Technol. 33 (2017) 971–986.
[44] N. Ott, P. Schmutz, C. Ludwig, A. Ulrich, Local, element-specific and time-resolved dissolution processes on a Mg-Y-RE alloy - Influence of inorganic species and buffering systems, Corros. Sci. 75 (2013) 201–211.
[45] S.V. Lamaka, B. Vaghefinazari, D. Mei, R.P. Petrauskas, D. Höche, M.L. Zheludkevich, Comprehensive screening of Mg corrosion inhibitors, Corros. Sci. 128 (2017) 224–240.
[46] J. Walker, S. Shadanbaz, N.T. Kirkland, E. Stace, T. Woodfield, M.P. Staiger, G.J. Dias, Magnesium alloys: predicting in vivo corrosion with in vitro immersion testing, J. Biomed. Mater. Res. Part B: Appl. Biomater. 100B (2012) 1134–1141.
[47] S. Naddaf Dezfuli, Z. Huan, J.M.C. Mol, M.A. Leeflang, J. Chang, J. Zhou, Influence of HEPES buffer on the local pH and formation of surface layer during in vitro degradation tests of magnesium in DMEM, Prog. Nat. Sci. 24 (2014) 531–538.
[48] K. Torne, A. Ornberg, J. Weissenrieder, The influence of buffer system and biological fluids on the degradation of magnesium, J. Biomed. Mater. Res. B Appl. Biomater. 105 (2017) 1490–1502.
[49] M.B. Kannan, H. Khakbaz, A. Yamamoto, Understanding the influence of HEPES buffer concentration on the biodegradation of pure magnesium: an electrochemical study, Mater. Chem. Phys. 197 (2017) 47–56.
[50] S.V. Lamaka, J. Gonzalez, D. Mei, F. Feyerabend, R. Willumeit-Römer, M.L. Zheludkevich, Local pH and its evolution near Mg alloy surfaces exposed to simulated body fluids, Adv. Mater. Interfaces 5 (2018) 1800169, https://doi.org/10.1002/admi.201800169.
[51] M.-C. Zhao, M. Liu, G.-L. Song, A. Atrens, Influence of pH and chloride ion concentration on the corrosion of Mg alloy ZE41, Corros. Sci. 50 (2008) 3168–3178.
[52] Y. Xin, K. Huo, H. Tao, G. Tang, P.K. Chu, Influence of aggressive ions on the degradation behavior of biomedical magnesium alloy in physiological environment, Acta Biomater. 4 (2008) 2008–2015.
[53] R.-C. Zeng, Y. Hu, S.-K. Guan, H.-Z. Cui, E.-H. Han, Corrosion of magnesium alloy AZ31: the influence of bicarbonate, sulphate, hydrogen phosphate and dihydrogen phosphate ions in saline solution, Corros. Sci. 86 (2014) 171–182.
[54] W. Ma, Y. Liu, W. Wang, Y. Zhang, Effects of electrolyte component in simulated body fluid on the corrosion behavior and mechanical integrity of magnesium, Corros. Sci. 98 (2015) 201–210.
[55] S. Johnston, M. Dargusch, A. Atrens, Building towards a standardised approach to biocorrosion studies: a review of factors influencing Mg corrosion in vitro pertinent to in vivo corrosion, Sci. China Mater. 61 (2017) 475–500.
[56] C. Ning, L. Zhou, Y. Zhu, Y. Li, P. Yu, S. Wang, T. He, W. Li, G. Tan, Y. Wang, C. Mao, Influence of Surrounding Cations on the Surface Degradation of Magnesium Alloy Implants under a Compressive Pressure, Langmuir 31 (2015) 13561–13570.
[57] M. Grabowski, D. Bluecher, M. Korte, S. Virtanen, Influence of Ca2+ in deicing salt on the corrosion behavior of AM50 magnesium alloy, Corrosion 70 (2014) 1008–1023.
[58] M. Grabowski, S. Virtanen, Cathodic corrosion of magnesium alloy AM50 in deicing salt solutions during "cathodic protection", Corrosion 73 (2017) 563–582.
[59] N.A. Agha, F. Feyerabend, B. Mihailova, S. Heidrich, U. Bismayer, R. Willumeit-Römer, Magnesium degradation influenced by buffering salts in concentrations typical of in vitro and in vivo models, Mater. Sci. Eng. C 58 (2016) 817–825.
[60] S. Lamaka, R.M. Souto, M.G. Ferreira, In-situ visualization of local corrosion by scanning ion-selective electrode technique (SIET), Microsc.: Sci. Technol. Appl. Educ. 3 (2010) 2162–2173.
[61] C.M.H. Ferreira, I.S.S. Pinto, E.V. Soares, H.M.V.M. Soares, (Un)suitability of the use of pH buffers in biological, biochemical and environmental studies and their interaction with metal ions - a review, RSC Adv. 5 (2015) 30989–31003.
[62] D. Hoche, C. Blawert, S.V. Lamaka, N. Scharnagl, C. Mendis, M.L. Zheludkevich, The effect of iron re-deposition on the corrosion of impurity-containing magnesium, J. Chem. Soc. Faraday Trans. 18 (2016) 1279–1291.
[63] S.V. Lamaka, D. Höche, R.P. Petrauskas, C. Blawert, M.L. Zheludkevich, A new concept for corrosion inhibition of magnesium: suppression of iron re-deposition, Electrochem. Commun. 62 (2016) 5–8.
[64] Chemical Equilibrium Diagrams, in https://www.kth.se/che/medusa/.
[65] S.V. Lamaka, O.V. Karavai, A.C. Bastos, M.L. Zheludkevich, M.G.S. Ferreira, Monitoring local spatial distribution of Mg2+, pH and ionic currents, Electrochem. Commun. 10 (2008) 259–262.
[66] O. Karavai, A. Bastos, M. Zheludkevich, M. Taryba, S. Lamaka, M. Ferreira, Localized electrochemical study of corrosion inhibition in microdefects on coated AZ31 magnesium alloy, Electrochim. Acta 55 (2010) 5401–5406.
[67] C. Wen, S. Guan, L. Peng, C. Ren, X. Wang, Z. Hu, Characterization and degradation behavior of AZ31 alloy surface modified by bone-like hydroxyapatite for implant applications, Appl. Surf. Sci. 255 (2009) 6433–6438.
[68] H. Wang, S. Guan, X. Wang, C. Ren, L. Wang, In vitro degradation and mechanical integrity of Mg–Zn–Ca alloy coated with Ca-deficient hydroxyapatite by the pulse electrodeposition process, Acta Biomater. 6 (2010) 1743–1748.
[69] X.B. Chen, N. Birbilis, T.B. Abbott, Effect of [Ca2+] and [PO43-] levels on the formation of calcium phosphate conversion coatings on die-cast magnesium alloy AZ91D, Corros. Sci. 55 (2012) 226–232.
[70] N.A. Agha, Z. Liu, F. Feyerabend, R. Willumeit-Römer, B. Gasharova, S. Heidrich, B. Mihailova, The effect of osteoblasts on the surface oxidation processes of biodegradable Mg and Mg-Ag alloys studied by synchrotron IR microspectroscopy, Mater. Sci. Eng.: C 91 (2018) 659–668.

[71] G. Williams, H.N. McMurray, R. Grace, Inhibition of magnesium localised corrosion in chloride containing electrolyte, Electrochim. Acta 55 (2010) 7824–7833.
[72] J. Grogan, D. Gastaldi, M. Castelletti, F. Migliavacca, G. Dubini, P. McHugh, A novel flow chamber for biodegradable alloy assessment in physiologically realistic environments, Rev. Sci. Instrum. 84 (2013) 094301.
[73] J. Wang, V. Giridharan, V. Shanov, Z. Xu, B. Collins, L. White, Y. Jang, J. Sankar, N. Huang, Y. Yun, Flow-induced corrosion behavior of absorbable magnesium-based stents, Acta Biomater. 10 (2014) 5213–5223.
[74] B. Zeller-Plumhoff, H. Helmholz, F. Feyerabend, T. Dose, F. Wilde, A. Hipp, F. Beckmann, R. Willumeit-Römer, J.U. Hammel, Quantitative characterization of degradation processes in situ by means of a bioreactor coupled flow chamber under physiological conditions using time-lapse SRμCT, Mater. Corros. 69 (2018) 298–306.

4.3 The influence of small-molecule bio-relevant organic compounds at low concentration on Mg corrosion

The following published paper was incorporated as Chapter 4.3 (with permission from Elsevier):

D. Mei, S.V. Lamaka, C. Feiler, M.L. Zheludkevich, The effect of small-molecule bio-relevant organic components at low concentration on the corrosion of commercially pure Mg and Mg-0.8Ca alloy: An overall perspective, Corrosion Science 153 (2019) 258-271. https://doi.org/10.1016/j.corsci.2019.03.039

D. Mei conceived and designed the study based on the discussion with S.V. Lamaka. D. Mei carried out the experimental work. C. Feiler made a contribution of setting up the automated recording function of the device used in hydrogen evolution tests. S.V. Lamaka, C. Feiler and M.L. Zheludkevich gave constructive comments on data analysis. All the authors contributed to the interpretation of the results and to writing of the paper.

Corrosion Science 153 (2019) 258–271

Contents lists available at ScienceDirect

Corrosion Science

journal homepage: www.elsevier.com/locate/corsci

The effect of small-molecule bio-relevant organic components at low concentration on the corrosion of commercially pure Mg and Mg-0.8Ca alloy: An overall perspective

Di Mei[a,*], Sviatlana V. Lamaka[a], Christian Feiler[a], Mikhail L. Zheludkevich[a,b]

[a] Magnesium Innovation Centre - MagIC, Institute of Materials Research, Helmholtz-Zentrum Geesthacht, Geesthacht, 21502, Germany
[b] Institute for Materials Science, Faculty of Engineering, Kiel University, Kiel, 24103, Germany

ARTICLE INFO

Keywords:
Magnesium
Corrosion
Degradation
Small-molecule organic components

ABSTRACT

The individual and combined influence of 53 small molecule bio-relevant organic compounds on the corrosion of CP Mg and Mg-0.8Ca is investigated. The results demonstrate that tested amino acids, vitamins and saccharides, do not critically influence the *in vitro* corrosion of tested materials. The presence of penicillin and streptomycin at low concentration in MEM has no significant influence on the corrosion, while higher concentration of streptomycin accelerates degradation. The similarity between MEM and SBF as corrosive medium for *in vitro* tests is also clarified. These results contribute to understanding the influence of organic compounds on *in vitro* corrosion of Mg.

1. Introduction

After years of research and development, magnesium and its alloys have become an important material for biodegradable implants for bone and cardiovascular applications [1–5]. For a biodegradable material, understanding its degradation mechanism and degradation rate are of paramount importance. A large number of studies focus on these aspects [6–8]. The *in vivo* corrosion tests are the most appropriate method to investigate the degradation behavior of biomedical magnesium. However, because of the limitations of *in vivo* animal trials, *in vitro* corrosion tests are indispensable [9,10] at the preliminary stages of development. Recent reviews conclude that the *in vivo* corrosion rate of biodegradable Mg does not fully correlate with corrosion rate that obtained by the *in vitro* tests [11,12]. Typically, slower degradation rate is observed *in vivo* compared to the same material tested *in vitro*. One of the reasons is that the existing *in vitro* test protocols were developed for the traditional inert biomaterials (i.e. stainless steels and titanium) rather than fast degrading magnesium and its alloys [11]. Although a recent standard provided suggestions about the medium selection [13], there is still no generally accepted medium for *in vitro* tests of Mg. Understanding other reasons causing the discrepancy between the corrosion rate of *in vivo* and *in vitro* is important for unravelling the details of high complexity degradation phenomena.

Initially, simple saline electrolyte was often used as the *in vitro* test medium. In a search for more appropriate testing media, a number of more complex solutions have been suggested as test media up to now [14,15], including Ringer solution [16], Hank's solutions [17–21], simulated body fluid (SBF) [22–28], as well as cell culture medium (MEM, DMEM, α-MEM) [17,29]. Besides, these media were modified by other components, for example protein, to mimic the real body fluid environment more accurately [17,30]. However, it is still not clear if any of these complex media are more suitable for *in vitro* corrosion tests. The cost of complex media is high and the influence of bacterial multiplication in complex media could not be ignored during long-term tests in an open environment. Although penicillin-streptomycin or UV light could be used to delay the contamination, the widespread application of the complex media is still constrained [31]. An optimal test medium for screening *in vitro* corrosion tests should be easy to prepare, representative and low cost [32]. Yet, a universal testing medium can hardly be created given the variation of possible *in vivo* corrosion environments (e.g. blood plasma, interstitial fluid, bile, urine, gastrointestinal fluid or saliva).

The simplification of the real body fluid appears to be a good choice for the development of test medium. Understanding the influence of body fluid components on the corrosion behavior of magnesium is prerequisite for this approach, due to the presence of a variety of components in real body fluid, such as inorganic salts, amino acids, vitamins, saccharides and several other organic components. The impact of inorganic ions on the corrosion behavior of magnesium have been fully described by a number of papers [33–37]. In our recent work,

* Corresponding author.
E-mail address: Di.Mei@hzg.de (D. Mei).

https://doi.org/10.1016/j.corsci.2019.03.039
Received 5 February 2019; Received in revised form 18 March 2019; Accepted 24 March 2019
Available online 30 March 2019

Table 1
The elemental composition of commercial pure Mg (CP Mg) and Mg-0.8Ca alloy.

	Element content/ wt. %										
	Fe	Cu	Ni	Al	Mn	Ce	Zn	Si	Ca	Zr	Mg
CP Mg	0.0342	0.00037	< 0.0002	0.00402	0.00237	0.0007	0.00046	0.00071	< 0.0001	< 0.0005	Bal.
Mg-0.8Ca	0.0046	0.0021	0.0019	0.024	0.052	0.001	0.0052	0.045	0.83	0.0035	Bal.

the individual effect and synergy of the inorganic ions in SBF have been studied [18,38]. The combination of Ca^{2+}, HPO_4^{2-} and HCO_3^- ions has been proven to slow down the corrosion rate of CP Mg. If at least one of this components is absent (in the medium), corrosion rates are several times higher [38]. This is due to the immediate formation of hydroxyapatite-like precipitates that stabilizes the local pH at the surface of degrading Mg below 8.5. In contrast to the widely spread common perception, the near surface pH of Mg degrading in physiological electrolyte is not highly alkaline [18,38].

Through the comparison between the corrosion rate of Mg in MEM and complex saline solution, it was found that the combination of amino acids, vitamins and glucose leads to accelerated corrosion rates [20,39]. However, the individual effect of standalone organic components have not been reported systematically. Although, there are over 20 species in human plasma or serum, only a limited amount of amino acids, such as cysteine, arginine, glycine and aspartic acid were considered in this regards in recent studies [17,40,41]. This is also the case for works on the influence of saccharides, only glucose was taken into account [40,42,43], although saccharides like galactose (for children), glucosamine and fructose also have relatively high concentration in plasma/serum. In addition, the effect of vitamins on corrosion of magnesium has not been considered systematically, even though several vitamins were found to inhibit corrosion of magnesium or other metals [44,45]. A number of other organic components in plasma/serum which are not included in common test media have also been tested as corrosion inhibitors [45]. Although the influence of a few organic components in plasma/serum on the corrosion of magnesium have been investigated, the concentration of the most of them in plasma/serum is one, two or even three orders of magnitude lower than the concentrations tested in previous reports [45,46]. However, it is well known that the influence of organic compounds on the corrosion of magnesium is strongly concentration dependent [45]. Thus, the limited understanding of the influence of the organic components at low concentration on the corrosion of magnesium restricts the development of *in vitro* corrosive media.

Except these small-molecule organic components from plasma/serum, other organic components that are often included in common test media also need to be considered, such as phenol red and penicillin with streptomycin. Phenol red is a commonly used pH indicator. It is added to the MEM cell culture media at low concentration (2.82×10^{-5} M). The combination of penicillin and streptomycin is often employed to avoid or delay the bacterial contamination in the *in vitro* cytocompatibility test of magnesium [47–49]. In our previous work, both the penicillin and the streptomycin at the concentration of 0.05 M were found to have a significant accelerating effect on the corrosion of magnesium in NaCl solution [45]. This, however, does not necessarily mean that the commercially available antibiotic penicillin-streptomycin accelerates the corrosion of magnesium when it is added in the cell culture media, since only the low amount of penicillin-streptomycin (1 vol. %) typically added to MEM. Common concentrations in MEM are 100 unit/ml for penicillin and 0.1 mg/ml for streptomycin, thus, the concentrations of both penicillin and streptomycin are around 10^{-4} M.

In this study, 53 bio-relevant organic compounds constituting plasma/serum or cell culture media were selected for investigation. The hydrogen evolution tests were performed to elucidate the influence of these organic components on the corrosion of magnesium. The individual and combined influence of group of amino acids was revealed, as well as the group of vitamins and saccharides. The influence of penicillin and streptomycin at different concentration on the corrosion of magnesium in MEM and SBF was also discussed. The main purpose of this work is to elucidate the influence of individual antibiotics, amino acids, vitamins, saccharides and their combinations on the corrosion of magnesium. This might contribute to better understanding of discrepancy of the *in vivo* vs *in vitro* corrosion rate of magnesium alloys and will help to facilitate the development of an appropriate corrosive media for *in vitro* corrosion tests.

2. Experimental

As-cast commercially pure Mg (CP Mg) and Mg-0.8Ca alloy were used in this study. These two materials are commonly used in biomedical research and they are also representatives for two types of magnesium alloy: Mg-0.8Ca includes anodically active second phases, while CP Mg suffers from iron-rich impurities acting as cathodic second phases. Optical discharge emission spectroscopy (SPECTROLAB with Spark Analyser Vision software, Germany) was employed to check the elemental composition of two materials, the results are listed in Table 1. In the hydrogen evolution tests, small metallic chips (produced by milling machine), which have large surface area (CP Mg: 47.7 ± 5.0 cm^2/g; Mg-0.8Ca: 52.3 ± 3.8 cm^2/g), was used instead of bulk samples.

The eudiometers (Art. Nr. 2591-10-500 from Neubert-Glas, Germany) combined with an electronic balance (OHAUS, SKX series) were used to perform the hydrogen evolution tests. 0.50 g of metallic chips were placed in a eudiometer container with 500 mL of electrolyte. During the test period, the electrolyte was constantly agitated by a magnetic stirrer. Fig. 1 shows the schematic of a eudiometer used for H_2 evolution test. Compared with the device described earlier [45], a distinct feature of the updated setup is that the corrosion rate was recorded automatically, and hence the change of corrosion rate could be recorded in more detail. Similar with previous works [50–52], the weight of water displaced from the eudiometer by evolved hydrogen was measured by the balance. The values were recorded every 15 min using USB data logger (OHAUS, 30268984) which is a great advantage compared to manual data recording (especially concerning overnight measurements). To process the obtained balance data files and to draw the hydrogen evolution plots in real time an in-house Python script was developed.

Three different basic electrolytes were used in this study, namely 0.85 wt. % NaCl solution (isotonic solution), complex saline solution (SBF, refer to [53] without Tris/HCl buffer) and Minimum Essential Media (MEM, Thermofisher, 61100-103). The detailed composition of these electrolytes is listed in Table 2. The HBSS (Hank's balance salt solution) is also shown for comparison since it is often used for corrosion testing of magnesium. Although SBF was used in this study instead of HBSS, based on published works [18,38,45] and our research result, the corrosion behavior of magnesium in these two media is comparable to their similar composition. To test the influence of individual organic components, 0.85 wt. % NaCl solution was used. Organic components were used as additives dissolved in NaCl, SBF or MEM and tested at initial pH of 6.8 ± 0.5 adjusted by NaOH or HCl. According to ref.

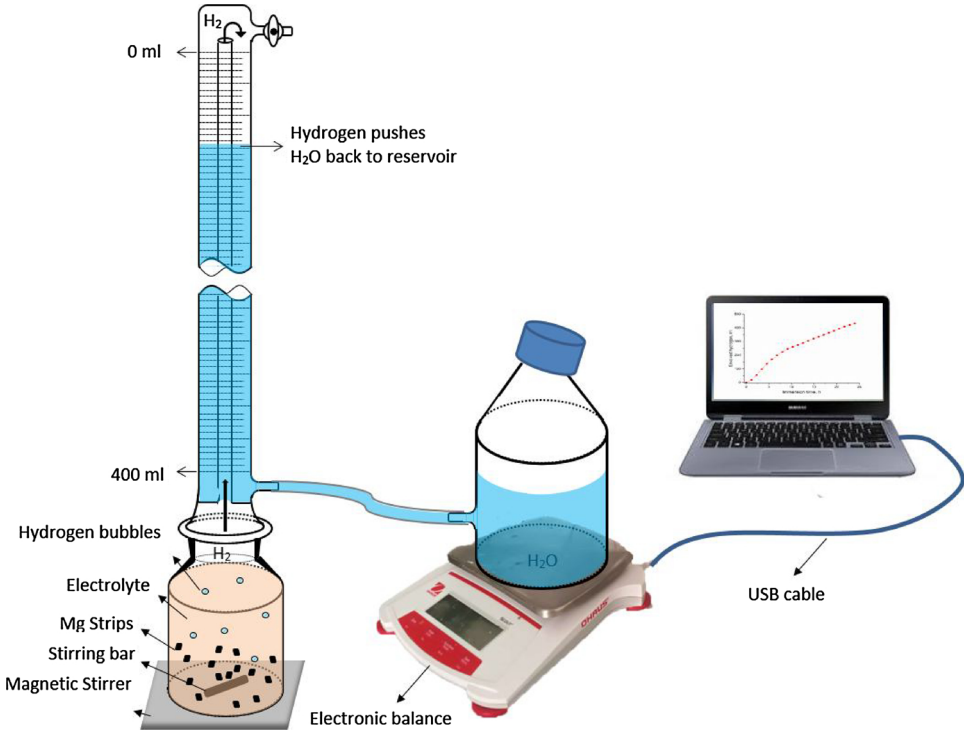

Fig. 1. The schematic setup of an eudiometer experiment used for H_2 evolution test.

Table 2
The compositions of three basic electrolytes (HBSS is also listed for comparison).

	Concentration/ mM			
	0.85 wt. % NaCl	SBF	MEM	HBSS
Na^+	145.4	142.0	144.4	142.5
K^+	–	5.0	5.3	5.8
Mg^{2+}	–	1.5	0.8	0.9
Ca^{2+}	–	2.5	1.8	1.3
Cl^-	145.4	147.8	126.1	146.8
HCO_3^-	–	4.2	26.2	4.2
HPO_4^{2-}/ H_2PO_4-	–	1.0	1.0	0.8
SO_4^{2-}	–	0.5	0.8	0.4
Synthetic pH buffer (i.e. Tris/ HCl, HEPES)	No	No	No	No
Amino acids (13 kinds)	–	–	848.0 mg/L	–
Vitamins (8 kinds)	–	–	8.1 mg/L	–
Glucose	–	–	5.5	5.5
Phenol red	–	–	10 mg/L	–
Initial pH value	5.6-5.9	7.35-7.45	7.0-7.4	7.0-7.4

[46,54,55], the concentration of each organic component was chosen so as to correspond to the concentration of this component in the blood plasma or MEM electrolyte. The individual and then combined influence of 20 common amino acids, 9 water-soluble vitamins, 4 saccharides were tested in NaCl and subsequently in SBF at initial pH of 7.1 ± 0.3 adjusted by NaOH/HCl. The influence of penicillin and streptomycin of three different concentrations was tested in MEM and SBF (where they are typically added to prevent the microbial growth). The impact of the investigated additives on the corrosion of magnesium is described by the inhibition efficiency (IE/ %), calculated according to H_2 evolution values after 20 h by the following equation:

$$IE/\ \%= \frac{V_{Reference} - V_{Additive}}{V_{Reference}} \times 100\,\%$$

Hydrogen evolution tests in reference solutions were repeated 3–6 times for reliability. The influence of groups or part of individual tests (which impact is relatively high) were repeated 2 or 3 times to verify the reproducibility.

For the electrochemical impedance spectroscopy (EIS) measurements, a conventional three-electrode setup was used, including of a working electrode (exposure area of 0.5 cm^2, electrolyte volume of 330 mL), a Pt wire coil counter electrode and a saturated Ag/AgCl reference electrode. Bulk samples (13 × 13 x 4 mm for CP Mg and 15 × 15 x 4 mm for Mg-0.8Ca) were used for the EIS. The samples were ground to 1200 grit with SiC paper before measurement, cleaned with ethanol and dried by pressurized air stream. EIS measurements were performed at open circuit potential (OCP), applying a sinusoidal perturbation with an amplitude of 10 mV RMS over a frequency range from 100 kHz to 0.1 Hz. The EIS curves were obtained by using a Gamry Interface 1000 potentiostat/galvanostat under constant steering condition at room temperature.

A scanning electron microscopy (TESCAN, Vega3 SB) was used to observe the surface morphologies of corroded magnesium and the chemical composition was obtained by the equipped energy dispersive X-ray spectrometer (EDS).

3. Results

3.1. The hydrogen evolution tests in three reference solutions

Fig. 2 shows the comparison of H_2 evolution curves of CP Mg by using automated and manual recording. The two curves in the same electrolyte are close to identical. It indicates that the automated recording function of the H_2 evolution test device works well. The average volume of evolved H_2 after 20 h immersion in each of these three electrolytes are listed in Table 3 and used as the references in the following work.

The corrosion rate for both investigated materials increases in the order SBF < MEM < NaCl, whereas the impact on the corrosion rate of CP Mg is significantly higher. These results are in good agreement with a study by Yamamoto [20] et al. In SBF, the combination of Ca^{2+},

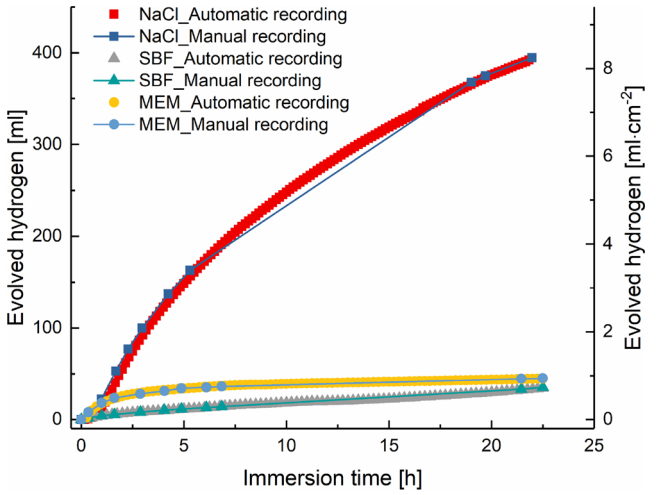

Fig. 2. Comparison of H_2 evolution test results of CP Mg by using automated recording and manual recording (in three basic electrolytes).

Table 3
The volumes of evolved H_2 after 20 h immersion in three reference solutions.

Reference solutions	H_2 evolved after 20 h immersion/ mL	
	Mg-0.8Ca	CP Mg
0.85 wt. % NaCl	62.8 ± 3.4	386.1 ± 22.7
SBF	32.1 ± 4.5	32.3 ± 6.5
MEM	44.4 ± 1.3	43.8 ± 1.3

Mg^{2+}, HPO_4^{2-} and HCO_3^- ions stimulates the formation of thin protective layer of hydroxyapatite-like compounds on the surface of Mg [38]. Compared with the corrosion rate of magnesium in SBF, CP Mg degraded more than 10 times faster in the NaCl solution. The corrosion rate of Mg-0.8Ca in NaCl solution was also two times faster compared to that in SBF. In MEM, the presence of organic components (amino acids, vitamins, glucose) led to a slight acceleration of the corrosion rate. It is noteworthy that, a great difference of corrosion rates of Mg-0.8Ca and CP Mg was observed in simple NaCl solution while the corrosion rate of the two tested materials is virtually identical in SBF and MEM electrolytes. This highlights the dominating role of the electrolyte on the degradation rate of magnesium.

3.2. Influence of amino acids on the corrosion of Mg-0.8Ca and CP Mg

The individual influence and the group effect of 20 amino acids which take part in the formation of protein [56] on the corrosion of CP Mg and Mg-0.8Ca is listed in Table 4. Additional four amino acids of relatively higher concentration in plasma or serum were also tested.

It is found that almost all of the amino acids accelerate the corrosion of Mg-0.8Ca, but the acceleration effect is not significant. 13 amino acids out of tested 24 exhibited weak inhibiting effect for the corrosion of CP Mg. The insignificant effects can be attributed to the low concentration of all the amino acids. In the case of Mg-0.8Ca alloy, the Mg_2Ca phase being the anode in the micro-galvanic coupling to the alloy matrix. In the early published works, Mg_2Ca phase was once regarded as cathodic phase in the galvanic couple between Mg_2Ca and α-Mg [57–59]. However, as the understanding deepens, more detail investigations prove the more negative corrosion potential of Mg_2Ca compared to Mg matrix [60–65]. The different corrosion mechanisms of Mg-0.8Ca and CP Mg lead to the dissimilar influence of amino acids on the corrosion of Mg-0.8Ca and CP Mg. The combination of the amino acids dissolved in NaCl has an additive effect. Corrosion of Mg-0.8Ca was accelerated by 70%, while corrosion of CP Mg was inhibited by 26% on average. However, the group effect of amino acids approaches zero when both Mg materials are exposed to SBF.

In this section, corrosion acceleration (for Mg-0.8Ca) and inhibition (for CP Mg) induced by the combination of amino acids observed in NaCl solution is leveled out once the same materials are exposed to SBF electrolytes containing the same combination of the amino acids.

Although most of amino acids tested individually have no significant influence on the corrosion of CP Mg, cysteine that forms complexes with Fe^{3+} characterized by high stability constants [66,67], demonstrates moderate inhibition effect on the corrosion of CP Mg. This is in good agreement with recent studies on the inhibition effect of iron complexing agents on the corrosion of pure Mg [68,69]. On the contrary, cysteine accelerates the corrosion of Mg-0.8Ca. This can be explained by the weaker influence of iron impurities on the corrosion of Mg-0.8Ca in conjunction with the ability of cysteine to bind with Ca^{2+} and Mg^{2+} [67] which is the predominant factor concerning this alloy. Hence, Mg-0.8Ca corrodes at higher rates in the presence of cysteine.

3.3. Influence of vitamins on the corrosion of Mg-0.8Ca and CP Mg

In this part, nine water soluble vitamins, namely ascorbic acid and eight different B vitamins, were tested. The results are listed in Table 5.

The individual and cumulative effect of nine tested vitamins on the corrosion of CP Mg and Mg-0.8Ca in NaCl solution was low in both NaCl and SBF solutions. This is most likely due to the very low concentration of the vitamins in the testing solutions. It has been shown earlier, that 0.05 M solutions of folic and ascorbic acids possess high inhibiting effect to several magnesium alloys, including CP Mg [45].

3.4. Influence of saccharides on the corrosion of Mg-0.8Ca and CP Mg

In this section, four monosaccharides (glucose, galactose, glucosamine and fructose) were tested. The results are listed in Table 6.

Glucosamine was found to cause a significant acceleration effect concerning the corrosion of Mg-0.8Ca alloy. This has also impacted the cumulative effect of saccharides measured in NaCl solution, while the acceleration waned in SBF. The group effect of saccharides was low on the corrosion of CP Mg in NaCl solution, which is in line with negligible influence of four individual saccharides. Surprisingly, the mixture of saccharides caused a strong acceleration of corrosion of CP Mg when added to SBF. This might be attributed to the complexation reaction between glucosamine and Ca^{2+} contained in SBF. A reasonable assumption is that the reaction leads to depletion of Ca^{2+} in SBF solution and this retards the formation of hydroxyapatite-like protective layer. Similarly, the acceleration effect of glucosamine on the corrosion of Mg-0.8Ca might be associated with the reaction between glucosamine and Ca^{2+} dissolved from the alloy. However, the stability constant of the complexes formed by Ca^{2+} and glucosamine is not available and fully grounded conclusion cannot be drawn.

Barring glucosamine, the other tested saccharides only influence the corrosion of Mg-0.8Ca and CP Mg slightly. Glucose is a component in common corrosive media, such as HBSS solution [70] and cell culture media [71]. It has been found to accelerate the corrosion of pure Mg and several Mg alloys [40,42,43,45]. However, the test concentration of glucose (2 g/L-50 g/L) in previous works were higher than the concentration in this work (1 g/L equal 5.5 mM contained in HBSS), while concentration of glucose in blood plasma varies around 0.6–1 mM for healthy adults. In a recent work, glucose with the concentration of 1 g/L was found to decrease the corrosion rate of AZ31 [72]. Comparing the published results and the results of this work, we conclude that the influence of glucose on the corrosion of magnesium is typically weak but concentration and alloy dependent.

Table 4
The individual influence and the group effect of amino acids on the corrosion of Mg-0.8Ca and CP Mg. (Red background color means the compound accelerates corrosion, IE < 0%; Yellow color means weak inhibition effect, 0% < IE < 40%; Green color means relatively moderate inhibition effect, IE > 40%; The same color-code is used in all the tables in this paper).

Amino acid	Concentration/ M	Mg-0.8Ca		CP Mg		Medium (Initial pH)
		Volume of H_2 (20 h) / mL	IE/ %	Volume of H_2 (20 h) / mL	IE/ %	
Alanine	8.53×10^{-4}	65.9	-5	424.8	-10	
Serine	1.90×10^{-4}	63.4	-1	338.4	12	
Aspartic	9.01×10^{-5}	55.6	11	374.2	3	
Proline	4.95×10^{-4}	74.6	-19	403.8	-5	
Glutamic	1.90×10^{-4}	66.8	-6	391.8	-1	
Cysteine	4.13×10^{-4}	82.3±7.3	-31±11	262.2±26.5	32±7	
Glycine	7.19×10^{-4}	69.1	-10	377.1	2	
Asparagine	1.00×10^{-4}	67.9±5.5	-8±8	353.1±28.3	9±7	
Leucine	3.96×10^{-4}	64.1	-2	375.3	3	
Isoleucine	3.20×10^{-4}	68.2	-9	364.8	6	NaCl (pH 6.8±0.5)
Methionine	1.01×10^{-4}	65.1	-4	375.1	3	
Arginine	2.07×10^{-4}	70.0	-12	389.2	-1	
Histidine	2.45×10^{-4}	71.7	-14	356.1	8	
Valine	3.59×10^{-4}	78.9±6.9	-26±11	406.4±1.4	-5±1	
Tryptophan	1.47×10^{-4}	68.2	-9	403.7	-5	
Threonine	2.69×10^{-4}	70.4	-12	388.0	0	
Phenylalanine	2.42×10^{-4}	73.4	-17	377.0	2	
Glutamine	7.25×10^{-4}	78.9	-26	401.3	-4	
Lysine	3.97×10^{-4}	68.9	-10	396.6	-3	
Tyrosine	1.38×10^{-4}	78.8	-26	375.4	3	
All above listed amino acids tested together		107.6±11.3	-70±18	285.1±15.7	26±4	NaCl (pH 6.8±0.5)
		29.0±6.0	11±18	30.4±1.4	5±4	SBF (pH 7.1±0.3)
Ornithine	1.06×10^{-4}	68.1	-8	391.4	-1	
α-Aminobutyric acid	1.94×10^{-5}	62.8	0	375.1	3	NaCl (pH 6.8±0.5)
Taurine	1.68×10^{-4}	72.2	-15	396.8	-3	
Cystine	9.90×10^{-5}	83.2±5.2	-34±8	303.4±14.5	21±4	

3.5. Influence of several organic compounds from Krebs cycle and other organic components on the corrosion of Mg-0.8Ca and CP Mg

In this section, several compounds participating in the Krebs cycle as well as other organic components present in plasma/serum and MEM were tested. The individual influence of these organic components on the corrosion of CP Mg and Mg-0.8Ca is listed in Table 7. Part of them have been previously tested as corrosion inhibitors for magnesium alloys [45]. Similar to the results in other sections, most of the chemicals of low concentration have minor influence on the corrosion of Mg-0.8Ca and CP Mg.

The influence of phenol red, a commonly used pH indicator, is rather weak. This supports the applicability of phenol red in cell culture media. Unlike the other chemicals, lecithin, a type of surfactant, emulsifies in aqueous solution and possesses certain inhibiting effect for both alloys. Similarly, uric acid in low concentration is also a weak corrosion inhibitor for both alloys.

3.6. Influence of antibiotics on the corrosion of Mg-0.8Ca and CP Mg

Penicillin and streptomycin are common antibiotics which are typically used in cell culture media to prevent the growth of bacteria but do not occur in the human body. Typically used concentration of penicillin-streptomycin in cell culture media is around 10^{-4} M. In our

Table 5
The individual influence and the group effect of vitamins on the corrosion of Mg-0.8Ca and CP Mg.

Vitamins	Concentration/ M	Mg-0.8Ca		CP Mg		Medium (Initial pH)
		Volume of H_2 (20 h) / mL	IE/ %	Volume of H_2 (20 h) / mL	IE/ %	
Ascorbic acid (VC)	1.14×10^{-4}	64.3±1.1	-2±2	333.8±5.0	14±1	NaCl (pH 6.8±0.5)
Folic acid (VB9)	2.27×10^{-6}	64.5	-3	365.4	5	
Inositol (VB8)	3.89×10^{-5}	67.2	-7	395.9	-3	
Riboflavin (VB2)	2.66×10^{-7}	68.5	-9	362.0	6	
Pyridoxine-HCl (VB6)	4.82×10^{-6}	67.2	-7	379.5	2	
Thiamine-HCl (VB1)	2.96×10^{-6}	59.7	5	363.3	6	
Nicotinamide (VB3)	8.19×10^{-6}	65.7	-5	398.3	-3	
Choline chloride (VB4)	7.16×10^{-6}	61.5	2	421.1	-9	
Calcium pantothenate (VB5)	2.10×10^{-6}	64.1	-2	401.8	-4	
All above listed vitamins tested together		68.9±1.5	-10±2	347.3±34.6	10±10	NaCl (pH 6.8±0.5)
		30.3±1.0	5±3	28.4±4.8	12±15	SBF (pH 7.1±0.3)

previous work, both of them (at high concentration of 0.05 M) were found to lead to serious corrosion for tested magnesium alloys in NaCl solution [45]. Only the corrosion of CP Mg with active iron-rich intermetallic particles was inhibited [45]. Three different concentrations of streptomycin and penicillin added either to SBF or MEM were tested. The results are listed in Table 8.

The influence of penicillin and streptomycin is alloy and concentration dependent. In general, they have similar influence on the corrosion of Mg in both electrolytes. This highlights the similarities of MEM and SBF as the media for the *in vitro* tests. As shown in Table 8, the combined effect of penicillin and streptomycin on the corrosion of CP Mg and Mg-0.8Ca in MEM and SBF are less than 30% at operating concentration of 10^{-4} M. The acceleration effect of streptomycin at higher concentrations (10^{-3} M or 10^{-2} M) on both alloys is rather significant. Streptomycin has been found to inhibit the corrosion of carbon-steel in seawater [73]. It was also shown to slightly inhibit the corrosion of CP Mg in NaCl solution [45]. However, when it is tested in MEM and SBF, the reactions between streptomycin and components of the used media should be taken into account. In clinical practice, calcium gluconate or other calcium salts are commonly used in the treatment of streptomycin poisoning based on the affinity of streptomycin for Ca^{2+}. Thus, the complexation reaction decreases the concentration of Ca^{2+} in used media. This accelerates the corrosion of magnesium. In case of Mg-0.8Ca alloy, streptomycin promotes the corrosion by binding with Ca^{2+} from alloy and media.

4. Discussion

The main purpose of this work is to establish an overview on the influence of small-molecule bio-relevant organic compounds on the corrosion of magnesium rather than to investigate the corrosion mechanism of magnesium in solutions containing organic components.

Table 6
The individual influence and the group effect of saccharides on the corrosion of Mg-0.8Ca and CP Mg.

Saccharides	Concentration/ M	Mg-0.8Ca		CP Mg		Medium (Initial pH)
		Volume of H_2 (20 h) / mL	IE/ %	Volume of H_2 (20 h) / mL	IE/ %	
Glucose	5.83×10^{-3}	76.5	-22	399.2	-3	NaCl (pH 6.8±0.5)
Galactose	1.11×10^{-3}	69.1	-10	362.8	6	
Glucosamine	4.97×10^{-3}	106.5±0.5	-69±1	386.5±0.3	0±1	
Fructose	4.44×10^{-4}	71.8	-14	374.5	3	
All above listed saccharides tested together		114.4±4.4	-82±7	369.1±7.7	4±2	NaCl (pH 6.8±0.5)
		29.7±6.4	8±20	41.2±1.6	-33±5	SBF (pH 7.1±0.3)

Table 7
The individual influence of several other organic components on the corrosion of Mg-0.8Ca and CP Mg.

Organic components	Concentration/ M	Mg-0.8Ca		CP Mg		Medium (Initial pH)
		Volume of H_2 (20 h) / mL	IE/ %	Volume of H_2 (20 h) / mL	IE/ %	
Phenol red	2.82×10^{-5}	66.5	-6	362.5	6	NaCl (pH 6.8±0.5)
β-Hydroxybutyric acid	9.00×10^{-6}	65.2	-4	391.4	-1	
Lactate	2.20×10^{-3}	62.6	0	395.1	-2	
Glucuronic acid	5.67×10^{-5}	66.9	-6	360.9	7	
Malic acid	6.70×10^{-5}	69.6	-11	375.3	3	
Creatinine	1.00×10^{-4}	79.5	-27	392.2	-2	
Glycerol	1.87×10^{-4}	60.2	4	399.5	-3	
Urea	6.66×10^{-3}	67.7	-8	340.1	12	
Uric acid	4.82×10^{-4}	51.9±4.4	17±7	294.8±23.2	24±6	
Citric acid	1.66×10^{-4}	60.3	4	356.9	8	
Succinic acid	4.23×10^{-5}	68.4	-9	397.2	-3	
Acetone	3.44×10^{-4}	65.0	-3	377.2	2	
Pyruvic acid	1.40×10^{-4}	72.7	-16	426.5	-10	
Lecithin	2.25 g/L	53.1±6.3	14±1	267.4±3.9	31±1	NaCl (pH 6.8±0.5) (emulsion)

Table 8
The influence of antibiotics on the corrosion of Mg-0.8Ca and CP Mg.

Antibiotics	Concentration/ M	Mg-0.8Ca		CP Mg		Medium (Initial pH)
		Volume of H_2 (20 h) / mL	IE/ %	Volume of H_2 (20 h) / mL	IE/ %	
Penicillin (Penicillin G sodium salt)	1×10^{-4} (0.036 g/L)	40.9±1.8	8±4	33.3±3.5	25±8	MEM (pH 7.1±0.3)
	1×10^{-3} (0.356 g/L)	29.7±5.7	33±13	43.4±4.4	1±11	
	1×10^{-2} (3.563 g/L)	34.6±5.3	23±12	43.4±9.2	3±21	
Streptomycin (Streptomycin sulfate salt)	1×10^{-4} (0.073 g/L)	36.3±1.3	18±3	40.3±2.7	8±6	
	1×10^{-3} (0.729 g/L)	79.9±2.6	-80±6	38.5±1.2	13±3	
	1×10^{-2} (7.287 g/L)	93.8±17.6	-115±40	95.5±17.9	-127±40	
Penicillin + Streptomycin	$1 \times 10^{-4} + 1 \times 10^{-4}$ (0.036 g/L + 0.073g/L)	36.9±1.3	17±3	33.9±1.9	23±4	
Penicillin (Penicillin G sodium salt)	1×10^{-4} (0.036 g/L)	23.9±7.5	26±23	17.7±0.5	45±2	SBF (pH 7.1±0.3)
	1×10^{-3} (0.356 g/L)	17.8±0.6	45±2	24.8±4.8	23±14	
	1×10^{-2} (3.563 g/L)	20.4±1.5	36±5	15.9±0.8	51±2	
Streptomycin (Streptomycin sulfate salt)	1×10^{-4} (0.073 g/L)	29.5±4.7	8±15	28.4±6.1	12±18	
	1×10^{-3} (0.729 g/L)	22.0±0.3	31±1	24.1±2.9	25±9	
	1×10^{-2} (7.287 g/L)	57.0±8.5	-78±26	45.3±0.8	-40±3	
Penicillin + Streptomycin	$1 \times 10^{-4} + 1 \times 10^{-4}$ (0.036 g/L + 0.073g/L)	26.0±1.5	19±5	28.5±7.4	12±23	

Table 9
The individual influence of selected organic compounds (at higher concentration) on the corrosion of Mg-0.8Ca and CP Mg.

Selected additives	Concentration/ M	Mg-0.8Ca Volume of H_2 (20 h) / mL	Mg-0.8Ca IE/ %	CP Mg Volume of H_2 (20 h) / mL	CP Mg IE/ %	Medium (Initial pH)
Cysteine	4.13×10^{-4}	82.3±7.3	-31±11	262.2±26.5	32±7	NaCl (pH 6.8±0.5)
	5.00×10^{-3}	100.9	-61	227.5	43	
	1.00×10^{-2}	127.9	-104	269.6	30	
Uric acid	4.82×10^{-4}	51.9±4.4	17±7	294.8±23.2	24±6	
	5.00×10^{-3}	34.2	46	85.3	80	
	1.00×10^{-2}	63.42	-1.0	104.0	73.1	
Ascorbic acid (VC)	1.14×10^{-4}	64.3±1.1	-2±2	333.8±5.0	14±1	
	5.00×10^{-3}	20.1	68	104.9	73	
	1.00×10^{-2}	30.8	51	82.0	79	
Lecithin	2.25 g/L (added)	53.1±6.3	14±1	267.4±3.9	31±1	NaCl (pH 6.8±0.5) (emulsion)
	5.00 g/L (added)	52.5	16	267.9	31	
	10.00 g/L (added)	50.6	20	220.9	43	

Although most of tested organic components at low concentration have no significant influence on the corrosion of CP Mg and Mg-0.8Ca, a number of interesting findings emerge from the results.

4.1. Influence of selected additives at higher concentration

The influence of individual amino acids on corrosion is somewhat different compared to the data previously reported [45,74]. Helal [74] et al. reported the inhibiting effect of a number of amino acids (tested at the concentration of 10^{-3} M) in chloride-free phthalate electrolyte measured for AZ71 alloy. In our previous paper, much higher concentrations of amino acids, namely 0.05 M, have been tested [45]. A decline in IE was clearly observed with decreasing concentration of amino acid. Among the amino acids tested in this study, cysteine at low concentration has relatively significant inhibition effect on the corrosion of CP Mg. Thus, its inhibition effect at higher concentration for CP Mg and Mg-0.8Ca was also tested (as shown in Table 9). It could be shown that the increase of the cysteine concentration led to an increase of IE for CP Mg. However, further increase in cysteine concentration (10 mM) lowers its IE. A similar result for Zn alloy was found by Shkirskiy et al. [75]. However, its effect on Mg-0.8Ca corrosion becomes more negative with the increase of concentration.

Selected organic compounds were also tested at higher concentrations, the results are shown in Table 9. All tested compounds exhibit a higher corrosion inhibition effect for CP Mg than for Mg-0.8Ca alloy. Lecithin at high concentration demonstrated limited corrosion inhibition effect owing to its emulsification rather than solubility. The ascorbic acid was the most effective corrosion inhibitor for both alloys with highest inhibiting efficiency reaching 79%.

4.2. The similar corrosion behaviors of Mg alloys in both MEM and SBF

Apart from the inorganic components common for SBF and MEM, the latter contains a variety of organic components, including amino acids, vitamins and glucose, which are mandatory for cell growth. In this study, it could be found that the organic compounds tested at physiological concentrations have no significant influence on the corrosion rate of magnesium. The addition of low concentration of antibiotics in both MEM and SBF also has limited influence on the corrosion of magnesium. This fact indicates the similarity of magnesium corrosion in both MEM and SBF.

The evolution of EIS spectra of CP Mg and Mg-0.8Ca was investigated in 0.85 wt. % NaCl, MEM and SBF for 24 h. Fig. 3 shows the Bode plots of CP Mg and Mg-0.8Ca after different immersion duration in three electrolytes. An interesting finding is that the hydrogen evolution and the evolution of impedance spectra are very similar for both alloys in MEM and SBF. However, the EIS spectra of two tested materials differ significantly in NaCl solution. When both alloys were immersed either in MEM or in SBF electrolytes, the additional time constant at high frequencies (about 10 kHz) continuously grew as the immersion time elapsed. This fact evidences the formation of an additional partially protective layer on the surface. This is not the case for the Bode plot evolutions of CP Mg and Mg-0.8Ca in NaCl as no additional time constant appeared at high frequency range. Furthermore, the EIS evolution of both materials in MEM and SBF at first 7 h were almost the same, while the evolutions of two materials in NaCl deviate significantly. This result provides a strong support on the applicability and representativeness of SBF for the *in vitro* corrosion tests. Nevertheless, the EIS curves after 24 h immersion have differences. It could be attributed to the consumption and depletion of Ca^{2+}, HPO_4^{2-} and HCO_3^- ions in electrolytes (EIS was done in stirred electrolyte, but the medium was not refreshed). This emphasizes the notion that maintaining constant composition of the electrolyte is necessary throughout the duration of the immersion tests.

Fig. 4 shows the morphologies of corroded CP Mg and Mg-0.8Ca after 24 h immersion in MEM and SBF. The elemental compositions of corrosion products in Fig. 4 given by EDS is listed in Table 10. From the morphology and EDS results, it is clear that the products formed on different alloys in these two media have similar features, low Ca-P content product layer combined with the clusters of product with higher Ca-P content. The similar dense layer of corrosion products is in agreement with similar corrosion rate of Mg in MEM and in SBF. These results indicate that the precipitates with similar protection effect were formed on different magnesium alloys in the same electrolyte. This is

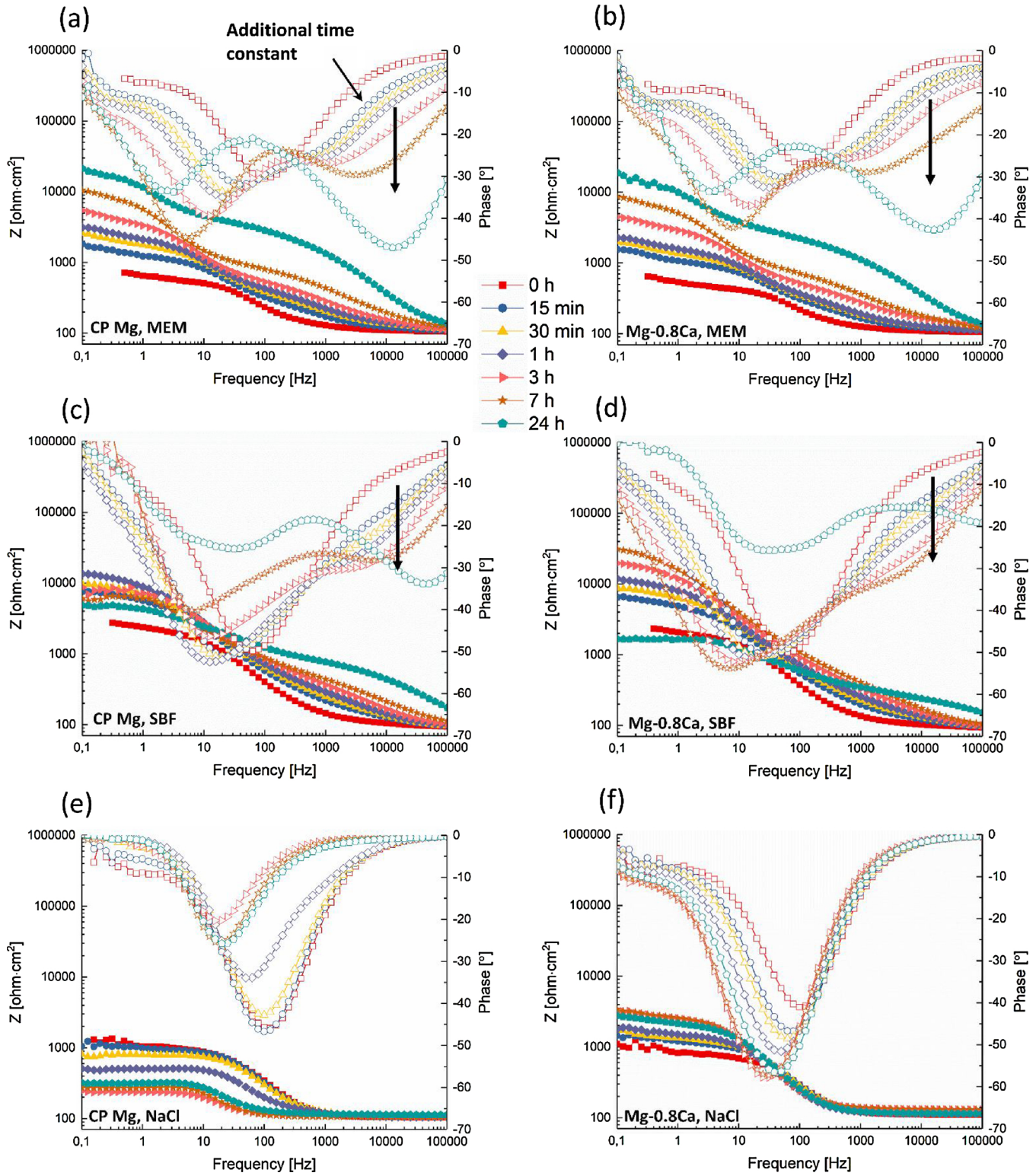

Fig. 3. Evolution of Bode plots for CP Mg (a, c, e) and Mg-0.8Ca (b, d, f) during 24 h immersion in MEM (a, b), SBF (c, d) and NaCl (e, f).

also in line with our previous work [18], similar local pH values were found during immersion of four different Mg alloys in HBSS electrolyte. The bulk pH changes of media after hydrogen evolution are shown in Fig. 5. It could be found that, even without pH buffer, the bulk pH changes of SBF and MEM after hydrogen evolution test are significantly lower than that of NaCl. The high final pH value of NaCl solution originates from the formation of $Mg(OH)_2$ products, however, it has poor blocking or passivation effect. For SBF and MEM, similar bulk pH changes reflect similar composition of main corrosion products. Fast formation of protective products layer in SBF and MEM inhibits further corrosion of magnesium and slows down the increase of pH value of media [18,38]. Similar corrosion behavior in both SBF and MEM points out the interchangeability between them. It should be noticed that the change of bulk pH of medium does not always have a direct relevance for the corrosion behavior of magnesium. For example, high corrosion rate of CP Mg has been found in the Tris-buffered SBF, even though the

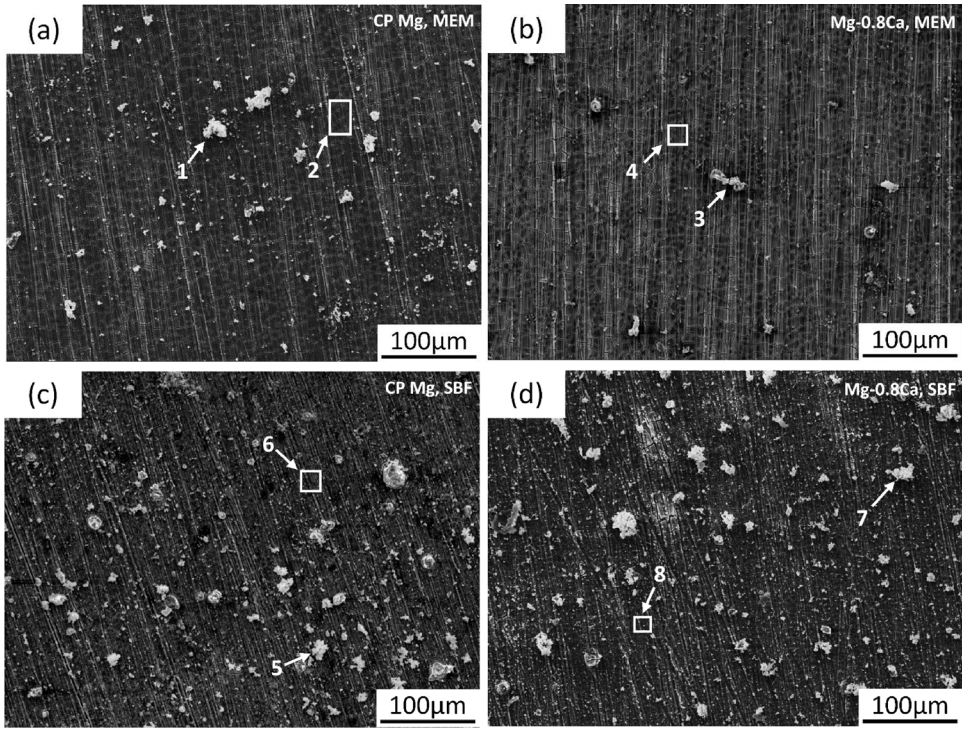

Fig. 4. Typical corrosion morphology of CP Mg (a, c) and Mg-0.8Ca (b, d) after 24 h immersion in MEM (a, b) and SBF (c, d).

bulk pH change after hydrogen evolution test was low [38]. It was explained by the continuous active surface reaction of Mg caused by Tris [38].

Our results show that the corrosion rates of tested materials in SBF and MEM are similar. However, several published works reported different results [12,76–78]. First of all, this can be explained by the fact that different materials and different test methods were used. In some cases, the corrosive media that used in published works are different with the media in this work, even though they have similar name, like SBF, m-SBF and r-SBF. HEPES and Tris, as the main components of other types of SBF, inhibit the formation of protective products layer and accelerate the corrosion of magnesium significantly [18,38,79]. In addition, cell culture media was used for the long-term *in vitro* tests at open environment, but the risk of media contamination was not always taken into account. All the above points can give rise to significantly faster degradation of Mg. This discrepancy points out to the urgent need for standardization of *in vitro* test protocols for biodegradable magnesium [80].

In this work, SBF (without synthetic pH buffer) was selected as the representative of inorganic simulated body fluids to be used. But it does not mean that the obtained results only could be applied to explain the phenomena in SBF. Other types of the inorganic simulated body fluid, like HBSS (with Ca^{2+} and Mg^{2+}, listed in Table 2) and EBSS [20], possess similar concentration of inorganic components. As we mentioned in experimental part, based on published works [18,38,45] and our research results, we believe that the corrosion behavior of magnesium in these inorganic simulated body fluid media is comparable. Therefore, the small-molecule organic components at low concentration should have similar influence on magnesium corrosion in SBF, HBSS and EBSS. In other words, the effect of small organic molecules of corrosion of Mg exposed to SBF are also relevant to the influence of these organic molecules on corrosion of Mg exposed to other inorganic simulated body fluids.

In general, the components of the electrolytes participate in the formation of the precipitates on the surface of corroded magnesium during the corrosion process. The alloy characteristics, such as composition, processing and grain orientation, obviously influences the degradation rate, while having only a limited influence on the composition and the protective ability of the precipitation layer. Two latter

Table 10
Composition of corrosion products on the CP Mg and Mg-0.8Ca given by EDS after 24 h immersion in MEM and SBF.

Sample /Electrolytes	Position	Elements/ at. %						
		C	O	Na	Mg	P	Cl	Ca
CP Mg / MEM	1	9.4	52.4	2.8	2.4	13.1	2.1	17.8
	2	9.0	37.1	1.4	37.3	8.6	0.2	6.4
Mg-0.8Ca / MEM	3	21.4	46.1	0.9	4.6	12.1	0.1	14.8
	4	9.0	35.9	1.0	39.3	8.4	0.1	6.3
CP Mg / SBF	5	8.6	49.5	2.1	3.9	17.7	0.5	17.7
	6	9.9	22.0	1.8	58.2	4.7	0.2	3.2
Mg-0.8Ca / SBF	7	8.0	50.0	0.6	5.5	16.4	0.1	19.4
	8	7.1	26.9	1.2	52.0	7.1	0.1	5.6

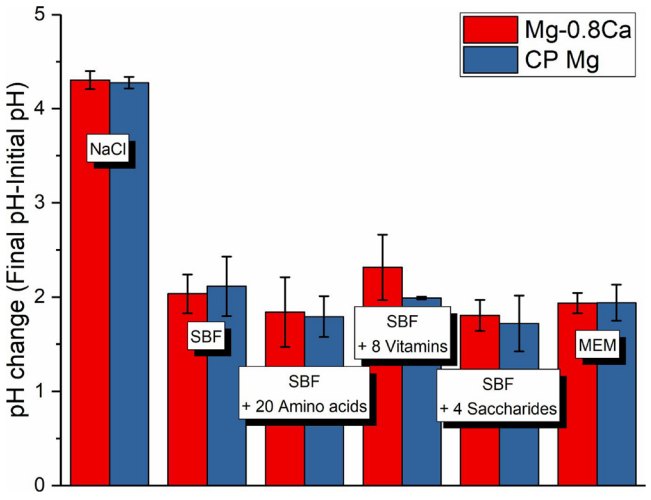

Fig. 5. The bulk pH change of selected media after hydrogen evolution test.

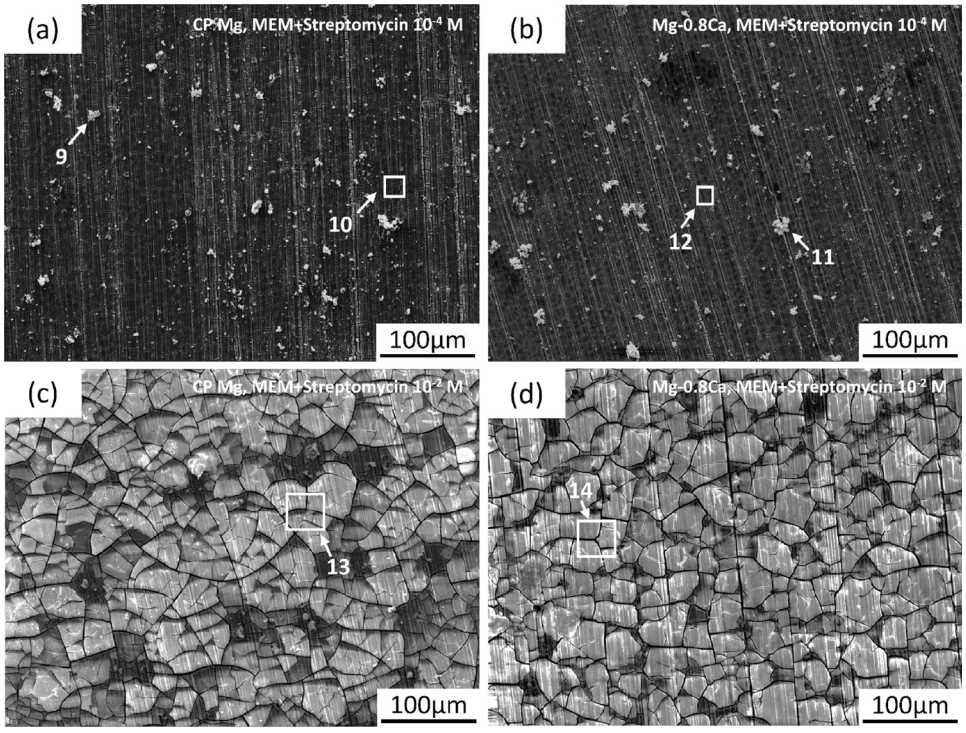

Fig. 6. Typical corrosion morphology of CP Mg (a, c) and Mg-0.8Ca (b, d) after 24 h immersion in MEM with streptomycin at the concentration of 10^{-4} M (a, b) and 10^{-2} M (c, d).

parameters are dominated by the electrolyte components. Therefore, the differences in degradation rate of magnesium alloys (caused by the elemental composition, phases and microstructural features of the materials) are best distinguished by the corrosion tests conducted in NaCl solution. These differences are leveled off during the immersion in simulated body fluids (such as SBF, HBSS, EBSS and MEM) because degradation is dominated by precipitation/conversion products especially at relatively early stages of corrosion. In line with this, similar corrosion behavior was observed for different magnesium alloys exposed either to MEM or to SBF. Although, from our results, the corrosion rate of CP Mg and Mg-0.8Ca in SBF or MEM is very similar, this might not hold true for all the magnesium alloys. However, it could be confirmed that the great difference in corrosion rate of different Mg alloys observed in simple NaCl solution is levelled off in SBF or MEM electrolytes.

4.3. The influence of streptomycin

Zhen [81] et al. reported the high corrosion rate of magnesium leads to the cells death. The corrosion rates of magnesium exposed to MEM and SBF are rather slow, but the influence of exogenous additives should be taken into account because of their potential corrosion acceleration effect. The test results indicate that addition of penicillin-streptomycin (at operating concentration) to MEM or SBF has no significant influence on the corrosion of magnesium. The cytocompatibility tests of Mg that performed presence of penicillin-streptomycin are not affected by these two antibiotics.

However, at high concentration (10^{-2} M) streptomycin significantly accelerate the corrosion of both tested materials. Fig. 6 shows the corrosion morphologies of corroded CP Mg and Mg-0.8Ca after 24 h immersion in MEM with streptomycin at the concentration of 10^{-4} M and 10^{-2} M. The compositions of corrosion products in Fig. 6 determined by EDS are listed in Table 11. It is clear that the corrosion morphologies and chemical compositions in MEM with low streptomycin concentration are similar to those in blank MEM, while the thick products and many deeper cracks appeared in the corrosion products in MEM with high streptomycin concentration (indicating poor corrosion resistance in this medium). This morphology is in good agreement with the conducted hydrogen evolution results. The evolution of EIS spectra of CP Mg and Mg-0.8Ca was investigated in MEM with streptomycin at concentration of 10^{-2} M and is shown in Fig. 7. Although the Ca-P content of corrosion products is also relatively high after 24 h immersion in MEM with high streptomycin concentration (shown in Table 11), there is no evident additional time constant observed at the

Table 11
Composition of corrosion products on the CP Mg and Mg-0.8Ca given by EDS after 24 h immersion in MEM with streptomycin at different concentration (10^{-4} M and 10^{-2} M).

Sample /Electrolytes	Position	Elements/ at. %						
		C	O	Na	Mg	P	Cl	Ca
CP Mg / MEM + 10^{-4} M	9	10.1	52.3	2.8	5.8	12.6	1.1	15.3
	10	9.5	38.7	1.7	34.0	9.0	0.2	6.9
Mg-0.8Ca / MEM + 10^{-4} M	11	15.6	57.6	0.9	4.7	9.7	0.4	11.1
	12	8.6	38.9	1.0	33.2	9.6	0.1	8.6
CP Mg / MEM + 10^{-2} M	13	9.2	57.5	1.4	5.2	12.6	0.1	14.0
Mg-0.8Ca / MEM + 10^{-2} M	14	8.5	56.3	0.9	6.1	13.3	0.1	14.8

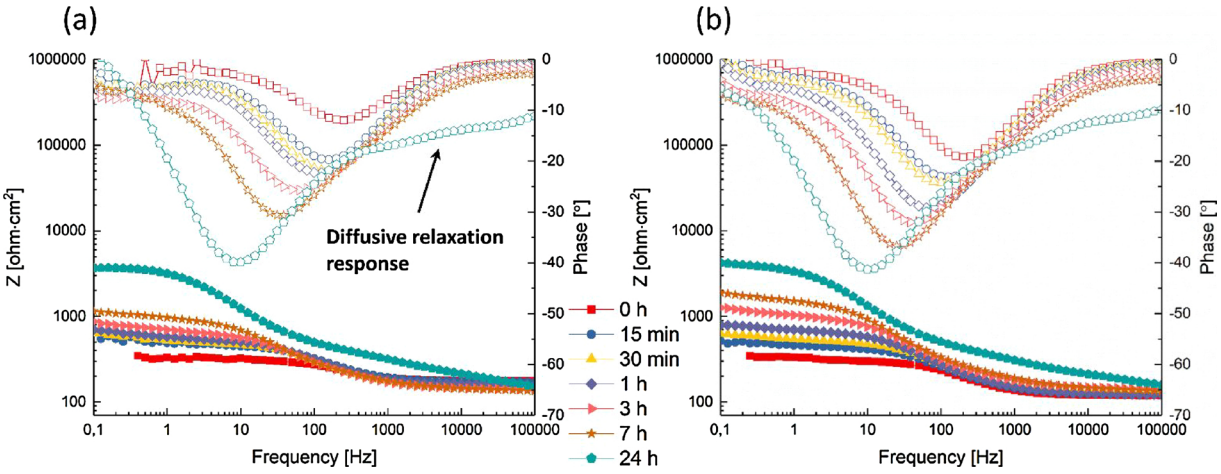

Fig. 7. Evolution of Bode plots for CP Mg (a) and Mg-0.8Ca (b) during 24 h immersion in MEM with streptomycin at concentration of 10^{-2} M.

high frequency range (shown in Fig. 7). Only after 24 h, a very diffusive relaxation response with minor barrier properties can be evidenced. Besides, the values of the low frequency impedance for both alloys at the earlier hours of immersion were one order of magnitude lower than that when the alloys were exposed to streptomycin-free SBF and MEM, compare to Fig. 3. This means that the formation of Ca-containing protective layer is delayed significantly suggesting possible complex formation between Ca^{2+} and streptomycin. This decreases the concentration of free Ca^{2+} in MEM and delays the formation of initially partially protective layer which is critical for the corrosion protection of magnesium in these media [38]. Apart from complex formation between streptomycin and Ca^{2+}, the possible complexation reactions between antibiotics and other metal ions might influence the corrosion behavior of other Mg alloys more significantly. Therefore, moderate caution is still necessary when adding antibiotics in the various tests media. Consequently, the affinity of antibiotics for ions like Ca^{2+} needs to be taken into account for future studies.

4.4. Additional remarks and outlook

All the tests in this work were carried out at ambient temperature (AT), while bio-degradation tests are usually done at 37 °C. Typically, the higher temperature leads to faster corrosion and can also shift chemical equilibria. However, Wagener et al. [32] compared the corrosion behavior of CP Mg in DMEM and SBF at AT and 37 °C. They concluded that the temperature only shows minor influence during the *in vitro* corrosion tests.

In this work, we have tested 53 chemicals, focusing only on the influence of small-molecule organic components on the corrosion of magnesium. The results shows that they have no critical influence on the corrosion of tested materials. A number of studies, which investigated the structure and chemical composition of Mg corrosion products exposed to cell culture media, suggested that the organic molecules influence the formation of corrosion products on magnesium [17,82]. Therefore, it is important to clarify our opinion in this case. From the research results in this work, although it could be found that the products formed on tested material in SBF and MEM have similar features. But the amount of product clusters (with higher Ca-P content) on the corroded Mg in MEM is less than that in SBF (as show in Fig. 4). It could be attributed to the presence of small-molecule organic components in MEM. Several organic components in MEM, like amino acids, were found to bind Ca^{2+} and Mg^{2+} [66]. Thus, the potential complexation reactions might influence the formation of product clusters with higher Ca-P content to certain extent. However, based on the results in this work, it could be concluded that the presence of organic compounds at low concentration does not critically influence the final corrosion rate. Similarly, streptomycin at low concentration has only low effect on degradation rate of Mg. Although the complexation effect between Ca^{2+} and streptomycin is explicit, its negative influence on corrosion rate is still not obvious at low concentration of antibiotics.

Previously, macromolecule organic components, like proteins, have been proven to have various stronger or weaker effects on the corrosion of magnesium [17,39,83–85]. These discrepancies could be attributed to the diversity of tested alloys, proteins and concentrations. Thus, the influence of protein on magnesium corrosion seems still worthy to be investigated in the future. Especially, in a recent review, Höhn [86] et al. pointed out that the interaction of protein on the surface of Mg and its effect on the formation of calcium phosphate containing products during the magnesium corrosion should be explored in more details.

The establishment of a set of appropriate *in vitro* test protocols is the target of many scientists who are working in this field. Many corrosion influencing factors have been considered, such as inorganic ions, organic compounds and macromolecules as well as medium sterilization [2,8,31,48,80,86,87]. In our recent work, we showed significant oxygen consumption as a result of cathodic oxygen reduction reaction during the corrosion of Mg [88]. The influence of oxygen might be another latent factor which leads to the discrepancy of magnesium corrosion rate measured *in vivo* and *in vitro*. Obviously, cell viability can be significantly influenced by concentration of dissolved oxygen.

Considering the diversity of *in vitro* test methods, the optimal corrosive media should be designed separately for different corrosion test methods. A single investigation does not suffice for predicting the overarching corrosion process, while a variety of *in vitro* corrosion test methods should be applied for comprehensively evaluation. In addition, because of the variety of physiological environment, different test methods or media should be employed for the implant materials that will be used in different part of body. Even so, the corrosion behavior of implant in human body is still difficult to be mimicked completely by the *in vitro* corrosion tests at present stage. In human body, a number of factors may influence the corrosion behavior, such as local inflammation (accompanied by the changes of local physiological environment) and the interaction between tissue and implant. These are difficult to mimic by *in vitro* corrosion tests. Although the experimental condition of *in vitro* corrosion tests can be made closer to the environment of real body, the *in vivo* animal trials are still irreplaceable in the developing magnesium for biomedical applications.

5. Conclusion

In this work, an automated logging of hydrogen evolution was established and experimentally tested. The individual influence and

group effect of 53 bio-relevant organic components on the corrosion of Mg-0.8Ca and CP Mg was investigated. The obtained results led us to the conclusion, that:

(1) The small-molecule organic components do not have a critical influence on the corrosion of Mg-0.8Ca and CP Mg *in vitro*. In general, the individual influence of small-molecule organic components at low concentration is not significant in NaCl solution. None of the cumulative effects of group of amino acids, vitamins and saccharides is significant when added in SBF.
(2) The addition of penicillin and streptomycin combination at 10^{-4} M in MEM also has no obvious effect on the corrosion of tested materials. However, the affinity of ions to antibiotics needs to be taken into account. Decreased concentration of free Ca^{2+} due to binding with the antibiotic results in higher corrosion rates of Mg.
(3) The individual test results point out promising corrosion inhibitors for Mg. Such as uric acid (for CP Mg) and ascorbic acid (for both CP Mg and Mg-Ca).
(4) Different magnesium alloys were found to have similar corrosion rate in the same medium (SBF or MEM). Similar corrosion behavior of the same alloy in SBF and MEM was also observed. These phenomena indicate that the corrosion of Mg in simulated body fluids (such as SBF, HBSS and MEM) is controlled by precipitation of the protective layer of corrosion products which is mainly controlled by the inorganic components of the electrolyte.
(5) The relatively simple solutions that contain all inorganic constituents (like SBF and HBSS) might be suitable *in vitro* test media for magnesium at open environment.

Data availability

The raw/processed data required to reproduce these findings cannot be shared at this time as the data also forms part of an ongoing study.

Acknowledgements

Mr. Di Mei thanks China Scholarship Council for the award of fellowship and funding (No. 201607040051). Dr. S. V. Lamaka acknowledges the financial support of Alexander von Humboldt Foundation via Experienced Researcher Grant. “MMDi” IDEA project funded by HZG is gratefully acknowledged. The technical support of Mr. Volker Heitmann and Mr. Ulrich Burmester during this work is gratefully acknowledged. The technical support of Mr. Tomasz Balicki from OHAUS Corporation is gratefully acknowledged.

References

[1] R. Zeng, W. Dietzel, F. Witte, N. Hort, C. Blawert, Progress and challenge for magnesium alloys as biomaterials, Adv. Eng. Mater. 10 (2008) B3–B14.
[2] Y.F. Zheng, X.N. Gu, F. Witte, Biodegradable metals, Mater. Sci. Eng. R Rep. 77 (2014) 1–34.
[3] Y. Chen, Z. Xu, C. Smith, J. Sankar, Recent advances on the development of magnesium alloys for biodegradable implants, Acta Biomater. 10 (2014) 4561–4573.
[4] D. Zhao, F. Witte, F. Lu, J. Wang, J. Li, L. Qin, Current status on clinical applications of magnesium-based orthopaedic implants: a review from clinical translational perspective, Biomaterials 112 (2017) 287–302.
[5] J. Wu, D. Zhao, J.M. Ohodnicki, B. Lee, A. Roy, R. Yao, S. Chen, Z. Dong, W.R. Heineman, P.N. Kumta, In vitro and in vivo evaluation of multiphase ultrahigh ductility Mg–Li–Zn alloys for cardiovascular stent application, ACS Biomater. Sci. Eng. 4 (2017) 919–932.
[6] S. Virtanen, Biodegradable Mg and Mg alloys: corrosion and biocompatibility, Mater. Sci. Eng. B 176 (2011) 1600–1608.
[7] M. Esmaily, J.E. Svensson, S. Fajardo, N. Birbilis, G.S. Frankel, S. Virtanen, R. Arrabal, S. Thomas, L.G. Johansson, Fundamentals and advances in magnesium alloy corrosion, Prog. Mater. Sci. 89 (2017) 92–193.
[8] S. Johnston, M. Dargusch, A. Atrens, Building towards a standardised approach to biocorrosion studies: a review of factors influencing Mg corrosion in vitro pertinent to in vivo corrosion, Sci. China Mater. 61 (2017) 475–500.
[9] N.T. Kirkland, N. Birbilis, M.P. Staiger, Assessing the corrosion of biodegradable magnesium implants: a critical review of current methodologies and their limitations, Acta Biomater. 8 (2012) 925–936.
[10] Z. Zhen, T.-f. Xi, Y.-f. Zheng, A review on in vitro corrosion performance test of biodegradable metallic materials, Trans. Nonferrous Met. Soc. China 23 (2013) 2283–2293.
[11] M.P. Staiger, F. Feyerabend, R. Willumeit, C.S. Sfeir, Y.F. Zheng, S. Virtanen, W.D. Müeller, A. Atrens, M. Peuster, P.N. Kumta, D. Mantovani, F. Witte, Summary of the panel discussions at the 2nd Symposium on Biodegradable Metals, Maratea, Italy, 2010, Mater. Sci. Eng. B 176 (2011) 1596–1599.
[12] A.H.M. Sanchez, B.J.C. Luthringer, F. Feyerabend, R. Willumeit, Mg and Mg alloys: how comparable are in vitro and in vivo corrosion rates? A review, Acta Biomater. 13 (2015) 16–31.
[13] Standard Guide for in Vitro Degradation Testing of Absorbable Metals, in: ASTM F3268-18a, ASTM International, 2018.
[14] E. Willbold, A. Weizbauer, A. Loos, J.-M. Seitz, N. Angrisani, H. Windhagen, J. Reifenrath, Magnesium alloys: a stony pathway from intensive research to clinical reality. Different test methods and approval-related considerations, J. Biomed. Mater. Res. A. 105 (2017) 329–347.
[15] J. Gonzalez, R.Q. Hou, E.P.S. Nidadavolu, R. Willumeit-Römer, F. Feyerabend, Magnesium degradation under physiological conditions – best practice, Bioact. Mater. 3 (2018) 174–185.
[16] A.D. Forero López, I.L. Lehr, S.B. Saidman, Anodisation of AZ91D magnesium alloy in molybdate solution for corrosion protection, J. Alloys. Compd. 702 (2017) 338–345.
[17] R.-Q. Hou, N. Scharnagl, F. Feyerabend, R. Willumeit-Römer, Exploring the effects of organic molecules on the degradation of magnesium under cell culture conditions, Corros. Sci. 132 (2018) 35–45.
[18] S.V. Lamaka, J. Gonzalez, D. Mei, F. Feyerabend, R. Willumeit-Romer, M.L. Zheludkevich, Local pH and its evolution near Mg alloy surfaces exposed to simulated body fluids, Adv. Mater. Interfaces 5 (2018) 1800169, , https://doi.org/10.1002/admi.201800169.
[19] J. Liu, X.L. Liu, T.F. Xi, C.C. Chu, A novel pseudo-protein-based biodegradable coating for magnesium substrates: in vitro corrosion phenomena and cytocompatibility, J. Mater. Chem. B 3 (2015) 878–893.
[20] A. Yamamoto, S. Hiromoto, Effect of inorganic salts, amino acids and proteins on the degradation of pure magnesium in vitro, Mater. Sci. Eng. C 29 (2009) 1559–1568.
[21] B.M. Wilke, L. Zhang, W. Li, C. Ning, C.-f. Chen, Y. Gu, Corrosion performance of MAO coatings on AZ31 Mg alloy in simulated body fluid vs. Earle’s balance salt solution, Appl. Surf. Sci. 363 (2016) 328–337.
[22] E. Willbold, X. Gu, D. Albert, K. Kalla, K. Bobe, M. Brauneis, C. Janning, J. Nellesen, W. Czayka, W. Tillmann, Y. Zheng, F. Witte, Effect of the addition of low rare earth elements (lanthanum, neodymium, cerium) on the biodegradation and biocompatibility of magnesium, Acta Biomater. 11 (2015) 554–562.
[23] Y. Feng, X. Ma, L. Chang, S. Zhu, S. Guan, Characterization and cytocompatibility of polydopamine on MAO-HA coating supported on Mg-Zn-Ca alloy, Surf. Interface Anal. 49 (2017) 1115–1123.
[24] J. Zhou, X. Zhang, Q. Li, Y. Liu, F. Chen, L. Li, Effect of the physiological stabilization process on the corrosion behaviour and surface biocompatibility of AZ91D magnesium alloy, J. Mater. Chem. B 1 (2013) 6213–6224.
[25] J. Sun, Y. Zhu, L. Meng, W. Wei, Y. Li, X. Liu, Y. Zheng, Controlled release and corrosion protection by self-assembled colloidal particles electrodeposited onto magnesium alloys, J. Mater. Chem. B 3 (2015) 1667–1676.
[26] J. Wang, Y. Zhou, Z. Yang, S. Zhu, L. Wang, S. Guan, Processing and properties of magnesium alloy micro-tubes for biodegradable vascular stents, Mater. Sci. Eng. C 90 (2018) 504–513.
[27] G.Z. Yang, H.W. Yang, L. Shi, T.L. Wang, W.C. Zhou, T. Zhou, W. Han, Z.Y. Zhang, W. Lu, J.Z. Hu, Enhancing corrosion resistance, osteoinduction, and antibacterial properties by Zn/Sr additional surface modification of magnesium alloy, ACS Biomater. Sci. Eng. 4 (2018) 4289–4298.
[28] M.B. Kannan, R. Walter, A. Yamamoto, Biocompatibility and in vitro degradation behavior of magnesium–calcium alloy coated with calcium phosphate using an unconventional electrolyte, ACS Biomater. Sci. Eng. 2 (2015) 56–64.
[29] L. Yang, L. Ma, Y. Huang, F. Feyerabend, C. Blawert, D. Höche, R. Willumeit-Römer, E. Zhang, K.U. Kainer, N. Hort, Influence of Dy in solid solution on the degradation behavior of binary Mg-Dy alloys in cell culture medium, Mater. Sci. Eng. C 75 (2017) 1351–1358.
[30] V. Wagener, S. Virtanen, Protective layer formation on magnesium in cell culture medium, Mater. Sci. Eng. C 63 (2016) 341–351.
[31] S. Johnston, Z. Shi, J. Venezuela, C. Wen, M.S. Dargusch, A. Atrens, Investigating Mg biocorrosion in vitro: lessons learned and recommendations, JOM (2019), https://doi.org/10.1007/s11837-019-03327-9.
[32] V. Wagener, S. Virtanen, Influence of electrolyte composition (Simulated body fluid vs. Dulbecco’s modified eagle’s medium), temperature, and solution flow on the biocorrosion behavior of commercially pure Mg, Corrosion 73 (2017) 1413–1422.
[33] M.-C. Zhao, M. Liu, G.-L. Song, A. Atrens, Influence of pH and chloride ion concentration on the corrosion of Mg alloy ZE41, Corros. Sci. 50 (2008) 3168–3178.
[34] Y. Xin, K. Huo, H. Tao, G. Tang, P.K. Chu, Influence of aggressive ions on the degradation behavior of biomedical magnesium alloy in physiological environment, Acta Biomater. 4 (2008) 2008–2015.
[35] R.-C. Zeng, Y. Hu, S.-K. Guan, H.-Z. Cui, E.-H. Han, Corrosion of magnesium alloy AZ31: the influence of bicarbonate, sulphate, hydrogen phosphate and dihydrogen phosphate ions in saline solution, Corros. Sci. 86 (2014) 171–182.
[36] W. Ma, Y. Liu, W. Wang, Y. Zhang, Effects of electrolyte component in simulated body fluid on the corrosion behavior and mechanical integrity of magnesium, Corros. Sci. 98 (2015) 201–210.
[37] S. Johnston, Z. Shi, A. Atrens, The influence of pH on the corrosion rate of high-purity Mg, AZ91 and ZE41 in bicarbonate buffered Hanks’ solution, Corros. Sci. 101

(2015) 182–192.
[38] D. Mei, S.V. Lamaka, J. Gonzalez, F. Feyerabend, R. Willumeit-Römer, M.L. Zheludkevich, The role of individual components of simulated body fluid on the corrosion behavior of commercially pure Mg, Corros. Sci. 147 (2018) 81–93.
[39] J. Walker, S. Shadanbaz, N.T. Kirkland, E. Stace, T. Woodfield, M.P. Staiger, G.J. Dias, Magnesium alloys: predicting in vivo corrosion with in vitro immersion testing, J. Biomed. Mater. Res. Part B Appl. Biomater. 100B (2012) 1134–1141.
[40] Y. Wang, L.-Y. Cui, R.-C. Zeng, S.-Q. Li, Y.-H. Zou, E.-H. Han, In vitro degradation of pure magnesium—the effects of glucose and/or amino acid, Materials 10 (2017) 725.
[41] Z. Fang, J. Wang, X. Yang, Q. Sun, Y. Jia, H. Liu, T. Xi, S. Guan, Adsorption of arginine, glycine and aspartic acid on Mg and Mg-based alloy surfaces: a first-principles study, Appl. Surf. Sci. 409 (2017) 149–155.
[42] L.-Y. Cui, X.-T. Li, R.-C. Zeng, S.-Q. Li, E.-H. Han, L. Song, In vitro corrosion of Mg–Ca alloy — the influence of glucose content, Front. Mater. Sci. 11 (2017) 284–295.
[43] R.C. Zeng, X.T. Li, S.Q. Li, F. Zhang, E.H. Han, In vitro degradation of pure Mg in response to glucose, Sci. Rep. 5 (2015) 13026.
[44] R. Fuchs-Godec, G. Zerjav, Corrosion resistance of high-level-hydrophobic layers in combination with Vitamin E – (α-tocopherol) as green inhibitor, Corros. Sci. 97 (2015) 7–16.
[45] S.V. Lamaka, B. Vaghefinazari, D. Mei, R.P. Petrauskas, D. Höche, M.L. Zheludkevich, Comprehensive screening of Mg corrosion inhibitors, Corros. Sci. 128 (2017) 224–240.
[46] H. Krebs, Chemical composition of blood plasma and serum, Annu. Rev. Biochem. 19 (1950) 409–430.
[47] F. Witte, F. Feyerabend, P. Maier, J. Fischer, M. Störmer, C. Blawert, W. Dietzel, N. Hort, Biodegradable magnesium–hydroxyapatite metal matrix composites, Biomaterials 28 (2007) 2163–2174.
[48] I. Marco, F. Feyerabend, R. Willumeit-Römer, O. Van der Biest, Degradation testing of Mg alloys in Dulbecco's modified eagle medium: influence of medium sterilization, Mater. Sci. Eng. C 62 (2016) 68–78.
[49] X. Song, L. Chang, J. Wang, S. Zhu, L. Wang, K. Feng, Y. Luo, S. Guan, Investigation on the in vitro cytocompatibility of Mg-Zn-Y-Nd-Zr alloys as degradable orthopaedic implant materials, J. Mater. Sci. Mater. Med. 29 (2018) 44.
[50] M. Curioni, The behaviour of magnesium during free corrosion and potentiodynamic polarization investigated by real-time hydrogen measurement and optical imaging, Electrochim. Acta 120 (2014) 284–292.
[51] M. Curioni, F. Scenini, T. Monetta, F. Bellucci, Correlation between electrochemical impedance measurements and corrosion rate of magnesium investigated by real-time hydrogen measurement and optical imaging, Electrochim. Acta 166 (2015) 372–384.
[52] S. Fajardo, G. Frankel, Gravimetric method for hydrogen evolution measurements on dissolving magnesium, J. Electrochem. Soc. 162 (2015) C693–C701.
[53] T. Kokubo, H. Takadama, How useful is SBF in predicting in vivo bone bioactivity? Biomaterials 27 (2006) 2907–2915.
[54] D. Rajdl, Clinical Biochemistry, Charles University in Prague, Faculty of Medicine in Pilsen, 2016.
[55] **55]** List of Human Blood Components, (2018) https://en.wikipedia.org/wiki/List_of_human_blood_components.
[56] I. Wagner, H. Musso, New naturally occurring amino acids, Angew. Chem. Int. Ed. Engl. 22 (1983) 816–828.
[57] W.-C. Kim, J.-G. Kim, J.-Y. Lee, H.-K. Seok, Influence of Ca on the corrosion properties of magnesium for biomaterials, Mater. Lett. 62 (2008) 4146–4148.
[58] J.-G. Kim, Y.-W. Kim, Advanced Mg-Mn-Ca sacrificial anode materials for cathodic protection, Mater. Corros. 52 (2001) 137–139.
[59] Z. Li, X. Gu, S. Lou, Y. Zheng, The development of binary Mg–Ca alloys for use as biodegradable materials within bone, Biomaterials 29 (2008) 1329–1344.
[60] A. Südholz, N. Kirkland, R. Buchheit, N. Birbilis, Electrochemical properties of intermetallic phases and common impurity elements in magnesium alloys, Electrochem. Solid-State Lett. 14 (2011) C5–C7.
[61] M. Deng, D. Höche, S.V. Lamaka, D. Snihirova, M.L. Zheludkevich, Mg-Ca binary alloys as anodes for primary Mg-air batteries, J. Power Sources 396 (2018) 109–118.
[62] Y.S. Jeong, W.J. Kim, Enhancement of mechanical properties and corrosion resistance of Mg–Ca alloys through microstructural refinement by indirect extrusion, Corros. Sci. 82 (2014) 392–403.
[63] J. Yang, J. Peng, E.A. Nyberg, F.-s. Pan, Effect of Ca addition on the corrosion behavior of Mg–Al–Mn alloy, Appl. Surf. Sci. 369 (2016) 92–100.
[64] H.R. Bakhsheshi-Rad, M.R. Abdul-Kadir, M.H. Idris, S. Farahany, Relationship between the corrosion behavior and the thermal characteristics and microstructure of Mg–0.5Ca–xZn alloys, Corros. Sci. 64 (2012) 184–197.
[65] J.W. Seong, W.J. Kim, Development of biodegradable Mg–Ca alloy sheets with enhanced strength and corrosion properties through the refinement and uniform dispersion of the Mg2Ca phase by high-ratio differential speed rolling, Acta Biomater. 11 (2015) 531–542.
[66] A. Martel, R. Smith, Critical stability constants, Amino Acids Vol. 1 Plenum Press, New York, 1974.
[67] G. Berthon, Critical evaluation of the stability constants of metal complexes of amino acids with polar side chains (Technical Report), Pure Appl. Chem. 67 (1995) 1117–1240.
[68] D. Höche, C. Blawert, S.V. Lamaka, N. Scharnagl, C. Mendis, M.L. Zheludkevich, The effect of iron re-deposition on the corrosion of impurity-containing magnesium, Phys. Chem. Chem. Phys. 18 (2016) 1279–1291.
[69] S.V. Lamaka, D. Höche, R.P. Petrauskas, C. Blawert, M.L. Zheludkevich, A new concept for corrosion inhibition of magnesium: suppression of iron re-deposition, Electrochem. Commun. 62 (2016) 5–8.
[70] J.H. Hanks, R.E. Wallace, Relation of oxygen and temperature in the preservation of tissues by refrigeration, Proc. Soc. Exp. Biol. Med. 71 (1949) 196–200.
[71] H. Eagle, Amino acid metabolism in mammalian cell cultures, Science 130 (1959) 432–437.
[72] L.-Y. Li, B. Liu, R.-C. Zeng, S.-Q. Li, F. Zhang, Y.-H. Zou, H.G. Jiang, X.-B. Chen, S.-K. Guan, Q.-Y. Liu, In vitro corrosion of magnesium alloy AZ31 — a synergetic influence of glucose and Tris, Front. Mater. Sci. 12 (2018) 184–197.
[73] M. Dehdab, Z. Yavari, M. Darijani, A. Bargahi, The inhibition of carbon-steel corrosion in seawater by streptomycin and tetracycline antibiotics: an experimental and theoretical study, Desalination 400 (2016) 7–17.
[74] N.H. Helal, W.A. Badawy, Environmentally safe corrosion inhibition of Mg–Al–Zn alloy in chloride free neutral solutions by amino acids, Electrochim. Acta 56 (2011) 6581–6587.
[75] V. Shkirskiy, P. Keil, H. Hintze-Bruening, F. Leroux, F. Brisset, K. Ogle, P. Volovitch, The effects of l-cysteine on the inhibition and accelerated dissolution processes of zinc metal, Corros. Sci. 100 (2015) 101–112.
[76] S. Agarwal, J. Curtin, B. Duffy, S. Jaiswal, Biodegradable magnesium alloys for orthopaedic applications: a review on corrosion, biocompatibility and surface modifications, Mater. Sci. Eng. C 68 (2016) 948–963.
[77] X. Gu, Y. Zheng, Y. Cheng, S. Zhong, T. Xi, In vitro corrosion and biocompatibility of binary magnesium alloys, Biomaterials 30 (2009) 484–498.
[78] Y. Li, P.D. Hodgson, Ce. Wen, The effects of calcium and yttrium additions on the microstructure, mechanical properties and biocompatibility of biodegradable magnesium alloys, J. Mater. Sci. 46 (2011) 365–371.
[79] L.-Y. Cui, Y. Hu, R.-C. Zeng, Y.-X. Yang, D.-D. Sun, S.-Q. Li, F. Zhang, E.-H. Han, New insights into the effect of Tris-HCl and Tris on corrosion of magnesium alloy in presence of bicarbonate, sulfate, hydrogen phosphate and dihydrogen phosphate ions, J. Mater. Sci. Technol. 33 (2017) 971–986.
[80] J. Wang, F. Witte, T. Xi, Y. Zheng, K. Yang, Y. Yang, D. Zhao, J. Meng, Y. Li, W. Li, Recommendation for modifying current cytotoxicity testing standards for biodegradable magnesium-based materials, Acta Biomater. 21 (2015) 237–249.
[81] Z. Zhen, X. Liu, T. Huang, T. Xi, Y. Zheng, Hemolysis and cytotoxicity mechanisms of biodegradable magnesium and its alloys, Mater. Sci. Eng. C 46 (2015) 202–206.
[82] N.A. Agha, Z. Liu, F. Feyerabend, R. Willumeit-Römer, B. Gasharova, S. Heidrich, B. Mihailova, The effect of osteoblasts on the surface oxidation processes of biodegradable Mg and Mg-Ag alloys studied by synchrotron IR microspectroscopy, Mater. Sci. Eng. C 91 (2018) 659–668.
[83] C.L. Liu, Y.J. Wang, R.C. Zeng, X.M. Zhang, W.J. Huang, P.K. Chu, In vitro corrosion degradation behaviour of Mg–Ca alloy in the presence of albumin, Corros. Sci. 52 (2010) 3341–3347.
[84] L. Yang, N. Hort, R. Willumeit, F. Feyerabend, Effects of corrosion environment and proteins on magnesium corrosion, Corros. Eng. Sci. Technol. 47 (2012) 335–339.
[85] V. Wagener, A.-S. Faltz, M.S. Killian, P. Schmuki, S. Virtanen, Protein interactions with corroding metal surfaces: comparison of Mg and Fe, Faraday Discuss. 180 (2015) 347–360.
[86] S. Höhn, S. Virtanen, A.R. Boccaccini, Protein adsorption on magnesium and its alloys: a review, Appl. Surf. Sci. 464 (2019) 212–219.
[87] A. Atrens, S. Johnston, Z. Shi, M.S. Dargusch, Viewpoint - understanding Mg corrosion in the body for biodegradable medical implants, Scr. Mater. 154 (2018) 92–100.
[88] E.L. Silva, S.V. Lamaka, D. Mei, M.L. Zheludkevich, The reduction of dissolved oxygen during magnesium corrosion, ChemistryOpen 7 (2018) 664–668.

4.4 The influence of protein on Mg corrosion

The following accepted paper was incorporated as Chapter 4.4:

D. Mei, C. Wang, S.V. Lamaka, M.L. Zheludkevich, Clarifying the influence of albumin on the initial stages of magnesium corrosion in Hank's Balanced Salt Solution, Journal of Magnesium and Alloys, (2020). https://doi.org/10.1016/j.jma.2020.07.002

D. Mei conceived and designed the study based on the discussion with S.V. Lamaka. D. Mei C. Wang and S.V. Lamaka carried out the experimental work. S.V. Lamaka and M.L. Zheludkevich gave constructive comments on data analysis. All the authors contributed to the interpretation of the results and to writing of the paper.

ARTICLE IN PRESS
JID: JMAA [m5+;August 6, 2020;14:54]

Available online at www.sciencedirect.com

ScienceDirect

Journal of Magnesium and Alloys xxx (xxxx) xxx

www.elsevier.com/locate/jma

Full Length Article

Clarifying the influence of albumin on the initial stages of magnesium corrosion in Hank's balanced salt solution

Di Mei[a,*], Cheng Wang[a], Sviatlana V. Lamaka[a], Mikhail L. Zheludkevich[a,b]

[a] *Magnesium Innovation Centre - MagIC, Institute of Materials Research, Helmholtz-Zentrum Geesthacht, Geesthacht 21502, Germany*
[b] *Institute for Materials Science, Faculty of Engineering, Kiel University, Kiel 24103, Germany*

Received 4 June 2020; received in revised form 1 July 2020; accepted 8 July 2020
Available online xxx

Abstract

The corrosion behavior of Mg, a promising biodegradable metallic material, in protein-containing pseudophysiological environment is still not fully understood. In this work, the influence of albumin on the corrosion behavior of commercially pure magnesium (CP Mg) is investigated during short-term tests in Hank's Balanced Salt Solution (HBSS). This work focuses on the reactions at the Mg/medium interface from the perspective of the interactions among albumin, media components and substrate. Hydrogen evolution tests demonstrate that the physiological amount of albumin (40 g L^{-1}) accelerates Mg corrosion in HBSS during the first few hours but slows down the degradation afterwards. The presence of albumin decreases the concentration of free Ca^{2+} in HBSS and delays formation of protective co-precipitation products on Mg surface. The evolution of local pH (differs from typically monitored bulk pH) near Mg/medium interface in albumin-containing HBSS is reported for the first time. Comparison of local and bulk pH values elucidates the pH buffering effect of albumin during the immersion period. Based on these results, adsorption, chelating and pH buffering effects are summarized as three important aspects of albumin influence on Mg corrosion. Additionally, constant replenishment of medium components is shown to be an influential factor during the Mg corrosion tests.

Keywords: Magnesium; Corrosion; Albumin; Biodegradable; Local pH.

1. Introduction

During the service period of metallic implant materials, the interaction between the implant and surrounding environment influences its surface states, which is an important factor for the degradation behavior of biodegradable metallic materials, such as Mg and its alloys [1–10]. Ion exchange, corrosion product formation and precipitation influenced by organic compounds are the important parts of these interactions. These are the research hotspots in the field of biomedical magnesium [8,9,11–18]. The synergy between inorganic ions and the formation of corrosion products on Mg surface has been clarified [19–23], the Ca^{2+}, carbonate and phosphate were found to have significant influences on Mg corrosion. Furthermore, to deepen the understanding of the in vivo degradation behavior of magnesium, a number of experimental works have focused on the influence of amino acids, vitamins, saccharides and other bio-relevant small molecule organic compounds on the Mg corrosion [24–26]. The results showed that these organic compounds influenced the corrosion behavior of Mg by altering the formation of corrosion products. However, at low, physiological concentrations, these compounds did not critically influence Mg corrosion rate.

In addition to small molecule organic compounds, the influence of macromolecule organic compounds, such as proteins, on the corrosion of magnesium has attracted a lot of deserved attention. However, there are discrepancies in the research results regarding the influence of protein on Mg corrosion in published works [6,27–29]. Liu [30] et al.

* Corresponding author.
E-mail address: di.mei@hzg.de (D. Mei).

https://doi.org/10.1016/j.jma.2020.07.002

investigated the corrosion behavior of Mg-Ca in albumin-containing NaCl solution. The results indicated that albumin at high concentrations significantly inhibited the corrosion of this alloy. Zhang [31] et al. reported that proteins slowed down the corrosion rate of Mg-Nd-Zn-Zr in cell culture medium. In contrast, Li [32] et al. investigated the influence of albumin on the corrosion behavior of Mg in Hank's Balanced Salt Solution (HBSS) and found that albumin inhibited Mg corrosion in the first 6 h but accelerated corrosion after long immersion times. Harandi [33] et al. provided similar results that BSA (bovine serum albumin) slowed the corrosion rate of magnesium in HBSS during the first 2 days and then increased it. Besides, Walker [27] et al. reported that the corrosion rate of several magnesium alloys in protein-containing MEM was significantly higher than that in Minimum Essential Medium (MEM), Earle's balanced salt solution (EBSS) and in vivo. Similar results were also proposed by Gu [34] et al. Certainly, these discrepancies may be attributed to different composition of test media, tested materials, and test conditions, e.g. static vs. dynamic. In addition, long-term tests in protein-containing media in an open environment allow for the growth of microbial life, which may significantly affect Mg corrosion [35,36].

At the present stage, the mechanistic understanding of the protein influence on the corrosion of Mg is still insufficient [5]. The barrier effect caused by protein adsorption has been used to explain its inhibitory effect. Hou [4] et al. experimentally investigated the influencing factors of protein adsorption on Mg in HBSS and Dulbecco's Modified Eagle Medium (DMEM). Protein absorption was found to slow down Mg degradation. Computational methods have also been employed to gain the insights into the action mechanism of organic molecules (such as amino acids, peptides and proteins) on Mg, the alloying elements and the surface status of samples were found to influence the adsorption of the organic molecules on Mg [37–41]. It is noteworthy that the adsorption effect of protein cannot be applied toward explaining all relative research results since protein is also found to accelerate Mg corrosion [27,28,34,42]. The chelating effect of protein on cations (e.g. Mg^{2+} and Ca^{2+}) was emphasized decades ago [43–45]. The consumption of Mg^{2+} by binding in chelate complexes undoubtedly shifts the chemical equilibria towards Mg corrosion reaction. Willumeit [46] et al. found that the addition of protein led to a less dense but thick corrosion product layer on the corroded Mg and noted that the binding of ions to proteins was the key for corrosion product formation in protein-containing media. Heakal [47] et al. also mentioned the possible binding effect of protein. It is noteworthy that the protein may not only chelate the dissolved Mg^{2+} from substrate, but also has affinity to other cations, like Ca^{2+}, in the complex corrosive media. This may be another influencing factor for Mg corrosion, given the principal role of Mg^{2+} and especially Ca^{2+} in interface stabilization. It has been found that Tris and streptomycin, as Ca^{2+} complexing agents, inhibit the formation of a protective layer on Mg surface in simulated body fluid [19,20,24]. This promotes Mg corrosion. Chelating effect of proteins in the course of Mg corrosion is worthy of further investigations. In addition, recent works reported that local pH in the diffusion layer near the interface of Mg exposed to simulated body fluid (SBF) and HBSS, differs significantly from the pH monitored in bulk electrolytes [19,20]. During the corrosion process of Mg, generated OH^- in the diffusion layer participates in the formation of corrosion products ($Mg(OH)_2$ but also Ca-P containing precipitates) and hence influences the corrosion kinetics. Thus, the pH buffering effect caused by functional groups in the chemical structure of protein, should be taken into account [48]. The buffered pH in protein-containing solution alters the test environment, which influences the corrosion behavior of Mg. At the present stage, understanding of the pH buffering effect of protein during Mg corrosion is still incomplete, especially, its influence on local pH at Mg/medium interface has not been reported.

Although, as previously mentioned, a number of publications investigated the influence of proteins on Mg corrosion, most of them focused on the interaction between proteins and substrates. Recently, the interaction between proteins and medium components was caught in a spot light of research interest. Yan [49] et al. reported that the synergistic effects of glucose and albumin decreased the corrosion rate of Mg in NaCl solution. However, as Höhn [5] et al. mentioned in a recent review that the understanding of protein interactions with Mg surfaces and their influence on Ca-P products formation in pseudophysiological solutions is still limited. Thus, we believe it is necessary to clarify the potential action mechanisms of protein on Mg corrosion in a complex pseudophysiological medium. It will be beneficial for the comprehensive understanding on the influence of protein on the reactions at the Mg/medium interface and its influence on the formation of Ca-P products. Furthermore, it will also help to elucidate the origin of different opinions about the protein influence on Mg corrosion in the previously published works.

In our recent works, a continuous electrochemical impedance spectroscopy (EIS) test has been proven to be an effective approach to investigate *in-situ* the formation of corrosion products and precipitation of protective layers on the Mg surface [20,24]. In addition, a scanning ion-selective electrode technique (SIET) has been employed to monitor the localized pH values near the Mg/medium interface during the corrosion process [19,20]. As compared to the pH monitoring of bulk electrolytes, the local pH has been proven to more accurately reflect the corrosion behavior of Mg [19,20]. Although these tests in protein-containing solution cannot be maintained for a long time due to the risk of contamination, short-term tests can still provide information, which contributes to understanding the influence of protein. In this work, hydrogen evolution test, EIS monitoring and local pH measurement are complementary employed to investigate the corrosion behavior of Mg in albumin-containing HBSS during a short-term test. Possible mechanisms of protein interaction with Mg are discussed. This work improves our understanding of the corrosion behavior of Mg in a complex pseudophysiological environment.

Please cite this article as: D. Mei, C. Wang and S.V. Lamaka et al., Clarifying the influence of albumin on the initial stages of magnesium corrosion in Hank's balanced salt solution, Journal of Magnesium and Alloys, https://doi.org/10.1016/j.jma.2020.07.002

Table 1
The elemental composition of commercially pure Mg (CP Mg).

	Element content/ wt.%										
	Fe	Cu	Ni	Al	Mn	Ce	Zn	Si	Ca	Zr	Mg
CP Mg	0.0342	0.00037	<0.0002	0.00402	0.00237	0.0007	0.00046	0.00071	<0.0001	<0.0005	Bal.

Table 2
The composition of Hank's balanced salt solution (HBSS).

	Concentration/mM
Na^+	142.8
K^+	5.8
Mg^{2+}	0.9
Ca^{2+}	1.3
Cl^-	146.8
HCO_3^-	4.2
HPO_4^{2-}/ $H_2PO_4^-$	0.8
SO_4^{2-}	0.4
Synthetic pH buffer (i.e. Tris/HCl, HEPES)	No
Initial pH value	7.0–7.4

2. Experimental

In this work, commercially pure Mg (CP Mg) was employed, its elemental compositions, obtained by optical discharge emission spectroscopy (SPECTROLAB with Spark Analyser Vision software, Germany), is listed in Table 1. Although CP Mg is not regarded as a potential implant material because of its unsatisfactory mechanical properties and corrosion resistance, it was selected as the research subject here to exclude the possible influence of alloying elements on corrosion and passivation mechanisms. In addition, due to the high risk of microbial contamination in protein-containing medium in the open environment, this fast corroding material (CP Mg) was employed here to shorten the test time and to obtain reliable results for analyzing the influence mechanisms of albumin. Small chips of CP Mg, which have a large surface area of 47.7 ± 5.0 cm^2/g, were used for the hydrogen evolution tests (electrolyte volume to sample surface area was 500 mL/23.85 cm^2=21 mL/cm^2). Eudiometers from Neubert-Glas, Germany (Art. Nr. 2591–10–5) combined with an electronic balance (OHAUS, SKX series) were used for a custom-made automated recording of the water weight displaced by evolved hydrogen [24,50]. Note that this is a closed setup, thus only the air initially entrapped (ca. 70 ml, equal to ca. 15 ml O_2) in the test bottle and the air initially dissolved in the electrolyte can possibly contribute to the oxygen reduction reaction [51], which otherwise might lead to a significant underestimation of the total cathodic reaction. The detailed description of the hydrogen evolution test can be found in our previous work [24].

HBSS was used as the corrosive medium; its detailed composition is listed in Table 2. 40 g L^{-1} Bovine serum albumin (BSA, Carl Roth, 8076.3) was added to the HBSS to investigate its influence. BSA-containing HBSS was referred to as HBSS+BSA. We choose to add 40 g L^{-1} of protein based on the concentration of albumin in human serum (35–52 g L^{-1}). The initial pH value of the HBSS was 7.2–7.3 and HBSS+BSA was 7.0 ± 0.1.

A conventional three-electrode setup was used for the EIS measurements. A CP Mg sample with a surface area of 0.5 cm^2 was exposed to 350 mL of electrolyte. A Pt wire coil was used as the counter electrode and a Ag/AgCl in saturated KCl solution was used as the reference electrode. The ground plates of $13 \times 13 \times 4$ mm (SiC paper up to 1200 grit) were used for the EIS measurements. Measurements were performed at open circuit potential (OCP) with an amplitude of 10 mV RMS over a frequency range from 100 kHz to 0.1 Hz by a Gamry Interface 1000 potentiostat/galvanostat under constant stirring conditions (200 rpm).

Scanning electron microscopy (TESCAN, Vega3 SB) at accelerating voltage of 15 kV was employed to observe the corrosion products morphology after a 24 h immersion in HBSS and HBSS+BSA. The elemental compositions of the corrosion products was tested by energy dispersive X-ray spectrometry (EDS).

Local pH measurements were performed in the HBSS electrolyte, in the diffusion layer directly adjacent to the surface of the corroding magnesium. The probes were positioned 50 ± 5 μm above the sample surface. The measurements were performed under hydrodynamic conditions (Medorex TL15E peristaltic pump) at a flow rate of 1.0 mL min^{-1} assuring full electrolyte renewal in the cell every 5 min. A commercial instrument for a scanning ion-selective electrode technique (SIET from Applicable Electronics) was used and controlled by LV4 software from Science Wares. A pH-sensitive microelectrode with a tip made of pH-sensitive glass from Unisense (pH-10, tip diameter was 10 μm, tip length was 50 μm) was employed. The samples were prepared by embedding CP Mg machined to a rod of 2 ± 0.2 mm in transparent epoxy resin (Buehler 20–3430064/20–3432–016) that, upon solidification, was ground up to 4000 grit.

The concentration of free Ca^{2+} in the medium was measured potentiometrically, employing Ca^{2+}-selective electrode (Perfection TM) and ion meter (SevenExcellence) both from Mettler Toledo.

The weight loss of CP Mg was measured three times after immersing the samples in HBSS and HBSS+BSA in a closed cell either under static or hydrodynamic conditions. In static conditions, the medium was changed once a day and the ratios of electrolyte volume to sample surface area (V/A) were 3:1 mL cm^{-2} and 10:1 mL cm^{-2}. In contrast, the medium was constantly renewed by a peristaltic pump at a rate of 0.5 mL min^{-1} under hydrodynamic conditions. After 3 days of immersion, the samples were cleaned with chromic acid (200 g L^{-1}) to remove the corrosion products, dried and weighed.

Please cite this article as: D. Mei, C. Wang and S.V. Lamaka et al., Clarifying the influence of albumin on the initial stages of magnesium corrosion in Hank's balanced salt solution, Journal of Magnesium and Alloys, https://doi.org/10.1016/j.jma.2020.07.002

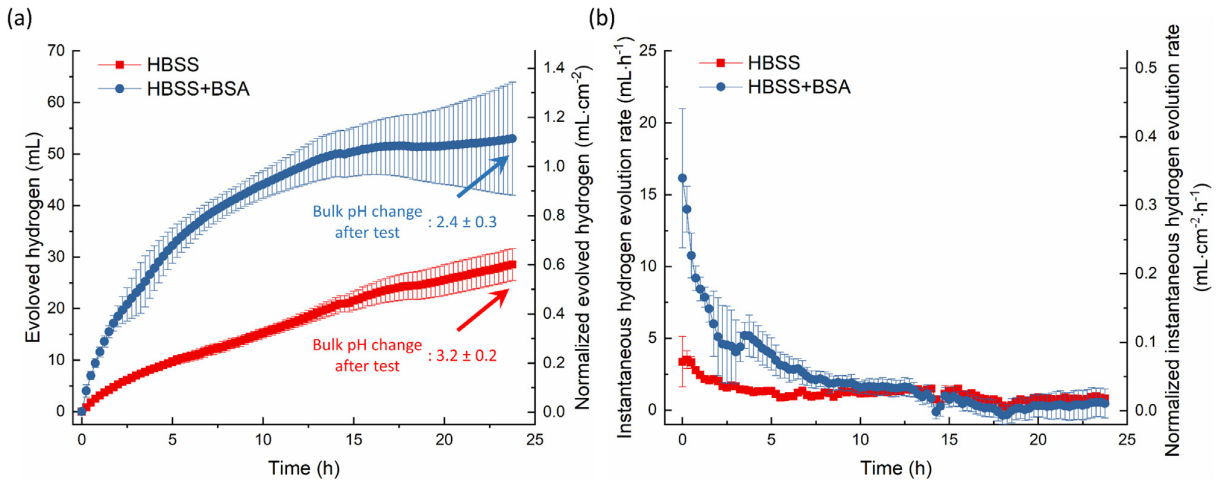

Fig. 1. (a) Hydrogen evolution curves of CP Mg during 24 h immersion in HBSS with and without 40 g·L^{-1} BSA; (b) Instantaneous hydrogen evolution rate derived from (a).

3. Results

3.1. Hydrogen evolution test

Fig. 1 shows the cumulative hydrogen evolution curves and instantaneous hydrogen evolution rate of CP Mg during 24 hours' immersion in HBSS and HBSS+BSA. Initially high degradation rate of Mg stabilized at lower, quasi-constant values after 5 (HBSS) to 10 (HBSS+BSA) hours of immersion. It further slightly decreased after 15 h for both samples and remained quasi-constant until the end of the measurement. During this time, the components of HBSS, such as Ca^{2+}, HCO_3^- and $HPO_4^{2-}/H_2PO_4^-$, were consumed [20] in the confined volume of the eudiometers. The presence of albumin in HBSS has a distinct effect on the corrosion behavior of Mg. During the first few hours of immersion, the Mg corrosion rate in HBSS+BSA was significantly higher than that in simple HBSS, but it gradually deceased over the immersion time. As shown in Fig. 1(b), initially, the instantaneous hydrogen evolution rate of CP Mg in HBSS+BSA was very high, but it became lower than the corrosion rate in a simple HBSS after 13 h of immersion. Although the Mg corrosion rate in HBSS+BSA was lower than that in simple HBSS at the second half of the measurement, according to the volume of evolved hydrogen after 24 h, BSA accelerates the corrosion of CP Mg in HBSS.

Another noteworthy point is that the pH change of the bulk electrolyte during measurements in HBSS and HBSS+BSA. What needs to be emphasized is that the initial pH value of the two media is similar (shown in Fig. 1(a), HBSS: 7.2; HBSS+BSA: 6.9–7.1), while the volume of evolved hydrogen in HBSS+BSA higher than that in HBSS (meaning that the amount of generated OH^- was also bigger). In this case, the smaller pH change of the albumin-containing solution (approximately 2 units in HBSS+BSA; 3 units in HBSS) indicates an additional pH buffering effect associated with albumin. Besides, the initial pH value of HBSS+BSA (6.9–7.1) is lower than that of HBSS (7.2–7.3). This is attributed to the weak acidity of albumin [52–54].

3.2. EIS evolution

Continuous EIS monitoring is an effective approach to investigate the formation of corrosion product layers and estimate their protective properties. Fig. 2 shows the evolution of Bode plots measured over Mg during 24 h immersion in HBSS with and without BSA. A striking feature of the Bode plots in simple HBSS was the presence of an additional time constant at the frequency of approximately 10 kHz (marked by arrow in Fig. 2(a,b)). A similar phenomenon has been emphasized in our previous research, performed in SBF [20,24]. This time constant was attributed to the growth of a semi-protective continuous layer containing Ca^{2+}, Mg^{2+}, $HPO_4^{2-}/H_2PO_4^-$ and HCO_3^-, which provides an important additional protection and slows down the corrosion rate.

However, the presence of BSA changed the Bode plots. During the first hour of immersion in HBSS+BSA, no additional time constant appeared in the high frequency range, as shown in Fig. 2(c). Even after 24 h of immersion, the additional time constant was still not easily observable at the frequency of 10 kHz, a typical manifestation frequency of the co-precipitation layer in the Bode plots obtained in HBSS+BSA (as shown in Fig. 2(d), marked by a dotted arrow).

In simple HBSS electrolyte, a rapid formation (within less than 15 min) of the co-precipitation layer provided protection against Mg corrosion, evidenced by a rapid growth of a high frequency time constant. However, in albumin-containing HBSS, its formation was delayed significantly. After 24 h in HBSS+BSA, the phase angle component of the Bode plot in high frequency domain has just taken the shape similar to that for the sample exposed to HBSS after 15 min. In addition, the evolution of the low frequency impedance of samples in the two media differs, while the initial Bode plots (upon first immersion) are very similar for the samples

Please cite this article as: D. Mei, C. Wang and S.V. Lamaka et al., Clarifying the influence of albumin on the initial stages of magnesium corrosion in Hank's balanced salt solution, Journal of Magnesium and Alloys, https://doi.org/10.1016/j.jma.2020.07.002

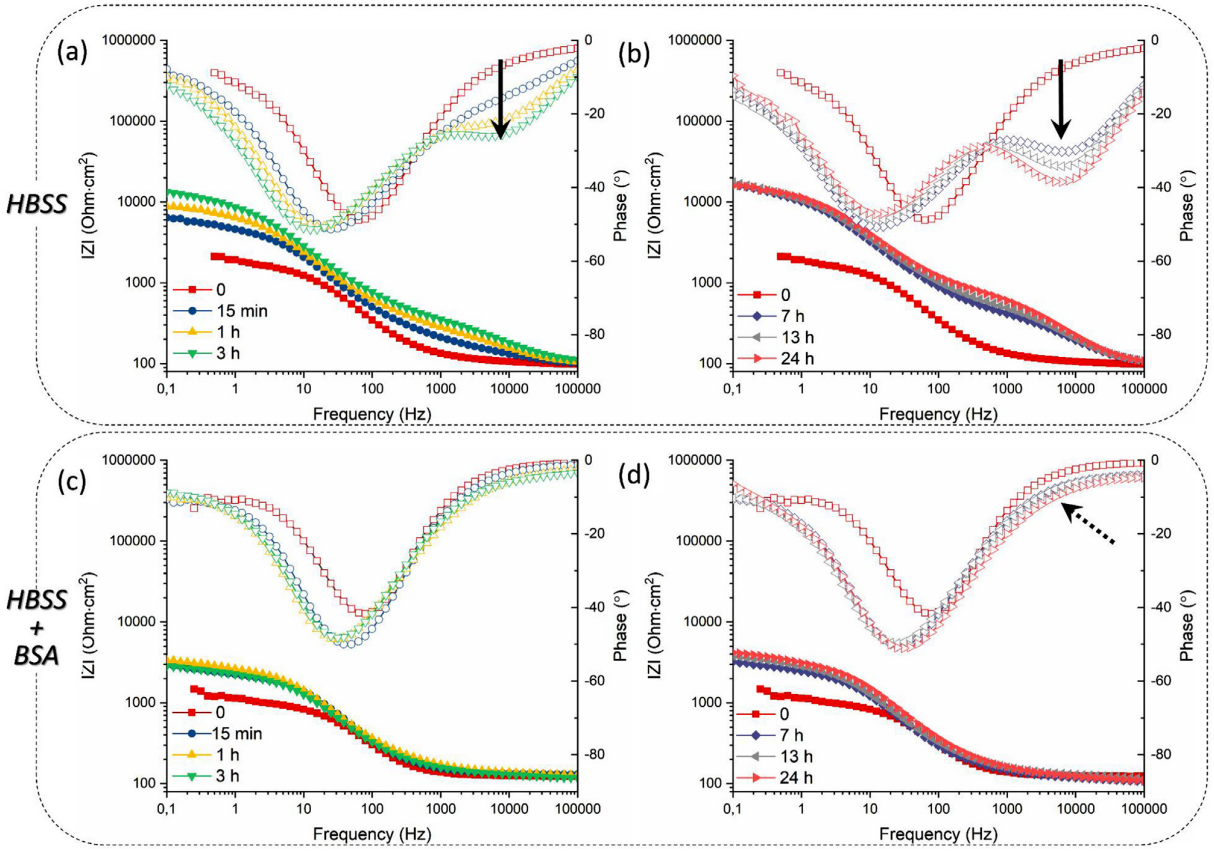

Fig. 2. Bode plots evolution of CP Mg during 24 h immersion in HBSS (a, b) and HBSS+BSA (c, d).

immersed in HBSS and HBSS+BSA. The low frequency value of impedance modulus increased during the first 3–7 h and then remained at the value of ca.18 kOhm·cm^2 until the end of the measurement for the sample immersed in HBSS. In contrast, the presence of albumin in HBSS caused the impedance to grow continuously but much lower during the entire test period, so that the low frequency impedance modulus was ca. 4 kOhm by the end of the immersion test. These EIS results correlate with the hydrogen evolution tests to some extent. At the early stage of immersion, the limited adsorption of protein and the suppressed formation of the co-precipitation layer caused the rapid corrosion of CP Mg in the albumin-containing HBSS. With increased immersion time, the synergy between the protein adsorption and formation of the precipitation layer provided protection against the corrosion of CP Mg, slowing down the corrosion rate.

3.3. Corrosion morphology

The corrosion morphology of CP Mg after a 24 h immersion in HBSS with and without albumin was investigated by SEM/EDS. Fig. 3 shows the typical corrosion morphology of CP Mg in HBSS. The elemental compositions of selected points and regions in Fig. 3 given by EDS are listed in Table 3. Similar morphologies have been reported in our previous works about Mg corrosion in SBF [20,24]. As shown in Fig. 3 (a, b), a distinct feature of the corrosion products was that the products with high Ca-P content formed clusters (point 1 and 2 in Fig. 3(b)) and a compact product layer with low Ca-P content (region 3 and 4 in Fig. 3(b)). The grinding scratches on Mg surface remained recognizable after the immersion, suggesting limited corrosion attack.

Table 3
Elemental composition of corrosion products on the CP Mg given by EDS after 24 h immersion in HBSS and HBSS+BSA.

Position	Elements/ at.%					
	C	O	Na	Mg	P	Ca
1	7.9	34.3	1.2	5.5	19.5	31.6
2	9.4	49.9	2.7	5.4	15.7	16.9
3	9.8	22.2	–	57.4	6.3	4.3
4	10.0	24.1	–	56.3	5.5	4.1
5	19.3	36.7	–	8.9	18.0	17.1
6	21.7	34.5	–	7.2	19.7	16.9
7	6.2	10.8	–	75.6	4.9	2.5

However, the addition of albumin in HBSS causes different corrosion morphologies of CP Mg. The typical corrosion morphologies of CP Mg in HBSS+BSA are shown in Fig. 4. The EDS results of the selected points and regions in Fig. 4 are also listed in Table 3.

Please cite this article as: D. Mei, C. Wang and S.V. Lamaka et al., Clarifying the influence of albumin on the initial stages of magnesium corrosion in Hank's balanced salt solution, Journal of Magnesium and Alloys, https://doi.org/10.1016/j.jma.2020.07.002

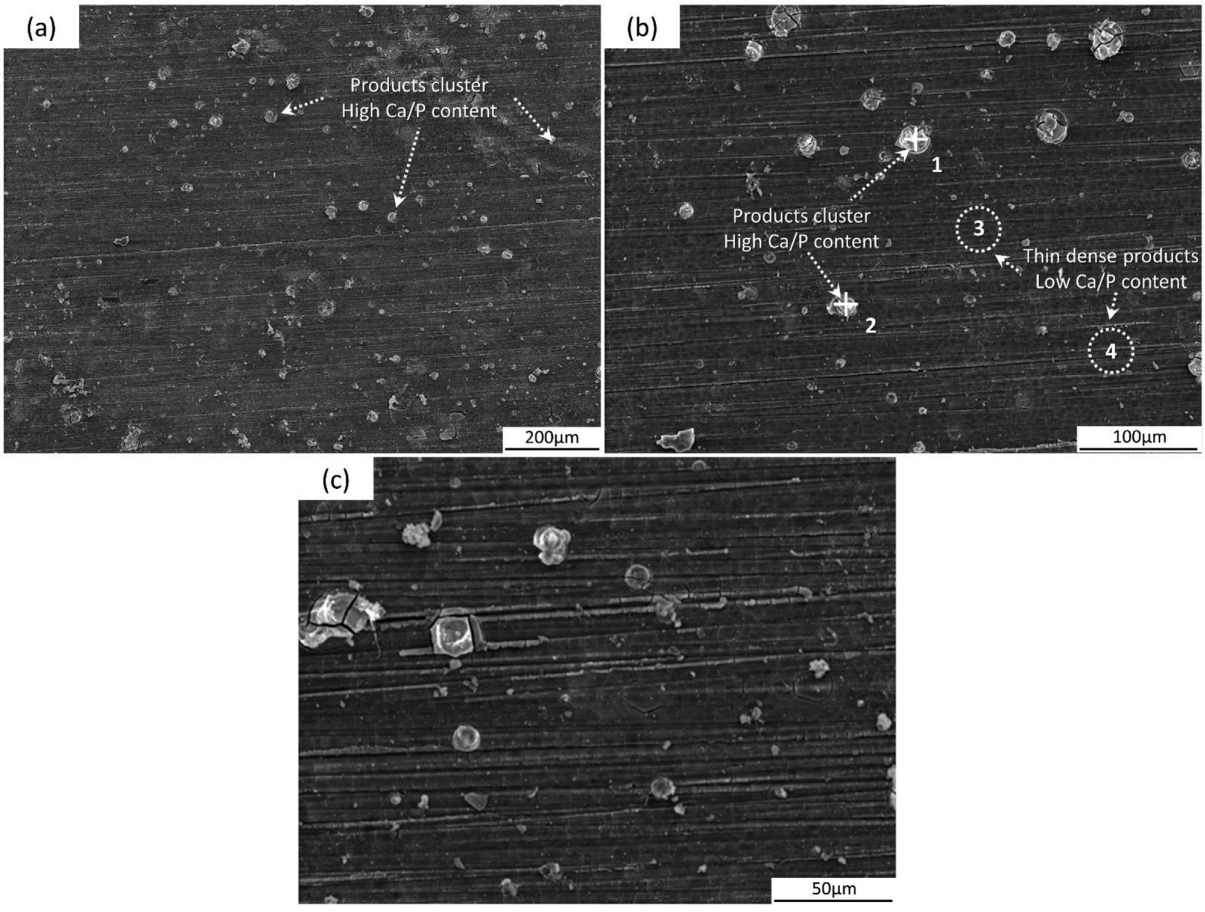

Fig. 3. Typical corrosion morphology of CP Mg after 24 h immersion in HBSS, SEM images.

The loose products with the layer structure in Fig. 4 were associated with the fast corrosion rate of magnesium in HBSS+BSA at the early stage of the hydrogen evolution test. This feature is not typical for the corrosion morphology of magnesium after immersion in simple HBSS. After the comparison between Figs. 3 and 4, it could be concluded that the addition of BSA inhibited the formation of product clusters with high Ca-P content. In contrast, the whole outer layer of the corrosion products (point 5 and 6 in Fig. 4) contained a high Ca-P content, while the inner layer (point 7 in Fig. 4) contained a low Ca-P content. In addition, the EDS mapping results of region 8 in Fig. 4 supported the different elemental compositions between outer and inner layers of the corrosion products formed on corroded surface of Mg exposed to HBSS+BSA.

The cracked morphology of the corrosion products in HBSS+BSA correlates well with the EIS results. Even though this morphology can be related to the drying and shrinkage, the corrosion products formed in HBSS+BSA is more characteristic for thicker but looser as compared with dense corrosion products that shown in Fig. 3. The less dense corrosion products in presence of albumin (Fig. 4) verified the delayed and limited formation of a semi-protective continuous layer of Ca^{2+}, Mg^{2+}, $HPO_4^{2-}/H_2PO_4^-$ and HCO_3^- (described by the change of a high frequency time constant in EIS evolution in Fig. 2).

3.4. Evolution of local pH near the corroded Mg surface

All the above measurements (the hydrogen evolution tests, EIS and immersion tests) were performed under stirring conditions but without constant renewal of the medium. To mimic the real service environment of the implant materials, the local pH near the surface of corroded CP Mg was measured during the corrosion test while constantly refreshing of the media.

Fig. 5 shows the point scan of local pH measurement on the surface of CP Mg immersed (under hydrodynamic conditions) in HBSS with and without BSA. The measurements captured the initial seconds of electrolyte contact with the sample surface. Technically, the pH micro-probe was positioned on the prepared sample and the measurement has started. Some seconds later, the electrolyte was added. This explains that the pH values in Fig. 5 are recorded from 50 s point on. Local pH values increased from the initial value of ca. 7.2 to above 9 within several seconds. The local pH in

Please cite this article as: D. Mei, C. Wang and S.V. Lamaka et al., Clarifying the influence of albumin on the initial stages of magnesium corrosion in Hank's balanced salt solution, Journal of Magnesium and Alloys, https://doi.org/10.1016/j.jma.2020.07.002

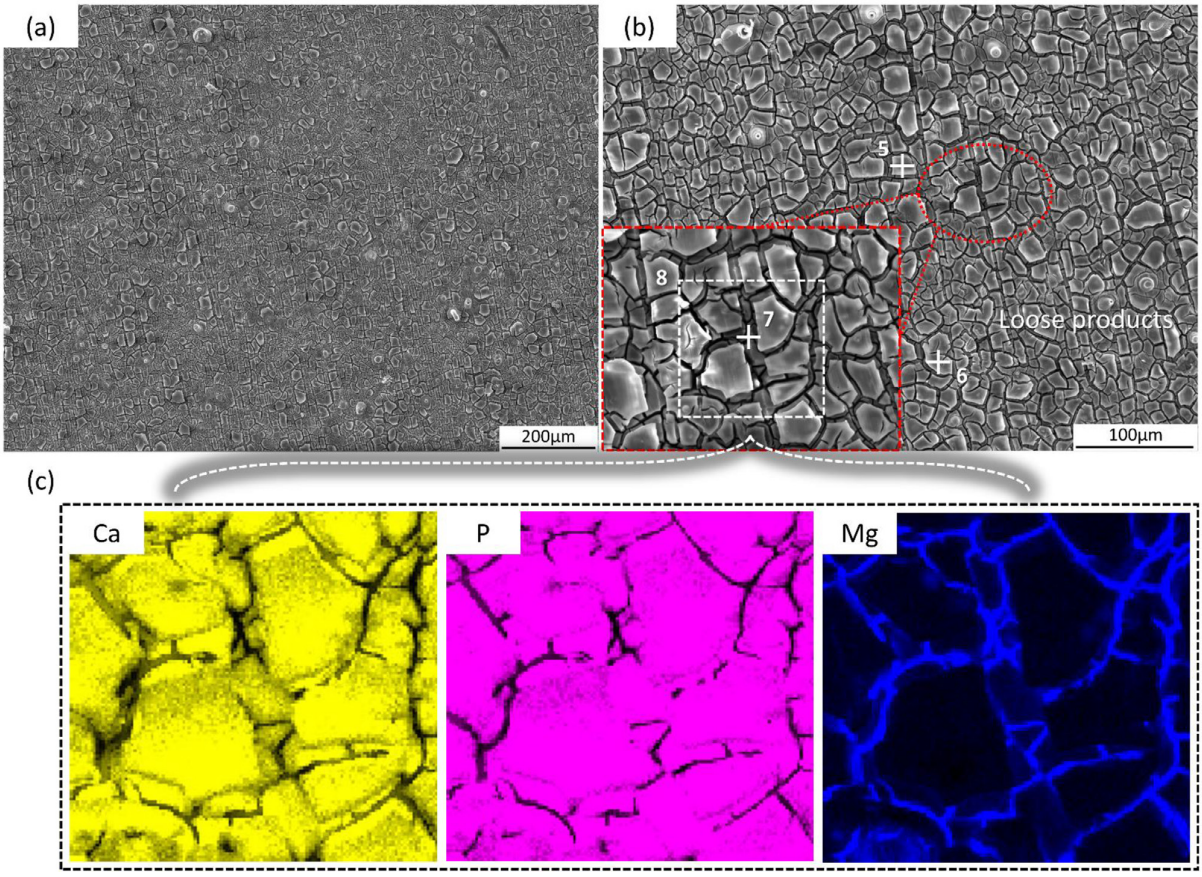

Fig. 4. Typical corrosion morphology by SEM (a, b) and EDS mapping (c) of CP Mg after 24 h immersion in HBSS+BSA.

the HBSS increased sharper and to higher values, up to 9.9, while it reached 9.6 in HBSS+BSA electrolyte. The measurement points for each sample are marked with a white cross in Fig. 5. The optical micrographs showed that the H_2 bubbles that appeared on the Mg surface in HBSS+BSA were smaller but more densely populated than those in simple HBSS, that testifies for higher rate of hydrogen generation, in line with similar conclusion reached by analyzing the hydrogen evolution by eudiometers, Section 3.1. The rapid corrosion of CP Mg was shown at the early stage of immersion in HBSS+BSA. Normally, rapid corrosion would indicate faster growing, high local pH [19,20]. However, the result in this work was different, and it confirmed the assumption about the pH buffering effect of albumin-containing HBSS. Meanwhile, the pH buffering mechanism of albumin was different from that of synthetic buffer (i.e. Tris, HEPES). While Tris and HEPES were not efficient in buffering the local pH [19,20], albumin effectively buffered both the local and bulk pH due to sufficient solubility and effective adsorption on the Mg surface.

In addition to the single point pH evolution, line scans of local pH measurements in HBSS with and without albumin were also performed under hydrodynamic conditions, Fig. 6. In simple HBSS, the local pH measured at the distance of 50 μm from the surface of sample was around 8.5 after first 10 min of immersion and slightly decreased to around 8.3–8.4 after 30 min of stabilization. Similarly, we have previously reported the fast stabilization of local pH in HBSS-like electrolytes over high purity Mg and Mg-2Ag, Mg-1.2Ca and Mg-Gd-Nd-Ca alloys [19,20]. After 1 hour's immersion, filiform corrosion occurred on the sample (marked by arrow in optical image in Fig. 6(a)). With propagation of filiform corrosion from the edge to the center of the sample, the line scan after 1.5 hours' immersion showed higher local pH values in the area of filiform corrosion. However, due to the component replenishment by constant renewal of the medium and continuous formation of passive layer containing Ca^{2+}, Mg^{2+}, $HPO_4^{2-}/H_2PO_4^-$ and HCO_3^-, the local pH decreased again afterwards. This indicates important protection effect of the components in HBSS on Mg corrosion.

In HBSS+BSA, as the immersion time elapses, the highest local pH decreased gradually to around 8.3 after 30 min. The highest local pH value was maintained below 8.5 within 6 h of immersion. Although the local pH in HBSS and HBSS+BSA showed similar maximal value, the local pH in HBSS+BSA always showed a marked fluctuation during the first 3 h of immersion, which was different from the evolution of local pH in HBSS. This pointed out the different originations of

Please cite this article as: D. Mei, C. Wang and S.V. Lamaka et al., Clarifying the influence of albumin on the initial stages of magnesium corrosion in Hank's balanced salt solution, Journal of Magnesium and Alloys, https://doi.org/10.1016/j.jma.2020.07.002

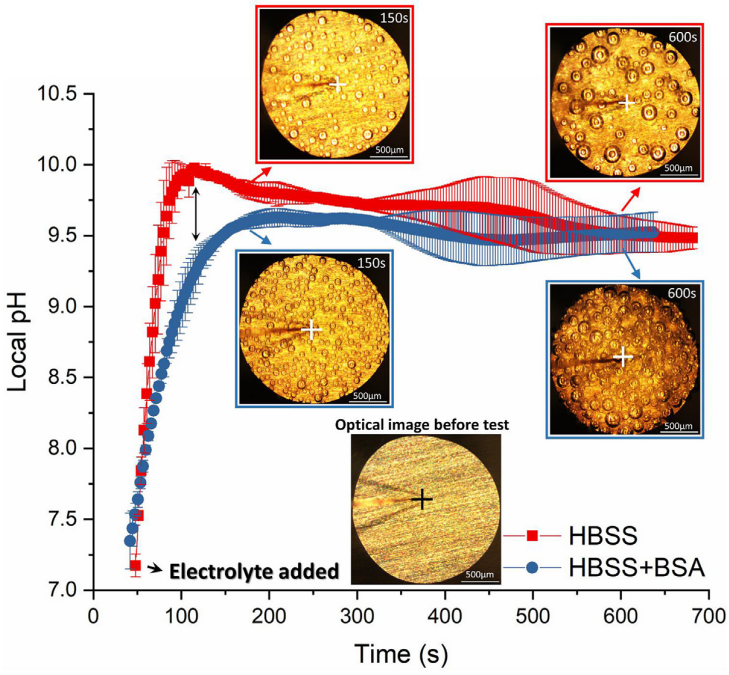

Fig. 5. Evolution of single point local pH at 50 μm from the surface of CP Mg immersed in HBSS or HBSS+BSA during the initial stage of immersion. Performed under hydrodynamic conditions, flow rate 1.0 mL/min. Optical micrographs show the visual appearance of two samples during the test. Multiple round features are the bubbles of evolved H_2.

low local pH in HBSS and HBSS+BSA. The formation of a dense co-precipitation layer of Ca^{2+}, Mg^{2+}, $HPO_4^{2-}/H_2PO_4^-$ and HCO_3^- slowed down the corrosion rate of Mg in simple HBSS and led to the stable and low local pH value in HBSS. In HBSS+BSA, as discussed in Section 3.2, BSA delayed the formation of the aforementioned dense protective precipitation layer. The addition of BSA activated the corrosion reaction at the Mg/medium interface and led to faster corrosion of CP Mg in HBSS+BSA than that in simple HBSS (as shown in Fig. 1). However, although the local pH did not show a higher value due to the pH buffering capacity of BSA, during the first 3 h of immersion, the distribution of local pH was uneven because of the activation effect of BSA on Mg corrosion (Fig. 6 (c, d)). As the immersion time increased, the combined albumin adsorption and corrosion products formed on the corroded Mg contributed to the stabilization of local pH in HBSS+BSA (as shown in Fig. 6(d) after 4.5 hours' immersion).

4. Discussion

4.1. The importance of component replenishment/ medium renewal during the tests

During the corrosion tests under static conditions, the medium composition changes depending on the substrate dissolution and precipitation of corrosion products. The latter contains the components of the medium, thus depleting its ionic load. This is an important notion that, if left without deserved attention, might distort our understanding of the corrosion behavior of magnesium alloys. The importance of a constant medium composition during corrosion tests have been already pointed out previously [55,56]. In spite of this, in most published works on immersion tests, the media were only refreshed after a fixed time interval (e.g. 1 day or 2–3 days) instead of continuous renewal. In commonly referred standards about immersion tests, there are several recommended V/A values. For example, V/A of 1.25–6.0 (depends on sample shape) in ISO 10993–12:2012 [57] and 20–40 in ASTM G31–72 (2004) [58] or ASTM G31–2012a [59].

Fig. 7 compares the weight loss of CP Mg after 3 days of immersion in HBSS with and without BSA under static and hydrodynamic conditions. With the timely renewal of the media, the weight loss of CP Mg in HBSS decreased significantly. In addition, the stability of the media compositions has an impact on the reproducibility of the parallel tests to some extent. A stable medium composition has a significant influence on the corrosion test results of Mg in HBSS, especially for long-term measurements. However, the test conditions do not have significant influence on Mg corrosion in HBSS+BSA. In this work, BSA decreased the weight loss of CP Mg under static conditions with a V/A of 3:1, while it did not show apparent effect on the weight loss under static conditions with a V/A of 10:1 and increased the weight loss under hydrodynamic condition. These results, demonstrating susceptibility to experimental conditions, highlight the urgency of standardization for the test protocols of biodegradable metallic materials.

Please cite this article as: D. Mei, C. Wang and S.V. Lamaka et al., Clarifying the influence of albumin on the initial stages of magnesium corrosion in Hank's balanced salt solution, Journal of Magnesium and Alloys, https://doi.org/10.1016/j.jma.2020.07.002

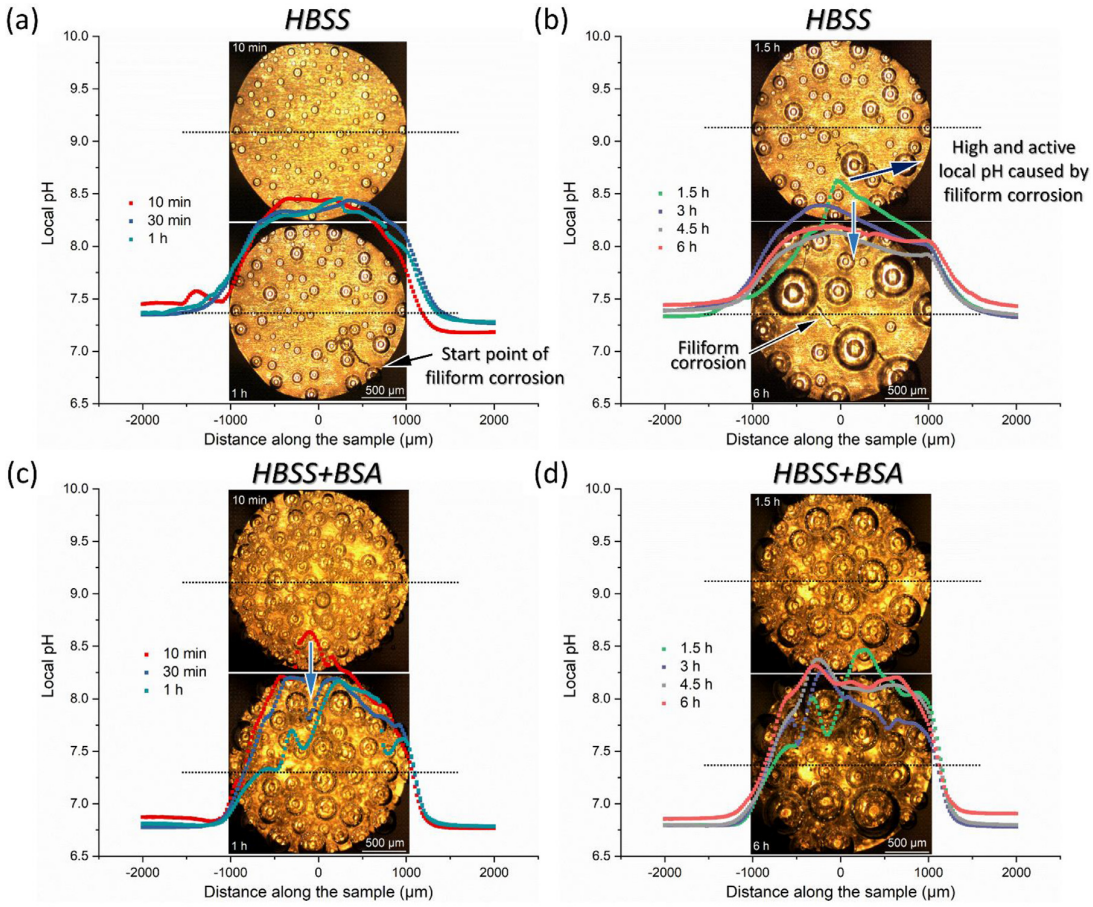

Fig. 6. Local pH measurements (line scan) at 50 μm from the surface of CP Mg immersed in (a, b) HBSS; (c, d) HBSS+BSA during immersion. All the measurements are performed under hydrodynamic conditions, flow rate 1.0 mL·min^{-1}. Optical micrographs show the visual appearance of two samples during the test. Multiple round features are the bubbles of evolved H_2. Dotted lines show the exact location of pH line scan.

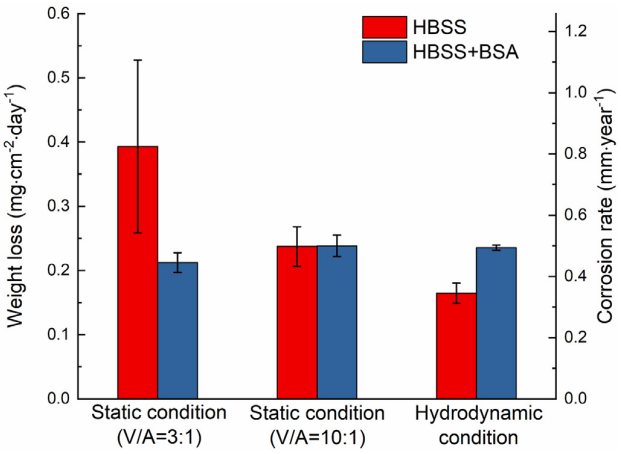

Fig. 7. Weight loss of CP Mg after 3 days immersion in HBSS with and without BSA under static conditions and hydrodynamic conditions.

To mimic the real service environment of implant materials, a timely, ideally constant renewal of the media should be performed. This should be considered as one of the essential factors when upgrading the setup for the Mg corrosion test.

4.2. Summary of the protein effect

In addition to the often-mentioned adsorption effect, the other two effects of albumin, including cation complexing and pH buffering, need to be discussed based on the results of this study. Complementary to the works previously published by different scientific groups, the real-time measurement methods used in this work provided detailed information about the influence of albumin on Mg corrosion in HBSS during up to 24 h period. Based on the above results and a number of relevant literatures, albumin interaction with corroding magnesium can be summarized to three factors: the barrier (adsorption), Ca^{2+}/Mg^{2+} chelation and pH buffering effects. Indeed, we did not provide direct evidence to prove the albumin adsorption in this work. However, the adsorption effect of proteins has been investigated and discussed for long time in the literatures. We deem that there is no need to provide even more results to support this recognized fact yet again.

It is noteworthy that the hydrogen evolution rate in both cases became similar after 10 h of immersion, which does not corresponded to the EIS results, that showed different low frequency impedance modulus value and time constant(s)

Please cite this article as: D. Mei, C. Wang and S.V. Lamaka et al., Clarifying the influence of albumin on the initial stages of magnesium corrosion in Hank's balanced salt solution, Journal of Magnesium and Alloys, https://doi.org/10.1016/j.jma.2020.07.002

after 10 h immersion. This discrepancy is most likely attributed to the different test conditions (such as V/A ratio, shape of tested material) of these two test methods. However, it could be found that the results obtained from two methods showed similar trend. The rapid hydrogen evolution of CP Mg in HBSS+BSA for the first few hours correlates with the delayed and limited formation of co-precipitation layers composed of Ca^{2+}, $HPO_4^{2-}/H_2PO_4^-$, HCO_3^- and Mg^{2+} (as described by the high frequency response in impedance spectra). Then, with the increase of immersion time, the synergy between albumin adsorption and co-precipitation layer formation inhibits further corrosion of CP Mg in HBSS+BSA (demonstrated by the decreased rate of hydrogen evolution). The second stage was verified to some extent by the dimly appeared additional time constant at high frequency range (marked by a dotted arrow in Fig. 2(d)) and the continuous increase of low frequency impedance modulus value. However, the opposite result has been reported by Wang [60] et al. The causes of this discrepancy are apparent. Apart from the tested material, the presence of Tris/HCl in the media [60] also has a significant influence. It has been shown in the literatures that Tris (as well as HEPES) accelerate degradation of Mg [20,61].

As presented in our previous works [19,20,24], compared with simple NaCl solution, SBF, HBSS, MEM or similar media possess pH buffering effects that originate from carbonate and phosphate components. The pH buffer capacity in these SBF-like electrolytes was attributed to the buffering effect of several ions (i.g. carbonates and phosphates) and the decreased concentration of generated OH- induced by the suppressed corrosion owing to the formed protective products layer. It is different from the buffering mechanism of common pH buffers, such as Tirs, HEPES or HCO_3^-/CO_2. Combining the hydrogen evolution and local pH results, at the initial stage of immersion in albumin-containing HBSS, the rapid corrosion of Mg did not lead to a high local pH value. This is because of the strengthened buffer capacity of HBSS by adding albumin. Approximately one-third of the amino acid functional groups in proteins can provide or accept hydrogen ions [48]. More specifically, the sidechains of glutamic and aspartic acid are comprised of carboxyl groups; lysine sidechains include an amino group; arginine sidechains contribute guanidyl groups; phenolic groups, sulfhydryl groups, imidazolyl groups can be found in the sidechains of tyrosine, cysteine and histidine, respectively. Almost all proteins contain terminal α-amino and α-carboxyl groups on polypeptide chains. All the above functional groups make protein a strong pH buffer, influencing the pH value of media during the corrosion test and then influencing the corrosion behavior of Mg.

The basic corrosion reaction of magnesium in a pseudo-physiological environment can be described by the following equations [20,51,62–67]:

Dissolution of the matrix:

Anodic reaction

$$Mg \rightarrow Mg^{2+} + 2e^- \quad (1)$$

Table 4
Concentration of free Ca^{2+} in HBSS and HBSS+BSA albumin measured potentiometrically with Ca^{2+}-selective electrode. The nominal concentration of Ca^{2+} in HBSS is 1.3 mM.

Medium	Concentration of Ca^{2+}/ mM
HBSS	1.23 ± 0.06
HBSS+BSA	0.81 ± 0.07

Cathodic reactions

$$\text{(Main)}\ 2e^- + 2H_2O \rightarrow 2OH^- + H_2 \uparrow \quad (2)$$

$$\text{(Secondary)}\ 4e^- + 2H_2O + O_2 \rightarrow 4OH^- \quad (3)$$

Precipitation from the media:

$$mMg^{2+} + nCa^{2+} + xH_2PO_4^-/HPO_4^{2-} + yHCO_3^- + zOH^- \rightarrow Mg_mCa_n(PO_4)_x(CO_3)_y(OH)_z \downarrow \quad (4)$$

Combining Eq. (2)–(4) and the obtained results, it can be concluded that the addition of albumin shifts the chemical equilibria of these reactions. More specifically, the consumption of OH^- caused by the pH buffering effect of albumin shifts the chemical equilibria of the reactions described by Eq. (2)–(3) to the right. Similarly, it also influences the formation of the protective co-precipitation product layer (described by $Mg_mCa_n(PO_4)_x(CO_3)_y(OH)_z$), as shown in Eq. (4). The concentration of free Ca^{2+} (measured potentiometrically with Ca^{2+}-selective electrode) in HBSS with and without albumin is listed in Table 4. The addition of albumin significantly reduces the concentration of free Ca^{2+} in HBSS (from 1.23 ± 0.06 mM to 0.81 ± 0.07 mM). This is a direct evidence for binding Ca^{2+} by albumin, as suggested earlier by different methods [44,45]. The complexation between albumin and metal cations shifts the chemical equilibrium of the reactions described by Eq. (3) to the left thus delaying the formation of the protective co-precipitation layer $Mg_mCa_n(PO_4)_x(CO_3)_y(OH)_z$. We would like to emphasize that the decreased concentration of free Ca^{2+} is not the only cause of the delayed formation of dense and protective co-precipitation layer on Mg surface in HBSS+BSA. The adsorption of albumin changes the surface state of Mg, which probably also influences the formation reaction of the product layer at the interface. Although the effect of protein may be caused by a number of factors, there is no doubt that the presence of albumin finally delays formation of dense and protective co-precipitation layer.

Fig. 8 depicts the mentioned mechanisms of albumin-magnesium interaction at the initial stages of immersion in HBSS. The barrier (adsorption), chelating and pH buffering effects are summarized. Based on the hydrogen evolution results in this work, at the initial stage of immersion in albumin-containing HBSS, the absence or delayed formation of co-precipitation layer leads to the fast corrosion of CP Mg. With increasing immersion time, the adsorption effect of albumin appears gradually. The barrier effect caused by the combination of adsorbed protein and tardily formed inorganic corrosion products slows down the corrosion. However, the above

Please cite this article as: D. Mei, C. Wang and S.V. Lamaka et al., Clarifying the influence of albumin on the initial stages of magnesium corrosion in Hank's balanced salt solution, Journal of Magnesium and Alloys, https://doi.org/10.1016/j.jma.2020.07.002

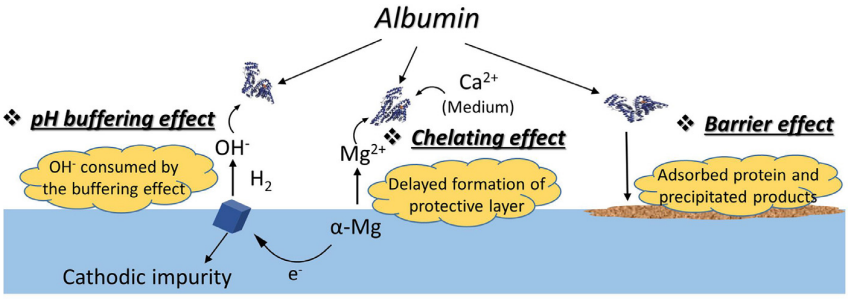

Fig. 8. Schematic illustration of influential factors of albumin on corrosion of CP Mg during short corrosion test in HBSS+BSA.

statements may not be regarded as the general description of the corrosion process of Mg in protein-containing pseudophysiological media. The question of whether the addition of protein accelerates or inhibits the corrosion of Mg cannot be answered unambiguously. As previously reported by other research groups, protein was found to inhibit Mg corrosion at the initial stage of test and accelerate it after long time immersion [32,33]. Even in this work, BSA showed different influence on the corrosion rate of Mg in different measurements. BSA was found to accelerate Mg corrosion based on 24 h hydrogen evolution test, while it showed different influence on Mg corrosion in 3 days weight loss measurements under various test conditions. It is clear that the testing media, tested materials, and test conditions significantly affect the final results of the albumin influence on Mg corrosion in a pseudophysiological environment. In any case, we do believe that the ultimate effect of protein on Mg corrosion originates from the synergy of three aforementioned mechanisms. It is reasonable to assume that the dominating factor(s) in these three mechanisms might differ depending on experimental conditions.

4.3. Outlook

Although the findings in this work were obtained from the tests with CP Mg, we believe they can be extended, at least in some parts, to other Mg alloys. Undoubtedly, it can be concluded that the addition of albumin significantly changes the corrosive environment and corrosion behavior of Mg. However, it does not mean that protein should be introduced into all corrosive media when studying magnesium for biomedical applications. For a long-term test in an open environment, protein-containing media may not be suitable. Specifically, after several days of immersion, the acidification of media induced by microbial proliferation significantly changes the test environment under unsterile conditions. That may also be one of the causes of the discrepancies between results in previously published works. Additionally, in some published works [30,68–70], the source of albumin is not mentioned. Fig. 9 shows cumulative hydrogen evolution curves of CP Mg in HBSS and HBSS with two different albumins: 40 $g{\cdot}L^{-1}$, BSA (from Carl Roth, Ref. 8076.3) and chicken egg albumin (CEA) (from Alfa Aesar, Ref. A16951). Although both of BSA and CEA significantly accelerated hydrogen

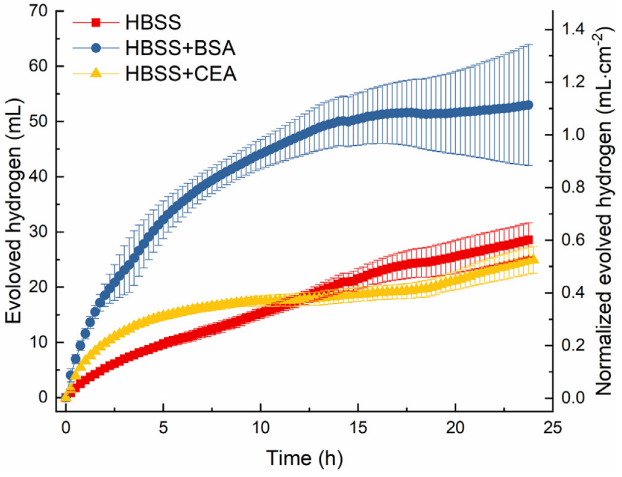

Fig. 9. Hydrogen evolution curves of CP Mg during 24 h immersion in HBSS, HBSS+BSA and HBSS+CEA.

evolution at first 2 h, they showed different acceleration capacity. According to the volume of evolved hydrogen after 24 hours' test, CEA slightly inhibited Mg corrosion, while BSA accelerated Mg corrosion. Based on this finding, it is evident that different sources of albumin may be one of the factors that influence the research results.

Notably, due to the complexity of magnesium corrosion in a pseudophysiological environment, the existing results of the protein influence on magnesium corrosion may still be fragmentary [5]. Thus, the further investigations about the influence of protein on Mg corrosion are still necessary. We are well aware that the test conditions in this work are far from a real body environment (37 °C and a controlled CO_2 concentration). However, we deem that our research is still an important step in understanding possible factors controlling Mg corrosion in a pseudophysiological environment. The stability of the local pH value near the corroded Mg induced by the addition of albumin in HBSS was clarified in this work. Moreover, the results show that the addition of albumin delays the formation of a protective co-precipitation product layer on Mg in HBSS. It is noteworthy that these effects originate from the general characteristics of the proteins. Thus, we believe the summarized mechanisms in this work are also applicable for other types of protein.

Please cite this article as: D. Mei, C. Wang and S.V. Lamaka et al., Clarifying the influence of albumin on the initial stages of magnesium corrosion in Hank's balanced salt solution, Journal of Magnesium and Alloys, https://doi.org/10.1016/j.jma.2020.07.002

As Höhn [5] et al. outlined in a recent review, the understanding of protein interactions with Mg surfaces and their influence on Ca-P product formation is still limited. We hope the results of this work open yet another facet of Mg-albumin interaction and improve the general understanding of these complex processes.

5. Conclusion

In this study, we investigated the corrosion behavior of CP Mg during up to 24 h in albumin-containing HBSS. The conclusions are listed below.

(1) The presence of BSA in HBSS buffers the pH of the electrolyte during the corrosion test. The bulk pH of HBSS+BSA only increases by approximately 2 units after the hydrogen evolution test, while the pH value increases by 3 units after immersion in simple HBSS. Even though the corrosion of CP Mg in HBSS+BSA is much faster, at the initial stage of immersion (first 1–2 min), the increase of local pH in HBSS+BSA is slower than that in HBSS.
(2) Although the local pH in HBSS and HBSS+BSA showed similar maximal value (8.5), the local pH in HBSS+BSA always showed a marked fluctuation during the first 3 h of immersion in contrast to stable local pH in HBSS. This indicates that different factors control low local pH in HBSS and HBSS+BSA.
(3) The addition of BSA decreases the concentration of free Ca^{2+} in HBSS by ca. 35% (from 1.23 to 0.81 mM) due to a chelating effect. During the first hours of immersion, the presence of BSA slows down the formation of a co-precipitation protective layer on the corroded CP Mg and leads to rapid corrosion, as shown by the hydrogen evolution test.
(4) Influence of BSA on the corrosion of Mg is susceptible to experimental conditions. Importance of replenishment of medium components during the corrosion tests was emphasized here and should be taken into account.
(5) The influence of albumin on Mg corrosion can be summarized in three aspects, namely, adsorption (the formation of a barrier layer), Ca^{2+}/Mg^{2+} chelation and pH buffering effects. The synergy of these three factors ultimately affects the corrosion of Mg in protein-containing HBSS.

Declaration of Competing Interest

The authors declare that they have no known competing financial interests or personal relationships that could have appeared to influence the work reported in this paper.

Acknowledgment

Mr. Di Mei and Mr. Cheng Wang thank China Scholarship Council for the award of fellowship and funding (No. 201607040051; 201806310128). “MMDi” IDEA project funded by HZG is gratefully acknowledged. The technical support of Mr. Volker Heitmann and Mr. Ulrich Burmester during this work is gratefully acknowledged.

References

[1] A. Shchukarev, M. Ransjö, Z.i. Mladenović, Intech. Open (2011).
[2] V. Wagener, A.S. Faltz, M.S. Killian, P. Schmuki, S. Virtanen, Faraday Discuss 180 (0) (2015) 347–360.
[3] Y.S. Hedberg, NPJ Mater. Degrad. 2 (1) (2018) 26.
[4] R. Hou, R. Willumeit-Römer, V.M. Garamus, M. Frant, J. Koll, F. Feyerabend, ACS Appl. Mater. Interfaces 10 (49) (2018) 42175–42185.
[5] S. Höhn, S. Virtanen, A.R. Boccaccini, Appl. Surf. Sci. 464 (2019) 212–219.
[6] R.Q. Hou, N. Scharnagl, R. Willumeit-Romer, F. Feyerabend, Acta Biomater. 98 (2019) 256–268.
[7] N. Sezer, Z. Evis, S.M. Kayhan, A. Tahmasebifar, M. Koç, J. Magnesium Alloys 6 (1) (2018) 23–43.
[8] M. Esmaily, J.E. Svensson, S. Fajardo, N. Birbilis, G.S. Frankel, S. Virtanen, R. Arrabal, S. Thomas, L.G. Johansson, Prog. Mater. Sci. 89 (2017) 92–193.
[9] S. Johnston, M. Dargusch, A. Atrens, Sci. China Mater. 61 (4) (2017) 475–500.
[10] J. Song, J. She, D. Chen, F. Pan, J. Magnesium Alloys 8 (1) (2020) 1–41.
[11] Y. Jang, B. Collins, J. Sankar, Y. Yun, Acta Biomater. 9 (10) (2013) 8761–8770.
[12] X.-B. Chen, C. Li, D. Xu, Bioactive Mater. 3 (1) (2018) 110–117.
[13] R. Hou, J. Victoria-Hernandez, P. Jiang, R. Willumeit-Romer, B. Luthringer-Feyerabend, S. Yi, D. Letzig, F. Feyerabend, Acta Biomater. 97 (2019) 608–622.
[14] Y. Yang, J. Zhou, Q. Chen, R. Detsch, X. Cui, G. Jin, S. Virtanen, A.R. Boccaccini, ACS Appl Mater Interfaces 11 (33) (2019) 29667–29680.
[15] D. Yu, H. Qiu, X. Mou, Z. Dou, N. Zhou, Q. Guo, N. Lyu, L. Lu, Z. Yang, N. Huang, ACS Biomater. Sci. Eng. 5 (9) (2019) 4331–4340.
[16] G. Yang, H. Yang, L. Shi, T. Wang, W. Zhou, T. Zhou, W. Han, Z. Zhang, W. Lu, J. Hu, ACS Biomater. Sci. Eng. 4 (12) (2018) 4289–4298.
[17] Z.-Z. Yin, W.-C. Qi, R.-C. Zeng, X.-B. Chen, C.-D. Gu, S.-K. Guan, Y.-F. Zheng, J. Magnesium Alloys 8 (1) (2020) 42–65.
[18] M. Liu, J. Wang, S. Zhu, Y. Zhang, Y. Sun, L. Wang, S. Guan, J. Magnesium Alloys 8 (1) (2020) 231–240.
[19] S.V. Lamaka, J. Gonzalez, D. Mei, F. Feyerabend, R. Willumeit-Römer, M.L. Zheludkevich, Adv. Mater. Interfaces 5 (18) (2018) 1800169.
[20] D. Mei, S.V. Lamaka, J. Gonzalez, F. Feyerabend, R. Willumeit-Römer, M.L. Zheludkevich, Corros. Sci. 147 (2019) 81–93.
[21] N.A. Agha, F. Feyerabend, B. Mihailova, S. Heidrich, U. Bismayer, R. Willumeit-Römer, Mater. Sci. Eng. 58 (2016) 817–825.
[22] X.B. Chen, N. Birbilis, T.B. Abbott, Corros. Sci. 55 (Supplement C) (2012) 226–232.
[23] A. Mohamed, A.M. El-Aziz, H.-G. Breitinger, J. Magnesium Alloys 7 (2) (2019) 249–257.
[24] D. Mei, S.V. Lamaka, C. Feiler, M.L. Zheludkevich, Corros. Sci. 153 (2019) 258–271.
[25] S.V. Lamaka, B. Vaghefinazari, D. Mei, R.P. Petrauskas, D. Höche, M.L. Zheludkevich, Corros. Sci. 128 (2017) 224–240.
[26] R.-Q. Hou, N. Scharnagl, F. Feyerabend, R. Willumeit-Römer, Corros. Sci. 132 (2018) 35–45.
[27] J. Walker, S. Shadanbaz, N.T. Kirkland, E. Stace, T. Woodfield, M.P. Staiger, G.J. Dias, J. Biomed. Mater. Res. Part B 100B (4) (2012) 1134–1141.
[28] N.T. Kirkland, J. Waterman, N. Birbilis, G. Dias, T.B.F. Woodfield, R.M. Hartshorn, M.P. Staiger, J. Mater. Sci. Mater. Med. 23 (2) (2012) 283–291.

Please cite this article as: D. Mei, C. Wang and S.V. Lamaka et al., Clarifying the influence of albumin on the initial stages of magnesium corrosion in Hank’s balanced salt solution, Journal of Magnesium and Alloys, https://doi.org/10.1016/j.jma.2020.07.002

[29] N.T. Kirkland, N. Birbilis, J. Walker, T. Woodfield, G.J. Dias, M.P. Staiger, J. Biomed. Mater. Res. Part B 95 (1) (2010) 91–100.
[30] C.L. Liu, Y.J. Wang, R.C. Zeng, X.M. Zhang, W.J. Huang, P.K. Chu, Corros. Sci. 52 (10) (2010) 3341–3347.
[31] J. Zhang, N. Kong, Y. Shi, J. Niu, L. Mao, H. Li, M. Xiong, G. Yuan, Corros. Sci. 85 (2014) 477–481.
[32] T. Li, Y. He, J. Zhou, S. Tang, Y. Yang, X. Wang, Mater. Lett. 217 (2018) 227–230.
[33] S.E. Harandi, P.C. Banerjee, C.D. Easton, R.K. Singh Raman, Mater. Sci. Eng. 80 (2017) 335–345.
[34] X. Gu, Y. Zheng, L. Chen, Biomed. Mater. 4 (6) (2009) 065011.
[35] I. Marco, F. Feyerabend, R. Willumeit-Römer, O. Van der Biest, Mater. Sci. Eng. 62 (2016) 68–78.
[36] S. Johnston, Z.M. Shi, J. Venezuela, C.E. Wen, M.S. Dargusch, A. Atrens, JOM 71 (4) (2019) 1406–1413.
[37] Y. Zhao, C. Qiao, Z. Fang, H. Wang, S. Zhu, J. Wang, J. Ren, S. Guan, Y. Jia, Langmuir 35 (52) (2019) 17009–17015.
[38] H. Wang, Z. Fang, Y. Zhao, S. Yao, J. Li, J. Wang, S. Zhu, C. Niu, Y. Jia, S. Guan, Appl. Surf. Sci. 512 (2020) 145725.
[39] Z. Fang, J. Wang, S. Zhu, X. Yang, Y. Jia, Q. Sun, S. Guan, PCCP 20 (5) (2018) 3602–3607.
[40] Z. Fang, J. Wang, X. Yang, Q. Sun, Y. Jia, H. Liu, T. Xi, S. Guan, Appl. Surf. Sci. 409 (2017) 149–155.
[41] Z. Fang, Y. Zhao, H. Wang, J. Wang, S. Zhu, Y. Jia, J.-H. Cho, S. Guan, Appl. Surf. Sci. 470 (2019) 893–898.
[42] A. Atrens, S. Johnston, Z. Shi, M.S. Dargusch, Scr. Mater. 154 (2018) 92–100.
[43] M. Kroll, R. Elin, Clin. Chem. 31 (2) (1985) 244–246.
[44] P. Maurer, E. Hohenester, J. Engel, Curr. Opin. Cell Biol. 8 (5) (1996) 609–617.
[45] W. Robertson, R. Marshall, G.N. Bowers, CRC Crit. Rev. Clin. Lab. Sci. 15 (2) (1981) 85–125.
[46] R. Willumeit, J. Fischer, F. Feyerabend, N. Hort, U. Bismayer, S. Heidrich, B. Mihailova, Acta Biomater. 7 (6) (2011) 2704–2715.
[47] F. El-Taib Heakal, A.M. Bakry, Mater. Chem. Phys. 220 (2018) 35–49.
[48] H.N. Christensen, Ann. N.Y. Acad. Sci. 133 (1) (1966) 34–40.
[49] W. Yan, Y.-J. Lian, Z.-Y. Zhang, M.-Q. Zeng, Z.-Q. Zhang, Z.-Z. Yin, L.-Y. Cui, R.-C. Zeng, Bioactive Mater. 5 (2) (2020) 318–333.
[50] C. Feiler, D. Mei, B. Vaghefinazari, T. Würger, R.H. Meißner, B.J.C. Luthringer-Feyerabend, D.A. Winkler, M.L. Zheludkevich, S.V. Lamaka, Corros. Sci. 163 (2019) 108245.
[51] E.L. Silva, S.V. Lamaka, D. Mei, M.L. Zheludkevich, Chem. Open 7 (8) (2018) 664–668.
[52] J. Figge, T. Rossing, V. Fencl, J. Lab. Clin. Med. 117 (6) (1991) 453–467.
[53] J. Figge, T. Mydosh, V. Fencl, J. Lab. Clin. Med. 120 (5) (1992) 713–719.
[54] H.E. Corey, Critical Care 9 (2) (2004) 184.
[55] J. Gonzalez, R.Q. Hou, E.P.S. Nidadavolu, R. Willumeit-Römer, F. Feyerabend, Bioactive Mater. 3 (2) (2018) 174–185.
[56] Standard Guide for in vitro Degradation Testing of Absorbable Metals, ASTM F3268-18a, ASTM International, 2018.
[57] NSAI, ISO 10993-12: 2012, 2012.
[58] A.S.f. Testing, Materials, ASTM G31-72: Standard Practice for Laboratory Immersion Corrosion Testing of Metals, ASTM, 2004.
[59] A. NACE, ASTMG31-12a, ASTM International, West Conshohocken, PA, 2012, p. 10.
[60] Y. Wang, C.S. Lim, C.V. Lim, M.S. Yong, E.K. Teo, L.N. Moh, Mater. Sci. Eng. 31 (3) (2011) 579–587.
[61] L.-Y. Cui, Y. Hu, R.-C. Zeng, Y.-X. Yang, D.-D. Sun, S.-Q. Li, F. Zhang, E.-H. Han, J. Mater. Sci. Technol. 33 (9) (2017) 971–986.
[62] Y. Song, D. Shan, R. Chen, F. Zhang, E.-H. Han, Mater. Sci. Eng. 29 (3) (2009) 1039–1045.
[63] A. Atrens, G.-L. Song, M. Liu, Z. Shi, F. Cao, M.S. Dargusch, Adv Eng Mater 17 (4) (2015) 400–453.
[64] P. Jiang, C. Blawert, N. Scharnagl, M.L. Zheludkevich, Corros. Sci. 153 (2019) 62–73.
[65] M. Strebl, M. Bruns, S. Virtanen, J. Electrochem. Soc. 167 (2) (2020) 021510.
[66] M. Strebl, S. Virtanen, J. Electrochem. Soc. 166 (11) (2019) C3001–C3009.
[67] D. Mei, S.V. Lamaka, X. Lu, M.L. Zheludkevich, Corros. Sci. 171 (2020) 108722.
[68] M. Kaseem, Y.G. Ko, Comp. Part B 176 (2019) 107225.
[69] R. Rettig, S. Virtanen, J Biomed. Mater. Res. Part A 88A (2) (2009) 359–369.
[70] W.-D. Mueller, M. Fernández Lorenzo de Mele, M.L. Nascimento, M. Zeddies, J. Biomed. Mater. Res. Part A 90A (2) (2009) 487–495.

Please cite this article as: D. Mei, C. Wang and S.V. Lamaka et al., Clarifying the influence of albumin on the initial stages of magnesium corrosion in Hank's balanced salt solution, Journal of Magnesium and Alloys, https://doi.org/10.1016/j.jma.2020.07.002

5. General discussion

In Chapter 4, the systematic works has been performed to investigate the influence of the medium components, including inorganic ions, synthetic pH buffers, small-molecule organic compounds, and macromolecule organic compound (protein), on Mg corrosion. The detail discussions about their mechanisms have been provided in the respective sections of Chapter 4.

In this chapter, based on the understandings about the influence of the media components on Mg corrosion, a more general discussion is provided to clarify the advantages, shortcomings, and applicability of several commonly used corrosive media in Mg corrosion tests and to outline the selection criteria of the medium for testing Mg degradation behavior. In addition, the discussion extends to the other biodegradable/bioabsorbable metallic materials, such as zinc and iron.

The following published paper was incorporated as Chapter 5:

D. Mei, S.V. Lamaka, X. Lu, M.L. Zheludkevich, Selecting medium for corrosion testing of bioabsorbable magnesium and other metals – a critical review, Corrosion Science, 171 (2020) 108722. https://doi.org/10.1016/j.corsci.2020.108722

D. Mei conceived the work based on the discussion with S.V. Lamaka and X. Lu. D. Mei and S.V. Lamaka carried out data collection and literature review. S.V. Lamaka, X. Lu and M.L. Zheludkevich gave constructive comments on refining the viewpoints. All the authors contributed to writing of the paper.

Corrosion Science 171 (2020) 108722

Contents lists available at ScienceDirect

Corrosion Science

journal homepage: www.elsevier.com/locate/corsci

Selecting medium for corrosion testing of bioabsorbable magnesium and other metals – A critical review

Di Mei[a,*], Sviatlana V. Lamaka[a], Xiaopeng Lu[b], Mikhail L. Zheludkevich[a,c]

[a] Magnesium Innovation Centre - MagIC, Institute of Materials Research, Helmholtz-Zentrum Geesthacht, Geesthacht, 21502, Germany
[b] Shenyang National Laboratory for Materials Science, Northeastern University, 3-11 Wenhua Road, Shenyang, 110819, China
[c] Institute for Materials Science, Faculty of Engineering, Kiel University, Kiel, 24103, Germany

ARTICLE INFO

Keywords:
Magnesium
Iron
Zinc
Corrosion medium
Bioabsorbable
Biodegradable

ABSTRACT

Corrosion testing of bioabsorbable metallic materials is important at material selection stage and for understanding their degradation mechanisms. A large variety of different corrosive media has been reported for evaluating degradation performance. This review takes magnesium as an example and focuses on discussing the advantages, shortcomings and applicability of commonly used corrosive media. The discrepancies between the published results disclosing Mg corrosion behavior often originate from non-comparable test media. This indicates the urgent need for verified corrosion test protocols. The media selection criteria are outlined. Additionally, the discussion extends to the other bioabsorbable metallic materials, such as zinc and iron.

1. Introduction

The application of magnesium [1–10], zinc [1,11–13] and iron [1,14,15] as bioabsorbable (or biodegradable) implant materials is a research hotspot in the field of novel metallic biomaterials, even though relevant investigations have been intensively performed for over a decade.

Magnesium is the most widely studied and most representative bioabsorbable metallic material. Of bioabsorbable metals, only magnesium-based implants are fully certified and are commercially available from the companies like BIOTRONIK (Magmaris®) [16], Syntellix AG (MAGNEZIX®) [17] and U&i (RESOMET®) [18]. On the other hand, the slower degradation rates of zinc and iron-based alloys make viable competition to magnesium [13,14]. In the recent years, a number of new alloys [19–27], processing routes [28–34] and surface modification methods [35–47] have been developed or applied to improve the anticorrosion and mechanical properties of Mg. A deep understanding of the corrosion behavior of Mg needs to be achieved prior to its wide application. Although there is still no clear quantitative relation between *in vivo* and *in vitro* corrosion behavior, corrosion tests are widely performed at the early stage of alloy development prior to much more expensive *in vivo* animal trails [48–50]. The selection of a corrosive media is an important part of the corrosion testing. Considering the main application potentials of Mg (vascular stent material and bone fixation material), the representative service environments are serum/plasma and interstitial fluid. Initially, isotonic solution (0.9 or 0.85 wt. % NaCl solution) was used as a corrosive medium. As understanding of the effects of body fluid components deepened, increasingly complex media have been used or designed for the corrosion test of Mg to make the test environment as close as possible to the real service environment. Ringer's solution, PBS (phosphate buffered saline), SBFs (simulated body fluids), HBSS (Hank's balanced salt solution) and cell culture medium are the representatives of test media. It is noteworthy that most of the media were not initially designed corrosion testing of bioabsorbable metals. For example, SBF (proposed by Kokubo [51] et al.) and m-SBF (proposed by Oyane [52] et al.) were designed for predicting the bone bioactivity of materials, PBS and Ringer's solution were designed for biological research, MEM (Minimum Essential medium) and DMEM (Dulbecco's modified Eagle's medium) were designed for cell cultures. The effect of components of these media on the corrosion of bioabsorbable metals was not understood when they were initially used.

Recently, a number of published papers focused on influence of individual components in corrosive media on Mg corrosion [48,53–59]. As important components of SBF, synthetic pH buffers (foreign to any of physiological fluids, e.g. Tris, HEPES) were shown to have a strong acceleration effect on Mg corrosion [48,58,60–66]. There is a viewpoint that the presence of synthetic pH buffer is necessary in the corrosion test media, to mimic the strong buffering capacity of the real body fluids [62]. However, recently published papers show that Tris and HEPES although have pH buffering effect over the bulk electrolyte,

* Corresponding author.
E-mail address: di.mei@hzg.de (D. Mei).

https://doi.org/10.1016/j.corsci.2020.108722
Received 26 March 2020; Received in revised form 24 April 2020; Accepted 28 April 2020
Available online 01 May 2020

cannot stabilize the local pH at the electrolyte/metal interface. It has been shown that local pH increases over 9.0 and even exceeds 10 in some locations of the interface immersed in Tris and HEPES containing SBF-like electrolytes [48,58]. This means that the corrosion process under *in vivo* conditions and in the presence of synthetic pH buffers are very different at the interface, which is the only place where it actually matters. In addition, the effect of a variety of inorganic ions on Mg corrosion has been investigated systematically, including carbonate, phosphate, sulfate and Ca^{2+}. Among them, the synergy between carbonate, phosphate and Ca^{2+} on the corrosion protection of Mg has been emphasized [48,58]. Besides, the influence of dozens of bio-relevant small-molecule organic compounds (constituting cell culture media) solely or combined in groups of amino acids, vitamins, saccharides and Kreb's cycle compounds, has also been explored [59,67–70]. The results showed that most of them have no critical influence on the corrosion rate owing to low physiological concentration. In addition, a series of works has been performed to investigate the influence of protein or a combination of proteins on Mg corrosion [71–77]. These fundamental works deepen the understanding of the importance of the corrosion media composition on the test outcome.

It should be noted that there is no universal medium for all the corrosion test methods due to the diversity of test conditions. As an example, a cell culture medium with protein mixture, which is regarded as the most suitable "simulated body fluid" [77], is an appropriate corrosive medium for weight loss measurements under cell culture conditions. However, due to a high risk of microbial development, they can hardly be used for long-term electrochemical tests in an open environment or for hydrogen evolution measurements. Conversely, NaCl solution has no risk of such contamination, but the electrolyte is too simplistic to predict the *in vivo* corrosion behavior of Mg. Therefore, it is necessary to sort the commonly used corrosive media and clarify the domains of their applicability.

Xin [78] et al. emphasized the importance of establishing corrosion test standards for biodegradable Mg several years ago. Through hundreds of related published papers, discrepancies between the experimental results from different research groups could be found [78,79]. Even if the same material was tested, the obtained corrosion rates often varied owing to different test media and test methods employed. At the initial screening stage of potential materials before an *in vivo* test, the absence of a generally accepted test protocol leads to obtaining half the results with twice the effort. Although an ASTM standard [80] has been enforced recently to provide guidelines for corrosion tests of bioabsorbable metallic materials, there is still no established test protocol.

Understanding the effects of corrosive media is not only beneficial for establishing generally accepted corrosion test protocols of Mg for biomedical application but also for promoting the development of bioabsorbable metallic materials in general [81]. In this review, we discuss several commonly used corrosive media for Mg. Based on the published literature and own research experience, the advantages and shortcomings of these media and their applicability are discussed. On this basis, the applicability of test media for other bioabsorbable metallic materials, like iron and zinc, is additionally discussed.

2. Commonly used corrosive media

The advantages, shortcomings and applicability of NaCl solution, complex saline solution, simulated body fluids, cell culture medium and protein-containing solutions are discussed below. As illustrated in Fig. 1, following the aforementioned sequence, from NaCl solution to protein-containing solutions, the complexity of corrosive media increases stepwise with the appearance of various inorganic ions, small-molecule organic compounds and proteins. The components of corrosive media become closer to that of real body fluid, e.g. serum/plasma and interstitial fluid. Table 1 lists the main components of these media.

2.1. Simple isotonic solution (NaCl solution)

As the most common medium for corrosion tests, NaCl solution is used in the corrosion tests of Mg for both engineering and biomedical applications [82,111–113]. NaCl solutions with concentrations of 0.85 wt.% or 0.9 wt.%, of the same osmolality as human plasma, is regarded as a simple isotonic solution. NaCl solution with other concentrations, such as 0.5 wt.% [114], 3.5 wt.% [47,113] and 0.05 M [115], has also been used in Mg corrosion tests but are not common when testing Mg for biomedical applications. Compared to more complex pseudophysiological electrolytes, such as HBSS and MEM, NaCl solution is a harsh medium that typically leads to significant corrosion attack. The basic corrosion reactions of Mg in aqueous solution can be described by the following equations [116–121]:

(Main, accompanied by hydrogen evolution reaction (HER))

$$Mg + 2H_2O \rightarrow Mg(OH)_2 + H_2\uparrow \quad (1)$$

(Secondary, accompanied by Oxygen reduction reaction (ORR))

$$2Mg + 2H_2O + O_2 \rightarrow 2Mg(OH)_2 \quad (2)$$

Virtually, at any initial pH of the bulk electrolyte, the local pH near the corroded Mg surface exposed to NaCl solution remains alkaline and the corrosion products consist primarily of $Mg(OH)_2$ and MgO. This surface film with porous structure cannot provide sufficient protection in Cl^--containing electrolytes. The visual appearance of a corroded pure Mg demonstrates the high aggressiveness of NaCl solution as a corrosive medium, Fig. 2. Since insufficiently protective corrosion products are formed, the corrosion tests in NaCl solution provide more information about the material itself. The influence of alloying elements, impurities, surface preparation, processing, grain size, orientation and microstructural features on Mg corrosion can be successfully reflected by the corrosion tests in NaCl [59]. However, by using NaCl solutions, the role of other multiple organic and inorganic components in body fluids is simplified to the role of ionic strength contributors. In serum/plasma and interstitial fluid, the combination of inorganic ions, such as carbonate, phosphate, and Ca^{2+}, significantly influences the rate and mechanism of Mg corrosion. On the other hand, the simplicity of NaCl solution makes it suitable for various corrosion tests with a low risk of contamination caused by the growth of microbial life.

Synthetic pH buffers (e.g. Tris, HEPES) have been introduced in simple NaCl to mimic the buffering capacity of real body fluids [63,66,84]. The results showed that the presence of the synthetic pH buffer accelerates Mg corrosion. This acceleration effect is attributed to the limited formation of the product layer due to the consumption of OH^- by the synthetic pH buffer. However, compared with the physiological buffers (phosphate/carbonate) in the human body, the mechanisms of Tris and HEPES are different and are discussed in Section 2.3 of this paper.

In summary, corrosion tests in NaCl solutions cannot reflect the complexity of real body fluids. Comparing to more complex media, NaCl solution is the most aggressive medium that is beneficial for differentiating the intrinsic corrosion susceptibility properties of the metallic substrates.

2.2. Complex saline solution

Phosphate buffered saline (PBS) is a commonly used solution in biological research and contains NaCl, KCl, KH_2PO_4 and Na_2HPO_4 salts. It has been used as a corrosive medium for testing the applicability of Mg alloys for biomedical application [61,85–88]. Compared with the simple NaCl solution, KH_2PO_4 and Na_2HPO_4 buffer the pH value of the medium in the range of 5.8–8.0 [122]. Most importantly, the phosphates in PBS can also slow down the corrosion rate of Mg owing to formation of a magnesium phosphate layer. The latter also buffers the local pH at the metal interface.

Xue [88] et al. investigated the corrosion behavior of Mg alloys in

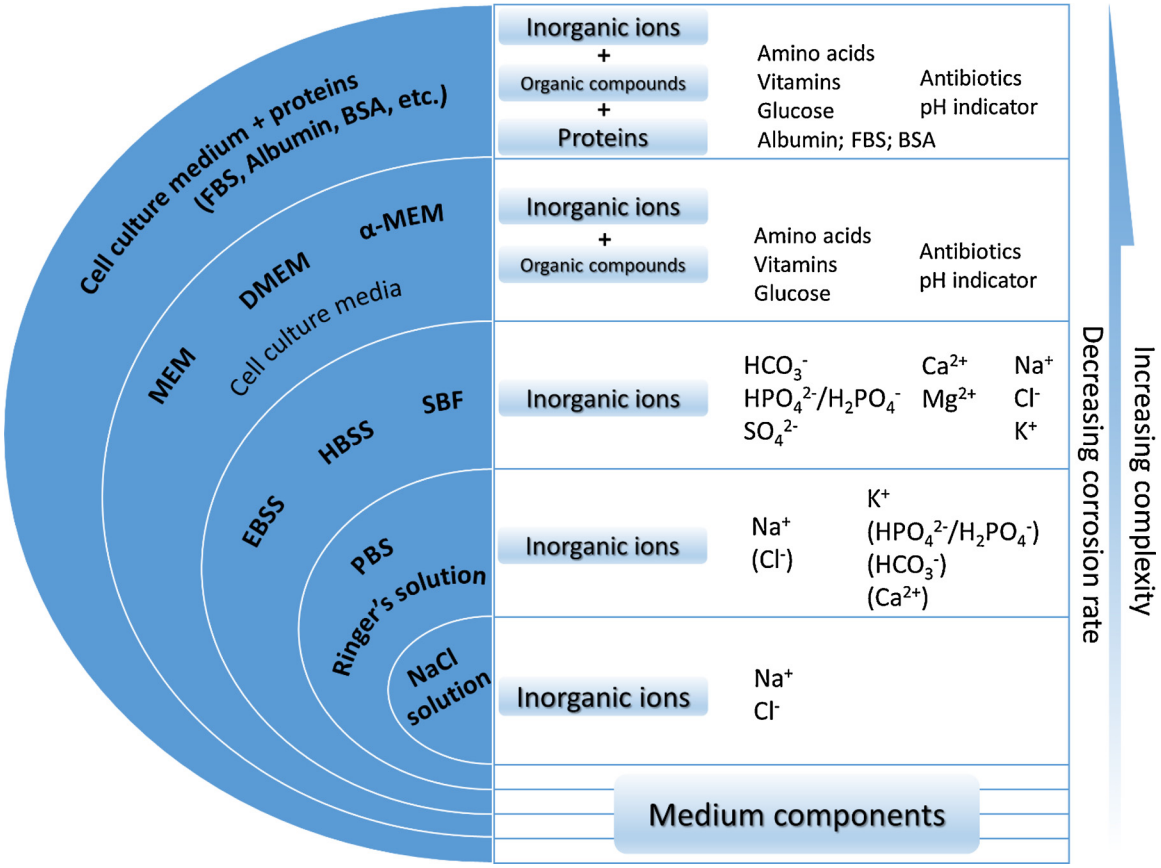

Fig. 1. Commonly used corrosive media for testing bio-absorbable metals. Typically, the corrosion rate of magnesium is decreased as a function of increasing complexity of the media. Ions in the brackets occasionally added to corresponding medium.

deionized water (DI water), PBS and Tris-buffered SBF. The slowest corrosion rate was found in DI water and PBS. However, the corrosion rate of Mg in PBS was higher than that in a cell culture medium as reported by Yun [123] et al. This can be attributed to the absence of several inorganic components, like Ca^{2+} and carbonate in PBS. In the following sections, the dominating role of inorganic ions (i.e. Ca^{2+}, carbonate and phosphates) on Mg corrosion protection is emphasized. Although Tris-buffered SBF that used in Xue's work [88] contains inorganic components similar to the cell culture medium, the presence of Tris, which is one of the commonly used synthetic pH buffers, significantly accelerated the corrosion rate of Mg, this is discussed in the next section.

Another type of complex saline electrolyte is Ringer's solution, which is a more complex isotonic solution relative to the body fluids of animals. Ringer's solution is named after Sydney Ringer, who investigated the cardiac perfusion fluid of frogs and its effect on maintaining a heart-beat in the 1880s [124–127]. In the following decades, other components were added to the original Ringer's solution. A number of modified solutions named Krebs-Ringer's solution [128], Ringer-Tyrode solution [129], and Ringer-Locke solution [130] were proposed for different animals and for different purposes. However, for corrosion testing of metallic biomaterials, the composition of the Ringer's solution is not strictly defined. There are at least three different recipes that have been used: with HCO_3^- [89–92], without HCO_3^- [93–95,131] or with lactate [132]. The difference causes greatly varying corrosion behavior when used with metallic biomaterials. In case of Mg, the combination of Ca^{2+}, HCO_3^- and alkaline pH at Mg interface, leads to formation of $CaCO_3$, which slows down the corrosion rate [118,133–135]. However, the insufficient inorganic ions (the absence of phosphates, compared to the components of human serum and interstitial fluid) in Ringer's solution lead to a relatively high corrosion rate of Mg. As an extreme example, the corrosion rate of AZ91 measured in Ringer's solution (with HCO_3^-) was found to be 92.0 ± 6.72 mm·year^{-1} [91], which is a hundred times higher than the *in vivo* degradation rate (0.7 ± 0.5 mm·year^{-1}) [136].

In general, the use of complex saline solutions as corrosive media for the corrosion test of Mg for biomedical application is not reliable. Compared with NaCl solution, the complex saline solutions provide a more complicated test environment. However, they lack several important inorganic ions (e.g. Ca^{2+}, carbonate or phosphates), which have a significant influence on Mg corrosion. This shortcoming allows rating corrosion tests in such media as of having limited informational value.

2.3. Simulated body fluids

"Simulated body fluids" is a general term referring to the media containing all the major inorganic ions (without bio-relevant organic compounds except for glucose) that are present in human serum and interstitial fluid. Common representatives are so-called simulated body fluid (SBF), Hank's balanced salt solution (HBSS) and Earle's balanced salt solution (EBSS). Typical compositions of these media are presented in Table 1.

SBF, HBSS and EBSS are typically constituted by similar inorganic components, while their concentration is slightly different. However, it is noteworthy that the composition of these media is not fixed, and several media with different components have the same or similar name in literatures. This can be confusing to readers and hampers the comparability of the results. As an example, electrolytes with Ca^{2+} [96,137–139] or without Ca^{2+} [67,140–142] are all named HBSS in the papers. Similarly, SBF also has multiple recipes with different concentrations of ions or different synthetic pH buffers [51,100,143]. In a

Table 1
The main components of commonly used corrosive media.

Medium	Concentration of components (mM)												
	Na^+	K^+	Mg^{2+}	Ca^{2+}	Cl^-	HCO_3^-	$HPO_4^{2-}/H_2PO_4^-$	SO_4^{2-}	Synthetic pH buffer	Glucose	Vitamins	Amino acids	Proteins
NaCl solution [59,82,83,84]	145.3-153.8	/	/	/	145.3-153.8	/	/	/	/	/	/	/	/
PBS [61,85,86,87,88]	146-157	4.1	/	/	140.6	/	9.5-11.5	/	/	/	/	/	/
Ringer's solution [89,90,91,92,93,94,95]	147-156.4	4.0-5.8	/	1.4-2.2	155.4-164.2	*2.4*	/	/	/	/	/	/	/
HBSS [67,74,77,96,97,98]	142.8	5.8	*0.8*	*1.2-2.5*	143.3-148.3	4.2	0.8	*0.4-0.8*	*50.5 (Tris)25.0-50.0 (HEPES)*	5.6	/	/	/
SBF [51,52,99,100,101]	142.0	5.0	1.0-1.5	2.5	103-148.8	4.2-27	1.0	0-0.5	*50.5 (Tris)25.0-75.0 (HEPES)*	/	/	/	/
EBSS [84,99,102,103,104]	144-151	5.4	0.4-0.8	1.8	125	26.2	0.9-1.0	0.4-0.8	/	5.6	/	/	/
Cell culture medium [59,84,102,105,106,107]	132.4-155.4	5.3	0.8	1.8	119.3-126.1	26.2-44	0.9-1.0	0.8	*15.0-75.0 (HEPES)*	5.6-25	8.1-31.6 mg/L	848 −1852 mg/L	/
Protein-containing solutions* [71,72,74,75,77,102,105,106,107,108,109,110]	132.4-155.4	5.3	0.8	1.8	119.3-126.1	26.2-44	0.9-1.0	0.8	*50.5 (Tris)15.0-75.0 (HEPES)*	5.6-25	8.1-31.6 mg/L	848 −1852 mg/L	10-20 vol. % FBS or 1-40 g/L albumin

"*Italic*" means this component is occasionally included as a part of these media.
* Mainly refer to protein containing cell culture medium/simulated body fluids.

number of published papers, detailed compositions of corrosive media employed for experiments were not listed or/and the usage of the pH buffer was not specified [75,88,144–149]. These problems hamper reliable comparison of the research results from different works.

The individual effect of inorganic ions constituting simulating body fluids (such as Cl^-, carbonate, phosphates, sulfate and Ca^{2+}) on corrosion rate has been largely explored. The presence of carbonate and phosphates slows down the corrosion rate of Mg, while the influence of sulfate is not significant [48,54,55,57,150]. The concentration of HCO_3^- influences not only the pH buffering capacity (as a part of a HCO_3^-/CO_2 buffer) but also the corrosion behavior of Mg. However, the concentration of HCO_3^- varies significantly in different simulated body fluids. For example, the concentration of HCO_3^- in r-SBF is ~27 mM, which is significantly higher than that in SBF (~4 mM) [51]. With increasing concentrations of HCO_3^- in Tris-buffered SBF, the corrosion rate of pure Mg decreases accordingly [150]. Phosphates often appear in the compositions of simulated body fluids. Under the physiological environment (pH: 7.35–7.45), HPO_4^{2-} and $H_2PO_4^-$ do coexist. In accordance with the deprotonation constants, the fraction of $H_2PO_4^-$ increases at pH lower than 7.3, while the fraction of HPO_4^{2-} dominates at pH above 7.3. It can be found that Ca^{2+} on its own has no significant influence on Mg corrosion [10], but the synergy between Ca^{2+}, Mg^{2+}, HCO_3^- and $H_2PO_4^-/HPO_4^{2-}$ induces a fast co-precipitation of these ions on the surface of Mg. Formed protective layer slows down the corrosion rate of commercially pure Mg (CP Mg) [48]. This also holds true for a number of alloys, including Mg-1.2Ca, Mg-2Ag and Mg-10Gd-1Nd-0.3Ca (E11) alloys [58,59]. Agha [141] et al. reported similar results that the synergy between Ca^{2+}, HCO_3^- and HPO_4^{2-} played an important role in the corrosion of highly pure Mg (HP Mg). It has been found that the corrosion of Mg alloys in simulated body fluids is dominated by the protective capacity of the formed corrosion products and is mainly controlled by the presence and concentration (activity) of specific inorganic components, such as Ca^{2+}, Mg^{2+}, HCO_3^- and $H_2PO_4^-/HPO_4^{2-}$ [58,59]. Thus, different Mg alloys possibly show similar corrosion rate and behavior in simulated body fluid even though they display different intrinsic corrosion resistance in NaCl solution. This point is verified by the results shown in Fig. 3, the corrosion behavior and corrosion rate of CP Mg and Mg-Ca in SBF (without Tris) are similar, while, in NaCl solution, two materials degrade at significantly different rate, over 6 times [59].

Glucose, phenol red and synthetic pH buffers, as the main components of simulated body fluids, have also attracted the research attention. Glucose and phenol red were found to have no significant influence on Mg corrosion [59,66]. However, the influence of pH buffers is significant. Tris, HEPES and HCO_3^-/CO_2, as commonly used pH buffers, have been introduced into different types of simulated body fluids. The aim for using a pH buffer is to mimic the humoral regulation in an animal body, but the selection of buffer should be more cautious. Tris and HEPES are synthetic buffers with sufficient buffer capacity that cover the pH range of the physiological environment. However, they accelerate the Mg corrosion owing to their pH buffering capacity and complexing effect [48,58,60,63]. Through the Scanning Ion-selective Electrode Technique (SIET) and Difference Viewer Imaging Technique (DVIT) measurements, these synthetic pH buffers have been shown to have no buffering effect on the local pH near the corroded Mg surface (Fig. 4(a, c)). Thus, the pH at the interface, the most important location in terms of pH stabilization is actually not fully stabilized by the synthetic pH buffers. On the contrary, HEPES and Tris delay the formation of a protective co-precipitate layer [48,58] due to local consumption of generated OH- and slight binding of Ca^{2+} and Mg^{2+}, thus lowering the concentration of the ionic species required for precipitate formation. The absence of co-precipitate layer leads to the high local pH. All these findings indicate that it is unreasonable to continue using these synthetic buffers for Mg corrosion tests. As an alternative to synthetic buffers, a natural pH buffer, HCO_3^-/CO_2, is commonly used in immersion tests under cell culture conditions. The reliability of $HCO_3^-/$

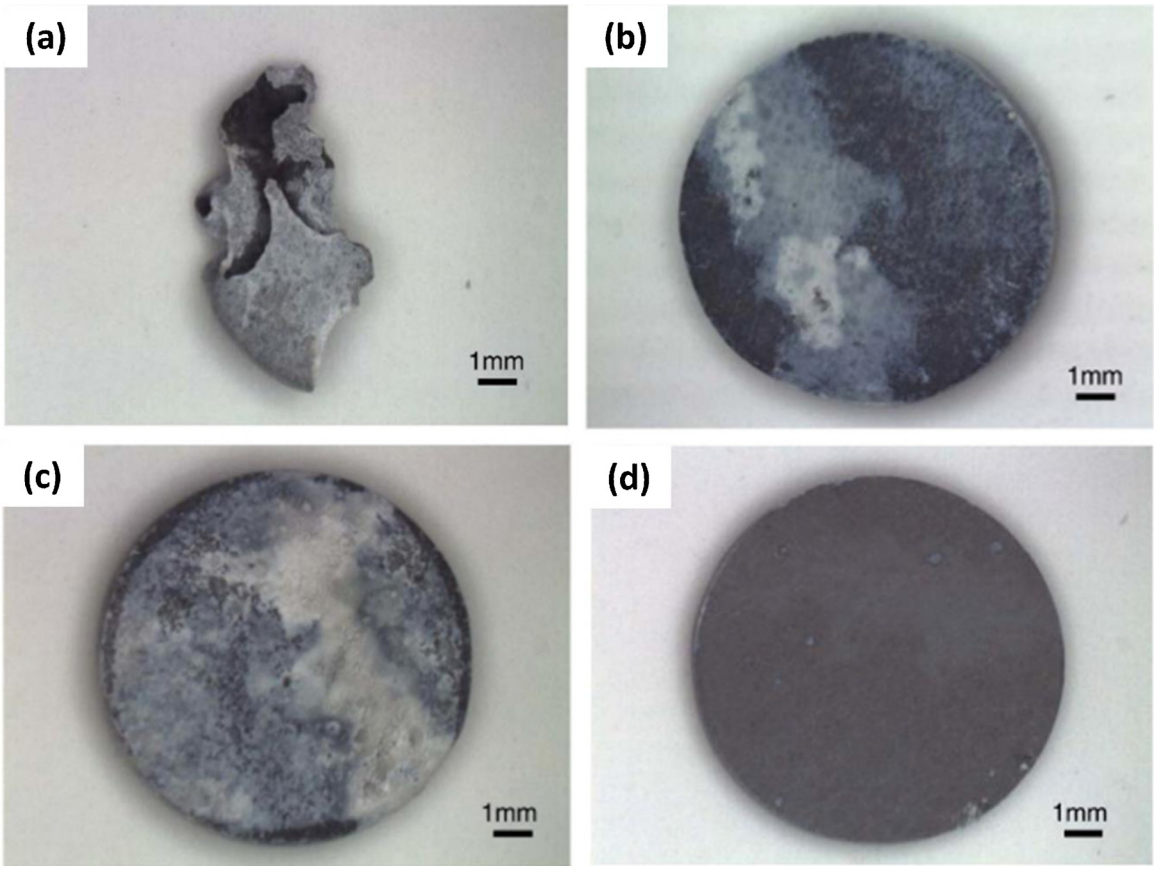

Fig. 2. Visual appearance of Mg disks after 14 d of immersion into NaCl solution (a), EBSS (b), MEM (c), and MEM + fetal bovine serum (d) [84]. Reprinted from Materials Science and Engineering: C, 29, A. Yamamoto, S. Hiromoto, Effect of inorganic salts, amino acids and proteins on the degradation of pure magnesium in vitro, 1559–1568, Copyright (2009), with permission from Elsevier.

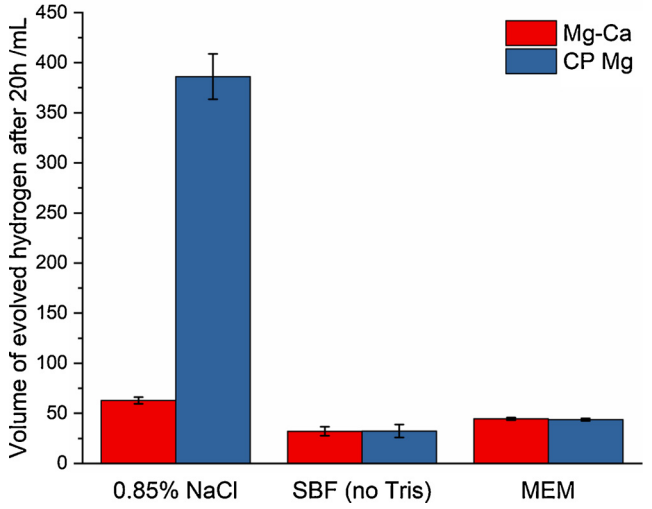

Fig. 3. The volumes of evolved hydrogen after 20 h immersion of Mg-0.8Ca alloy and CP Mg in 0.85% NaCl solution, SBF (no Tris) and MEM. This graph was drawn based on the results reported in Ref. [59].

CO_2 buffer originates from three factors: high buffering capacity, constant supply of CO_2 and similarity of corrosion mechanism/formed corrosion products to those occurring *in vivo*. The HCO_3^-/CO_2 buffer, which has a dual effect due to its buffering capacity and inhibition of corrosion, maintains the pH value of the medium within the local pH values of 7.8-8.5. More specifically, the chemical equilibrium between $H_2CO_3(CO_2)$, HCO_3^-, and CO_3^{2-} in the electrolyte provides the pH buffering capacity. Meanwhile, the carbonate from $NaHCO_3$ and the dissolution of CO_2 strengthens the formation of the above mentioned co-precipitate layer [78] that slows down the Mg corrosion and decreases the concentration of generated OH^- in the diffusion layer. However, due to technical arrangements of the methods, the HCO_3^-/CO_2 buffer cannot be easily applied in hydrogen evolution and electrochemical tests. On the other hand, even in the simulated body fluid without additional supply of CO_2, the bulk and local pH are maintained in the same pH range due to the formation of a protective layer (as shown in Fig. 4(b, d)) [48,58,59]. Thus, the usage of the simulated body fluids without additional pH buffers is acceptable. However, in this case, it is of paramount importance to maintain constant medium composition and to avoid the depletion of the media components.

In general, simulated body fluids are suitable for corrosion tests, but the synthetic pH buffers should not be added in the test media. Compared with the tests that performed in NaCl and complex saline solutions, the corrosion tests in simulated body fluids lead to the formation of corrosion products similar to those found *in vivo*. However, different Mg alloys tested in simulated body fluids show similar corrosion rates due to similar composition of the quasi-protective corrosion products. This levels out the difference between the degradation rates/mechanisms of different Mg alloys, which is more apparent in NaCl electrolyte.

2.4. Cell culture medium

A number of cell culture media have been designed for *in vitro* cell biology research, which include not only inorganic ions but also small-molecule organic components. In corrosion research of metallic biomaterials, cell culture media have been employed as a corrosive

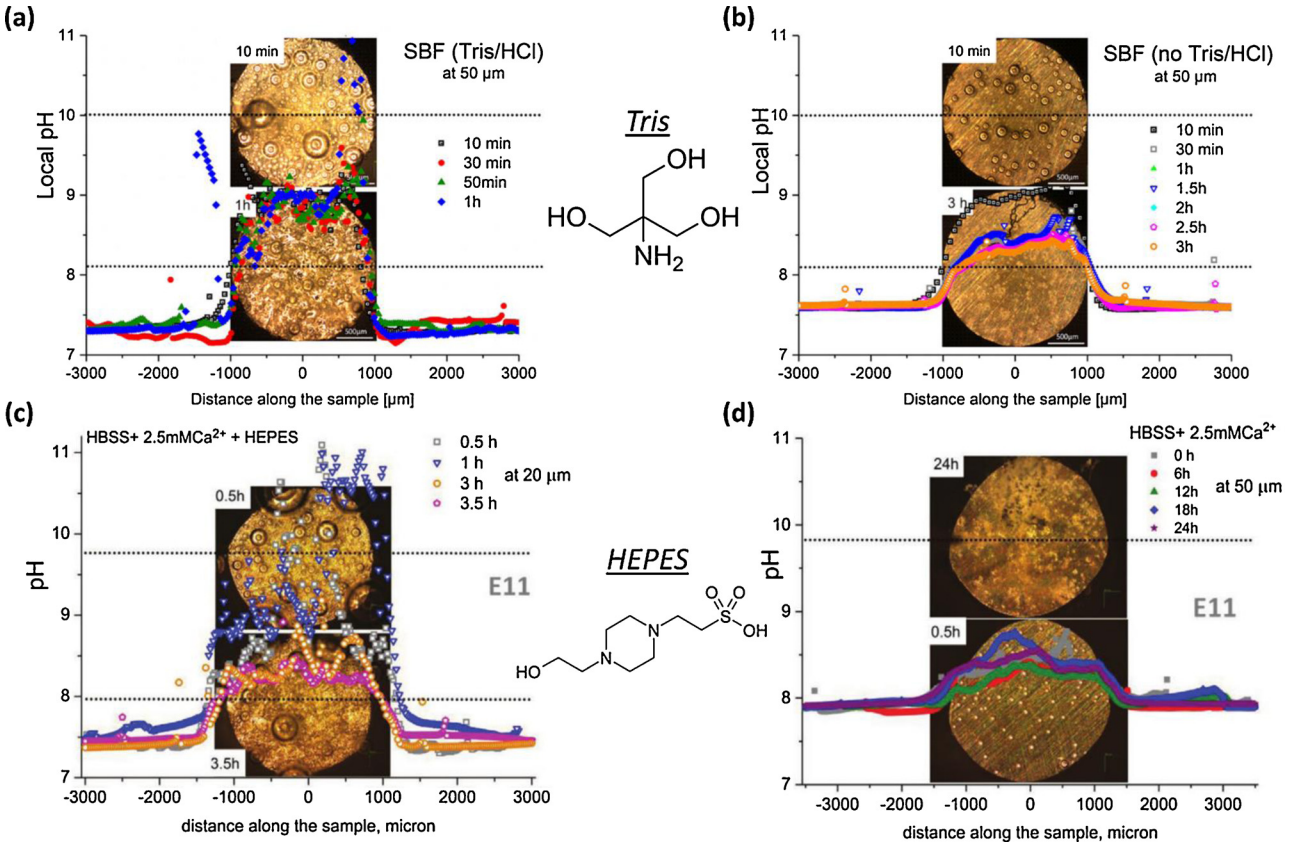

Fig. 4. Local pH measurements of CP Mg (a, b) and E11 (Mg-10Gd-1Nd-0.3Ca) (c, d) immersed in (a) SBF with Tris/HCl; (b) SBF without Tris/HCl; (c) HBSS + Ca with HEPES; (d) HBSS + Ca without HEPES. Performed under hydrodynamic conditions [48,58]. Reprinted from Corrosion Science, 147, D. Mei, S.V. Lamaka, J. Gonzalez, F. Feyerabend, R. Willumeit-Römer, M.L. Zheludkevich, The role of individual components of simulated body fluid on the corrosion behavior of commercially pure Mg, 81–93, Copyright (2019), with permission from Elsevier. Reprinted from Advanced Materials Interfaces, S.V. Lamaka, J. Gonzalez, D. Mei, F. Feyerabend, R. Willumeit-Römer, M.L. Zheludkevich, Local pH and Its Evolution Near Mg Alloy Surfaces Exposed to Simulated Body Fluids, 1,800,169, Copyright (2018), with permission from John Wiley and Sons.

medium due to its similarities with interstitial fluid.

Similar to simulated body fluids, cell culture medium is a type of mild corrosive medium. The difference in the corrosion rate between different Mg alloys is leveled out in cell culture medium. Wagener [105] et al. found that Ca-P products (similar to those formed in simulated body fluids) were formed on Mg surface during an immersion test in DMEM. Chen [151] et al. and Gnedenkov [152,153] et al. reported similar electrochemical test results for AZ31, Mg-*Zn*-Ca, Mg-Li and MA8 alloys during a short immersion test in MEM. In our previous work [59], two types of Mg, CP Mg and Mg-0.8Ca, demonstrated have similar corrosion rates and corrosion products after exposure in MEM.

The obvious difference between simulated body fluid and cell culture medium is that there are bio-relevant organic compounds in the latter one. Yamamoto [84] et al. found that the presence of amino acids and vitamins in EBSS accelerated the corrosion of Mg, but the results showed that the acceleration was only mild. Recently, the influence of small-molecule organic compounds has been investigated systemically [59,66,68,154]. Several individual amino acids, vitamins, saccharides, antibiotics and other organic compounds at high concentrations (0.05 M) were found to inhibit or accelerate Mg corrosion [66]. However, the concentration of organic compounds in cell culture media and plasma/serum is rather low, typically ranging from 10^{-4} M to 10^{-6} M [155]. Although these organic compounds are considered to influence the formation of corrosion products on corroded Mg to a certain extent [67,154], these bio-relevant small-molecules at lower concentrations do not critically influence cumulative corrosion rate of Mg in simulated body fluids or a cell culture medium [59]. As shown in Fig. 5, the impedance spectra of CP Mg and Mg-0.8Ca in both SBF and MEM show similar feature, which is a continuous growth of an additional time constant at high frequency range, which indicates the formation of protective continuous co-precipitate layer on the surface. The SEM images of CP Mg and Mg-0.8Ca after 24 h immersion in MEM and SBF also provides information that corrosion products on two alloys in two different media had similar morphology (Fig. 6). Combined with Fig. 3, which shows similar hydrogen evolution results of Mg alloys in SBF and MEM, it can be concluded that, similar to the tests in the simulated body fluid, the corrosion behavior of Mg in the cell culture medium is also mainly dominated by the inorganic components, namely a combination of Ca^{2+}, HCO_3^-, $H_2PO_4^-/HPO_4^{2-}$ and Mg^{2+}. These results indicate the similarity between the cell culture media and simulated body fluids. The similar weight loss of different Mg alloys after immersion in MEM and EBSS confirms this [102].

However, as a type of corrosive media, the obvious weakness of the cell culture media is that they are easily contaminated by microbial life that readily grows in the presence of the organic nutrients. Fig. 7 shows the hydrogen evolution curve coupled with the bulk pH change during 100 h of immersion using a flow-through cell in an open environment. The corrosion rate of MA8 Mg alloy sharply increases after ca. 30 h of immersion in MEM [152]. This is accompanied by the notable acidification of the bulk MEM caused by metabolic products of microbial life growth in MEM. Phenol red, a pH indicator that is one of the common components in cell culture media, can easily reveal this acidification by color change. It is an effective additive to the corrosive media to show the microbial life growth, that does not influence Mg corrosion [59].

In practice, antibiotics and UV light are applied to delay microbial

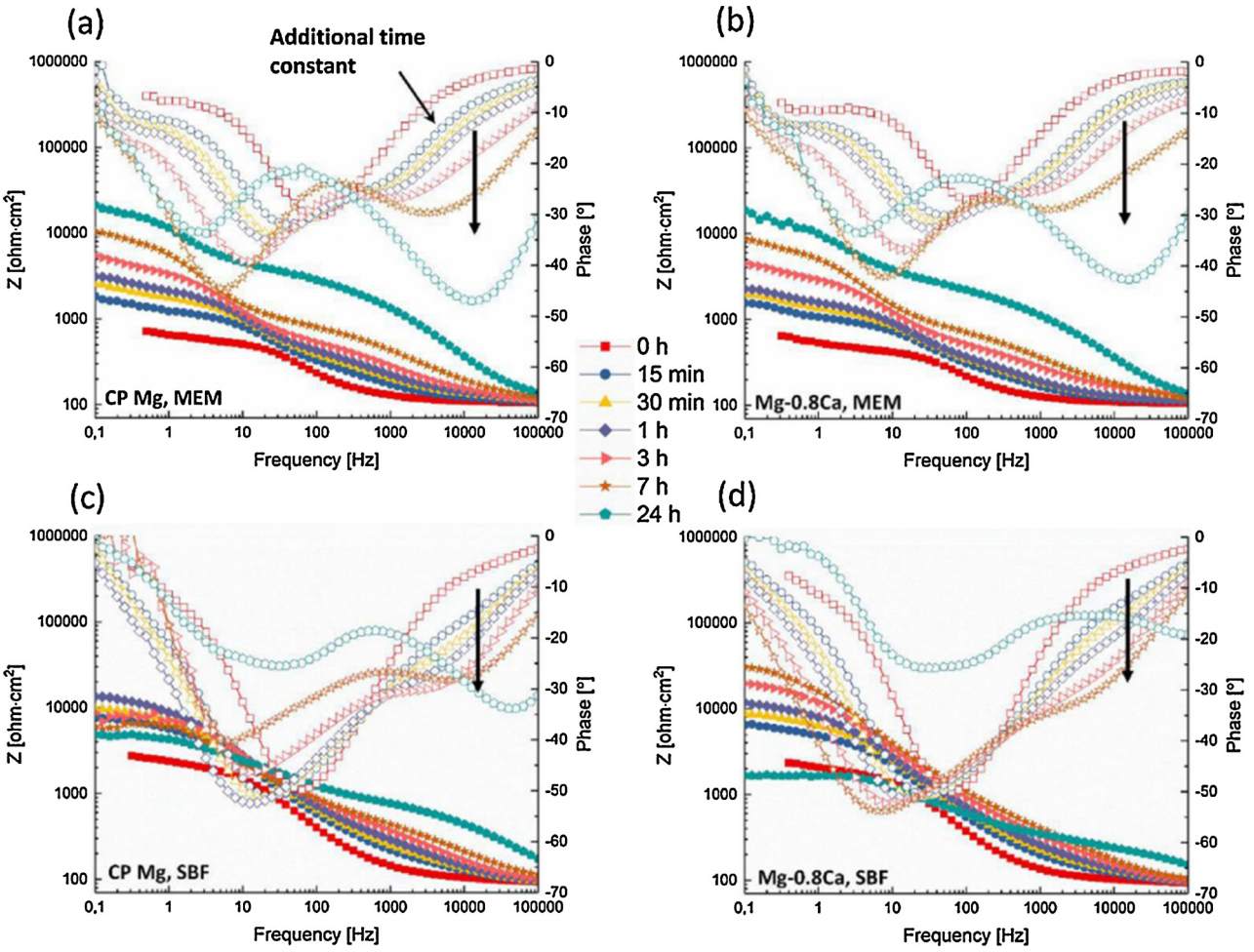

Fig. 5. Evolution of Bode plots for CP Mg (a, c) and Mg-0.8Ca (b, d) during 24 h immersion in MEM (a, b), SBF (c, d). The arrows mark the growth of additional time constant at high frequency range, which is attributed precipitation of continuous protective layer formed only in presence of Ca^{2+}, HCO_3^-, $H_2PO_4^-/HPO_4^{2-}$ and Mg^{2+} [59]. Reprinted from Corrosion Science, 153, D. Mei, S.V. Lamaka, C. Feiler, M.L. Zheludkevich, The effect of small-molecule bio-relevant organic components at low concentration on the corrosion of commercially pure Mg and Mg-0.8Ca alloy: An overall perspective, 258–271, Copyright (2019), with permission from Elsevier.

contamination. However, the effect of UV light cannot be maintained over a long period of time [156]. It has been verified that the low concentration of antibiotics (100 IU·mL^{-1} of penicillin and 100 μg mL^{-1} of streptomycin [157–161], which corresponds to the concentration of ca. 1E-4 M) does not influence the degradation rate of Mg to a high degree [59]. Meanwhile, at higher concentrations (1E-3 M and 1E-2 M), penicillin and streptomycin significantly accelerate Mg corrosion [59]. These findings highlight the inapplicability of a cell culture medium for long-term tests in an open environment where the sterile conditions are hard to maintain. Simulated body fluid is a reliable alternative for cell culture medium for the corrosion tests at an open environment: similar corrosion rates and corrosion products were observed upon immersion of Mg alloys in the cell culture medium and simulated body fluids.

2.5. Protein-containing media

Part of real human body fluids, such as plasma, cerebrospinal fluid and lymphatic fluid, consists of inorganic ions, small-molecule organic compounds and proteins. For example, there are over 30 g·L^{-1} albumin and over 20 g·L^{-1} globulin in human plasma/serum [77]. The presence of proteins adds another dimension to interactions with implant surfaces. Protein has been introduced into corrosive media to make the test environment more similar to blood plasma.

A number of related works have been published, and proteins were shown to have various acceleration or inhibition effects on the Mg corrosion. Liu [108] et al. investigated the corrosion behavior of Mg-Ca in albumin-containing NaCl solution and found that 1 g·L^{-1} and 10 g·L^{-1} of albumin showed an inhibition effect on the corrosion. Heakal [72] et al. also found that the competition between albumin, OH^- and Cl^- inhibited the corrosion of AZ80 in albumin-containing NaCl solution. Li [75] et al. investigated the corrosion behavior of Mg-*Zn*-Zr-Sc in HBSS with and without albumin. The results show that albumin inhibits corrosion during the first 6 h but accelerates it at longer immersion times. Harandi [71] et al. observed similar test results that showed the presence of BSA (bovine serum albumin) in HBSS increased the corrosion resistance of AZ91D during the first 2 days but then decreased it. Gu [110] et al. presented that FBS (fetal bovine serum) had the opposite impact on the corrosion of Mg-Ca and AZ series alloys in DMEM. However, there was no sterile test environment mentioned in these papers. Thus, these findings might not reflect the real corrosion behavior of Mg in a protein-containing media because of the high chance of media contamination during the long term immersion [162]. Under cell culture conditions in sterile environment, Zhang [106] et al. found that the addition of 10% FBS slowed down the corrosion rate of Mg-Nd-*Zn*-Zr in M199 cell culture medium. Johnson [109] et al. found that the addition of FBS had little impact on the degradation of pure Mg but increased the weight loss of Mg-Y in DMEM. Hou [74,77] et al. investigated the influence of protein adsorption and compared the effect of a single protein and protein mixtures on Mg corrosion in HBSS

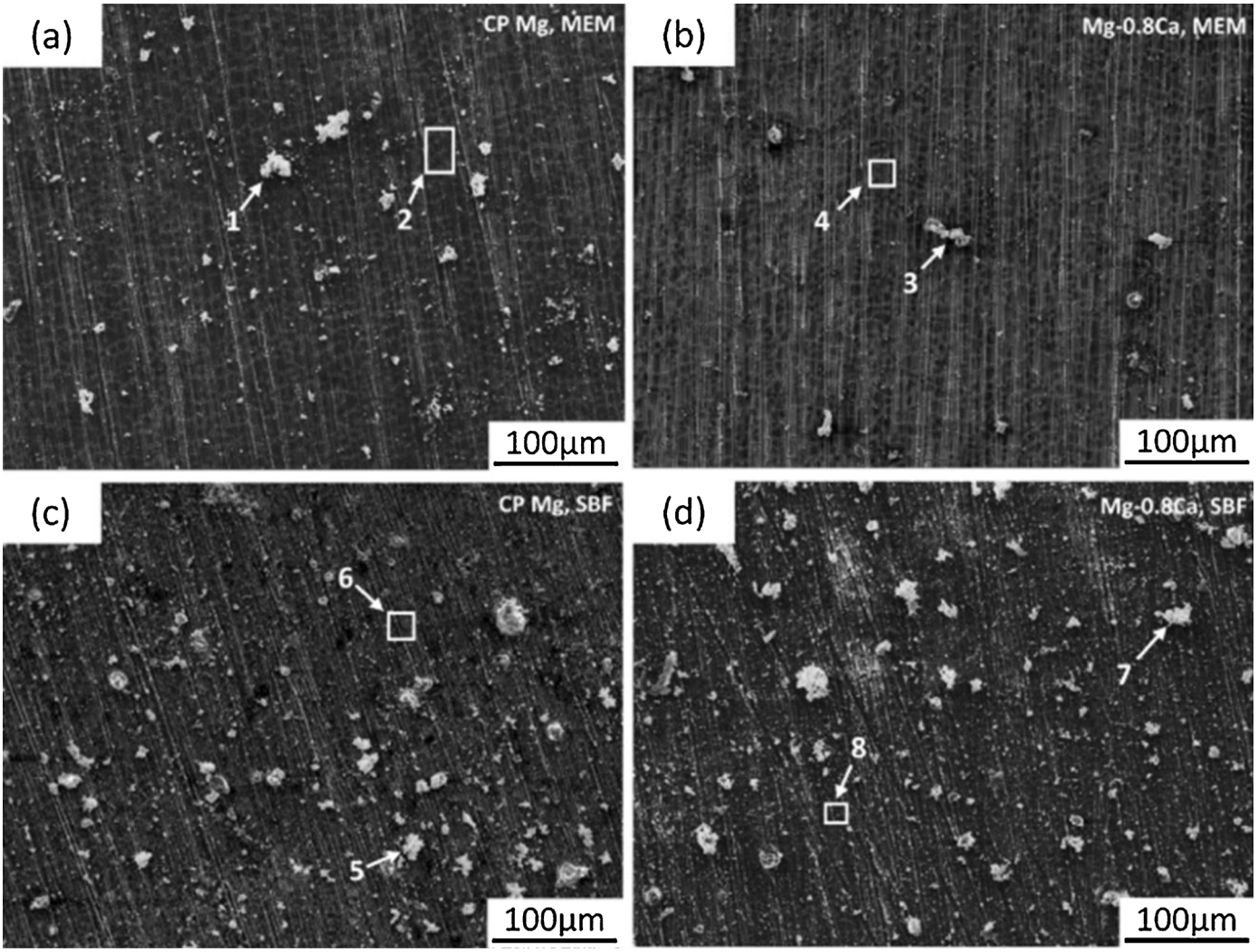

Fig. 6. Typical corrosion morphology of CP Mg (a, c) and Mg-0.8Ca (b, d) after 24 h immersion in MEM (a, b) and SBF (c, d) [59]. Reprinted from Corrosion Science, 153, D. Mei, S.V. Lamaka, C. Feiler, M.L. Zheludkevich, The effect of small-molecule bio-relevant organic components at low concentration on the corrosion of commercially pure Mg and Mg-0.8Ca alloy: An overall perspective, 258–271, Copyright (2019), with permission from Elsevier.

(without Ca^{2+}), HBSS-Ca and cell culture medium under cell culture condition (sterile environment, 37 °C and 5% CO_2). Through the obtained results, proteins or their mixture were found to have various effects on Mg degradation in different basic media. As shown in Fig. 8, the protein mixture (BSA + fibrinogen (Fib)) accelerates Mg corrosion in DMEM, which is different from that in HBSS and HBSS-Ca.

In many papers, FBS was simply regarded as the protein supply in test media. For corrosion tests under cell culture conditions, a routine addition of FBS is 10–20 vol. % [74,77,83,84,142,163–168]. This means that the real added amount of albumin is only approximately 2.0–7.2 $g{\cdot}L^{-1}$ [169], which is significantly lower than the concentration of albumin in serum (35–52 $g{\cdot}L^{-1}$). Most importantly, in addition to albumin, FBS also contains various inorganic ions, antibodies, hormones and growth factors [169,170]. These extra components make the cell culture medium more complicated and might also have influence on Mg corrosion. Kirkland and Walker [98,102,171] et al. investigated the corrosion rate of Mg in MEM with different protein additions. The results show that 10% FBS (means 2.0–3.6 $g{\cdot}L^{-1}$ albumin in the medium) slows down the corrosion of Mg-0.8Ca, while the addition of BSA at a concentration of 40 $g{\cdot}L^{-1}$ significantly accelerates the corrosion rate of several Mg alloys (including Mg-0.8Ca).

In a recent work, monitoring of local pH vs. bulk pH of an albumin-containing HBSS revealed the pH buffering effect of albumin, which extended all the way to the Mg/electrolyte interface [172]. In addition, considering the high concentration and complex structure of protein, the complexation between protein and metal cations has a notable effect [173–175]. Both types of ions are affected: the cations constituting the media and those dissolved from the alloy. Wagener [105] et al. noted that the presence of protein in DMEM seemed to inhibit the formation of a product layer. It can be found that the addition of protein delays the formation of the co-precipitation layer in pseudo-physiological media (the formation of the layer is described by Eq. (3), refer to [48,116–118,176]).

$$mMg^{2+} + nCa^{2+} + xH_2PO_4^-/HPO_4^{2-} + yHCO_3^- + zOH^- \rightarrow Mg_mCa_n(PO_4)_x(CO_3)_y(OH)_z\downarrow \quad (3)$$

In general, the synergy between the adsorption, chelating and pH buffering effect (all caused by protein) influence Mg corrosion in protein-containing pseudophysiological media.

Obviously, given the different protein sources, concentrations, tested materials and test environments, the effect of protein on Mg corrosion is still controversial. Although the influence of protein on the Mg corrosion is still not fully understood, protein-containing media can be used to predict the corrosion behavior of Mg because of their similar composition to blood plasma. Given the demanding sterile environment, the application of a protein-containing cell culture medium for

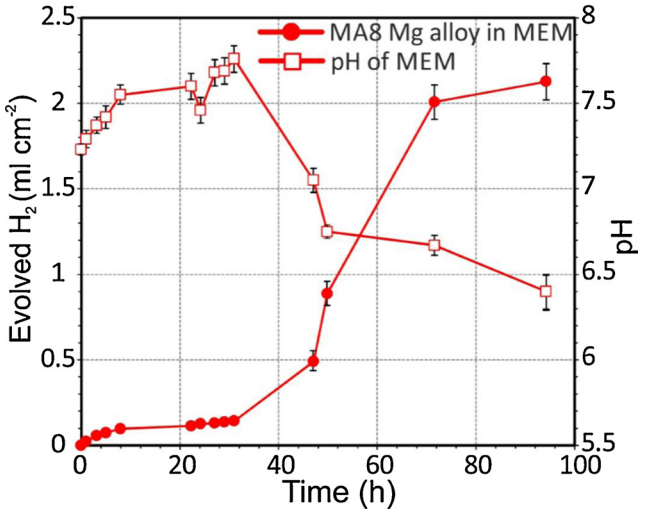

Fig. 7. Normalized hydrogen evolution curve coupled with bulk pH change of MEM for MA8 Mg alloy during 100 h of immersion. Tests were carried out using flow-through cell [152]. Reprinted from Corrosion Science, A.S. Gnedenkov, D. Mei, S.V. Lamaka, S.L. Sinebryukhov, D.V. Mashtalyar, I.E. Vyaliy, M.L. Zheludkevich, S.V. Gnedenkov, Localized currents and pH distribution studied during corrosion of MA8 Mg alloy in the cell culture medium, 108,689, Copyright (2020), with permission from Elsevier.

long-term measurement (e.g. for hydrogen evolution or EIS measurements) in an open environment is not practical.

As a summary, Fig. 9 depicts the corrosion behavior of Mg in all the above-mentioned media. The discussions above are outlined briefly in Table 2.

3. Discussion and outlook

3.1. Compatibility of the corrosive media and test methods

An immersion/weight loss measurement is the most direct method to measure the corrosion rate of Mg [177]. All of the aforementioned media can be used for weight loss measurements, and a natural buffer, HCO_3^-/CO_2, is easier to be applied (under incubator-type conditions). The weight loss is a non-continuous test method. At the early stage of the test in mild media (important for understanding the corrosion mechanism of Mg), the peculiarities of the corrosion behavior accompanied by the fast formation of protective co-precipitate/adsorption layer are not observable by the weight loss measurement. Considering the occasional requirement of environment, the weight loss test is suitable to investigate the long-term corrosion behavior in the organics-containing media, such as a cell culture medium or protein-containing media. However, the cleaning procedure (by chromic acid, according to ASTM G1-03) of the weight loss measurement might dissolve minute amounts of the Mg matrix and secondary phases [49,178]. This may lead to a slightly overestimated corrosion rate calculated by weight loss method.

As shown in Eq. (1), the corrosion of Mg alloys is accompanied by the generation of hydrogen. The hydrogen evolution test can indirectly reflect the corrosion rate of Mg. As a high-efficiency test method, hydrogen evolution has been used in a high-throughput screening of corrosion inhibitors employing the materials of high surface area and hence producing considerable amount of hydrogen [66]. Johnson [156,179] et al. found that, in HBSS, the Mg corrosion rate measured by the hydrogen evolution test is slower than that found by weight loss measurements due to the possible dissolution of evolved hydrogen. In addition to the possible hydrogen dissolution, the consumption of oxygen may also influence the volume of evolved gas (the secondary reaction during the Mg corrosion, shown as Eq. (2)). The relative contribution of ORR to total cathodic process is smaller for faster corroding substrates and higher for slower corroding Mg alloys or mild media, like HBSS and MEM [180]. The contribution of ORR can be reduced if the tests are run in closed eudiometers that entrap only fixed minimal amount of air at the beginning of the test. Additionally, the medium might be purged with hydrogen and nitrogen to decrease concentration of dissolved air and to decrease the solubility of hydrogen generated during Mg degradation [181]. These findings indicate that hydrogen evolution results may not be suitable to precisely calculate the corrosion rate of Mg [156]. However, an important advantage of this method is that it is continuous and can be easily automated. As such, it is still effective to compare the corrosion resistance of different materials or the aggressiveness of different media. The minute change in the corrosion behavior can be shown by this continuous test method, especially when it is performed with automatic recording [59,182]. The bio-relevant organics-containing solutions are not recommended for long-term hydrogen evolution tests due to the high danger of microbial contamination that greatly accelerates the degradation rate of Mg. On the other hand, HCO_3^-/CO_2 buffer can be introduced in the chamber for the hydrogen evolution test [179,183], as shown in Fig. 10.

Potentiodynamic polarization (PDP) and EIS are two frequently used electrochemical test methods. As a non-continuous destructive test method, PDP cannot easily reflect the influence of the growth of the protective product layer on the long-term corrosion behavior in mild media. However, in simple media, such as NaCl, it can be used to make a qualitative comparison between the corrosion resistances of different materials. As a nondestructive test method, EIS measurements can be used to study the degradation behavior of a substrate. Continuous EIS monitoring provides information about the formation of an adsorption and corrosion product layers, which is important for understanding the corrosion behavior of Mg in pseudo-physiological media [48,59,72,184]. In most cases, electrochemical corrosion tests are performed in an open environment. Thus, organics-free media are

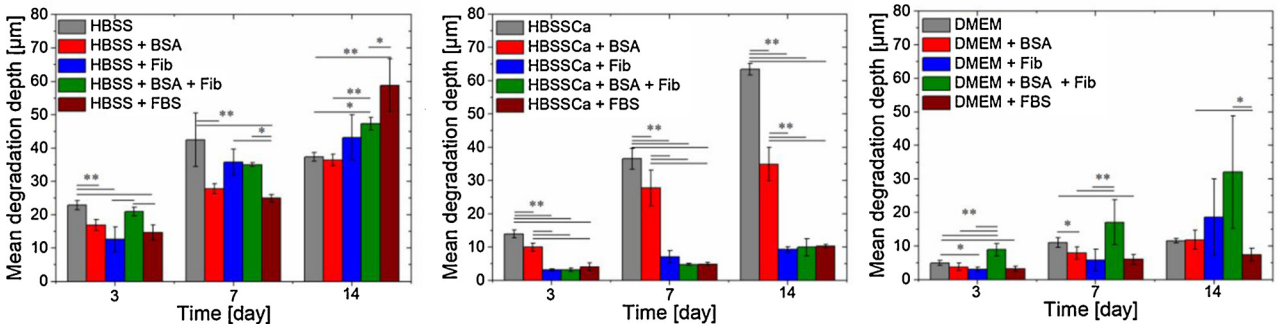

Fig. 8. Mean degradation depths of pure Mg in different media after different immersion time (significant differences are depicted by the solid line, Significance level: (*): $p < 0.05$, (**): $p < 0.01$) [77]. Reprinted from Acta Biomaterialia, 98, R.Q. Hou, N. Scharnagl, R. Willumeit-Romer, F. Feyerabend, Different effects of single protein vs. protein mixtures on magnesium degradation under cell culture conditions, 256–268, Copyright (2019), with permission from Elsevier.

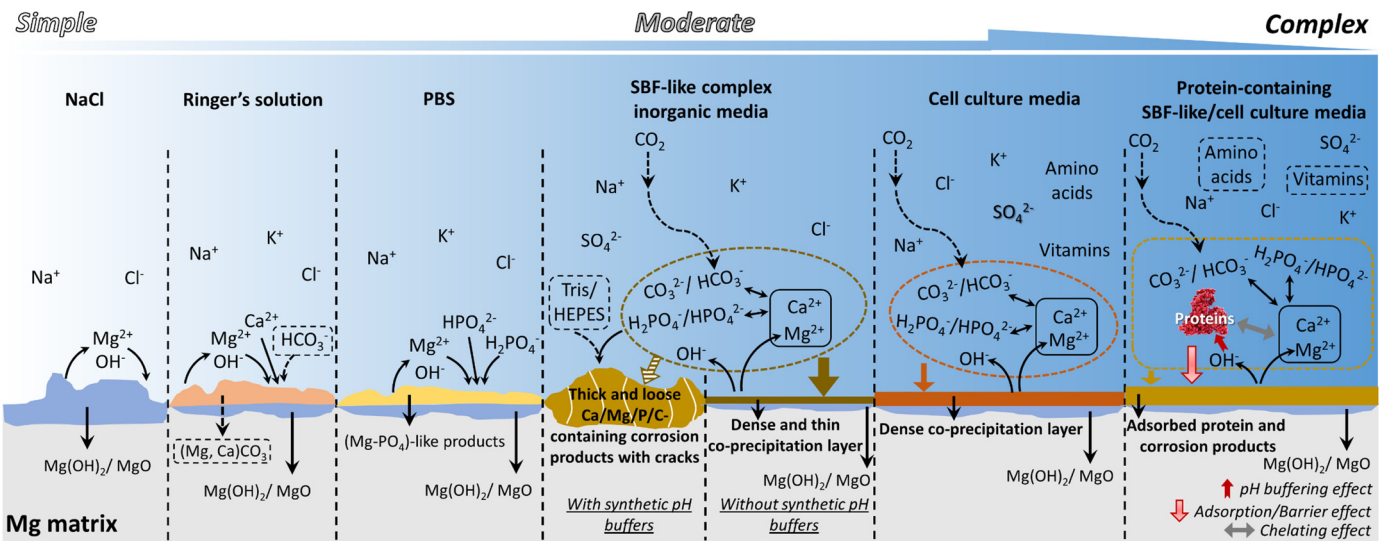

Fig. 9. Schematic illustration of the corrosion behavior of Mg in the commonly used media.

suitable for this. Certainly, long-term electrochemical tests in organics-containing media are also possible in sterile environments, but special facilities are required in this case.

Although the accumulation of microbial life in organic-containing media is uncontrollable in an open environment, its significant impact on Mg corrosion does not appear immediately. However, for long-term tests (longer than 3 days in our experience [152]) in an open environment, organics-containing media are not recommended.

The advantages and shortcomings of commonly used test methods discussed in this section are briefly summarized in Table 3.

3.2. A stable test environment during the corrosion tests

The service environment of the implants in human body is maintained nearly constant because of the continuous body fluid circulation. Thus, in order to mimic a real body environment, a stable test environment, including a stabilized pH (around a physiological value) during the test period and constant medium composition, is desirable for Mg corrosion tests for biomedical applications.

As discussed in section 2.3, synthetic pH buffers are not recommended to be introduced into corrosive media to stabilize the pH value. Through local pH measurements in SBF/HBSS under hydrodynamic conditions, it was found that the local pH value is not highly alkaline [48,58,172]. The pH at interface varies in the range between 8.0–8.6 if the important trio of ions (Ca^{2+}, HCO_3^-, $H_2PO_4^-/HPO_4^{2-}$) is present in the medium in physiological amounts. Similarly, the local measurement in albumin-containing HBSS shows that the local pH value near the corroded CP Mg surface, and the bulk pH of the media are even slightly lower, in the range of 8.0–8.5 [172]. All these local pH measurements, which were performed under hydrodynamic conditions without any added synthetic pH buffer. Under this condition, the medium composition is maintained constant by constant replenishment of ions consumed from the medium. The pH value of mild test media (e.g. SBF-like media, cell culture medium) without a buffer system may not change drastically under hydrodynamic conditions during the test period. It is stabilized by i) the dissolved ions ($H_2PO_4^-/HPO_4^{2-}$ and CO_2/HCO_3^-) and ii) by the precipitating products (as soon as more OH^- is generated due to cathodic reaction, more Ca-carbonate-phosphate containing corrosion products are formed that consume excessive alkalinity). Fig. 11 depicts the main origins of stable test environment under hydrodynamic conditions.

Hydrogen evolution tests in MEM have been conducted under real-time hydrodynamic conditions without any buffer system [152]. As shown in Fig. 6, the bulk pH of MEM can be maintained under 7.8 during the first 30 h of immersion (before contamination, owing to the microbial growth acidifies the medium) [152]. During tests under real-time hydrodynamic conditions, the renewal of the media replenishes the protective components (e.g. Ca^{2+}, carbonate, phosphate) that

Table 2
Summary of advantages, shortcomings and applicability of the reviewed media.

Medium	Suitability at an open environment	Risk of microbial contamination	Applicable research purposes / Remarks
NaCl solution	Yes	Low	The corrosion resistance of material itself is revealed. Can be used for initial screening tests for alloy selection.
Complex saline solution(e.g. PBS, (modified) Ringer's solution, etc.)	Yes	Low	Not recommended due to the varying composition and lack of important components
Simulated body fluids(e.g. SBF, HBSS, EBSS, etc.)	Yes	Low	Due to formation of corrosion product from the media, the corrosion resistance of metal substrates is revealed to lesser extent compared to simple NaCl solution. Ca^{2+}, Mg^{2+} need to be included. Can be used for initial screening test.
Cell culture medium(e.g. MEM, DMEM, α-MEM, M199, etc.)	Only up to 1 to 3 day(s) (based on our experience)	High	Similar with simulated body fluids.
Protein-contain solution(mainly refer to cell culture medium/simulated body fluids with protein addition)	Only up to 1 to 3 day(s) (based on our experience)	High	Most closely represents the blood plasma environment. Suitable for understanding the corrosion resistance of materials, as well as the formation of corrosion product from media. Can be used at advanced stages of implant development for corrosion tests.

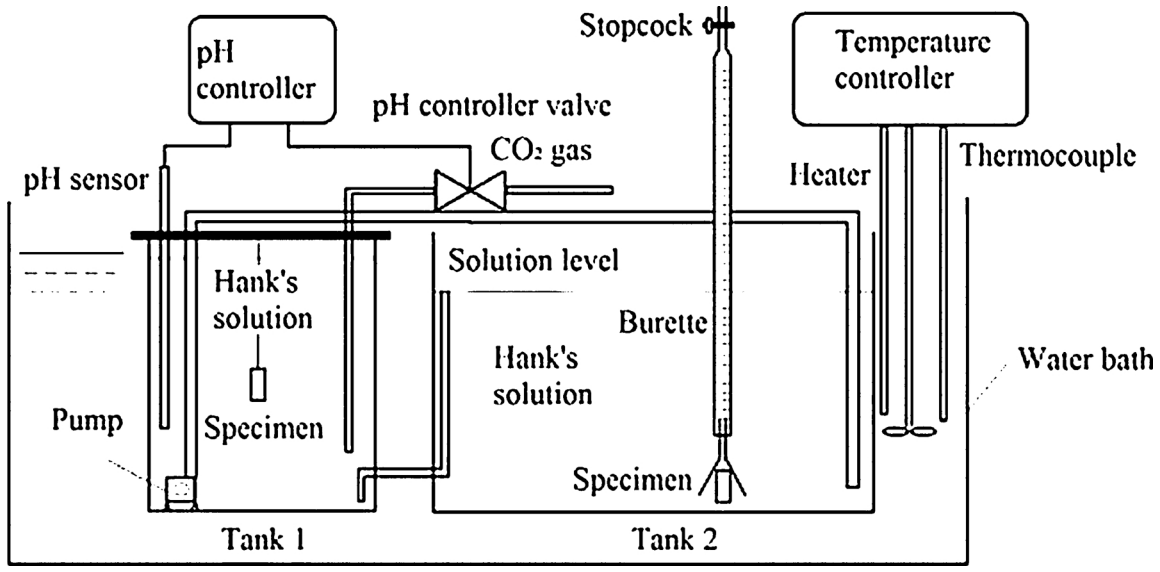

Fig. 10. Schematic of the experimental immersion apparatus under HCO_3^-/CO_2 buffer condition [179]. Reprinted from Corrosion Science, 101, S. Johnston, Z. Shi, A. Atrens, The influence of pH on the corrosion rate of high-purity Mg, AZ91 and ZE41 in bicarbonate buffered Hanks' solution, 182–192, Copyright (2015), with permission from Elsevier.

participate in precipitation of hydroxyapatite-like compounds and results in the long-term stability of formed protective layer. The renewal of media during the corrosion tests was previously emphasized in published works [49,80]. However, most tests are performed under semi-static conditions, which is not acceptable for many types of measurements. In ref. [67,77], the media used in the corrosion tests under cell culture conditions were refreshed at fixed intervals. However, compared with a real-time dynamic condition, this semi-static condition probably does not completely supplement the necessary protective components of the media due to their rapid consumption. Several recent publications reported the technical developments of the flow through cells for continuous supply of the fresh media [185–187].

In summary, the importance of stable test environment during corrosion tests of Mg has been recognized. During the corrosion tests in mild media (e.g. SBF-like media, cell culture medium), the continuous renewal of media is beneficial to maintain the test environment.

Besides media components, another noteworthy environmental factor in corrosion tests is temperature. Considering the target service environment of bioabsorbable Mg, the tests with ambient temperature of 37°C are desirable, while part of published works were performed at room temperature (RT) [78]. Temperature may have two opposite effects on the corrosion behavior of bioabsorbable Mg. Higher temperature typically leads to more active corrosion reaction. However, in pseudophysiological media, rapid corrosion probably promotes the precipitation of $Mg_mCa_n(PO_4)_x(CO_3)_y(OH)_z$ that provides better protection of Mg against corrosion afterwards. Wagener [188] et al. have compared the corrosion behavior of Mg at two different temperatures (RT and 37°C) by using the electrochemical tests (EIS and PDP). The results show that temperature change (from RT to 37°C) only have minor influence on Mg corrosion in SBF and DMEM. It is probably to be attributed to the combination of the aforementioned dual effects. In general, the influence of temperature on Mg corrosion is still not fully understood. More effort should be devoted to relevant research to clarify the effects of temperature on Mg corrosion. It is of significant importance for the establishment of internationally accepted test protocols of corrosion tests for bioabsorbable Mg-base materials.

3.3. Status of corrosion tests

In an animal body, implantation causes changes in the local physiological environment (e.g. local inflammation). The reaction between body tissue and implant materials influences the corrosive environment around the implantation position [189]. In addition, during the service period, mechanical stress also influences the corrosion of implanted materials [190–192]. These factors are not easily reflected synthetically by corrosion tests. Thus, it seems unrealistic to fully simulate the *in vivo* response through corrosion tests [4].

As discussed in section 3.1, none of the commonly used corrosion

Table 3
Summary of advantages and shortcomings of commonly used test methods.

Test method	Advantages	Shortcomings
Weight loss	Most reliable Direct method for one point calculation of corrosion rate Easily controlled test environment	Non-continuous. Does not reveal varying corrosion rate throughout the immersion Low sensitivity at the initial stages
Hydrogen evolution	Continuous Can be automated Can be performed in closed eudiometers	Performed in open environment in most cases Might show underestimated values of corrosion rate due to secondary ORR and solubility of H_2 in aqueous media
Potentiodynamic polarization	Fast measurement	Non-continuous Open environment measurement in most cases Very often low correlation with long-term weight loss measurements
Electrochemical impedance spectroscopy	Continuous *In situ* investigation of protective properties of forming corrosion products	Performed in open environment in most cases

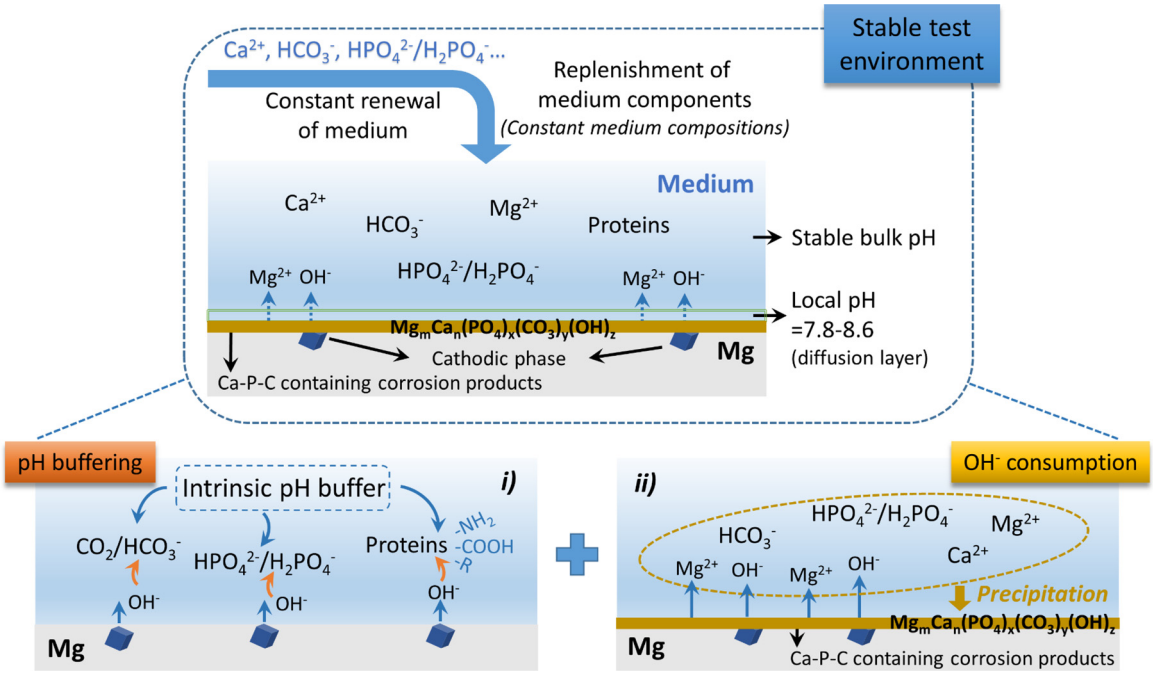

Fig. 11. Schematic illustration of stable test environment under hydrodynamic conditions.

test methods can alone answer all the questions about Mg corrosion. Due to their respective characteristics, the corrosion rate measured by corrosion tests cannot fully reflect the *in vivo* corrosion rate, which also varies. Therefore, we deem that the purpose of corrosion tests should be to screen for the best performing metallic materials, organic and inorganic coatings and various additives such as drugs or corrosion modulators and understand their interplay. Certainly, performance evaluation criteria should come from the agreement within the scientific community.

In mild corrosive media, e.g. SBF, HBSS, EBSS or MEM, the difference in corrosion rate of different Mg alloys is smaller than that in a simple NaCl solution [59,84]. At the early stage of the screening procedure, they might not be appropriate corrosive media since similar corrosion behavior is observed when different alloys are tested [59]. In contrast, corrosion tests in a simple NaCl solution provide more information about the corrosion resistance of the material itself. However, this does not mean that the corrosion test in NaCl solution is sufficient at the early screening stage of Mg for biomedical application. It is noteworthy that secondary phases and impurities in alloys may play different roles during corrosion in NaCl solution and in pseudo-physiological media. In general, the Volta potential difference between the secondary phases and matrix causes the galvanic corrosion of Mg. In the NaCl solution, more secondary phases normally lead to more serious corrosion. But in pseudophysiological media, the corrosion promotes the precipitation of a protective product layer, which inhibits further corrosion [48]. Because of the different corrosion mechanisms of Mg in NaCl solution and pseudophysiological media, tests in both types of electrolytes are complementary. As a widely accepted fact, animals have a complex internal body environment and a great variety of body fluids, including plasma/serum, tissue fluid, urine, cerebrospinal fluid, saliva, etc. [193]. This fact points out the importance of a differentiated design of corrosive media for corrosion tests depending on the tailored application. The target of the corrosion tests should be screening out the best candidates for the target service environment. In this case, harsh test environments are reasonable.

In some cases, the chemical composition of Mg alloys also influences the selection of media [98,102]. For the corrosion tests performed in organics-containing media, the possible complexation reactions need to be considered between organic components of media and metal ions generated by alloying element during the corrosion. It can be an accelerating factor for the corrosion of specific Mg alloys. For example, compared to the corrosion rate in simple NaCl solution, the addition of glucosamine accelerated the corrosion of Mg-Ca alloy in NaCl solution due to the reaction between glucosamine and Ca^{2+} (dissolved from the alloy), but glucosamine had no critical influence on the corrosion of CP Mg the same medium [59]. In addition, similar reactions also influence Mg corrosion in complex media, like SBF and MEM. An example of this point is that the addition of streptomycin accelerated Mg corrosion in MEM and SBF due to the suppressed formation of protective products layer caused by the complexation reaction between streptomycin and Ca^{2+} (as the component of media) [59].

3.4. Factors to consider when running corrosion tests

It is certain that corrosion tests will continue playing important role in the field of biomedical implants. However, the lack of widely accepted test protocols has led to insufficient comparability of experimental results from different groups [49,194]. This fact significantly affects the sustainable development of Mg alloys as implant materials. Herein, the authors would like to provide several considerable suggestions about corrosion tests.

a) The timely renewal of the medium and the influence of oxygen are both worthy of consideration during the Mg corrosion tests, especially for long-term measurements in an open environment.
b) The possible change of corrosion behavior or test environment induced by a potential complexation reactions between organic compounds, including small- and macromolecule compounds, and inorganic ions (media components or dissolved from the materials) should be taken into account.
c) Some of components in cell culture media, including but not limited to antibiotics, pH indicators and synthetic pH buffers, are not the components of the real service environment of implants. They may bias the corrosion rate and judgement of the biocompatibility of the tested materials.

4. Medium selection for other bioabsorbable metallic materials

Similarly to Mg, all aforementioned media, including NaCl solution [195,196], PBS [197], Ringer's solution [198], HBSS [199–201], SBF [202–206], cell culture media [207,208] and protein-containing solutions [208–210] have been used for testing corrosion behavior of zinc, iron and their alloys as bioabsorbable materials. Thus, it is of paramount importance to discuss the selection of suitable medium for obtaining valuable and reliable experimental results about the corrosion of zinc and iron. The brief discussion is given in the following sections.

4.1. Iron and its alloys

Unlike Mg alloys, biodegradable iron alloys are typically designed in a way to increase their degradation rate in physiological environments [201,211–214]. Therefore, it is very important to select a suitable corrosive medium for evaluating the degradation behavior of iron and its alloys.

However, not much of comparative work has been done on the influence of media components on corrosion of iron for biodegradable implant application. Based on independent experimental results from different research groups, it was found that the corrosion behavior of iron seems not susceptible to the change of medium compositions, as much as magnesium. As an example, the corrosion rate of pure iron in HBSS is 0.138 ± 0.011 mm·year^{-1} [215]. It is similar to that of 0.10 ± 0.01 mm·year^{-1} [204] in HEPES-buffered r-SBF. This low dependency on pH equilibria of surrounding media can be explained by rapid formation of iron oxide/hydroxides are relatively low pH (< 3) [216]. Even in 0.9% NaCl solution, the most aggressive medium, the corrosion rate of pure iron remains rather low, around 0.2 mm·year^{-1} [195].

The *in vivo* animal trials show no significant difference of corrosion rate between different iron alloys at the same implantation site [217], although these iron alloys show different corrosion rate in corrosion tests [217,218]. It is indicated that the existing corrosion test media and test methods cannot well predict the *in vivo* corrosion rate of iron and its alloys. Therefore, for iron and its alloys, the main purpose of corrosion tests is not to screen out the materials with acceptable corrosion resistance (that should be faster than that of pure iron), but to deepen the understandings of their corrosion behavior in pseudo-/ physiological environment. For this purpose, pseudophysiological media are suitable, such as simulated body fluids, cell culture media and protein-containing solutions. In animal body, the Ca, P-rich corrosion products form on the implanted iron materials [217]. This phenomenon can be mimicked by the application of pseudophysiological media (e.g. SBF, HBSS and cell culture media). As shown in Fig. 12, in SBF-like media, the continuous EIS measurements of iron and its alloys show the constantly growing additional time constant at the high frequency range [219,220], which is similar to the phenomenon of Mg corrosion in similar media (as shown in Fig. 5). It can be attributed to precipitation of Ca, P-rich products from the medium caused by the slight increase of local pH in cathodic sites during corrosion of iron. Anodic sites are typically characterized by local acidification [221], owing to significant degree of hydrolysis of Fe^{2+} and Fe^{3+} ions [216]. This leads to high susceptibility of iron-based materials to pitting corrosion [201,222].

4.2. Zinc and its alloys

A number of works have been performed to compare the corrosion behavior of zinc in various media. Liu [223] et al. investigated the corrosion behavior of pure Zn in four different electrolytes, including HBSS, Tris-buffered SBF, DMEM and DMEM + 10% FBS. After 7 days' immersion, the weight loss results showed that pure zinc has lowest corrosion rate of 0.01-0.02 mm·year^{-1} in DMEM and DMEM + FBS, followed by approximately 0.03 mm·year^{-1} in HBSS and 0.06-0.08 mm·year^{-1} in Tris-buffered SBF [223]. Presumably, Tris has acceleration effect on the corrosion of zinc as on Mg corrosion. Similarly, other independent experimental results confirmed this finding, zinc alloys showed corrosion rate of around 0.08 mm·year^{-1} in HBSS (no synthetic buffer) [224–226] and had higher corrosion rate (0.2-0.3 mm·year^{-1}) in Tris-buffered SBF [227–229].

Liu [230] et al. compared the influence of buffer system on the corrosion of pure zinc in SBF. It was found that zinc shows extremely low corrosion rate (0.005 mm·year^{-1}) in buffer-free SBF, but all pH buffers, including HEPES (0.082 mm·year^{-1}), Tris/HCl (0.04 mm·year^{-1}) and $NaHCO_3/CO_2$ (0.037 mm·year^{-1}), accelerate its corrosion. Considered the *in vivo* corrosion rate of pure zinc stent in rabbit artery (0.03 mm·year^{-1}) [231], Liu et al. provisionally concluded that SBF with Tris/HCl or $NaHCO_3/CO_2$ buffer can be employed to investigate the corrosion behavior of zinc for vascular stent applications, since zinc has similar corrosion rate in buffered SBF and *in vivo*. On the other hand, similarity of degradation rate should not be the only selection criteria for the pH buffer. We believe the selection of pH buffer should be more cautious. Tris/HCl is foreign to any of physiological fluid and possesses Ca^{2+}-complexing and OH^--consuming effects that delay formation of Ca-P-rich precipitation products. The corrosion tests in Tris-buffered media might be not beneficial for deepening the understanding of zinc corrosion behavior in pseudo-/ physiological environment. The local pH measurements might be helpful to verify whether synthetic pH buffers (e.g. Tris/HCl and HEPES) activates the metal/media interface reaction during zinc corrosion, as they do for Mg corrosion process. Similar to iron and its alloys, zinc shows good

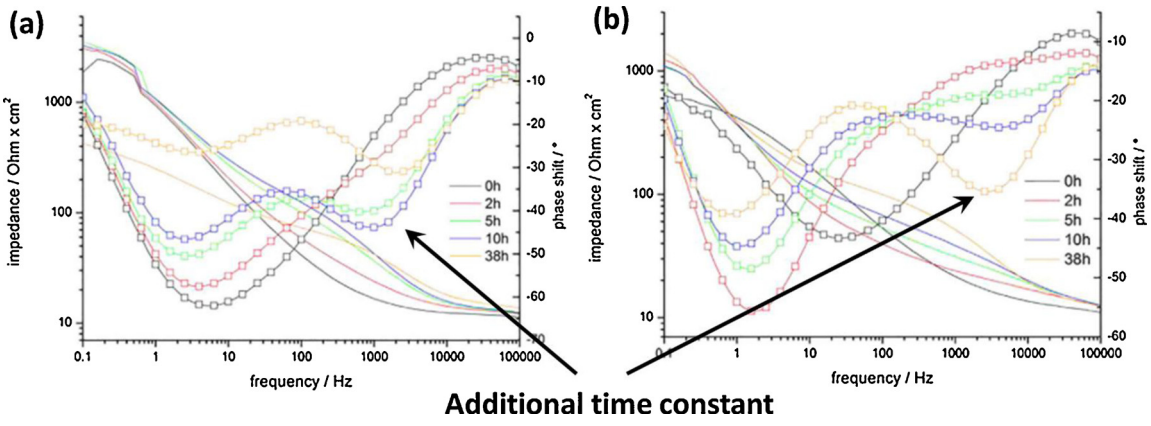

Fig. 12. Evolution of Bode plots for (a) FeMn and (b) FeMn-Ag in SBF over 38 h [219]. Reprinted from Materials and Corrosion, 68, M. Wiesener, K. Peters, A. Taube, A. Keller, K.-P. Hoyer, T. Niendorf, G. Grundmeier, Corrosion properties of bioresorbable FeMn-Ag alloys prepared by selective laser melting, 1028–1036, Copyright (2017), with permission from John Wiley and Sons.

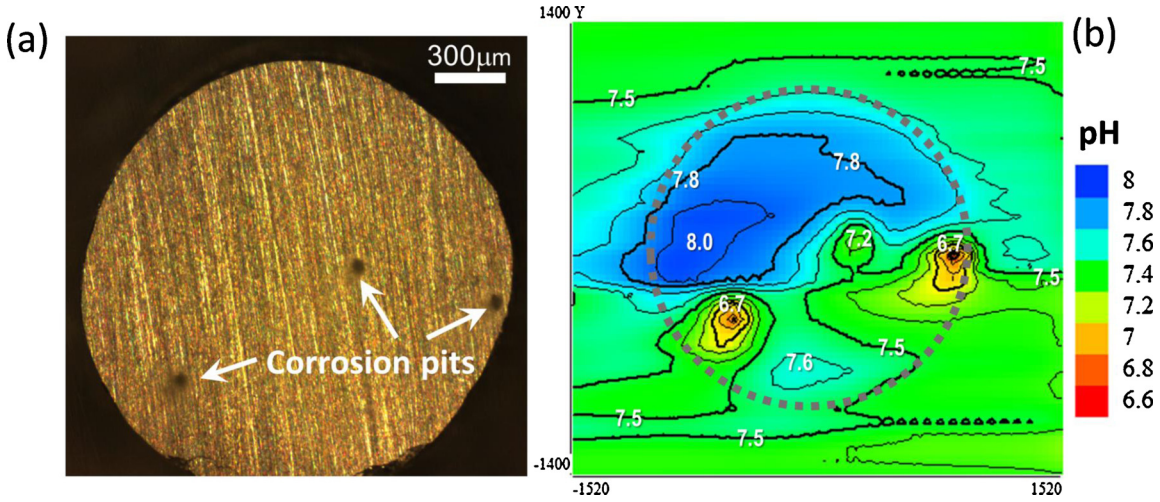

Fig. 13. a) The visual appearance of the Zn-4Mg alloy after 4 h of immersion in SBF and b) corresponding pH mapping revealing slight acidification in the location of optically visible pits [232].

corrosion resistance in corrosion tests but is also prone to pitting corrosion, though to lesser extent compared to Fe-based alloys. Even in mild medium, as shown in Fig. 13, the local pH near the surface of Zn-4Mg alloy after 4 h' immersion in SBF showed the local acidification at corrosion pits [232]. On the other hand, with the presence of BSA, Liu [209] et al. reported the uniform corrosion behavior of pure zinc in artificial plasma owing to rapid adsorption of albumin.

Corrosion tests are essential for a better understanding about the corrosion behavior of zinc in pseudo-/ physiological environment. In this case, the complex media (e.g. simulated body fluids, cell culture media and protein-containing solutions), which have similar components to that of physiological fluids (such as serum/plasma and interstitial fluid), should be considered to get closer to the real service environment.

4.3. General discussion

Due to the short research time of iron-based and zinc-based bioabsorbable materials, there is the lack of systematic investigation about the influence of media components on their corrosion behavior. The above discussion is rather basic and open. Typically, even in the mild media (SBF-like media without synthetic pH buffer), the corrosion rates of magnesium are significant higher than that of iron and zinc (as shown in Fig. 14). Due to different corrosion mechanisms and intrinsic corrosion resistance among magnesium, zinc and iron, the previous discussion about media selection obtained in the field of bioabsorbable Mg cannot be directly applied to zinc and iron. However, considering the similar potential biomedical applications of magnesium, iron and zinc, we believe that several general principles can be cautiously extended to the works having their subjects iron and zinc. Firstly, the suitable test medium should be selected based on specific research purpose. Secondly, the risk of microbial contamination of the complex media in the open environment should be always considered. Media acidification caused by growth of microbial life might significantly bias the degradation rates. Third, the addition of components (which are foreign to body fluids) in the media should be cautious because their effect, obvious in case of Mg, might be overshadowed by slower degradation rates of Fe and Zn based alloys.

Although magnesium, zinc and iron are all regarded as promising bioabsorbable materials, their corrosion mechanisms are different. The main cathodic reaction for Mg corrosion is hydrogen evolution reaction (HER), while it is oxygen reduction reaction (ORR) for iron and zinc. Thus, there is a concern that the oxygen consuming during the corrosion process of iron or zinc implants in animal body might cause the hypoxia of surroundings and lead to tissue necrosis. Since recently, this concern also applies to Mg owing to recently discovered contribution of ORR to the total cathodic reaction in Mg (shown in Eq. 2).

The corrosion of zinc and iron is limited by diffusion of oxygen and influenced by the availability of oxygen in the test environment to a great extent. The partial pressure of oxygen (PaO_2) in human body is controlled by the uninterrupted breathing. However, in corrosion tests, the PaO_2 of the test environment is usually uncontrolled. Besides, the concentration of dissolved oxygen at the interface of corroding metal differs from that in the bulk electrolyte. As we suggested in section 3.4, more attention should be paid on the influence of oxygen in the corrosion tests of bioabsorbable metallic materials. It is desirable to perform the corrosion tests under the controllable PaO_2 based on the different target service environments [201]. This is especially important for iron and zinc, as their corrosion rates are predetermined by diffusion limited ORR cathodic reaction.

5. Summary and outlook

In this review, we discussed the applicability of several commonly used corrosive media when testing Mg for biomedical implant applications. The advantages and shortcomings for different tests, and the scopes of application of these media are clarified. The discussion also extends to the other bioabsorbable metallic materials, such as zinc and iron. It can be concluded that the complementary use of multiple test methods and media is beneficial to obtain comprehensive information about the corrosion behavior of bioabsorbable metallic materials. Based on the review, several opinions about medium selection for corrosion tests of bioabsorbable metallic materials are listed below:

a) For works that are going to be published, a detailed composition of the corrosive media needs to be listed. Providing only a name, such as HBSS or SBF, is insufficient since a number of different media have same/similar names. This information is necessary for comparing the experimental results across different research groups.
b) Synthetic pH buffers (e.g. Tris/HCl and HEPES) should not be involved in corrosion tests, especially for Mg and its alloys.
c) The corrosion tests performed in NaCl solution provide more information about the intrinsic corrosion resistance of material itself. In contrast, the tests in the complex media (e.g. simulated body fluids and protein-containing solutions) are influenced by the media components to large extent.
d) The nutrients-containing media (e.g. cell culture media and protein-containing solutions) are not suitable for long-term tests in an open

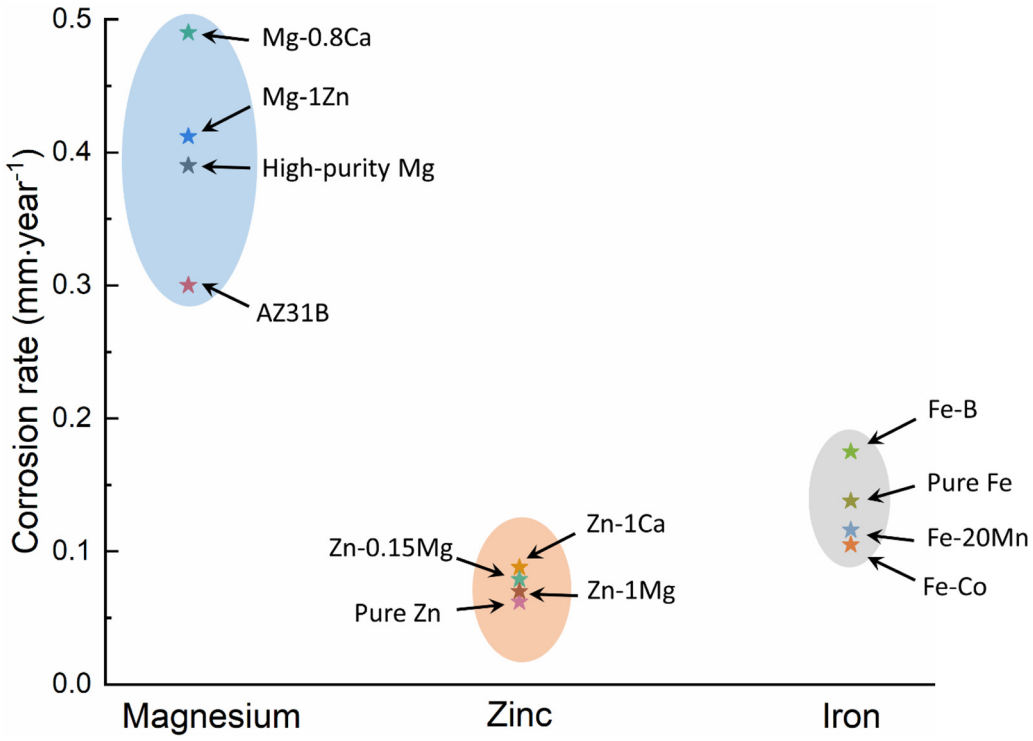

Fig. 14. The representative degradation rates of magnesium, zinc and iron in SBF-like media (without synthetic pH buffer) obtained by weight loss measurement. This graph was drawn based on the results reported in Ref. [102,201,215,220,224,225,233,234].

environment because of high risk of microbial contamination.

e) The introduction of components, which are not the parts of the target service environment, in the test media should be cautious. It might cause the misunderstanding when evaluating the corrosion behavior/resistance of bioabsorbable metallic materials.

Considering various test media and test methods that are being applied for the screening and prediction of degradation behavior, it is urgent to establish clear corrosion test protocols to provide comparable research results and to boost the synergy of research in biodegradable metal community.

CRediT authorship contribution statement

Di Mei: Conceptualization, Investigation, Visualization, Writing - original draft, Writing - review & editing. **Sviatlana V. Lamaka:** Conceptualization, Investigation, Supervision, Writing - review & editing. **Xiaopeng Lu:** Conceptualization, Writing - review & editing. **Mikhail L. Zheludkevich:** Conceptualization, Supervision, Writing - review & editing.

Declaration of Competing Interest

The authors declare that they have no known competing financial interests or personal relationships that could have appeared to influence the work reported in this paper.

Acknowledgement

Mr. Di Mei thanks China Scholarship Council for the award of fellowship and funding (No. 201607040051). Mr. Di Mei acknowledges the support of EFC Young Scientist Grant (2019) founded by European Federation of Corrosion (EFC) and Chinese Society for Corrosion and Protection (CSCP). “MMDi” IDEA project funded by HZG is gratefully acknowledged. Dr. Xiaopeng Lu would like to acknowledge the financial support from National Natural Science Foundation of China (No. U1737102), Mobility Programme (M-0056) of the Sino-German Center and the Fundamental Research Funds for the Central Universities (N2002009). Mr. Di Mei thanks Mr. Cheng Wang (HZG) for the helpful discussion.

References

[1] Y.F. Zheng, X.N. Gu, F. Witte, Biodegradable metals, Mater. Sci. Eng. R Rep. 77 (2014) 1–34.
[2] F. Witte, N. Hort, C. Vogt, S. Cohen, K.U. Kainer, R. Willumeit, F. Feyerabend, Degradable biomaterials based on magnesium corrosion, Curr. Opin. Solid State Mater. Sci. 12 (2008) 63–72.
[3] R. Zeng, W. Dietzel, F. Witte, N. Hort, C. Blawert, Progress and challenge for magnesium alloys as biomaterials, Adv. Eng. Mater. 10 (2008) B3–B14.
[4] Z. Zhen, T.-f. Xi, Y.-f. Zheng, A review on in vitro corrosion performance test of biodegradable metallic materials, Trans. Nonferrous Met. Soc. China 23 (2013) 2283–2293.
[5] Y. Liu, Y. Zheng, X.H. Chen, J.A. Yang, H. Pan, D. Chen, L. Wang, J. Zhang, D. Zhu, S. Wu, K.W.K. Yeung, R.C. Zeng, Y. Han, S. Guan, Fundamental theory of biodegradable metals—definition, criteria, and design, Adv. Funct. Mater. 29 (2019) 1805402.
[6] D. Zhao, F. Witte, F. Lu, J. Wang, J. Li, L. Qin, Current status on clinical applications of magnesium-based orthopaedic implants: a review from clinical translational perspective, Biomaterials 112 (2017) 287–302.
[7] Y. Chen, Z. Xu, C. Smith, J. Sankar, Recent advances on the development of magnesium alloys for biodegradable implants, Acta Biomater. 10 (2014) 4561–4573.
[8] X. Gu, Y. Zheng, Y. Cheng, S. Zhong, T. Xi, In vitro corrosion and biocompatibility of binary magnesium alloys, Biomaterials 30 (2009) 484–498.
[9] M. Esmaily, J.E. Svensson, S. Fajardo, N. Birbilis, G.S. Frankel, S. Virtanen, R. Arrabal, S. Thomas, L.G. Johansson, Fundamentals and advances in magnesium alloy corrosion, Prog. Mater. Sci. 89 (2017) 92–193.
[10] R. Willumeit-Römer, The interface between degradable Mg and tissue, JOM 71 (2019) 1447–1455.
[11] J. Venezuela, M.S. Dargusch, The influence of alloying and fabrication techniques on the mechanical properties, biodegradability and biocompatibility of zinc: a comprehensive review, Acta Biomater. 87 (2019) 1–40.
[12] E. Mostaed, M. Sikora-Jasinska, J.W. Drelich, M. Vedani, Zinc-based alloys for degradable vascular stent applications, Acta Biomater. 71 (2018) 1–23.
[13] P.K. Bowen, J. Drelich, J. Goldman, Zinc exhibits ideal physiological corrosion behavior for bioabsorbable stents, Adv. Mater. 25 (2013) 2577–2582.
[14] M. Schinhammer, A.C. Hänzi, J.F. Löffler, P.J. Uggowitzer, Design strategy for biodegradable Fe-based alloys for medical applications, Acta Biomater. 6 (2010)

1705–1713.
[15] H.-S. Han, S. Loffredo, I. Jun, J. Edwards, Y.-C. Kim, H.-K. Seok, F. Witte, D. Mantovani, S. Glyn-Jones, Current status and outlook on the clinical translation of biodegradable metals, Mater. Today 23 (2019) 57–71.
[16] BIOTRONIK, in https://www.biotronik.com/en-de/products/coronary/magmaris.
[17] Syntellix A.G., in https://www.syntellixA.G.de/en/products/product-overview/all.html.
[18] U&i, in http://www.youic.com/m/sub02/list.php?ca_id=10.
[19] G. Song, Control of biodegradation of biocompatable magnesium alloys, Corros. Sci. 49 (2007) 1696–1701.
[20] N. Li, Y. Zheng, Novel magnesium alloys developed for biomedical application: a review, J. Mater. Sci. Technol. 29 (2013) 489–502.
[21] H. Qin, Y. Zhao, Z. An, M. Cheng, Q. Wang, T. Cheng, Q. Wang, J. Wang, Y. Jiang, X. Zhang, G. Yuan, Enhanced antibacterial properties, biocompatibility, and corrosion resistance of degradable Mg-Nd-Zn-Zr alloy, Biomaterials 53 (2015) 211–220.
[22] L. Yang, L. Ma, Y. Huang, F. Feyerabend, C. Blawert, D. Höche, R. Willumeit-Römer, E. Zhang, K.U. Kainer, N. Hort, Influence of Dy in solid solution on the degradation behavior of binary Mg-Dy alloys in cell culture medium, Mater. Sci. Eng. C 75 (2017) 1351–1358.
[23] R.L. Liu, J.R. Scully, G. Williams, N. Birbilis, Reducing the corrosion rate of magnesium via microalloying additions of group 14 and 15 elements, Electrochim. Acta 260 (2018) 184–195.
[24] P. Jiang, C. Blawert, R. Hou, N. Scharnagl, J. Bohlen, M.L. Zheludkevich, Microstructural influence on corrosion behavior of MgZnGe alloy in NaCl solution, J. Alloys. Compd. 783 (2019) 179–192.
[25] J. Wang, H. Zhou, L. Wang, S. Zhu, S. Guan, Microstructure, mechanical properties and deformation mechanisms of an as-cast Mg–Zn–Y–Nd–Zr alloy for stent applications, J. Mater. Sci. Technol. 35 (2019) 1211–1217.
[26] J. Wang, L. Wang, S. Guan, S. Zhu, C. Ren, S. Hou, Microstructure and corrosion properties of as sub-rapid solidification Mg–Zn–Y–Nd alloy in dynamic simulated body fluid for vascular stent application, J. Mater. Sci. Mater. Med. 21 (2010) 2001–2008.
[27] J.-L. Wang, S. Mukherjee, D.R. Nisbet, N. Birbilis, X.-B. Chen, In vitro evaluation of biodegradable magnesium alloys containing micro-alloying additions of strontium, with and without zinc, J. Mater. Chem. B 3 (2015) 8874–8883.
[28] K. Matsubara, Y. Miyahara, Z. Horita, T. Langdon, Developing superplasticity in a magnesium alloy through a combination of extrusion and ECAP, Acta Mater. 51 (2003) 3073–3084.
[29] G.-L. Song, Z. Xu, Effect of microstructure evolution on corrosion of different crystal surfaces of AZ31 Mg alloy in a chloride containing solution, Corros. Sci. 54 (2012) 97–105.
[30] C.Z. Zhang, S.J. Zhu, L.G. Wang, R.M. Guo, G.C. Yue, S.K. Guan, Microstructures and degradation mechanism in simulated body fluid of biomedical Mg–Zn–Ca alloy processed by high pressure torsion, Mater. Des. 96 (2016) 54–62.
[31] J. Wang, Y. Zhou, Z. Yang, S. Zhu, L. Wang, S. Guan, Processing and properties of magnesium alloy micro-tubes for biodegradable vascular stents, Mater. Sci. Eng. C Mater. Biol. Appl. 90 (2018) 504–513.
[32] M. Gholami-Kermanshahi, V.D. Neubert, M. Tavakoli, F. Pastorek, B. Smola, V. Neubert, Effect of ECAP processing on corrosion behavior and mechanical properties of the ZFW MP magnesium alloy as a biodegradable implant material, Adv. Eng. Mater. 20 (2018) 1800121.
[33] W. Zhang, L. Tan, D. Ni, J. Chen, Y.-C. Zhao, L. Liu, C. Shuai, K. Yang, A. Atrens, M.-C. Zhao, Effect of grain refinement and crystallographic texture produced by friction stir processing on the biodegradation behavior of a Mg-Nd-Zn alloy, J. Mater. Sci. Technol. 35 (2019) 777–783.
[34] C. Zhang, S. Guan, L. Wang, S. Zhu, J. Wang, R. Guo, Effect of solution pretreatment on homogeneity and corrosion resistance of biomedical Mg-Zn-Ca alloy processed by high pressure torsion, Adv. Eng. Mater. 19 (2017) 1600326.
[35] H. Wang, S. Guan, X. Wang, C. Ren, L. Wang, In vitro degradation and mechanical integrity of Mg–Zn–Ca alloy coated with Ca-deficient hydroxyapatite by the pulse electrodeposition process, Acta Biomater. 6 (2010) 1743–1748.
[36] J. Wang, J. Tang, P. Zhang, Y. Li, J. Wang, Y. Lai, L. Qin, Surface modification of magnesium alloys developed for bioabsorbable orthopedic implants: a general review, J. Biomed. Mater. Res. Part B Appl. Biomater. 100B (2012) 1691–1701.
[37] H. Hornberger, S. Virtanen, A.R. Boccaccini, Biomedical coatings on magnesium alloys - A review, Acta Biomater. 8 (2012) 2442–2455.
[38] J. Yang, X. Lu, C. Blawert, S. Di, M.L. Zheludkevich, Microstructure and corrosion behavior of Ca/P coatings prepared on magnesium by plasma electrolytic oxidation, Surf. Coat. Technol. 319 (2017) 359–369.
[39] M. Mohedano, B. Luthringer, B. Mingo, F. Feyerabend, R. Arrabal, P. Sanchez-Egido, C. Blawert, R. Willumeit-Römer, M. Zheludkevich, E. Matykina, Bioactive plasma electrolytic oxidation coatings on Mg-Ca alloy to control degradation behaviour, Surf. Coat. Technol. 315 (2017) 454–467.
[40] Y. Feng, X. Ma, L. Chang, S. Zhu, S. Guan, Characterization and cytocompatibility of polydopamine on MAO-HA coating supported on Mg-Zn-Ca alloy, Surf. Interface Anal. 49 (2017) 1115–1123.
[41] X. Lu, C. Blawert, D. Tolnai, T. Subroto, K.U. Kainer, T. Zhang, F. Wang, M.L. Zheludkevich, 3D reconstruction of plasma electrolytic oxidation coatings on Mg alloy via synchrotron radiation tomography, Corros. Sci. 139 (2018) 395–402.
[42] C. Song, Y. Yang, Y. Zhou, L. Wang, S. Zhu, J. Wang, R. Zeng, Y. Zheng, S. Guan, Electrochemical polymerization of dopamine with/without subsequent PLLA coating on Mg-Zn-Y-Nd alloy, Mater. Lett. 252 (2019) 202–206.
[43] L. Chen, J. Li, S. Wang, S. Zhu, C. Zhu, B. Zheng, G. Yang, S. Guan, Surface modification of the biodegradable cardiovascular stent material Mg–Zn–Y–Nd alloy via conjugating REDV peptide for better endothelialization, J. Mater. Res. 33 (2018) 4123–4133.
[44] Y. Chen, X. Lu, S.V. Lamaka, P. Ju, C. Blawert, T. Zhang, F. Wang, M.L. Zheludkevich, Active protection of Mg alloy by composite PEO coating loaded with corrosion inhibitors, Appl. Surf. Sci. 504 (2020) 144462.
[45] X.B. Chen, N. Birbilis, T.B. Abbott, Effect of [Ca2+] and [PO43-] levels on the formation of calcium phosphate conversion coatings on die-cast magnesium alloy AZ91D, Corros. Sci. 55 (2012) 226–232.
[46] X.-B. Chen, K. Chong, T. Abbott, N. Birbilis, M. Easton, Biocompatible strontium-phosphate and manganese-phosphate conversion coatings for magnesium and its alloys, Surface Modification of Magnesium and Its Alloys for Biomedical Applications, Elsevier, 2015, pp. 407–432.
[47] X. Lu, Y. Chen, C. Zhang, T. Zhang, B. Yu, H. Xu, F. Wang, Formation mechanism and corrosion performance of phosphate conversion coatings on AZ91 and Mg-Gd-Y-Zr alloy, J. Electrochem. Soc. 165 (2018) C601–C607.
[48] D. Mei, S.V. Lamaka, J. Gonzalez, F. Feyerabend, R. Willumeit-Römer, M.L. Zheludkevich, The role of individual components of simulated body fluid on the corrosion behavior of commercially pure Mg, Corros. Sci. 147 (2019) 81–93.
[49] J. Gonzalez, R.Q. Hou, E.P.S. Nidadavolu, R. Willumeit-Römer, F. Feyerabend, Magnesium degradation under physiological conditions – best practice, Bioact. Mater. 3 (2018) 174–185.
[50] M.P. Staiger, F. Feyerabend, R. Willumeit, C.S. Sfeir, Y.F. Zheng, S. Virtanen, W.D. Müeller, A. Atrens, M. Peuster, P.N. Kumta, D. Mantovani, F. Witte, Summary of the Panel Discussions at the 2nd Symposium on Biodegradable Metals, Maratea, Italy, 2010, Materials Science and Engineering: B, 176, 2011, pp. 1596–1599.
[51] T. Kokubo, H. Takadama, How useful is SBF in predicting in vivo bone bioactivity? Biomaterials 27 (2006) 2907–2915.
[52] A. Oyane, H.-M. Kim, T. Furuya, T. Kokubo, T. Miyazaki, T. Nakamura, Preparation and assessment of revised simulated body fluids, J. Biomed. Mater. Res. A. 65A (2003) 188–195.
[53] M.-C. Zhao, M. Liu, G.-L. Song, A. Atrens, Influence of pH and chloride ion concentration on the corrosion of Mg alloy ZE41, Corros. Sci. 50 (2008) 3168–3178.
[54] Y. Xin, K. Huo, H. Tao, G. Tang, P.K. Chu, Influence of aggressive ions on the degradation behavior of biomedical magnesium alloy in physiological environment, Acta Biomater. 4 (2008) 2008–2015.
[55] R.-C. Zeng, Y. Hu, S.-K. Guan, H.-Z. Cui, E.-H. Han, Corrosion of magnesium alloy AZ31: the influence of bicarbonate, sulphate, hydrogen phosphate and dihydrogen phosphate ions in saline solution, Corros. Sci. 86 (2014) 171–182.
[56] W. Ma, Y. Liu, W. Wang, Y. Zhang, Effects of electrolyte component in simulated body fluid on the corrosion behavior and mechanical integrity of magnesium, Corros. Sci. 98 (2015) 201–210.
[57] S. Johnston, M. Dargusch, A. Atrens, Building towards a standardised approach to biocorrosion studies: a review of factors influencing Mg corrosion in vitro pertinent to in vivo corrosion, Sci. China Mater. 61 (2017) 475–500.
[58] S.V. Lamaka, J. Gonzalez, D. Mei, F. Feyerabend, R. Willumeit-Römer, M.L. Zheludkevich, Local pH and its evolution near Mg alloy surfaces exposed to simulated body fluids, Adv. Mater. Interfaces 5 (2018) 1800169.
[59] D. Mei, S.V. Lamaka, C. Feiler, M.L. Zheludkevich, The effect of small-molecule bio-relevant organic components at low concentration on the corrosion of commercially pure Mg and Mg-0.8Ca alloy: an overall perspective, Corros. Sci. 153 (2019) 258–271.
[60] Y. Xin, P.K. Chu, Influence of Tris in simulated body fluid on degradation behavior of pure magnesium, Mater. Chem. Phys. 124 (2010) 33–35.
[61] Y. Xin, T. Hu, P.K. Chu, Influence of test solutions on in vitro studies of biomedical magnesium alloys, J. Electrochem. Soc. 157 (2010) C238–C243.
[62] S. Naddaf Dezfuli, Z. Huan, J.M.C. Mol, M.A. Leeflang, J. Chang, J. Zhou, Influence of HEPES buffer on the local pH and formation of surface layer during in vitro degradation tests of magnesium in DMEM, Prog. Nat. Sci. 24 (2014) 531–538.
[63] L.-Y. Cui, Y. Hu, R.-C. Zeng, Y.-X. Yang, D.-D. Sun, S.-Q. Li, F. Zhang, E.-H. Han, New insights into the effect of Tris-HCl and Tris on corrosion of magnesium alloy in presence of bicarbonate, sulfate, hydrogen phosphate and dihydrogen phosphate ions, J. Mater. Sci. Technol. 33 (2017) 971–986.
[64] M.B. Kannan, H. Khakbaz, A. Yamamoto, Understanding the influence of HEPES buffer concentration on the biodegradation of pure magnesium: an electrochemical study, Mater. Chem. Phys. 197 (2017) 47–56.
[65] K. Torne, A. Ornberg, J. Weissenrieder, The influence of buffer system and biological fluids on the degradation of magnesium, J. Biomed. Mater. Res. B Appl. Biomater. 105 (2017) 1490–1502.
[66] S.V. Lamaka, B. Vaghefinazari, D. Mei, R.P. Petrauskas, D. Höche, M.L. Zheludkevich, Comprehensive screening of Mg corrosion inhibitors, Corros. Sci. 128 (2017) 224–240.
[67] R.-Q. Hou, N. Scharnagl, F. Feyerabend, R. Willumeit-Römer, Exploring the effects of organic molecules on the degradation of magnesium under cell culture conditions, Corros. Sci. 132 (2018) 35–45.
[68] Y. Wang, L.-Y. Cui, R.-C. Zeng, S.-Q. Li, Y.-H. Zou, E.-H. Han, In vitro degradation of pure magnesium - the effects of glucose and/or amino acid, Materials 10 (2017) 725.
[69] R.C. Zeng, X.T. Li, S.Q. Li, F. Zhang, E.H. Han, In vitro degradation of pure Mg in response to glucose, Sci. Rep. 5 (2015) 13026.
[70] L.-Y. Cui, X.-T. Li, R.-C. Zeng, S.-Q. Li, E.-H. Han, L. Song, In vitro corrosion of Mg-Ca alloy - the influence of glucose content, Front. Mater. Sci. 11 (2017) 284–295.
[71] S.E. Harandi, P.C. Banerjee, C.D. Easton, R.K. Singh Raman, Influence of bovine serum albumin in Hanks' solution on the corrosion and stress corrosion cracking of a magnesium alloy, Mater. Sci. Eng. C 80 (2017) 335–345.
[72] F. El-Taib Heakal, A.M. Bakry, Serum albumin can influence magnesium alloy degradation in simulated blood plasma for cardiovascular stenting, Mater. Chem.

Phys. 220 (2018) 35–49.
[73] Y.S. Hedberg, Role of proteins in the degradation of relatively inert alloys in the human body, Npj Mater. Degrad. 2 (2018) 26.
[74] R. Hou, R. Willumeit-Römer, V.M. Garamus, M. Frant, J. Koll, F. Feyerabend, Adsorption of Proteins on Degradable Magnesium - Which Factors are Relevant? ACS Appl. Mater. Interfaces 10 (2018) 42175–42185.
[75] T. Li, Y. He, J. Zhou, S. Tang, Y. Yang, X. Wang, Influence of albumin on in vitro degradation behavior of biodegradable Mg-1.5Zn-0.6Zr-0.2Sc alloy, Mater. Lett. 217 (2018) 227–230.
[76] S. Höhn, S. Virtanen, A.R. Boccaccini, Protein adsorption on magnesium and its alloys: a review, Appl. Surf. Sci. 464 (2019) 212–219.
[77] R.Q. Hou, N. Scharnagl, R. Willumeit-Romer, F. Feyerabend, Different effects of single protein vs. Protein mixtures on magnesium degradation under cell culture conditions, Acta Biomater. 98 (2019) 256–268.
[78] Y. Xin, T. Hu, P.K. Chu, In vitro studies of biomedical magnesium alloys in a simulated physiological environment: a review, Acta Biomater. 7 (2011) 1452–1459.
[79] F. Feyerabend, 8 - in vitro analysis of magnesium corrosion in orthopaedic biomaterials, in: P. Dubruel, S. Van Vlierberghe (Eds.), Biomaterials for Bone Regeneration, Woodhead Publishing, 2014, pp. 225–269.
[80] Standard Guide for in Vitro Degradation Testing of Absorbable Metals, in: ASTM F3268-18a, ASTM International, 2018.
[81] Y. Zhang, J. Xu, Y.C. Ruan, M.K. Yu, M. O'Laughlin, H. Wise, D. Chen, L. Tian, D. Shi, J. Wang, S. Chen, J.Q. Feng, D.H.K. Chow, X. Xie, L. Zheng, L. Huang, S. Huang, K. Leung, N. Lu, L. Zhao, H. Li, D. Zhao, X. Guo, K. Chan, F. Witte, H.C. Chan, Y. Zheng, L. Qin, Implant-derived magnesium induces local neuronal production of CGRP to improve bone-fracture healing in rats, Nat. Med. 22 (2016) 1160–1169.
[82] K. Yan, H. Liu, N. Feng, J. Bai, H. Cheng, J. Liu, F. Huang, Preparation of a single-phase Mg–6Zn alloy via ECAP-stimulated solution treatment, J. Magnes. Alloy. 7 (2019) 305–314.
[83] P. Minárik, E. Jablonská, R. Král, J. Lipov, T. Ruml, C. Blawert, B. Hadzima, F. Chmelík, Effect of equal channel angular pressing on in vitro degradation of LAE442 magnesium alloy, Mater. Sci. Eng. C 73 (2017) 736–742.
[84] A. Yamamoto, S. Hiromoto, Effect of inorganic salts, amino acids and proteins on the degradation of pure magnesium in vitro, Mater. Sci. Eng. C 29 (2009) 1559–1568.
[85] C. Schille, M. Braun, H.P. Wendel, L. Scheideler, N. Hort, H.P. Reichel, E. Schweizer, J. Geis-Gerstorfer, Corrosion of experimental magnesium alloys in blood and PBS: a gravimetric and microscopic evaluation, Mater. Sci. Eng. B 176 (2011) 1797–1801.
[86] W.D. Mueller, M. Fernandez Lorenzo de Mele, M.L. Nascimento, M. Zeddies, Degradation of magnesium and its alloys: dependence on the composition of the synthetic biological media, J. Biomed. Mater. Res. A. 90 (2009) 487–495.
[87] M. Alvarez-Lopez, M.D. Pereda, J. Del Valle, M. Fernandez-Lorenzo, M. Garcia-Alonso, O.A. Ruano, M. Escudero, Corrosion behaviour of AZ31 magnesium alloy with different grain sizes in simulated biological fluids, Acta Biomater. 6 (2010) 1763–1771.
[88] D. Xue, Y. Yun, Z. Tan, Z. Dong, M.J. Schulz, In vivo and in vitro degradation behavior of magnesium alloys as biomaterials, J. Mater. Sci. Technol. 28 (2012) 261–267.
[89] M.I. Jamesh, G. Wu, Y. Zhao, D.R. McKenzie, M.M.M. Bilek, P.K. Chu, Electrochemical corrosion behavior of biodegradable Mg–Y–RE and Mg–Zn–Zr alloys in Ringer's solution and simulated body fluid, Corros. Sci. 91 (2015) 160–184.
[90] F. Rosalbino, S. De Negri, A. Saccone, E. Angelini, S. Delfino, Bio-corrosion characterization of Mg–Zn–X (X = Ca, Mn, Si) alloys for biomedical applications, J. Mater. Sci. Mater. Med. 21 (2010) 1091–1098.
[91] N.M. Chelliah, P. Padaikathan, R. Kumar, Evaluation of electrochemical impedance and biocorrosion characteristics of as-cast and T4 heat treated AZ91 Mg-alloys in Ringer's solution, J. Magnes. Alloy. 7 (2019) 134–143.
[92] M. Jamesh, S. Kumar, T.S.N. Sankara Narayanan, Corrosion behavior of commercially pure Mg and ZM21 Mg alloy in Ringer's solution – long term evaluation by EIS, Corros. Sci. 53 (2011) 645–654.
[93] A.D. Forero López, I.L. Lehr, S.B. Saidman, anodisation of AZ91D magnesium alloy in molybdate solution for corrosion protection, J. Alloys. Compd. 702 (2017) 338–345.
[94] S. Feliu, L. Veleva, F. García-Galvan, Effect of temperature on the corrosion behavior of biodegradable AZ31B magnesium alloy in ringer's physiological solution, Metals 9 (2019) 591.
[95] D. Mareci, G. Bolat, J. Izquierdo, C. Crimu, C. Munteanu, I. Antoniac, R. Souto, Electrochemical characteristics of bioresorbable binary MgCa alloys in Ringer's solution: revealing the impact of local pH distributions during in-vitro dissolution, Mater. Sci. Eng. C 60 (2016) 402–410.
[96] J. Tkacz, K. Slouková, J. Minda, J. Drábiková, S. Fintová, P. Doležal, J. Wasserbauer, Influence of the composition of the hank's balanced salt solution on the corrosion behavior of AZ31 and AZ61 magnesium alloys, Metals 7 (2017) 465.
[97] K.Y. Chiu, M.H. Wong, F.T. Cheng, H.C. Man, Characterization and corrosion studies of fluoride conversion coating on degradable Mg implants, Surf. Coat. Technol. 202 (2007) 590–598.
[98] N.T. Kirkland, N. Birbilis, J. Walker, T. Woodfield, G.J. Dias, M.P. Staiger, In-vitro dissolution of magnesium-calcium binary alloys: clarifying the unique role of calcium additions in bioresorbable magnesium implant alloys, J. Biomed. Mater. Res. Part B Appl. Biomater. 95 (2010) 91–100.
[99] B.M. Wilke, L. Zhang, Electrochemical investigations of polycaprolactone-coated AZ31 Mg alloy in Earle's balance salt solution and conventional simulated body fluid, JOM 68 (2016) 1701–1710.
[100] L. Müller, F.A. Müller, Preparation of SBF with different HCO3- content and its influence on the composition of biomimetic apatites, Acta Biomater. 2 (2006) 181–189.
[101] L. Chen, Y. Sheng, H. Zhou, Z. Li, X. Wang, W. Li, Influence of a MAO + PLGA coating on biocorrosion and stress corrosion cracking behavior of a magnesium alloy in a physiological environment, Corros. Sci. 148 (2019) 134–143.
[102] J. Walker, S. Shadanbaz, N.T. Kirkland, E. Stace, T. Woodfield, M.P. Staiger, G.J. Dias, Magnesium alloys: predicting in vivo corrosion with in vitro immersion testing, J. Biomed. Mater. Res. Part B Appl. Biomater. 100B (2012) 1134–1141.
[103] B.M. Wilke, L. Zhang, W. Li, C. Ning, C.-f. Chen, Y. Gu, Corrosion performance of MAO coatings on AZ31 Mg alloy in simulated body fluid vs, Earle's Balance Salt Solution, Applied Surface Science 363 (2016) 328–337.
[104] J. Zhang, L. Zhang, B.M. Wilke, W. Li, C. Ning, T. Chowdhury, Corrosion behaviour of microarc-oxidised magnesium alloy in Earle's balanced salt solution, Surf. Innov. 5 (2017) 43–53.
[105] V. Wagener, S. Virtanen, Protective layer formation on magnesium in cell culture medium, Mater. Sci. Eng. C 63 (2016) 341–351.
[106] J. Zhang, N. Kong, Y. Shi, J. Niu, L. Mao, H. Li, M. Xiong, G. Yuan, Influence of proteins and cells on in vitro corrosion of Mg–Nd–Zn–Zr alloy, Corros. Sci. 85 (2014) 477–481.
[107] S. Agarwal, M.-N. Labour, D. Hoey, B. Duffy, J. Curtin, S. Jaiswal, Enhanced corrosion resistance and cytocompatibility of biomimetic hyaluronic acid functionalised silane coating on AZ31 Mg alloy for orthopaedic applications, J. Mater. Sci. Mater. Med. 29 (2018) 144.
[108] C.L. Liu, Y.J. Wang, R.C. Zeng, X.M. Zhang, W.J. Huang, P.K. Chu, In vitro corrosion degradation behaviour of Mg–Ca alloy in the presence of albumin, Corros. Sci. 52 (2010) 3341–3347.
[109] I. Johnson, W. Jiang, H. Liu, The effects of serum proteins on magnesium alloy degradation in vitro, Sci. Rep. 7 (2017) 14335.
[110] X. Gu, Y. Zheng, L. Chen, Influence of artificial biological fluid composition on the biocorrosion of potential orthopedic Mg–Ca, AZ31, AZ91 alloys, Biomed. Mater. 4 (2009) 065011.
[111] B. Hadzima, M. Mhaede, F. Pastorek, Electrochemical characteristics of calcium-phosphatized AZ31 magnesium alloy in 0.9% NaCl solution, J. Mater. Sci. Mater. Med. 25 (2014) 1227–1237.
[112] A. Pardo, M. Merino, A.E. Coy, R. Arrabal, F. Viejo, E. Matykina, Corrosion behaviour of magnesium/aluminium alloys in 3.5 wt.% NaCl, Corros. Sci. 50 (2008) 823–834.
[113] X.P. Lu, Y. Li, P.F. Ju, Y. Chen, J.S. Yang, K. Qian, T. Zhang, F.H. Wang, Unveiling the inhibition mechanism of an effective inhibitor for AZ91 Mg alloy, Corros. Sci. 148 (2019) 264–271.
[114] J.J. Yang, C. Blawert, S.V. Lamaka, K.A. Yasakau, L. Wang, D. Laipple, M. Schieda, S.C. Di, M.L. Zheludkevich, Corrosion inhibition of pure Mg containing a high level of iron impurity in pH neutral NaCl solution, Corros. Sci. 142 (2018) 222–237.
[115] S.V. Gnedenkov, S.L. Sinebryukhov, V.S. Egorkin, D.V. Mashtalyar, I.E. Vyaliy, K.V. Nadaraia, I.M. Imshinetskiy, A.I. Nikitin, E.P. Subbotin, A.S. Gnedenkov, Magnesium fabricated using additive technology: specificity of corrosion and protection, J. Alloys. Compd. 808 (2019) 151629.
[116] A. Atrens, G.-L. Song, M. Liu, Z. Shi, F. Cao, M.S. Dargusch, Review of recent developments in the field of magnesium corrosion, Adv. Eng. Mater. 17 (2015) 400–453.
[117] E.L. Silva, S.V. Lamaka, D. Mei, M.L. Zheludkevich, The reduction of dissolved oxygen during magnesium corrosion, ChemistryOpen 7 (2018) 664–668.
[118] P. Jiang, C. Blawert, N. Scharnagl, M.L. Zheludkevich, Influence of water purity on the corrosion behavior of Mg0.5ZnX (X=Ca, Ge) alloys, Corros. Sci. 153 (2019) 62–73.
[119] M. Strebl, S. Virtanen, Real-time monitoring of atmospheric magnesium alloy corrosion, J. Electrochem. Soc. 166 (2019) C3001–C3009.
[120] M. Strebl, M. Bruns, S. Virtanen, Editors' choice—respirometric in situ methods for real-time monitoring of corrosion rates: part I. Atmospheric corrosion, J. Electrochem. Soc. 167 (2020) 021510.
[121] Y. Li, X. Lu, K. Wu, L. Yang, T. Zhang, F. Wang, Exploration the inhibition mechanism of sodium dodecyl sulfate on Mg alloy, Corros. Sci. (2020) 108559, https://doi.org/10.1016/j.corsci.2020.108559.
[122] B. Krajewska, W. Zaborska, The effect of phosphate buffer in the range of pH 5.80–8.07 on jack bean urease activity, J. Mol. Catal., B Enzym. 6 (1999) 75–81.
[123] Y. Yun, Z. Dong, D. Yang, M.J. Schulz, V.N. Shanov, S. Yarmolenko, Z. Xu, P. Kumta, C. Sfeir, Biodegradable Mg corrosion and osteoblast cell culture studies, Mater. Sci. Eng. C 29 (2009) 1814–1821.
[124] S. Ringer, Regarding the action of hydrate of soda, hydrate of ammonia, and hydrate of potash on the ventricle of the frog's heart, J. Physiol. (Lond.) 3 (1882) 195.
[125] S. Ringer, Concerning the influence exerted by each of the constituents of the blood on the contraction of the ventricle, J. Physiol. (Lond.) 3 (1882) 380–393.
[126] S. Ringer, A further contribution regarding the influence of the different constituents of the blood on the contraction of the heart, J. Physiol. (Lond.) 4 (1883) 29–42.
[127] S. Ringer, A third contribution regarding the influence of the inorganic constituents of the blood on the ventricular contraction, J. Physiol. (Lond.) 4 (1883) 222–225.
[128] H.A. Krebs, K. Henseleit, Untersuchungen uber die harnstoffbildung im tierkörper, Hoppe-Seyler s Zeitschrift für physiologische Chemie 210 (1932) 33–66.
[129] M. Tyrode, The mode of action of some purgative salts, Arch. Int. Pharmacodyn.

Ther. (1910) 205–209.
[130] F. Locke, O. Rosenheim, Contributions to the physiology of the isolated heart: the consumption of dextrose by mammalian cardiac muscle, J. Physiol. (Lond.) 36 (1907) 205.
[131] A. Zakiyuddin, K. Yun, K. Lee, Corrosion behavior of as-cast and hot rolled pure magnesium in simulated physiological media, Met. Mater. Int. 20 (2014) 1163–1168.
[132] C. Vasilescu, S.I. Drob, E.I. Neacsu, J.C. Mirza Rosca, Surface analysis and corrosion resistance of a new titanium base alloy in simulated body fluids, Corros. Sci. 65 (2012) 431–440.
[133] M. Grabowski, D. Bluecher, M. Korte, S. Virtanen, Influence of Ca2+ in deicing salt on the corrosion behavior of AM50 magnesium alloy, Corrosion 70 (2014) 1008–1023.
[134] M. Grabowski, D. Bluecher, M. Korte, S. Virtanen, The influence of Ca2+ in deicing salt on the chemistry of corrosion products formed on AM50 magnesium alloy—calcareous deposition, Corrosion 71 (2015) 703–725.
[135] F.Y. Cao, C. Zhao, J. You, J.J. Hu, D.J. Zheng, G.L. Song, The inhibitive effect of artificial seawater on magnesium corrosion, Adv. Eng. Mater. 21 (2019) 1900363.
[136] N.I. Zainal Abidin, B. Rolfe, H. Owen, J. Malisano, D. Martin, J. Hofstetter, P.J. Uggowitzer, A. Atrens, The in vivo and in vitro corrosion of high-purity magnesium and magnesium alloys WZ21 and AZ91, Corros. Sci. 75 (2013) 354–366.
[137] Y. Al-Abdullat, S. Tsutsumi, N. Nakajima, M. Ohta, H. Kuwahara, K. Ikeuchi, Surface modification of magnesium by NaHCO3 and corrosion behavior in Hank's solution for new biomaterial applications, Mater. Trans. 42 (2001) 1777–1780.
[138] H. Kuwahara, Y. Al-Abdullat, N. Mazaki, S. Tsutsumi, T. Aizawa, Precipitation of magnesium apatite on pure magnesium surface during immersing in Hank's solution, Mater. Trans. 42 (2001) 1317–1321.
[139] T.-W. Kim, H.-S. Lee, D.-H. Kim, H.-H. Jin, K.-H. Hwang, J.K. Lee, H.-C. Park, S.-Y. Yoon, In situ synthesis of magnesium-substituted biphasic calcium phosphate and in vitro biodegradation, Mater. Res. Bull. 47 (2012) 2506–2512.
[140] D. Tie, F. Feyerabend, N. Hort, R. Willumeit, D. Hoeche, XPS studies of magnesium surfaces after exposure to Dulbecco's modified eagle medium, Hank's buffered salt solution, and simulated body fluid, Adv. Eng. Mater. 12 (2010) B699–B704.
[141] N.A. Agha, F. Feyerabend, B. Mihailova, S. Heidrich, U. Bismayer, R. Willumeit-Römer, Magnesium degradation influenced by buffering salts in concentrations typical of in vitro and in vivo models, Mater. Sci. Eng. C 58 (2016) 817–825.
[142] R. Willumeit, J. Fischer, F. Feyerabend, N. Hort, U. Bismayer, S. Heidrich, B. Mihailova, Chemical surface alteration of biodegradable magnesium exposed to corrosion media, Acta Biomater. 7 (2011) 2704–2715.
[143] M. Zuo, W. Wang, H. Wu, L. Yang, J. Yan, J. Ni, S. Zhang, Y. Song, J. Wang, X. Zhang, In vitro degradation and mineralization of high-purity magnesium in three physiological fluids, Mater. Lett. 240 (2019) 279–283.
[144] D.-B. Liu, B. Wu, X. Wang, M.-F. Chen, Corrosion and wear behavior of an Mg–2Zn–0.2 Mn alloy in simulated body fluid, Rare Metals 34 (2015) 553–559.
[145] J. Waterman, A. Pietak, N. Birbilis, T. Woodfield, G. Dias, M. Staiger, Corrosion resistance of biomimetic calcium phosphate coatings on magnesium due to varying pretreatment time, Mater. Sci. Eng. B 176 (2011) 1756–1760.
[146] W. Wang, J. Han, X. Yang, M. Li, P. Wan, L. Tan, Y. Zhang, K. Yang, Novel biocompatible magnesium alloys design with nutrient alloying elements Si, Ca and Sr: structure and properties characterization, Mater. Sci. Eng. B 214 (2016) 26–36.
[147] M. Zhang, W.-L. Deng, X.-N. Yang, Y.-K. Wang, X.-Y. Zhang, R.-Q. Hang, K.-K. Deng, X.-B. Huang, In vitro biodegradability of Mg–2Gd–xZn alloys with different Zn contents and solution treatments, Rare Metals 38 (2019) 620–628.
[148] M.-Z. Ge, J.-Y. Xiang, L. Yang, J. Wang, Effect of laser shock peening on the stress corrosion cracking of AZ31B magnesium alloy in a simulated body fluid, Surf. Coat. Technol. 310 (2017) 157–165.
[149] T. Li, H. Zhang, Y. He, N. Wen, X. Wang, Microstructure, Mechanical Properties and In Vitro Degradation Behavior of a Novel Biodegradable Mg–1.5Zn–0.6Zr–0.2Sc Alloy, J. Mater. Sci. Technol. 31 (2015) 744–750.
[150] Y. Xin, T. Hu, P.K. Chu, Degradation behaviour of pure magnesium in simulated body fluids with different concentrations of HCO3, Corros. Sci. 53 (2011) 1522–1528.
[151] X.-B. Chen, C. Li, D. Xu, Biodegradation of Mg-14Li alloy in simulated body fluid: a proof-of-concept study, Bioact. Mater. 3 (2018) 110–117.
[152] A.S. Gnedenkov, D. Mei, S.V. Lamaka, S.L. Sinebryukhov, D.V. Mashtalyar, I.E. Vyaliy, M.L. Zheludkevich, S.V. Gnedenkov, Localized currents and pH distribution studied during corrosion of MA8 Mg alloy in the cell culture medium, Corros. Sci. (2020) 108689, https://doi.org/10.1016/j.corsci.2020.108689.
[153] A.S. Gnedenkov, S.V. Lamaka, S.L. Sinebryukhov, D.V. Mashtalyar, V.S. Egorkin, I.M. Imshinetskiy, A.G. Zavidnaya, M.L. Zheludkevich, S.V. Gnedenkov, Electrochemical behaviour of the MA8 Mg alloy in minimum essential medium, Corros. Sci. (2020) 108552, https://doi.org/10.1016/j.corsci.2020.108552.
[154] Y. Wang, B.H. Ding, S.Y. Gao, X.B. Chen, R.C. Zeng, L.Y. Cui, S.J. Li, S.Q. Li, Y.H. Zou, E.H. Han, S.K. Guan, Q.Y. Liu, In vitro corrosion of pure Mg in phosphate buffer solution-Influences of isoelectric point and molecular structure of amino acids, Mater. Sci. Eng. C Mater. Biol. Appl. 105 (2019) 110042.
[155] H. Krebs, Chemical composition of blood plasma and serum, Annu. Rev. Biochem. 19 (1950) 409–430.
[156] S. Johnston, Z.M. Shi, J. Venezuela, C.E. Wen, M.S. Dargusch, A. Atrens, Investigating Mg biocorrosion in vitro: lessons learned and recommendations, JOM 71 (2019) 1406–1413.
[157] N.A. Agha, Z. Liu, F. Feyerabend, R. Willumeit-Römer, B. Gasharova, S. Heidrich, B. Mihailova, The effect of osteoblasts on the surface oxidation processes of biodegradable Mg and Mg-Ag alloys studied by synchrotron IR microspectroscopy, Mater. Sci. Eng. C 91 (2018) 659–668.
[158] S. Yoshizawa, A. Brown, A. Barchowsky, C. Sfeir, Magnesium ion stimulation of bone marrow stromal cells enhances osteogenic activity, simulating the effect of magnesium alloy degradation, Acta Biomater. 10 (2014) 2834–2842.
[159] N. Ostrowski, B. Lee, N. Enick, B. Carlson, S. Kunjukunju, A. Roy, P.N. Kumta, Corrosion protection and improved cytocompatibility of biodegradable polymeric layer-by-layer coatings on AZ31 magnesium alloys, Acta Biomater. 9 (2013) 8704–8713.
[160] D. Hong, P. Saha, D.-T. Chou, B. Lee, B.E. Collins, Z. Tan, Z. Dong, P.N. Kumta, In vitro degradation and cytotoxicity response of Mg–4% Zn–0.5% Zr (ZK40) alloy as a potential biodegradable material, Acta Biomater. 9 (2013) 8534–8547.
[161] H.M. Mousa, A.P. Tiwari, J. Kim, S.P. Adhikari, C.H. Park, C.S. Kim, A novel in situ deposition of hydroxyapatite nanoplates using anodization/hydrothermal process onto magnesium alloy surface towards third generation biomaterials, Mater. Lett. 164 (2016) 144–147.
[162] I. Marco, F. Feyerabend, R. Willumeit-Römer, O. Van der Biest, Degradation testing of Mg alloys in Dulbecco's modified eagle medium: influence of medium sterilization, Mater. Sci. Eng. C 62 (2016) 68–78.
[163] H. Hornberger, F. Witte, N. Hort, W.D. Mueller, Effect of fetal calf serum on the corrosion behaviour of magnesium alloys, Mater. Sci. Eng. B 176 (2011) 1746–1755.
[164] G.Z. Jia, C.X. Chen, J. Zhang, Y.C. Wang, R. Yue, B.J.C. Luthringer-Feyerabend, R. Willumeit-Roemer, H. Zhang, M.P. Xiong, H. Huang, G.Y. Yuan, F. Feyerabend, In vitro degradation behavior of Mg scaffolds with three-dimensional interconnected porous structures for bone tissue engineering, Corros. Sci. 144 (2018) 301–312.
[165] A. Witecka, A. Bogucka, A. Yamamoto, K. Máthis, T. Krajňák, J. Jaroszewicz, W. Święszkowski, In vitro degradation of ZM21 magnesium alloy in simulated body fluids, Mater. Sci. Eng. C 65 (2016) 59–69.
[166] L. Yang, N. Hort, D. Laipple, D. Höche, Y. Huang, K.U. Kainer, R. Willumeit, F. Feyerabend, Element distribution in the corrosion layer and cytotoxicity of alloy Mg–10Dy during in vitro biodegradation, Acta Biomater. 9 (2013) 8475–8487.
[167] F. Witte, F. Feyerabend, P. Maier, J. Fischer, M. Störmer, C. Blawert, W. Dietzel, N. Hort, Biodegradable magnesium–hydroxyapatite metal matrix composites, Biomaterials 28 (2007) 2163–2174.
[168] A. Pietak, P. Mahoney, G.J. Dias, M.P. Staiger, Bone-like matrix formation on magnesium and magnesium alloys, J. Mater. Sci. Mater. Med. 19 (2008) 407–415.
[169] P.J. Price, E.A. Gregory, Relationship between in vitro growth promotion and biophysical and biochemical properties of the serum supplement, In Vitro 18 (1982) 576–584.
[170] G. Gstraunthaler, Alternatives to the use of fetal bovine serum: serum-free cell culture, ALTEX-Alternatives to animal experimentation 20 (2003) 275–281.
[171] N.T. Kirkland, J. Waterman, N. Birbilis, G. Dias, T.B.F. Woodfield, R.M. Hartshorn, M.P. Staiger, Buffer-regulated biocorrosion of pure magnesium, J. Mater. Sci. Mater. Med. 23 (2012) 283–291.
[172] D. Mei, C. Wang, S.V. Lamaka, M.L. Zheludkevich, Clarifying the influence of albumin on the initial stages of magnesium corrosion in Hank's Balanced Salt Solution, Submitted.
[173] W. Robertson, R. Marshall, G.N. Bowers, Ionized calcium in body fluids, CRC Crit. Rev. Clin. Lab. Sci. 15 (1981) 85–125.
[174] M. Kroll, R. Elin, Relationships between magnesium and protein concentrations in serum, Clin. Chem. 31 (1985) 244–246.
[175] P. Maurer, E. Hohenester, J. Engel, Extracellular calcium-binding proteins, Curr. Opin. Cell Biol. 8 (1996) 609–617.
[176] Y. Song, D. Shan, R. Chen, F. Zhang, E.-H. Han, Biodegradable behaviors of AZ31 magnesium alloy in simulated body fluid, Mater. Sci. Eng. C 29 (2009) 1039–1045.
[177] N.T. Kirkland, N. Birbilis, M. Staiger, Assessing the corrosion of biodegradable magnesium implants: a critical review of current methodologies and their limitations, Acta Biomater. 8 (2012) 925–936.
[178] Y. Jin, C. Blawert, F. Feyerabend, J. Bohlen, M. Silva Campos, S. Gavras, B. Wiese, D. Mei, M. Deng, H. Yang, R. Willumeit-Römer, Time-sequential corrosion behaviour observation of micro-alloyed Mg-0.5Zn-0.2Ca alloy via a quasi-in situ approach, Corros. Sci. 158 (2019) 108096.
[179] S. Johnston, Z. Shi, A. Atrens, The influence of pH on the corrosion rate of high-purity Mg, AZ91 and ZE41 in bicarbonate buffered Hanks' solution, Corros. Sci. 101 (2015) 182–192.
[180] C. Wang, D. Mei, S.V. Lamaka, M.L. Zheludkevich, Oxygen Reduction Reaction During Magnesium Corrosion, Submitted.
[181] A.D. King, N. Birbilis, J.R. Scully, Accurate electrochemical measurement of magnesium corrosion rates; a combined impedance, mass-loss and hydrogen collection study, Electrochim. Acta 121 (2014) 394–406.
[182] C. Feiler, D. Mei, B. Vaghefinazari, T. Würger, R.H. Meißner, B.J.C. Luthringer-Feyerabend, D.A. Winkler, M.L. Zheludkevich, S.V. Lamaka, In silico screening of modulators of magnesium dissolution, Corros. Sci. 163 (2019) 108245.
[183] M. Schinhammer, J. Hofstetter, C. Wegmann, F. Moszner, J.F. Löffler, P.J. Uggowitzer, On the immersion testing of degradable implant materials in simulated body fluid: active pH regulation using CO2, Adv. Eng. Mater. 15 (2013) 434–441.
[184] Y. Liu, M. Curioni, Z. Liu, Correlation between electrochemical impedance measurements and corrosion rates of Mg-1Ca alloy in simulated body fluid, Electrochim. Acta 264 (2018) 101–108.
[185] J. Wang, V. Giridharan, V. Shanov, Z. Xu, B. Collins, L. White, Y. Jang, J. Sankar, N. Huang, Y. Yun, Flow-induced corrosion behavior of absorbable magnesium-based stents, Acta Biomater. 10 (2014) 5213–5223.
[186] A.P. Md Saad, A. Syahrom, Study of dynamic degradation behaviour of porous magnesium under physiological environment of human cancellous bone, Corros. Sci. 131 (2018) 45–56.

[187] B. Zeller-Plumhoff, H. Helmholz, F. Feyerabend, T. Dose, F. Wilde, A. Hipp, F. Beckmann, R. Willumeit-Römer, J.U. Hammel, Quantitative characterization of degradation processes in situ by means of a bioreactor coupled flow chamber under physiological conditions using time-lapse SRμCT, Mater. Corros. 69 (2018) 298–306.
[188] V. Wagener, S. Virtanen, Influence of electrolyte composition (Simulated body fluid vs. Dulbecco's modified eagle's medium), temperature, and solution flow on the biocorrosion behavior of commercially pure Mg, Corrosion 73 (2017) 1413–1422.
[189] A. Atrens, S. Johnston, Z. Shi, M.S. Dargusch, Viewpoint - understanding Mg corrosion in the body for biodegradable medical implants, Scr. Mater. 154 (2018) 92–100.
[190] Y. Gao, L. Wang, L. Li, X. Gu, K. Zhang, J. Xia, Y. Fan, Effect of stress on corrosion of high-purity magnesium in vitro and in vivo, Acta Biomater. 83 (2019) 477–486.
[191] M. Liu, J. Wang, S. Zhu, Y. Zhang, Y. Sun, L. Wang, S. Guan, Corrosion fatigue of the extruded Mg–Zn–Y–Nd alloy in simulated body fluid, J. Magnes. Alloy. 8 (2020) 231–240.
[192] D. Bian, W. Zhou, Y. Liu, N. Li, Y. Zheng, Z. Sun, Fatigue behaviors of HP-Mg, Mg–Ca and Mg–Zn–Ca biodegradable metals in air and simulated body fluid, Acta Biomater. 41 (2016) 351–360.
[193] S. Hu, J.A. Loo, D.T. Wong, Human body fluid proteome analysis, Proteomics 6 (2006) 6326–6353.
[194] A.H.M. Sanchez, B.J.C. Luthringer, F. Feyerabend, R. Willumeit, Mg and Mg alloys: how comparable are in vitro and in vivo corrosion rates? A review, Acta Biomater. 13 (2015) 16–31.
[195] D. Vojtech, J. Kubasek, J. Capek, I. Pospisilova, Comparative mechanical and corrosion studies on magnesium, zinc and iron alloys as biodegradable metals, Mater. Technol 49 (2015) 877–882.
[196] A. Drynda, T. Hassel, F.W. Bach, M. Peuster, In vitro and in vivo corrosion properties of new iron–manganese alloys designed for cardiovascular applications, J. Biomed. Mater. Res. Part B Appl. Biomater. 103 (2015) 649–660.
[197] Y. Chen, W. Zhang, M.F. Maitz, M. Chen, H. Zhang, J. Mao, Y. Zhao, N. Huang, G. Wan, Comparative corrosion behavior of Zn with Fe and Mg in the course of immersion degradation in phosphate buffered saline, Corros. Sci. 111 (2016) 541–555.
[198] K. Törne, M. Larsson, A. Norlin, J. Weissenrieder, Degradation of zinc in saline solutions, plasma, and whole blood, J. Biomed. Mater. Res. Part B Appl. Biomater. 104 (2016) 1141–1151.
[199] X. Liu, J. Sun, F. Zhou, Y. Yang, R. Chang, K. Qiu, Z. Pu, L. Li, Y. Zheng, Micro-alloying with Mn in Zn–Mg alloy for future biodegradable metals application, Mater. Des. 94 (2016) 95–104.
[200] E. Zhang, H. Chen, F. Shen, Biocorrosion properties and blood and cell compatibility of pure iron as a biodegradable biomaterial, J. Mater. Sci. Mater. Med. 21 (2010) 2151–2163.
[201] B. Liu, Y.F. Zheng, Effects of alloying elements (Mn, Co, Al, W, Sn, B, C and S) on biodegradability and in vitro biocompatibility of pure iron, Acta Biomater. 7 (2011) 1407–1420.
[202] Y. Li, P. Pavanram, J. Zhou, K. Lietaert, P. Taheri, W. Li, H. San, M.A. Leeflang, J.M.C. Mol, H. Jahr, A.A. Zadpoor, Additively manufactured biodegradable porous zinc, Acta Biomater. 101 (2020) 609–623.
[203] C. Xiao, L. Wang, Y. Ren, S. Sun, E. Zhang, C. Yan, Q. Liu, X. Sun, F. Shou, J. Duan, H. Wang, G. Qin, Indirectly extruded biodegradable Zn-0.05wt%Mg alloy with improved strength and ductility: in vitro and in vivo studies, J. Mater. Sci. Technol. 34 (2018) 1618–1627.
[204] Y. Li, H. Jahr, K. Lietaert, P. Pavanram, A. Yilmaz, L.I. Fockaert, M.A. Leeflang, B. Pouran, Y. Gonzalez-Garcia, H. Weinans, J.M.C. Mol, J. Zhou, A.A. Zadpoor, Additively manufactured biodegradable porous iron, Acta Biomater. 77 (2018) 380–393.
[205] H. Dong, J. Zhou, S. Virtanen, Fabrication of ZnO nanotube layer on Zn and evaluation of corrosion behavior and bioactivity in view of biodegradable applications, Appl. Surf. Sci. 494 (2019) 259–265.
[206] B. Jia, H. Yang, Y. Han, Z. Zhang, X. Qu, Y. Zhuang, Q. Wu, Y. Zheng, K. Dai, In vitro and in vivo studies of Zn-Mn biodegradable metals designed for orthopedic applications, Acta Biomater. (2020), https://doi.org/10.1016/j.actbio.2020.03.009.
[207] J. Kubásek, D. Vojtěch, E. Jablonská, I. Pospíšilová, J. Lipov, T. Ruml, Structure, mechanical characteristics and in vitro degradation, cytotoxicity, genotoxicity and mutagenicity of novel biodegradable Zn–Mg alloys, Mater. Sci. Eng. C 58 (2016) 24–35.
[208] J. Čapek, J. Kubásek, D. Vojtěch, E. Jablonská, J. Lipov, T. Ruml, Microstructural, mechanical, corrosion and cytotoxicity characterization of the hot forged FeMn30(wt.%) alloy, Mater. Sci. Eng. C 58 (2016) 900–908.
[209] L. Liu, Y. Meng, A.A. Volinsky, H.-J. Zhang, L.-N. Wang, Influences of albumin on in vitro corrosion of pure Zn in artificial plasma, Corros. Sci. 153 (2019) 341–356.
[210] P. Li, C. Schille, E. Schweizer, E. Kimmerle-Müller, F. Rupp, A. Heiss, C. Legner, U.E. Klotz, J. Geis-Gerstorfer, L. Scheideler, Selection of extraction medium influences cytotoxicity of zinc and its alloys, Acta Biomater. 98 (2019) 235–245.
[211] S. Reuter, C. Georges, P. Jacques, Optimisation of the corrosion rate of iron-based alloys for bioresorbable stent applications by surface acidification, 9th Symposium on Biodegradable Metals for Biomedical Applications (2017).
[212] H. Hermawan, D. Dubé, D. Mantovani, Degradable metallic biomaterials: design and development of Fe–Mn alloys for stents, J. Biomed. Mater. Res. A. 93A (2010) 1–11.
[213] H. Hermawan, A. Purnama, D. Dube, J. Couet, D. Mantovani, Fe–Mn alloys for metallic biodegradable stents: degradation and cell viability studies, Acta Biomater. 6 (2010) 1852–1860.
[214] E. Mouzou, C. Paternoster, R. Tolouei, A. Purnama, P. Chevallier, D. Dubé, F. Prima, D. Mantovani, In vitro degradation behavior of Fe–20Mn–1.2C alloy in three different pseudo-physiological solutions, Mater. Sci. Eng. C 61 (2016) 564–573.
[215] C.S. Obayi, R. Tolouei, C. Paternoster, S. Turgeon, B.A. Okorie, D.O. Obikwelu, G. Cassar, J. Buhagiar, D. Mantovani, Influence of cross-rolling on the microtexture and biodegradation of pure iron as biodegradable material for medical implants, Acta Biomater. 17 (2015) 68–77.
[216] S. Lamaka, R.M. Souto, M.G. Ferreira, In-situ visualization of local corrosion by scanning ion-selective electrode technique (SIET), microscopy: science, technology, applications and education 3 (2010) 2162–2173.
[217] T. Kraus, F. Moszner, S. Fischerauer, M. Fiedler, E. Martinelli, J. Eichler, F. Witte, E. Willbold, M. Schinhammer, M. Meischel, P.J. Uggowitzer, J.F. Löffler, A. Weinberg, Biodegradable Fe-based alloys for use in osteosynthesis: outcome of an in vivo study after 52weeks, Acta Biomater. 10 (2014) 3346–3353.
[218] M. Schinhammer, P. Steiger, F. Moszner, J.F. Löffler, P.J. Uggowitzer, Degradation performance of biodegradable FeMnC(Pd) alloys, Mater. Sci. Eng. C 33 (2013) 1882–1893.
[219] M. Wiesener, K. Peters, A. Taube, A. Keller, K.-P. Hoyer, T. Niendorf, G. Grundmeier, Corrosion properties of bioresorbable FeMn-Ag alloys prepared by selective laser melting, Mater. Corros. 68 (2017) 1028–1036.
[220] M.S. Dargusch, A. Dehghan-Manshadi, M. Shahbazi, J. Venezuela, X. Tran, J. Song, N. Liu, C. Xu, Q. Ye, C. Wen, Exploring the role of manganese on the microstructure, mechanical properties, biodegradability, and biocompatibility of porous iron-based scaffolds, ACS Biomater. Sci. Eng. 5 (2019) 1686–1702.
[221] M. Taryba, S. Lamaka, D. Snihirova, M. Ferreira, M. Montemor, W. Wijting, S. Toews, G. Grundmeier, The combined use of scanning vibrating electrode technique and micro-potentiometry to assess the self-repair processes in defects on "smart" coatings applied to galvanized steel, Electrochim. Acta 56 (2011) 4475–4488.
[222] L. Guo, S.R. Street, H.B. Mohammed-Ali, M. Ghahari, N. Mi, S. Glanvill, A. Du Plessis, C. Reinhard, T. Rayment, A.J. Davenport, The effect of relative humidity change on atmospheric pitting corrosion of stainless steel 304L, Corros. Sci. 150 (2019) 110–120.
[223] X. Liu, H.T. Yang, Y. Liu, P. Xiong, H. Guo, H.H. Huang, Y.F. Zheng, Comparative studies on degradation behavior of pure zinc in various simulated body fluids, JOM 71 (2019) 1414–1425.
[224] E. Mostaed, M. Sikora-Jasinska, A. Mostaed, S. Loffredo, A.G. Demir, B. Previtali, D. Mantovani, R. Beanland, M. Vedani, Novel Zn-based alloys for biodegradable stent applications: design, development and in vitro degradation, J. Mech. Behav. Biomed. Mater. 60 (2016) 581–602.
[225] H.F. Li, X.H. Xie, Y.F. Zheng, Y. Cong, F.Y. Zhou, K.J. Qiu, X. Wang, S.H. Chen, L. Huang, L. Tian, L. Qin, Development of biodegradable Zn-1X binary alloys with nutrient alloying elements Mg, Ca and Sr, Sci. Rep. 5 (2015) 10719.
[226] C. Shen, X. Liu, B. Fan, P. Lan, F. Zhou, X. Li, H. Wang, X. Xiao, L. Li, S. Zhao, Z. Guo, Z. Pu, Y. Zheng, Mechanical properties, in vitro degradation behavior, hemocompatibility and cytotoxicity evaluation of Zn–1.2Mg alloy for biodegradable implants, RSC Adv. 6 (2016) 86410–86419.
[227] H. Gong, K. Wang, R. Strich, J.G. Zhou, In vitro biodegradation behavior, mechanical properties, and cytotoxicity of biodegradable Zn–Mg alloy, J. Biomed. Mater. Res. Part B Appl. Biomater. 103 (2015) 1632–1640.
[228] H.R. Bakhsheshi-Rad, E. Hamzah, H.T. Low, M. Kasiri-Asgarani, S. Farahany, E. Akbari, M.H. Cho, Fabrication of biodegradable Zn-Al-Mg alloy: mechanical properties, corrosion behavior, cytotoxicity and antibacterial activities, Mater. Sci. Eng. C 73 (2017) 215–219.
[229] M.S. Dambatta, S. Izman, D. Kurniawan, H. Hermawan, Processing of Zn-3Mg alloy by equal channel angular pressing for biodegradable metal implants, J. King Saud Univ. - Sci. 29 (2017) 455–461.
[230] X. Liu, H.T. Yang, P. Xiong, W.T. Li, E.H. Huang, Y.F. Zheng, Comparative studies of Tris-HCl, HEPES and NaHCO3/CO2 buffer systems on the biodegradation behaviour of pure Zn in NaCl and SBF solutions, Corros. Sci. 157 (2019) 205–219.
[231] H. Yang, C. Wang, C. Liu, H. Chen, Y. Wu, J. Han, Z. Jia, W. Lin, D. Zhang, W. Li, W. Yuan, H. Guo, H. Li, G. Yang, D. Kong, D. Zhu, K. Takashima, L. Ruan, J. Nie, X. Li, Y. Zheng, Evolution of the degradation mechanism of pure zinc stent in the one-year study of rabbit abdominal aorta model, Biomaterials 145 (2017) 92–105.
[232] S. Lamaka, M. Zheludkevich, Evolution of local pH and dissolved oxygen concentration during in vitro degradation of pure Zn and Zn-Mg alloys, 10th Symposium on Biodegradable Metals for Biomedical Applications (2018).
[233] D. Vojtěch, J. Kubásek, J. Šerák, P. Novák, Mechanical and corrosion properties of newly developed biodegradable Zn-based alloys for bone fixation, Acta Biomater. 7 (2011) 3515–3522.
[234] Y. Ren, J. Huang, B. Zhang, K. Yang, Preliminary study of biodegradation of AZ31B magnesium alloy, Front. Mater. Sci. China 1 (2007) 401–404.

6. Conclusions and outlook

The influence of inorganic ions and selected organic compounds on Mg corrosion has been investigated in this work. The main findings and conclusions are listed below:

(1) Synthetic pH buffer (Tris/HCl) significantly accelerates Mg corrosion. Considering it is not the component of any physiological fluid, synthetic pH buffer should not be used for Mg corrosion tests related to biomedical applications.

(2) In SBF-like media (e.g. SBF, HBSS, MEM etc.), the synergy of Ca^{2+}, HCO_3^- and $HPO_4^{2-}/H_2PO_4^-$ affects the corrosion behavior of Mg by the formation of additional protective co-precipitation layer on Mg surface, mostly composed of Mg/Ca-carbonates and Mg/Ca phosphates. This phenomenon was indicated by the appearance of the additional time constant at the high frequency range during the continuous EIS tests.

(3) The tested 53 small-molecule bio-relevant organic compounds at low concentration do not critically influence Mg corrosion in NaCl solution, SBF, or MEM. The similar corrosion behavior of Mg was observed in MEM and SBF during the short test period. However, bearing in mind the presence of nutrients, cell culture media (MEM or other similar ones) are not suitable for the long-term corrosion test at the open environment due to the high risk of microbial contamination.

(4) Proteins ultimately affect the corrosion of Mg in HBSS through the combination of three effects, adsorption, chelation of Mg^{2+} and Ca^{2+} and pH buffering effecting local and bulk electrolyte. The dominated factor(s) among these three effects vary. The effect of protein on Mg corrosion is susceptible to the test method, test condition, alloy, exposure time and protein sources.

(5) The additives that influence the free concentration of trio of ions (Ca^{2+}, HCO_3^- and $HPO_4^{2-}/H_2PO_4^-$) inhibit the formation of aforementioned (point 2) protective co-precipitation layer and increase the corrosion rate of Mg in SBF-like media. For example, in this work, albumin and streptomycin at high concentration (over 0.01 M) were found to be delaying the formation of co-precipitation layer because of their affinity to Ca^{2+}.

(6) Compared to bulk pH, the evolution of local pH near the corroding Mg surface (in the diffusion layer) provides more insights into Mg corrosion behavior. The low and stable local pH (below 8.5) in SBF (w/o synthetic pH buffer) and HBSS verified the slight corrosion of Mg alloys and different nature of corrosion products in this type of medium compared to that in NaCl solution and media with synthetic buffers. The local pH measurement in HBSS+BSA showed the buffering effect of albumin, which differs from that of synthetic pH buffers. The latter typically only buffer the bulk pH of the media.

(7) In Mg corrosion test, the corrosive medium should be selected according to the research purpose. For example, the corrosion tests in NaCl solution provide more information

about the intrinsic corrosion resistance of tested materials, while the tests performed in HBSS or MEM are influenced by the media components to large extent. Thus, multiple corrosive media should be used at different stages of material development in order to obtain comprehensive information about the corrosion behavior of Mg.

In this thesis, several test methods, continuous EIS and local pH measurements, have been proven to be effective approaches to investigate the corrosion behavior of Mg in pseudophysiological media. They are helpful for further investigation. As mentioned earlier in the thesis, at the present stage, the lack of the general acceptable test protocols restricts the rapid development of biodegradable Mg. In order to establish the relevant standards, fundamental contribution of experts is necessary to clarify the influence of test media and test conditions. The main content of this thesis focused on the influence of media components. However, we are aware that not only the media components, but also the test conditions influence the Mg corrosion. In terms of test condition, we performed preliminarily tests to compare the corrosion rate of Mg under both static condition and hydrodynamic condition, but some other parameters, like temperature and partial pressure of oxygen in the test environment, were not considered in this work. They are worthy for the further investigation.

Bibliography

[1] F. Witte, N. Hort, C. Vogt, S. Cohen, K.U. Kainer, R. Willumeit, F. Feyerabend, Degradable biomaterials based on magnesium corrosion, Current Opinion in Solid State and Materials Science, 12 (2008) 63-72.

[2] F. Kaiser, K. Kainer, Magnesium alloys and technology, John Wiley & Sons, 2003.

[3] T. Zhang, Z. Tao, J. Chen, Magnesium–air batteries: from principle to application, Materials Horizons, 1 (2014) 196-206.

[4] C. Blawert, N. Hort, K. Kainer, Automotive applications of magnesium and its alloys, Trans. Indian Inst. Met, 57 (2004) 397-408.

[5] A.A. Luo, Magnesium casting technology for structural applications, journal of Magnesium and Alloys, 1 (2013) 2-22.

[6] F. Cheng, J. Chen, Metal–air batteries: from oxygen reduction electrochemistry to cathode catalysts, Chemical Society Reviews, 41 (2012) 2172-2192.

[7] M.A. Rahman, X. Wang, C. Wen, High energy density metal-air batteries: a review, Journal of The Electrochemical Society, 160 (2013) A1759-A1771.

[8] M. Deng, D. Höche, D. Snihirova, L. Wang, B. Vaghefinazari, S.V. Lamaka, M.L. Zheludkevich, CHAPTER 12 Aqueous Mg Batteries, in: Magnesium Batteries: Research and Applications, The Royal Society of Chemistry, 2020, pp. 275-308.

[9] R. Zeng, W. Dietzel, F. Witte, N. Hort, C. Blawert, Progress and Challenge for Magnesium Alloys as Biomaterials, Advanced Engineering Materials, 10 (2008) B3-B14.

[10] Y.F. Zheng, X.N. Gu, F. Witte, Biodegradable metals, Materials Science and Engineering: R: Reports, 77 (2014) 1-34.

[11] Y. Chen, Z. Xu, C. Smith, J. Sankar, Recent advances on the development of magnesium alloys for biodegradable implants, Acta Biomaterialia, 10 (2014) 4561-4573.

[12] D. Zhao, F. Witte, F. Lu, J. Wang, J. Li, L. Qin, Current status on clinical applications of magnesium-based orthopaedic implants: A review from clinical translational perspective, Biomaterials, 112 (2017) 287-302.

[13] J. Wu, D. Zhao, J.M. Ohodnicki, B. Lee, A. Roy, R. Yao, S. Chen, Z. Dong, W.R. Heineman, P.N. Kumta, In Vitro and in Vivo Evaluation of Multiphase Ultrahigh Ductility Mg–Li–Zn Alloys for Cardiovascular Stent Application, ACS Biomaterials Science & Engineering, 4 (2017) 919-932.

[14] A. Atrens, G.-L. Song, M. Liu, Z. Shi, F. Cao, M.S. Dargusch, Review of Recent Developments in the Field of Magnesium Corrosion, Advanced Engineering Materials, 17 (2015) 400-453.

[15] P. Jiang, C. Blawert, N. Scharnagl, M.L. Zheludkevich, Influence of water purity on the corrosion behavior of Mg0.5ZnX (X=Ca, Ge) alloys, Corrosion Science, 153 (2019) 62-73.

[16] E.L. Silva, S.V. Lamaka, D. Mei, M.L. Zheludkevich, The Reduction of Dissolved Oxygen During Magnesium Corrosion, ChemistryOpen, 7 (2018) 664-668.

[17] M. Strebl, S. Virtanen, Real-Time Monitoring of Atmospheric Magnesium Alloy Corrosion, Journal of The Electrochemical Society, 166 (2019) C3001-C3009.

[18] M. Strebl, M. Bruns, S. Virtanen, Editors' Choice—Respirometric in Situ Methods for Real-Time Monitoring of Corrosion Rates: Part I. Atmospheric Corrosion, Journal of The Electrochemical Society, 167 (2020) 021510.

[19] L. Wang, T. Shinohara, B.-P. Zhang, Influence of Deaerated Condition on the Corrosion Behavior of AZ31 Magnesium Alloy in Dilute NaCl Solutions, MATERIALS TRANSACTIONS, 50 (2009) 2563-2569.

[20] D. Snihirova, M. Taryba, S.V. Lamaka, M.F. Montemor, Corrosion inhibition synergies on a model Al-Cu-Mg sample studied by localized scanning electrochemical techniques, Corrosion Science, 112 (2016) 408-417.

[21] S. Thomas, N.V. Medhekar, G.S. Frankel, N. Birbilis, Corrosion mechanism and hydrogen evolution on Mg, Current Opinion in Solid State and Materials Science, 19 (2015) 85-94.

[22] M. Esmaily, J.E. Svensson, S. Fajardo, N. Birbilis, G.S. Frankel, S. Virtanen, R. Arrabal, S. Thomas, L.G. Johansson, Fundamentals and advances in magnesium alloy corrosion, Progress in Materials Science, 89 (2017) 92-193.

[23] W. Beetz, XXXIV. On the development of hydrogen from the anode, The London, Edinburgh, and Dublin Philosophical Magazine and Journal of Science, 32 (1866) 269-278.

[24] A. Atrens, W. Dietzel, The negative difference effect and unipositive Mg+, Advanced Engineering Materials, 9 (2007) 292-297.

[25] A. Seyeux, M. Liu, P. Schmutz, G. Song, A. Atrens, P. Marcus, ToF-SIMS depth profile of the surface film on pure magnesium formed by immersion in pure water and the identification of magnesium hydride, Corrosion Science, 51 (2009) 1883-1886.

[26] M. Curioni, The behaviour of magnesium during free corrosion and potentiodynamic polarization investigated by real-time hydrogen measurement and optical imaging, Electrochimica Acta, 120 (2014) 284-292.

[27] M. Taheri, J.R. Kish, N. Birbilis, M. Danaie, E.A. McNally, J.R. McDermid, Towards a Physical Description for the Origin of Enhanced Catalytic Activity of Corroding Magnesium Surfaces, Electrochimica Acta, 116 (2014) 396-403.

[28] D. Höche, C. Blawert, S.V. Lamaka, N. Scharnagl, C. Mendis, M.L. Zheludkevich, The effect of iron re-deposition on the corrosion of impurity-containing magnesium, Physical Chemistry Chemical Physics, 18 (2016) 1279-1291.

[29] L. Yang, G. Liu, L. Ma, E. Zhang, X. Zhou, G. Thompson, Effect of iron content on the corrosion of pure magnesium: Critical factor for iron tolerance limit, Corrosion Science, 139 (2018) 421-429.

[30] S.V. Lamaka, B. Vaghefinazari, D. Mei, R.P. Petrauskas, D. Höche, M.L. Zheludkevich, Comprehensive screening of Mg corrosion inhibitors, Corrosion Science, 128 (2017) 224-240.

[31] A.S.f.T. Materials, ASTM B94-18 Standard Specification for Magnesium-Alloy Die Castings, in, ASTM, 2018.

[32] A.S.f.T. Materials, ASTM B91-17 Standard Specification for Magnesium-Alloy Forgings, in, ASTM, 2017.

[33] J. Liu, Y. Song, J. Chen, P. Chen, D. Shan, E.-H. Han, The Special Role of Anodic Second Phases in the Micro-galvanic Corrosion of EW75 Mg Alloy, Electrochimica Acta, 189 (2016) 190-195.

[34] Y.-J. Feng, L. Wei, X.-B. Chen, M.-C. Li, Y.-F. Cheng, Q. Li, Unexpected cathodic role of Mg41Sm5 phase in mitigating localized corrosion of extruded Mg-Sm-Zn-Zr alloy in NaCl solution, Corrosion Science, 159 (2019) 108133.

[35] A. Südholz, N. Kirkland, R. Buchheit, N. Birbilis, Electrochemical properties of intermetallic phases and common impurity elements in magnesium alloys, Electrochemical and Solid-State Letters, 14 (2011) C5-C7.

[36] M. Deng, D. Höche, S.V. Lamaka, D. Snihirova, M.L. Zheludkevich, Mg-Ca binary alloys as anodes for primary Mg-air batteries, Journal of Power Sources, 396 (2018) 109-118.

[37] Y. Jin, C. Blawert, F. Feyerabend, J. Bohlen, M. Silva Campos, S. Gavras, B. Wiese, D. Mei, M. Deng, H. Yang, R. Willumeit-Römer, Time-sequential corrosion behaviour observation of micro-alloyed Mg-0.5Zn-0.2Ca alloy via a quasi-in situ approach, Corrosion Science, 158 (2019) 108096.

[38] Y.S. Jeong, W.J. Kim, Enhancement of mechanical properties and corrosion resistance of Mg–Ca alloys through microstructural refinement by indirect extrusion, Corrosion Science, 82 (2014) 392-403.

[39] Z. Szklarska-Smialowska, Pitting corrosion of aluminum, Corrosion Science, 41 (1999) 1743-1767.

[40] M.P. Brady, G. Rother, L.M. Anovitz, K.C. Littrell, K.A. Unocic, H.H. Elsentriecy, G.L. Song, J.K. Thomson, N.C. Gallego, B. Davis, Film Breakdown and Nano-Porous Mg(OH)2Formation from Corrosion of Magnesium Alloys in Salt Solutions, Journal of The Electrochemical Society, 162 (2015) C140-C149.

[41] M. Danaie, R.M. Asmussen, P. Jakupi, D.W. Shoesmith, G.A. Botton, The role of aluminum distribution on the local corrosion resistance of the microstructure in a sand-cast AM50 alloy, Corrosion Science, 77 (2013) 151-163.

[42] C. MAŽURANIĆ, H. Bilinski, B. Matković, Reaction products in the system MgCl2 ‐ NaOH ‐ H2O, Journal of The American Ceramic Society, 65 (1982) 523-526.

[43] L. Urwongse, C.A. Sorrell, The System MgO ‐ MgCl2 ‐ H2O at 23° C, Journal of the American Ceramic Society, 63 (1980) 501-504.

[44] I. Giner, O. Ozcan, G. Grundmeier, In situ AFM studies of the stability of MgO(100) in aqueous electrolytes, Corrosion Science, 87 (2014) 51-59.

[45] F. Cao, C. Zhao, J. You, J. Hu, D. Zheng, G.-L. Song, The Inhibitive Effect of Artificial Seawater on Magnesium Corrosion, Advanced Engineering Materials, 21 (2019) 1900363.

[46] M. Grabowski, D. Bluecher, M. Korte, S. Virtanen, Influence of Ca2+ in Deicing Salt on the Corrosion Behavior of AM50 Magnesium Alloy, Corrosion, 70 (2014) 1008-1023.

[47] M. Grabowski, D. Bluecher, M. Korte, S. Virtanen, The Influence of Ca2+ in Deicing Salt on the Chemistry of Corrosion Products Formed on AM50 Magnesium Alloy—Calcareous Deposition, Corrosion, 71 (2015) 703-725.

[48] N.I. Zainal Abidin, B. Rolfe, H. Owen, J. Malisano, D. Martin, J. Hofstetter, P.J. Uggowitzer, A. Atrens, The in vivo and in vitro corrosion of high-purity magnesium and magnesium alloys WZ21 and AZ91, Corrosion Science, 75 (2013) 354-366.

[49] A.H.M. Sanchez, B.J.C. Luthringer, F. Feyerabend, R. Willumeit, Mg and Mg alloys: How comparable are in vitro and in vivo corrosion rates? A review, Acta Biomaterialia, 13 (2015) 16-31.

[50] S.V. Lamaka, J. Gonzalez, D. Mei, F. Feyerabend, R. Willumeit-Römer, M.L. Zheludkevich, Local pH and Its Evolution Near Mg Alloy Surfaces Exposed to Simulated Body Fluids, Advanced Materials Interfaces, 5 (2018) 1800169.

[51] Chemical Equilibrium Diagrams, in, https://www.kth.se/che/medusa/.

[52] R.-Q. Hou, N. Scharnagl, F. Feyerabend, R. Willumeit-Römer, Exploring the effects of organic molecules on the degradation of magnesium under cell culture conditions, Corrosion Science, 132 (2018) 35-45.

[53] G. Song, Control of biodegradation of biocompatable magnesium alloys, Corrosion Science, 49 (2007) 1696-1701.

[54] J. Wang, L. Wang, S. Guan, S. Zhu, C. Ren, S. Hou, Microstructure and corrosion properties of as sub-rapid solidification Mg–Zn–Y–Nd alloy in dynamic simulated body fluid for vascular stent application, Journal of Materials Science: Materials in Medicine, 21 (2010) 2001-2008.

[55] N. Li, Y. Zheng, Novel Magnesium Alloys Developed for Biomedical Application: A Review, Journal of Materials Science & Technology, 29 (2013) 489-502.

[56] H. Qin, Y. Zhao, Z. An, M. Cheng, Q. Wang, T. Cheng, Q. Wang, J. Wang, Y. Jiang, X. Zhang, G. Yuan, Enhanced antibacterial properties, biocompatibility, and corrosion resistance of degradable Mg-Nd-Zn-Zr alloy, Biomaterials, 53 (2015) 211-220.

[57] R.L. Liu, J.R. Scully, G. Williams, N. Birbilis, Reducing the corrosion rate of magnesium via microalloying additions of group 14 and 15 elements, Electrochimica Acta, 260 (2018) 184-195.

[58] J. Wang, J. Tang, P. Zhang, Y. Li, J. Wang, Y. Lai, L. Qin, Surface modification of magnesium alloys developed for bioabsorbable orthopedic implants: A general review, Journal of Biomedical Materials Research Part B: Applied Biomaterials, 100B (2012) 1691-1701.

[59] H. Hornberger, S. Virtanen, A.R. Boccaccini, Biomedical coatings on magnesium alloys - A review, Acta Biomaterialia, 8 (2012) 2442-2455.

[60] G. Wu, J.M. Ibrahim, P.K. Chu, Surface design of biodegradable magnesium alloys — A review, Surface and Coatings Technology, 233 (2013) 2-12.

[61] X. Lu, C. Blawert, D. Tolnai, T. Subroto, K.U. Kainer, T. Zhang, F. Wang, M.L. Zheludkevich, 3D reconstruction of plasma electrolytic oxidation coatings on Mg alloy via synchrotron radiation tomography, Corrosion Science, 139 (2018) 395-402.

[62] J. Yang, C. Blawert, S.V. Lamaka, D. Snihirova, X. Lu, S. Di, M.L. Zheludkevich, Corrosion protection properties of inhibitor containing hybrid PEO-epoxy coating on magnesium, Corrosion Science, 140 (2018) 99-110.

[63] G.-L. Song, Z. Xu, Effect of microstructure evolution on corrosion of different crystal surfaces of AZ31 Mg alloy in a chloride containing solution, Corrosion Science, 54 (2012) 97-105.

[64] C.Z. Zhang, S.J. Zhu, L.G. Wang, R.M. Guo, G.C. Yue, S.K. Guan, Microstructures and degradation mechanism in simulated body fluid of biomedical Mg–Zn–Ca alloy processed by high pressure torsion, Materials & Design, 96 (2016) 54-62.

[65] F. Pan, X. Chen, T. Yan, T. Liu, J. Mao, W. Luo, Q. Wang, J. Peng, A. Tang, B. Jiang, A novel approach to melt purification of magnesium alloys, Journal of Magnesium and Alloys, 4 (2016) 8-14.

[66] Y. Dai, X.-H. Chen, T. Yan, A.-T. Tang, D. Zhao, Z. Luo, C.-Q. Liu, R.-J. Cheng, F.-S. Pan, Improved Corrosion Resistance in AZ61 Magnesium Alloys Induced by Impurity Reduction, Acta Metallurgica Sinica (English Letters), 33 (2020) 225-232.

[67] H. Matsubara, Y. Ichige, K. Fujita, H. Nishiyama, K. Hodouchi, Effect of impurity Fe on corrosion behavior of AM50 and AM60 magnesium alloys, Corrosion Science, 66 (2013) 203-210.

[68] J.I. Kim, H.N. Nguyen, B.S. You, Y.M. Kim, Effect of Y addition on removal of Fe impurity from magnesium alloys, Scripta Materialia, 162 (2019) 355-360.

[69] R. Liu, M. Hurley, A. Kvryan, G. Williams, J. Scully, N. Birbilis, Controlling the corrosion and cathodic activation of magnesium via microalloying additions of Ge, Scientific reports, 6 (2016) 28747.

[70] S. Fajardo, J. Bosch, G.S. Frankel, Anomalous hydrogen evolution on AZ31, AZ61 and AZ91 magnesium alloys in unbuffered sodium chloride solution, Corrosion Science, 146 (2019) 163-171.

[71] M. Liu, G.-L. Song, Impurity control and corrosion resistance of magnesium–aluminum alloy, Corrosion Science, 77 (2013) 143-150.

[72] Z. Hu, R.L. Liu, S.K. Kairy, X. Li, H. Yan, N. Birbilis, Effect of Sm additions on the microstructure and corrosion behavior of magnesium alloy AZ91, Corrosion Science, 149 (2019) 144-152.

[73] P. Minárik, R. Král, M. Janeček, Effect of ECAP processing on corrosion resistance of AE21 and AE42 magnesium alloys, Applied Surface Science, 281 (2013) 44-48.

[74] K. Matsubara, Y. Miyahara, Z. Horita, T. Langdon, Developing superplasticity in a magnesium alloy through a combination of extrusion and ECAP, Acta materialia, 51 (2003) 3073-3084.

[75] J. Gao, S. Guan, Z. Ren, Y. Sun, S. Zhu, B. Wang, Homogeneous corrosion of high pressure torsion treated Mg–Zn–Ca alloy in simulated body fluid, Materials Letters, 65 (2011) 691-693.

[76] K. Edalati, A. Yamamoto, Z. Horita, T. Ishihara, High-pressure torsion of pure magnesium: Evolution of mechanical properties, microstructures and hydrogen storage capacity with equivalent strain, Scripta Materialia, 64 (2011) 880-883.

[77] N. Saikrishna, G.P.K. Reddy, B. Munirathinam, B.R. Sunil, Influence of bimodal grain size distribution on the corrosion behavior of friction stir processed biodegradable AZ31 magnesium alloy, Journal of magnesium and alloys, 4 (2016) 68-76.

[78] W. Woo, H. Choo, D. Brown, P. Liaw, Z. Feng, Texture variation and its influence on the tensile behavior of a friction-stir processed magnesium alloy, Scripta materialia, 54 (2006) 1859-1864.

[79] B. Jiang, Q. Xiang, A. Atrens, J. Song, F. Pan, Influence of crystallographic texture and grain size on the corrosion behaviour of as-extruded Mg alloy AZ31 sheets, Corrosion Science, 126 (2017) 374-380.

[80] B. Wang, D. Xu, J. Dong, W. Ke, Effect of the crystallographic orientation and twinning on the corrosion resistance of an as-extruded Mg–3Al–1Zn (wt.%) bar, Scripta Materialia, 88 (2014) 5-8.

[81] G.-L. Song, Z. Xu, Crystal orientation and electrochemical corrosion of polycrystalline Mg, Corrosion Science, 63 (2012) 100-112.

[82] F.C. Walsh, C.T.J. Low, R.J.K. Wood, K.T. Stevens, J. Archer, A.R. Poeton, A. Ryder, Plasma electrolytic oxidation (PEO) for production of anodised coatings on lightweight metal (Al, Mg, Ti) alloys, Transactions of the IMF, 87 (2009) 122-135.

[83] S.V. Lamaka, G. Knörnschild, D.V. Snihirova, M.G. Taryba, M.L. Zheludkevich, M.G.S. Ferreira, Complex anticorrosion coating for ZK30 magnesium alloy, Electrochimica Acta, 55 (2009) 131-141.

[84] J.H. Gao, X.Y. Shi, B. Yang, S.S. Hou, E.C. Meng, F.X. Guan, S.K. Guan, Fabrication and characterization of bioactive composite coatings on Mg–Zn–Ca alloy by MAO/sol–gel, Journal of Materials Science: Materials in Medicine, 22 (2011) 1681-1687.

[85] J.H. Gao, S.K. Guan, J. Chen, L.G. Wang, S.J. Zhu, J.H. Hu, Z.W. Ren, Fabrication and characterization of rod-like nano-hydroxyapatite on MAO coating supported on Mg–Zn–Ca alloy, Applied Surface Science, 257 (2011) 2231-2237.

[86] L. Chen, Y. Sheng, H. Zhou, Z. Li, X. Wang, W. Li, Influence of a MAO + PLGA coating on biocorrosion and stress corrosion cracking behavior of a magnesium alloy in a physiological environment, Corrosion Science, 148 (2019) 134-143.

[87] X.B. Chen, N. Birbilis, T.B. Abbott, Review of Corrosion-Resistant Conversion Coatings for Magnesium and Its Alloys, Corrosion, 67 (2011) 035005-035001-035005-035016.

[88] R. Maurya, A.R. Siddiqui, K. Balani, An environment-friendly phosphate chemical conversion coating on novel Mg-9Li-7Al-1Sn and Mg-9Li-5Al-3Sn-1Zn alloys with remarkable corrosion protection, Applied Surface Science, 443 (2018) 429-440.

[89] X.B. Chen, N. Birbilis, T.B. Abbott, Effect of [Ca2+] and [PO43-] levels on the formation of calcium phosphate conversion coatings on die-cast magnesium alloy AZ91D, Corrosion Science, 55 (2012) 226-232.

[90] Z. Chunyan, L. Shangju, Y. Baoxing, L. Xiaopeng, C. Xiao-Bo, Z. Tao, W. Fuhui, Ratio of total acidity to pH value of coating bath: A new strategy towards phosphate conversion coatings with optimized corrosion resistance for magnesium alloys, Corrosion Science, (2019).

[91] S.-Y. Jian, Y.-R. Chu, C.-S. Lin, Permanganate conversion coating on AZ31 magnesium alloys with enhanced corrosion resistance, Corrosion Science, 93 (2015) 301-309.

[92] Y. Ma, N. Li, D. Li, M. Zhang, X. Huang, Characteristics and corrosion studies of vanadate conversion coating formed on Mg–14 wt% Li–1 wt% Al–0.1 wt% Ce alloy, Applied surface science, 261 (2012) 59-67.

[93] L. Niu, S.-H. Chang, X. Tong, G. Li, Z. Shi, Analysis of characteristics of vanadate conversion coating on the surface of magnesium alloy, Journal of alloys and compounds, 617 (2014) 214-218.

[94] A.S. Hamdy, M. Farahat, Chrome-free zirconia-based protective coatings for magnesium alloys, Surface and Coatings Technology, 204 (2010) 2834-2840.

[95] Y. Yang, C. Tsai, Y. Huang, C. Lin, Formation mechanism and properties of titanate conversion coating on AZ31 magnesium alloy, Journal of The Electrochemical Society, 159 (2012) C226.

[96] C. Lin, H. Lin, K. Lin, W. Lai, Formation and properties of stannate conversion coatings on AZ61 magnesium alloys, Corrosion science, 48 (2006) 93-109.

[97] F. Zucchi, A. Frignani, V. Grassi, G. Trabanelli, C. Monticelli, Stannate and permanganate conversion coatings on AZ31 magnesium alloy, Corrosion Science, 49 (2007) 4542-4552.

[98] G. Zhang, L. Wu, A. Tang, Y. Ma, G.-L. Song, D. Zheng, B. Jiang, A. Atrens, F. Pan, Active corrosion protection by a smart coating based on a MgAl-layered double hydroxide on a cerium-modified plasma electrolytic oxidation coating on Mg alloy AZ31, Corrosion Science, 139 (2018) 370-382.

[99] Y. Chen, X. Lu, S.V. Lamaka, P. Ju, C. Blawert, T. Zhang, F. Wang, M.L. Zheludkevich, Active protection of Mg alloy by composite PEO coating loaded with corrosion inhibitors, Applied Surface Science, 504 (2020) 144462.

[100] A.F. Galio, S.V. Lamaka, M.L. Zheludkevich, L.F.P. Dick, I.L. Müller, M.G.S. Ferreira, Inhibitor-doped sol–gel coatings for corrosion protection of magnesium alloy AZ31, Surface and Coatings Technology, 204 (2010) 1479-1486.

[101] Z.-Z. Yin, W.-C. Qi, R.-C. Zeng, X.-B. Chen, C.-D. Gu, S.-K. Guan, Y.-F. Zheng, Advances in coatings on biodegradable magnesium alloys, Journal of Magnesium and Alloys, 8 (2020) 42-65.

[102] J. Hu, D. Zeng, Z. Zhang, T. Shi, G.-L. Song, X. Guo, 2-Hydroxy-4-methoxy-acetophenone as an environment-friendly corrosion inhibitor for AZ91D magnesium alloy, Corrosion Science, 74 (2013) 35-43.

[103] M. Antonijevic, M. Petrovic, Copper corrosion inhibitors. A review, Int. J. Electrochem. Sci, 3 (2008) 1-28.

[104] K. Xhanari, M. Finšgar, Organic corrosion inhibitors for aluminum and its alloys in chloride and alkaline solutions: A review, Arabian Journal of Chemistry, (2016).

[105] K. Xhanari, M. Finšgar, M.K. Hrnčič, U. Maver, Ž. Knez, B. Seiti, Green corrosion inhibitors for aluminium and its alloys: a review, RSC Advances, 7 (2017) 27299-27330.

[106] M. Finšgar, J. Jackson, Application of corrosion inhibitors for steels in acidic media for the oil and gas industry: A review, Corrosion Science, 86 (2014) 17-41.

[107] A.E. Somers, B.R.W. Hinton, C. de Bruin-Dickason, G.B. Deacon, P.C. Junk, M. Forsyth, New, environmentally friendly, rare earth carboxylate corrosion inhibitors for mild steel, Corrosion Science, 139 (2018) 430-437.

[108] G. Williams, H.N. McMurray, R. Grace, Inhibition of magnesium localised corrosion in chloride containing electrolyte, Electrochimica Acta, 55 (2010) 7824-7833.

[109] D. Huang, J. Hu, G.-L. Song, X. Guo, Inhibition effect of inorganic and organic inhibitors on the corrosion of Mg–10Gd–3Y–0.5Zr alloy in an ethylene glycol solution at ambient and elevated temperatures, Electrochimica Acta, 56 (2011) 10166-10178.

[110] M.D. Pereda, C. Alonso, L. Burgos-Asperilla, J.A. del Valle, O.A. Ruano, P. Perez, M.A. Fernández Lorenzo de Mele, Corrosion inhibition of powder metallurgy Mg by fluoride treatments, Acta Biomaterialia, 6 (2010) 1772-1782.

[111] G. Wang, M. Zhang, R. Wu, Molybdate and molybdate/permanganate conversion coatings on Mg–8.5 Li alloy, Applied Surface Science, 258 (2012) 2648-2654.

[112] N. Dinodi, A.N. Shetty, Alkyl carboxylates as efficient and green inhibitors of magnesium alloy ZE41 corrosion in aqueous salt solution, Corrosion Science, 85 (2014) 411-427.

[113] A. Frignani, V. Grassi, F. Zanotto, F. Zucchi, Inhibition of AZ31 Mg alloy corrosion by anionic surfactants, Corrosion Science, 63 (2012) 29-39.

[114] H. Gao, Q. Li, Y. Dai, F. Luo, H.X. Zhang, High efficiency corrosion inhibitor 8-hydroxyquinoline and its synergistic effect with sodium dodecylbenzenesulphonate on AZ91D magnesium alloy, Corrosion Science, 52 (2010) 1603-1609.

[115] X.P. Lu, Y. Li, P.F. Ju, Y. Chen, J.S. Yang, K. Qian, T. Zhang, F.H. Wang, Unveiling the inhibition mechanism of an effective inhibitor for AZ91 Mg alloy, Corrosion Science, 148 (2019) 264-271.

[116] D. Höche, S.V. Lamaka, B. Vaghefinazari, T. Braun, R.P. Petrauskas, M. Fichtner, M.L. Zheludkevich, Performance boost for primary magnesium cells using iron complexing agents as electrolyte additives, Scientific Reports, 8 (2018) 7578.

[117] J.J. Yang, C. Blawert, S.V. Lamaka, K.A. Yasakau, L. Wang, D. Laipple, M. Schieda, S.C. Di, M.L. Zheludkevich, Corrosion inhibition of pure Mg containing a high level of iron impurity in pH neutral NaCl solution, Corrosion Science, 142 (2018) 222-237.

[118] S.V. Lamaka, D. Höche, R.P. Petrauskas, C. Blawert, M.L. Zheludkevich, A new concept for corrosion inhibition of magnesium: Suppression of iron re-deposition, Electrochemistry Communications, 62 (2016) 5-8.

[119] C. Feiler, D. Mei, B. Vaghefinazari, T. Würger, R.H. Meißner, B.J.C. Luthringer-Feyerabend, D.A. Winkler, M.L. Zheludkevich, S.V. Lamaka, In silico screening of modulators of magnesium dissolution, Corrosion Science, 163 (2019) 108245.

[120] A. Maltseva, S.V. Lamaka, K.A. Yasakau, D. Mei, D. Kurchavov, M.L. Zheludkevich, G. Lefèvre, P. Volovitch, In situ surface film evolution during Mg aqueous corrosion in presence of selected carboxylates, Corrosion Science, (2020) 108484.

[121] M.C. Merino, A. Pardo, R. Arrabal, S. Merino, P. Casajús, M. Mohedano, Influence of chloride ion concentration and temperature on the corrosion of Mg–Al alloys in salt fog, Corrosion Science, 52 (2010) 1696-1704.

[122] M.-C. Zhao, M. Liu, G.-L. Song, A. Atrens, Influence of pH and chloride ion concentration on the corrosion of Mg alloy ZE41, Corrosion Science, 50 (2008) 3168-3178.

[123] R. Ambat, N.N. Aung, W. Zhou, Studies on the influence of chloride ion and pH on the corrosion and electrochemical behaviour of AZ91D magnesium alloy, Journal of Applied Electrochemistry, 30 (2000) 865-874.

[124] H. Altun, S. Sen, Studies on the influence of chloride ion concentration and pH on the corrosion and electrochemical behaviour of AZ63 magnesium alloy, Materials & Design, 25 (2004) 637-643.

[125] C. Taltavull, Z. Shi, B. Torres, J. Rams, A. Atrens, Influence of the chloride ion concentration on the corrosion of high-purity Mg, ZE41 and AZ91 in buffered Hank's solution, Journal of Materials Science: Materials in Medicine, 25 (2014) 329-345.

[126] R.-C. Zeng, Y. Hu, S.-K. Guan, H.-Z. Cui, E.-H. Han, Corrosion of magnesium alloy AZ31: The influence of bicarbonate, sulphate, hydrogen phosphate and dihydrogen phosphate ions in saline solution, Corrosion Science, 86 (2014) 171-182.

[127] Y. Xin, T. Hu, P.K. Chu, Degradation behaviour of pure magnesium in simulated body fluids with different concentrations of HCO3, Corrosion Science, 53 (2011) 1522-1528.

[128] Z. Li, G.-L. Song, S. Song, Effect of bicarbonate on biodegradation behaviour of pure magnesium in a simulated body fluid, Electrochimica Acta, 115 (2014) 56-65.

[129] W. Ma, Y. Liu, W. Wang, Y. Zhang, Effects of electrolyte component in simulated body fluid on the corrosion behavior and mechanical integrity of magnesium, Corrosion Science, 98 (2015) 201-210.

[130] N.A. Agha, F. Feyerabend, B. Mihailova, S. Heidrich, U. Bismayer, R. Willumeit-Römer, Magnesium degradation influenced by buffering salts in concentrations typical of in vitro and in vivo models, Materials Science and Engineering: C, 58 (2016) 817-825.

[131] Y. Jang, B. Collins, J. Sankar, Y. Yun, Effect of biologically relevant ions on the corrosion products formed on alloy AZ31B: An improved understanding of magnesium corrosion, Acta Biomaterialia, 9 (2013) 8761-8770.

[132] C. Ning, L. Zhou, Y. Zhu, Y. Li, P. Yu, S. Wang, T. He, W. Li, G. Tan, Y. Wang, C. Mao, Influence of Surrounding Cations on the Surface Degradation of Magnesium Alloy Implants under a Compressive Pressure, Langmuir, 31 (2015) 13561-13570.

[133] R. Willumeit-Römer, The Interface Between Degradable Mg and Tissue, JOM, 71 (2019) 1447-1455.

[134] F. Cao, C. Zhao, G.-L. Song, D. Zheng, The corrosion of pure Mg accelerated by haze pollutant ammonium sulphate, Corrosion Science, 150 (2019) 161-174.

[135] Q. Jiang, K. Zhang, X. Li, Y. Li, M. Ma, G. Shi, J. Yuan, The corrosion behaviors of Mg–7Gd–5Y‑1Nd–0.5Zr alloy under (NH4)2SO4, NaCl and Ca(NO3)2 salts spray condition, Journal of Magnesium and Alloys, 1 (2013) 230-234.

[136] C. Zhao, F. Cao, G.-L. Song, Corrosivity of haze constituents to pure Mg, Journal of Magnesium and Alloys, 8 (2020) 150-162.

[137] N.T. Kirkland, J. Waterman, N. Birbilis, G. Dias, T.B.F. Woodfield, R.M. Hartshorn, M.P. Staiger, Buffer-regulated biocorrosion of pure magnesium, Journal of Materials Science: Materials in Medicine, 23 (2012) 283-291.

[138] M.B. Kannan, H. Khakbaz, A. Yamamoto, Understanding the influence of HEPES buffer concentration on the biodegradation of pure magnesium: An electrochemical study, Materials Chemistry and Physics, 197 (2017) 47-56.

[139] S.S. Jamali, S.E. Moulton, D.E. Tallman, M. Forsyth, J. Weber, G.G. Wallace, Applications of scanning electrochemical microscopy (SECM) for local characterization of AZ31 surface during corrosion in a buffered media, Corrosion Science, 86 (2014) 93-100.

[140] Y. Xin, P.K. Chu, Influence of Tris in simulated body fluid on degradation behavior of pure magnesium, Materials Chemistry and Physics, 124 (2010) 33-35.

[141] L.-Y. Cui, Y. Hu, R.-C. Zeng, Y.-X. Yang, D.-D. Sun, S.-Q. Li, F. Zhang, E.-H. Han, New insights into the effect of Tris-HCl and Tris on corrosion of magnesium alloy in presence of bicarbonate, sulfate,

hydrogen phosphate and dihydrogen phosphate ions, Journal of Materials Science & Technology, 33 (2017) 971-986.

[142] A. Yamamoto, S. Hiromoto, Effect of inorganic salts, amino acids and proteins on the degradation of pure magnesium in vitro, Materials Science and Engineering: C, 29 (2009) 1559-1568.

[143] N.H. Helal, W.A. Badawy, Environmentally safe corrosion inhibition of Mg–Al–Zn alloy in chloride free neutral solutions by amino acids, Electrochimica Acta, 56 (2011) 6581-6587.

[144] Z. Fang, J. Wang, X. Yang, Q. Sun, Y. Jia, H. Liu, T. Xi, S. Guan, Adsorption of arginine, glycine and aspartic acid on Mg and Mg-based alloy surfaces: A first-principles study, Applied Surface Science, 409 (2017) 149-155.

[145] Y. Wang, B.H. Ding, S.Y. Gao, X.B. Chen, R.C. Zeng, L.Y. Cui, S.J. Li, S.Q. Li, Y.H. Zou, E.H. Han, S.K. Guan, Q.Y. Liu, In vitro corrosion of pure Mg in phosphate buffer solution-Influences of isoelectric point and molecular structure of amino acids, Mater Sci Eng C Mater Biol Appl, 105 (2019) 110042.

[146] Y. Zhao, C. Qiao, Z. Fang, H. Wang, S. Zhu, J. Wang, J. Ren, S. Guan, Y. Jia, Inverted Hydration Layers on Bio-Magnesium Surfaces in the Initial Degradation Stage and their Influence on Adsorption of Amino Acid Analogues: The Metadynamics Simulations, Langmuir, 35 (2019) 17009-17015.

[147] L.-Y. Cui, X.-T. Li, R.-C. Zeng, S.-Q. Li, E.-H. Han, L. Song, In vitro corrosion of Mg-Ca alloy - The influence of glucose content, Frontiers of Materials Science, 11 (2017) 284-295.

[148] R.C. Zeng, X.T. Li, S.Q. Li, F. Zhang, E.H. Han, In vitro degradation of pure Mg in response to glucose, Sci Rep, 5 (2015) 13026.

[149] Blood proteins, in, https://en.wikipedia.org/wiki/Blood_proteins.

[150] C.L. Liu, Y.J. Wang, R.C. Zeng, X.M. Zhang, W.J. Huang, P.K. Chu, In vitro corrosion degradation behaviour of Mg–Ca alloy in the presence of albumin, Corrosion Science, 52 (2010) 3341-3347.

[151] F. El-Taib Heakal, A.M. Bakry, Serum albumin can influence magnesium alloy degradation in simulated blood plasma for cardiovascular stenting, Materials Chemistry and Physics, 220 (2018) 35-49.

[152] T. Li, Y. He, J. Zhou, S. Tang, Y. Yang, X. Wang, Influence of albumin on in vitro degradation behavior of biodegradable Mg-1.5Zn-0.6Zr-0.2Sc alloy, Materials Letters, 217 (2018) 227-230.

[153] S.E. Harandi, P.C. Banerjee, C.D. Easton, R.K. Singh Raman, Influence of bovine serum albumin in Hanks' solution on the corrosion and stress corrosion cracking of a magnesium alloy, Materials Science and Engineering: C, 80 (2017) 335-345.

[154] J. Walker, S. Shadanbaz, N.T. Kirkland, E. Stace, T. Woodfield, M.P. Staiger, G.J. Dias, Magnesium alloys: Predicting in vivo corrosion with in vitro immersion testing, Journal of Biomedical Materials Research Part B: Applied Biomaterials, 100B (2012) 1134-1141.

[155] X. Gu, Y. Zheng, L. Chen, Influence of artificial biological fluid composition on the biocorrosion of potential orthopedic Mg–Ca, AZ31, AZ91 alloys, Biomedical Materials, 4 (2009) 065011.

[156] I. Johnson, W. Jiang, H. Liu, The Effects of Serum Proteins on Magnesium Alloy Degradation in Vitro, Sci Rep, 7 (2017) 14335.

[157] R. Hou, R. Willumeit-Römer, V.M. Garamus, M. Frant, J. Koll, F. Feyerabend, Adsorption of Proteins on Degradable Magnesium - Which Factors are Relevant?, ACS Applied Materials & Interfaces, 10 (2018) 42175-42185.

[158] R.Q. Hou, N. Scharnagl, R. Willumeit-Romer, F. Feyerabend, Different effects of single protein vs. protein mixtures on magnesium degradation under cell culture conditions, Acta Biomater, 98 (2019) 256-268.

[159] N.T. Kirkland, N. Birbilis, J. Walker, T. Woodfield, G.J. Dias, M.P. Staiger, In-vitro dissolution of magnesium-calcium binary alloys: Clarifying the unique role of calcium additions in bioresorbable magnesium implant alloys, Journal of Biomedical Materials Research Part B: Applied Biomaterials, 95 (2010) 91-100.

[160] R. Willumeit, J. Fischer, F. Feyerabend, N. Hort, U. Bismayer, S. Heidrich, B. Mihailova, Chemical surface alteration of biodegradable magnesium exposed to corrosion media, Acta Biomaterialia, 7 (2011) 2704-2715.

[161] J. Yang, J. Peng, E.A. Nyberg, F.-s. Pan, Effect of Ca addition on the corrosion behavior of Mg–Al–Mn alloy, Applied Surface Science, 369 (2016) 92-100.

[162] H.R. Bakhsheshi-Rad, M.R. Abdul-Kadir, M.H. Idris, S. Farahany, Relationship between the corrosion behavior and the thermal characteristics and microstructure of Mg–0.5Ca–xZn alloys, Corrosion Science, 64 (2012) 184-197.

[163] J.W. Seong, W.J. Kim, Development of biodegradable Mg–Ca alloy sheets with enhanced strength and corrosion properties through the refinement and uniform dispersion of the Mg2Ca phase by high-ratio differential speed rolling, Acta Biomaterialia, 11 (2015) 531-542.

[164] T. Kokubo, H. Takadama, How useful is SBF in predicting in vivo bone bioactivity?, Biomaterials, 27 (2006) 2907-2915.

[165] H. Krebs, Chemical composition of blood plasma and serum, Annual review of biochemistry, 19 (1950) 409-430.

[166] D. Rajdl, Clinical Biochemistry, Charles University in Prague, Faculty of Medicine in Pilsen, 2016.

[167] List of human blood components, in, https://en.wikipedia.org/wiki/List_of_human_blood_components.

[168] A. Michnik, K. Michalik, A. Kluczewska, Z. Drzazga, Comparative DSC study of human and bovine serum albumin, Journal of thermal analysis and calorimetry, 84 (2006) 113-117.

[169] C. Wang, D. Mei, l. Wang, M. Deng, S.V. Lamaka, M.L. Zheludkevich, High Rate Oxygen Reduction Reaction during Corrosion of Ultra-High-Purity Magnesium Submitted.

[170] D. Mei, S.V. Lamaka, C. Feiler, M.L. Zheludkevich, The effect of small-molecule bio-relevant organic components at low concentration on the corrosion of commercially pure Mg and Mg-0.8Ca alloy: An overall perspective, Corrosion Science, 153 (2019) 258-271.

[171] A. NACE, ASTMG31-12a, Standard Guide for Laboratory Immersion Corrosion Testing of Metals, ASTM International, West Conshohocken, PA, (2012) 10.

Appendix

1. List of symbols and abbreviations

BSA	Bovine serum albumin
CEA	Chicken egg albumin
CP Mg	Commercially pure Mg
DMEM	Dulbecco's Modified Eagle's Medium
EBSS	Earle's balanced salt solution
EDS	Energy dispersive X-rays spectroscopy
EIS	Electrochemical impedance spectroscopy
FBS	Fetal bovine serum
HBSS	Hank's balanced salt solution
HEPES	4-(2-Hydroxyethyl)piperazine-1-ethanesulfonic acid
IE	Inhibition efficiency
OCP	Open circuit potential
PaO_2	Partial pressure of oxygen
PBS	Phosphate buffered saline
SBF	Simulated body fluid
SEM	Scanning electron microscopy
SIET	Scanning ion-selective electrode technique
Tris	Tris(hydroxyethyl)aminomethane
MEM	Minimum essential medium
Mg	Magnesium
Mg-0.8Ca	Mg-0.8 wt.% Ca alloy
V/A	Ratio of electrolyte volume to sample surface area
XRD	X-ray diffraction

2. Publications during candidature

The published/accepted journal papers (first author & corresponding author) included in this thesis:

[1] ***D. Mei***, S.V. Lamaka, J. Gonzalez, F. Feyerabend, R. Willumeit-Römer, M.L. Zheludkevich, The role of individual components of simulated body fluid on the corrosion behavior of commercially pure Mg, Corrosion Science, 147 (2019) 81-93. https://doi.org/10.1016/j.corsci.2018.11.011

This paper was incorporated in this thesis as **Chapter 4.2**.

[2] ***D. Mei***, S.V. Lamaka, C. Feiler, M.L. Zheludkevich, The effect of small-molecule bio-relevant organic components at low concentration on the corrosion of commercially pure Mg and Mg-0.8Ca alloy: An overall perspective, Corrosion Science, 153 (2019) 258-271. https://doi.org/10.1016/j.corsci.2019.03.039

This paper was incorporated in this thesis as **Chapter 4.3**.

[3] ***D. Mei***, C. Wang, S.V. Lamaka, M.L. Zheludkevich, Clarifying the influence of albumin on the initial stages of magnesium corrosion in Hank's Balanced Salt Solution, Journal of Magnesium and Alloys, (2020). https://doi.org/10.1016/j.jma.2020.07.002

This paper was incorporated in this thesis as **Chapter 4.4**.

[4] ***D. Mei***, S.V. Lamaka, X. Lu, M.L. Zheludkevich, Selecting medium for corrosion testing of bioabsorbable magnesium and other metals – a critical review, Corrosion Science, 171 (2020) 108722. https://doi.org/10.1016/j.corsci.2020.108722

This paper was incorporated in this thesis as **Chapter 5**.

The co-authored published journal papers:

[5] C. Feiler, ***D. Mei***, B. Vaghefinazari, T. Würger, R. H. Meißner, B. J. C. Luthringer-Feyerabend, D. A. Winkler, M. L. Zheludkevich, S. V. Lamaka, In silico Screening of Modulators of Magnesium Dissolution, Corrosion Science, 163 (2020) 108245. https://doi.org/10.1016/j.corsci.2020.108722

This paper was not incorporated in this thesis, while its content is related to the influence of organic molecules on Mg corrosion. D. Mei participated in the collection of preliminary experimental data, conducted verification experiments of the simulation results and gave comments on data analysis.

[6] C. Feiler, ***D. Mei***, B. J. C. Luthringer-Feyerabend, S. V. Lamaka , M. L. Zheludkevich, Rational Design of Effective Mg Degradation Modulators, Corrosion, 2020, https://doi.org/10.5006/3597

This paper was not incorporated in this thesis, while its content is related to the influence of organic molecules on Mg corrosion. D. Mei participated in the collection of preliminary experimental data, conducted verification experiments of the simulation results and gave comments on data analysis.

[7] A.S. Gnedenkov, ***D. Mei***, S.V. Lamaka, S.L. Sinebryukhov, D.V. Mashtalyar, I.E. Vyaliy, M.L. Zheludkevich, S.V. Gnedenkova, Localized currents and pH distribution studied during corrosion of MA8 Mg alloy in the cell culture medium, 170 (2020) 108689. https://doi.org/10.1016/j.corsci.2020.108689

This paper was not incorporated in this thesis, while its content is related to the corrosion behavior of Mg in complex pseudophysiological medium. D. Mei conducted the corrosion tests of MA8 Mg alloy in the cell culture medium and gave comments on data analysis.

[8] S.V. Lamaka, B. Vaghefinazari, ***D. Mei***, R.P. Petrauskas, D. Höche, M.L. Zheludkevich, Comprehensive Screening of Mg Corrosion Inhibitors, Corrosion Science, 128 (2017) 224-240. https://doi.org/10.1016/j.corsci.2017.07.011

This paper was not incorporated in this thesis, while its content is related to the influence of organic molecules on Mg corrosion. D. Mei conducted part of corrosion tests and gave comments on data analysis.

[9] S.V. Lamaka, J. Gonzalez, ***D. Mei***, F. Feyerabend, R. Willumeit-Römer, M.L. Zheludkevich, Local pH and Its Evolution Near Mg Alloy Surfaces Exposed to Simulated Body Fluids, Advanced Materials Interfaces, 5 (2018) 1800169. https://doi.org/10.1002/admi.201800169

This paper was not incorporated in this thesis, while its content is related to the corrosion behavior of Mg in complex pseudophysiological medium. D. Mei conducted the corrosion tests in this work and gave comments on data analysis.

[10] E.L. Silva, S.V. Lamaka, ***D. Mei***, M.L. Zheludkevich, The Reduction of Dissolved Oxygen During Magnesium Corrosion, ChemistryOpen, 7 (2018) 664-668. https://doi.org/10.1002/open.201800076

This paper was not incorporated in this thesis, while its content is involved is related to the corrosion behavior of Mg in aqueous solutions. D. Mei conducted the hydrogen evolution tests in this work and gave comments on data analysis.

[11] A. Maltseva, S.V. Lamaka, K.A. Yasakau, ***D. Mei***, D. Kurchavov, M.L. Zheludkevich, G. Lefèvre, P. Volovitch, *In situ* surface film evolution during aqueous corrosion of magnesium in presence of selected carboxylates, Corrosion Science, 171 (2020) 108484. https://doi.org/10.1016/j.corsci.2020.108484

This paper was not incorporated in this thesis, while its content is related to the influence of organic molecules on Mg corrosion. D. Mei conducted part of corrosion tests and gave comments on data analysis.

[12] Y. Jin, C. Blawert, H. Yang, B. Wiese, F. Feyerabend, J. Bohlen, ***D. Mei***, M. Deng, M. Silva Campos, N. Scharnagl, K. Strecker, J. Bode, C. Vogt, R. Willumeit-Römer, Microstructure-corrosion behaviour relationship of micro-alloyed Mg-0.5Zn alloy with the addition of Ca, Sr, Ag, In and Cu, Materials & Design, 195 (2020) 108980. https://doi.org/10.1016/j.matdes.2020.108980

This paper was not incorporated in this thesis. D. Mei participated in the data analysis.

[13] Y. Jin, C. Blawert, F. Feyerabend, J. Bohlen, M. Silva Campos, S. Gavras, B. Wiese, ***D. Mei***, M. Deng, H. Yang, R. Willumeit-Römer, Time-sequential corrosion behaviour observation of micro-alloyed Mg-0.5Zn-0.2Ca alloy via a quasi-in situ approach, Corrosion Science, 158 (2019) 108096. https://doi.org/10.1016/j.corsci.2019.108096

This paper was not incorporated in this thesis. D. Mei participated in the data analysis.

Acknowledgment

After finishing this thesis, it is my pleasure to express sincere gratitude to the people who have contributed to my research works during the past four years in HZG.

First and foremost, I would like to express my deep gratitude to my supervisor, Prof. Dr. Mikhail L. Zheludkevich, to give the opportunity to me to start my PhD study at a such great and active department. His guidance and help led to the accomplishment of my work here. With his support, I had opportunities to go to academic conferences and published scientific papers. I would also like to thank Prof. dr. ir. J.M.C. (Arjan) Mol for being my second academic supervisor and his valuable suggestions to this dissertation. I am sincerely grateful to Prof. Dr. rer. nat. Franz Faupel for being the president of my defense committee and Prof. Dr. Regine Willumeit-Römer for her suggestions to my work.

I would like to appreciate my daily supervisor, Dr. Sviatlana V. Lamaka. Her work enthusiasm deeply inspired me. She showed me the efforts and rigor that a scientist should have, and encouraged me to continue to work in the field of scientific research. Without her help, it is impossible for me to finish my PhD in time. I really learned a lot from her, not only in scientific part.

I would like to thank Mr. Ulrich Burmester, Mr. Volker Heitmann and Mr. Gert Wiese for the technical help during my research works. I am very grateful to Dr. Xiaopeng Lu, who helped me a lot when I first arrived Germany and gave the beneficial discussions about my research. My deep gratitude to my officemate, Dr. Silva Campos, for helping me in the daily life. Many thanks to Ms. Anissa Bouali, Mr. Vinodh Korrapati for the friendly atmosphere that they provided in Room 409. I would like to thank Dr. Christian Feiler, Dr. Carsten Blawert, Dr. Nico Scharnagl, Dr. Daniel Höche, Dr. Darya Snihirova, Dr. Maria Serdechnova and all the colleagues in WZK department for their assistance during my study.

I would like to acknowledge the Chinese Community in HZG. Undoubtedly, these Chinese friends made me feel warm like in my family, although in a foreign country. Thanks for the fun that they brought into my life, in the festival parties, weekend games, and even daily lunches.

I gratefully acknowledge the funding from China Scholarship Council (CSC) for the financial support for my PhD study in Germany.

Finally, I would like to thank my parents and my grandparents for their years of nurturing, for their understanding and support on every decision that I made. To my uncle, Prof. Lei Wang, the beacon of my life, thanks his guidance and suggestions at key points in my life. To my uncles, aunts and cousins and all my friends, thanks their love and support. To my love, Bing, thank you for your appearing, accompanying, as well as the perseverance and dedication for our relationship.